UNIVERSIDADE NOVA DE LISBOA
Faculdade de Ciências e Tecnologia

Cristina Maria Grade Couto da Silva Cordas

Electrochemical Studies of Electron Transfer Proteins and Electroactive Biofilms

LISBOA
2007

Cristina Maria Grade Couto da Silva Cordas

Electrochemical Studies of Electron Transfer Proteins and Electroactive Biofilms

Dissertação apresentada para obtenção do Grau de Doutor em Bioquímica-especialidade Bioquímica Física, pela Universidade Nova de Lisboa, Faculdade de Ciências e Tecnologia.

LISBOA
2007

Nº de arquivo

“copyright”

Agradecimentos

Em primeiro lugar quero agradecer ao meu Supervisor, Prof. José J. G. Moura, por me ter recebido no seu grupo e dado a oportunidade da realização deste trabalho, a sua total disponibilidade para a resolução de todos os problemas, as discussões científicas e, não menos importante, a sua amizade.

À Prof. Isabel Moura agradeço a sua disponibilidade para ajudar sempre que foi necessário e por me acolher também no seu laboratório.

Agradeço também aos Profs. Pedro Tavares e Alice Pereira por todas as discussões de resultados, pela sua sempre total disponibilidade para ajudar em tudo o que fosse necessário e pela amizade e carinho que sempre me dispensaram. A integridade pessoal e científica que sempre demonstraram é um modelo que me faz acreditar nas pessoas e na ciência.

Gostaria de agradecer também a todos os colegas do laboratório, presentes e os que já saíram, a sua contribuição, e em particular, aos amigos do Lab.407, pelo companheirismo e ajudas. Sem vós, Filipe, Rui Almeida, Susana, Rui Duarte, Carlos e Américo (membros honorários do 407) tudo teria sido muito mais difícil.

Ao Tiago Guerra e à Catarina Xavier agradeço ainda as suas contribuições no tema dos biofilmes e a compreensão pela minha falta de tempo.

Quero agradecer ainda ao CQFB/Dep. Química pelas condições de trabalho proporcionadas.

Agradeço à Fundação para a Ciência e Tecnologia (BOLSA SFRH / BD / 2917 / 2000) e ao Projecto EA-Biofilms (NEST-508866) pelos financiamentos que permitiram o desenvolvimento dos trabalhos.

Gostaria de agradecer, muito especialmente, à minha amiga Alda Fundo. Agradeço a sua amizade sincera, o seu apoio incondicional, em todas as horas e em todas as áreas da vida, científica e pessoal, sem o qual tenho a certeza de que não teria sido possível concluir mais esta etapa.

Agradeço ainda ao Henrique, não só pelo incentivo para a conclusão da tese, mas também por me ter ajudado a ter uma nova perspectiva do trabalho e da vida.

Aos meus pais agradeço tudo. O apoio incondicional, a paciência e o carinho. A sua compreensão pela minha “ausência” presente.

A todos, muito obrigada.

Abstract

Abstract

Bioelectrochemistry has been recognized as a very important technique to get relevant thermodynamic and kinetic information on diverse complex biological systems. From the determination of redox potentials of metallic centers in small electron carrier proteins to the resolution of more complex mechanisms in highly organised enzymes, and even whole bacteria systems, the application of dynamic electrochemical techniques has proved to be a powerful tool that has allowed to get deeper in the understanding of such systems.

In the present thesis electrochemical techniques were used to study diverse biochemical systems. Different approaches have been used, namely the classic bulk systems in which the reactive species are in solution and immobilised systems where proteins are physically constrained at the electrode surface. Within these, also alternative methods were used, as membrane electrodes and physical adsorption of the biological material.

Several systems of different complexity were object of study.

Simple Enzymes

Small non-hemic proteins, essentially related to electron transfer processes, with iron-sulfur centers, as desulforedoxin and other related iron-sulfur proteins, associated with oxidative stress protection, namely superoxide reductases, were investigated by cyclic and square wave voltammetry; its redox potentials and pH dependence were determined.

Complex Enzymes and Catalytic Systems

Nitrogen Cycle Enzymes

Enzymes taking part in the nitrogen cycle were studied, namely the periplasmic nitrate reductase isolated from *Desulfovibrio desulfuricans* ATCC 27774 and nitric oxide reductase purifed from *Pseudomonas nautica* 617. The first one, responsible

for the nitrate reduction to nitrite, is the only known monomeric nitrate reductase biding an iron-sulfur center and a molybdopterin co-factor. In this work it was possible, for the first time, to observe the individual metal centers voltammetric features. The electrocatalytic activity was also evaluated. The second enzyme, nitric oxide reductase, promotes the two electrons reduction of NO to N_2O. In this unique work it was possible to obtain data from a nitric oxide reductase resulting from direct electron transfer assays, accomplished by cyclic voltammetry. The demonstration of the catalytic activity towards the oxygen reduction was achieved and the reduction and catalysis of NO was also observed by direct electrochemistry. The pH dependence of the catalytic center redox process was evaluated and it was possible to show that the immobilized enzyme retained its native properties.

Production and Consumption of Hydrogen

Hydrogenase (Hase), isolated from *Desulfovibrio gigas (Dg)*, is a multicenter enzyme that catalyses the interconversion between H_2 and H^+, and that is involved in the dissimilatory sulphate reduction pathway. In this work, the direct electrochemistry of the *Dg* Hase, in bulk solution and also immobilised by adsorption, in turnover and non-turnover conditions was studied. For the first time the redox features of the enzyme metallic centers in non-catalytic conditions and without the addition of any of the known enzyme inhibitors were attained. Besides, it was possible to tune the activation and inactivation of the enzyme by dynamic potential control.

Approach to *in vivo* systems

Finally, the electrochemical behaviour of biofilms formed from pure cultures of sulphate reducing bacteria, namely *Desulfovibrio desulfuricans* ATCC 27774 was studied. The response of the biofilm on the electrodes was evaluated by the ratio of current obtained in the presence/absence of the biofilm and its stability in time. For the first time it was possible to observe that pure culture biofilms of sulphate reducing bacteria are electroactive.

SYMBOLS AND ABBREVIATIONS

Symbols

ν	scan rate
A_{geom}	geometric area
c	concentration
n	number of electrons
E	potential
E_{app}	applied potential
E_p	peak potential
E_{pa}	anodic peak potential
E_{pc}	cathodic peak potential
$E^{o'}$	formal redox potential
ΔE	potential difference
f	frequency
F	Faraday constant
g	Electronic *g* factor
i	current density
i_{cat}	catalytic current density
i_{max}	catalytic current at the maximum turnover rate
I	current
I_b	backwards current
I_f	forward current
I_p	maximum peak current
I_{pa}	maximum anodic peak current
I_{pc}	maximum cathodic peak current
k_s	rate constant
k_{sh}	heterogeneous rate constant
K_M	Michaelis constant
l	thickness
R	ideal gas constant
T	temperature
U	specific activity

V	volume
$W_{1/2}$	peak width
ν	scan rate

Abreviations

CA	chronoamperometry
CE	counter electrode
CV	cyclic voltammetry
Cys	cysteine
Cyt. oxidase	Cytochrome oxidase
Cyt. *c_3*	Cytochrome *c_3*
DFT	density functional theory
D. desulfuricans	*Desulfovibrio desulfuricans*
Dfx	desulfoferredoxin
Dg	*Desulfovibrio gigas*
D. gigas	*Desulfovibrio gigas*
D. desulfuricans	*Desulfovibrio desulfuricans*
DMSO	dimethylsulfoxide
DSA	dimensionally stable anode
D. vulgaris	*Desulfovibrio vulgaris*
Dx	desulforedoxin
E. coli	*Escherichia coli*
ENDOR	electron-nuclear double resonance
EPR	electronic paramagnetic resonance
EPS	exopolysacharides
EXAFS	extended X-ray absorption fine structure
GC	glassy carbon
Hase	hydrogenase
His	histidine
Glu	glutamate
MGD	bis-molybdopterin guanine dinucleotide
NAP	periplasmic nitrate reductase
NAR	respiratory nitrate reductase
NHE	normal hydrogen electrode

Nlr	neelaredoxin
O.D.	optical density
NOR	nitric oxide reductase
PDB	protein data bank
PG	pyrolytic graphite
P. aeruginosa	*Pseudomonas aeruginosa*
P. denitrificans	*Paracoccus denitrificans*
P. pantotrophus	*Paracoccus pantotrophus*
Re	*Ralstonia eutropha*
SCE	saturated calomel electrode
SEM	scanning electron microscopy
SOR	superoxide reductase
SRB	sulphate reducing bacteria
SS	stainless steel
SWV	square wave voltammetry
T. pallidum	*Treponema pallidum*
Tp	*Treponema pallidum*
Tris-HCl	Tris(hydroxymethyl)methylamine hydrochloride
UV	ultraviolet
WE	working electrode

GENERAL INDEX

FIGURES INDEX

CHAPTER I

CHAPTER II

CHAPTER V

TABLES INDEX

Chapter I

Bioelectrochemistry: a tool for the study of biological systems

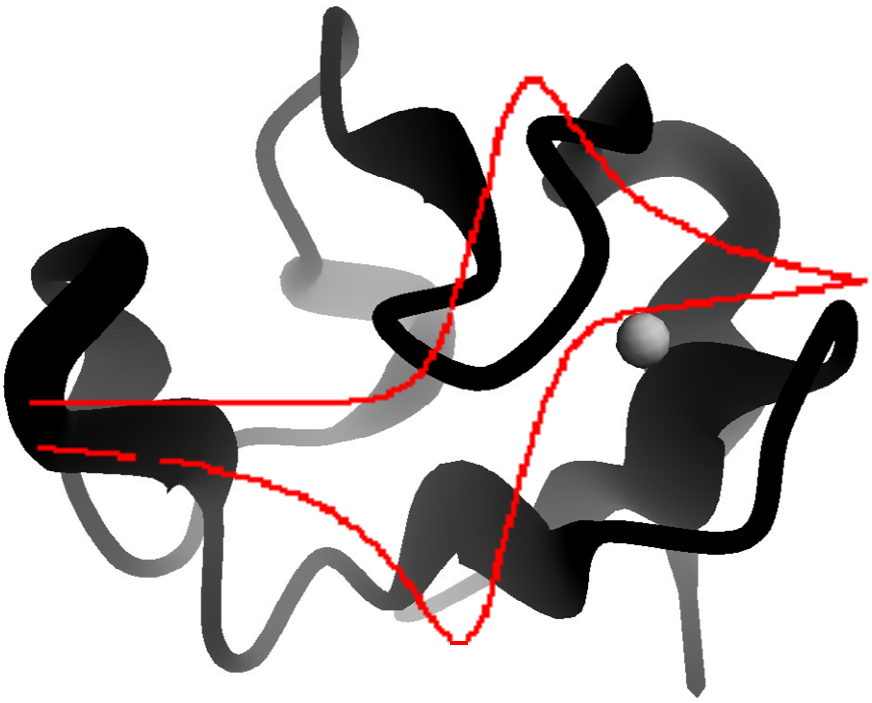

Bioelectrochemistry: a tool for the study of biological systems

I.1 Electrochemistry in biological systems

The application of electrochemical methods to the study of biological systems has started in the late XVIII century with the work of Luigi Galvani in which he observed the frog's legs contraction as the result of an applied electrical current[1]. Since then bioelectrochemistry has developed and spread into different areas, that can be designated as faradaic bioelectrochemistry, membrane potentials and currents resulting from the ionic transport through membranes[2].

Dynamic electrochemical techniques, such as cyclic voltammetry or square wave voltammetry, are currently used to determine formal reduction potentials in systems with small, low molecular weight proteins, such as cytochromes and ferredoxins, that, in general, present well defined and reversible electrochemical behaviour[3-5].

More recently, the acquisition of thermodynamic and kinetic information on the redox reactions of proteins/enzymes, through the use of dynamic electrochemistry was extended to larger proteins of considerable molecular weight and multiple redox centres[6, 7].

It can be considered that an efficient electronic transfer occurs when the electrode substitutes the physiological redox partner of the proteins and the analysis of the obtained response allows the understanding of the its structure and function[8]. This can be observe in different systems, such as the hydrogenase direct response, where it was possible to observe the redox centres and the electrocatalytic activity of the enzyme (see Chapter V), as schematized in figure I.1.

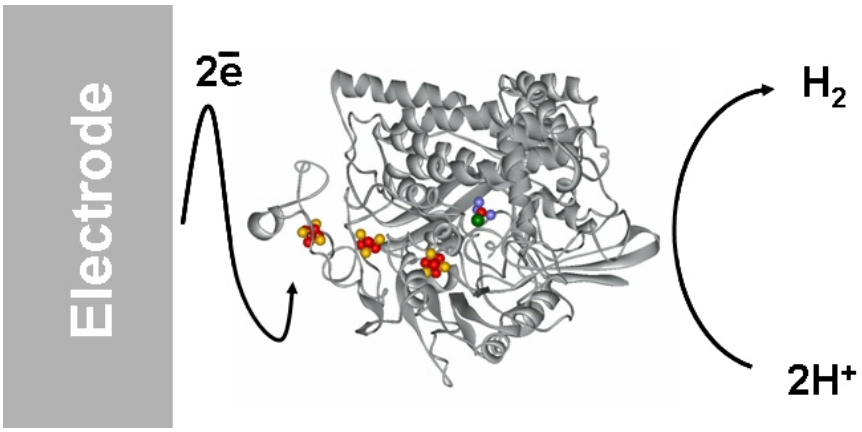

Figure I.1 Schematic representation of the hydrogenase enzyme interaction with the electrode.

I.2 Immobilisation of proteins on electrode surfaces

Several methods have been used to achieve the electronic transfer from and through the proteins and the electrode, from a classical bulk electrochemical approach, in which the biomolecules are in solution, with or without the use of chemical mediators, to other innovative methods such as immobilisation of the biological material, in different matrixes or using membrane electrodes, or even by physical or chemical adsorption of proteins on electrode surfaces[9-11]. Some of these new approaches of immobilisation are schematized on figure I.2.

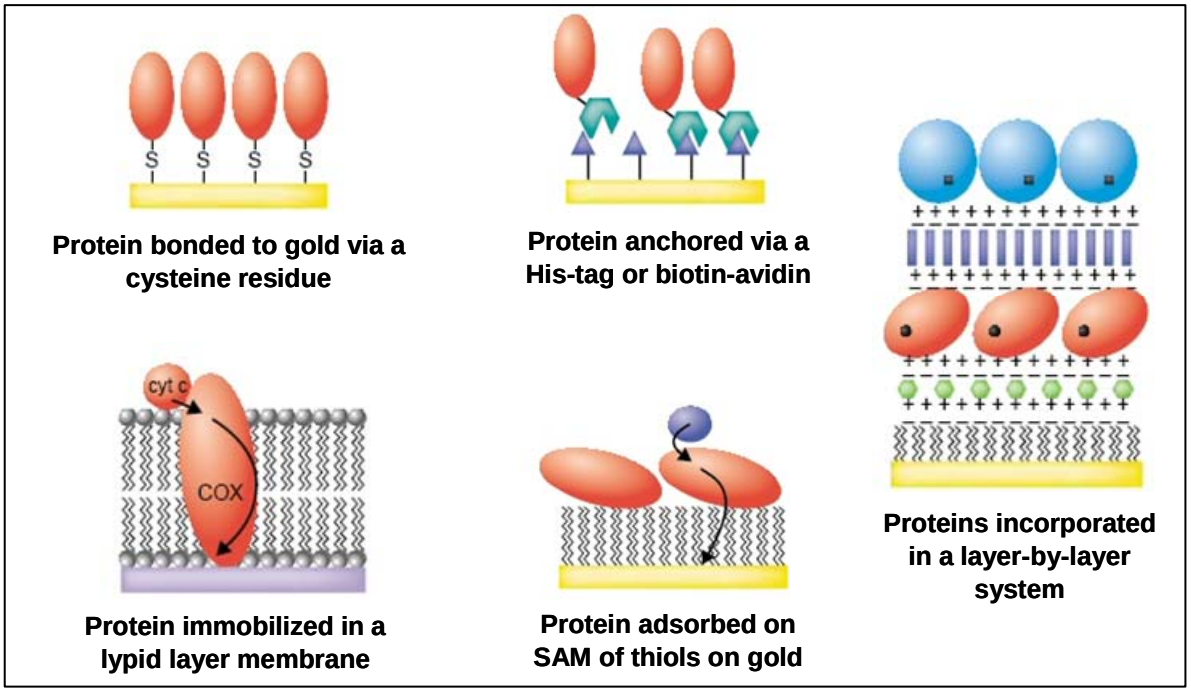

Figure I.2 Schematic representation of some methods for the immobilisation of proteins on electrodes (adapted from Gilardi *et al*, 2001)[8].

The immobilisation of proteins on surfaces has demonstrated to be an efficient method to achieve electron transfer between the proteins and the electrodes with high transfer rates. Amongst the possible methods, physical immobilisation by adsorption or by entrapment on cellulose membranes has been extensively used by the inherent advantages such as the easy of preparation, low cost and simplification of the theoretical analysis (no diffusional systems)[6, 9, 11]. A schematic representation of these two methods is displayed on figure I.3.

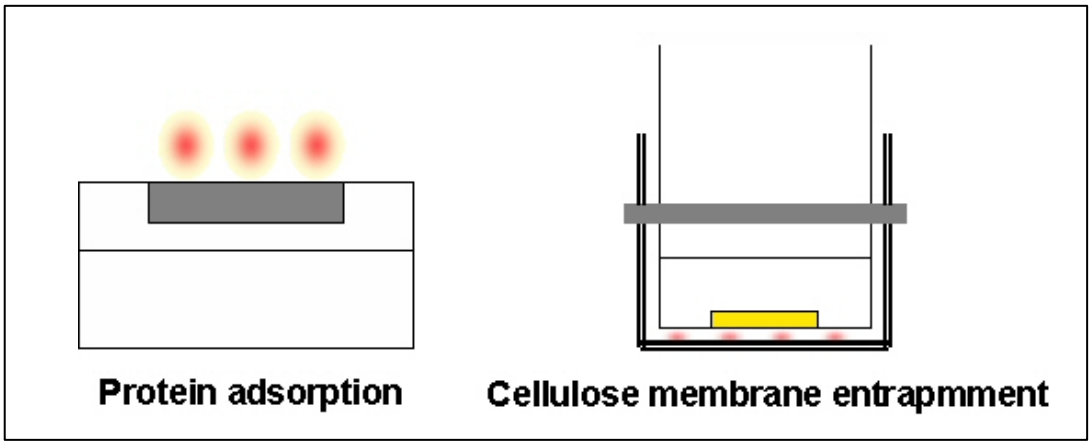

Figure I.3 Schematic representation of the adsorption and the physical immobilisation by the use of cellulose membranes.

These approaches, however, strongly depend of the protein surface interaction with the electrode, where the superficial charges of the protein play a key role[6]. A solution to overtake the electrostatic barrier, that commonly occurs, is the use of several promoters that can facilitate the interaction of proteins with electrode surfaces. For this purpose the addition of molecules with thiol or amino groups, such as bis(4-pyridyl) disulphite, polylysine, and neomycine are amongst the most currently used[12, 13]. An example of the key role of the protein surface charge was observed in the current work with the periplasmic nitrate reductase (see Chapter III). In fact, this enzyme presents quite different electrochemical behaviour on gold and graphite electrodes that was attributed to its orientation towards the two materials. A schematic representation illustrating this orientation is presented on figure I.4.

The immobilisation on surfaces has open new insights to the new applications, such as nanodevices, biofuel cells and biosensors[8, 14, 15].

The direct, not mediated, electrochemistry of proteins can provide information on the mechanisms of complex enzymes, its kinetics, energetics and catalysis. In particular with the protein immobilized on the surface electrode the problem of the protein diffusion, usually slow and rate determining is overcome[16]. The electrochemical of physical adsorbed proteins, at close monolayer level, has been extensively studied recently using the so-called *protein film voltammetry*[2]. The proteins immobilised, using this later or other immobilisation techniques, should retain its structure and function, which is simple to prove in the case of enzymes, where its catalytic properties, as for instance its K_M, can be compared with classic assays in solution.

The protein environment can, however, change some of its properties. Several reports can be found in the literature for formal potential shifts due to the adsorption[16].

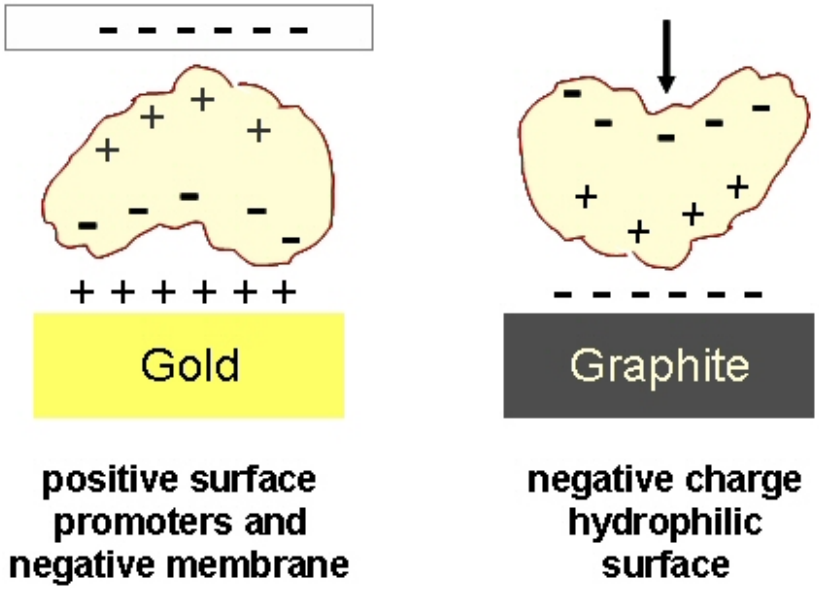

Figure I.4 Schematic representation of the orientation of the nitrate reductase enzyme on gold and graphite electrodes.

As already mentioned, the surface material used for the adsorption is determinant for the success of the direct electrochemical response. One of the most used electrodes is carbon, in particular graphite, since proteins in general seem to present better affinity with this material. This may be due not only to the known carbon surface functionalities (C-O groups) but also because these electrodes frequently have grain boundaries that result in surface defects that can act as catalytic sites[17, 18].

I.3 Bioelectrocatalysis

Electron-transfer enzymes have been extensively studied by electrochemical methods, either in mediated and no-mediated bioelectrocatalytic systems. In figure I.5 a scheme of the direct and the mediated electrocatalysis is presented.

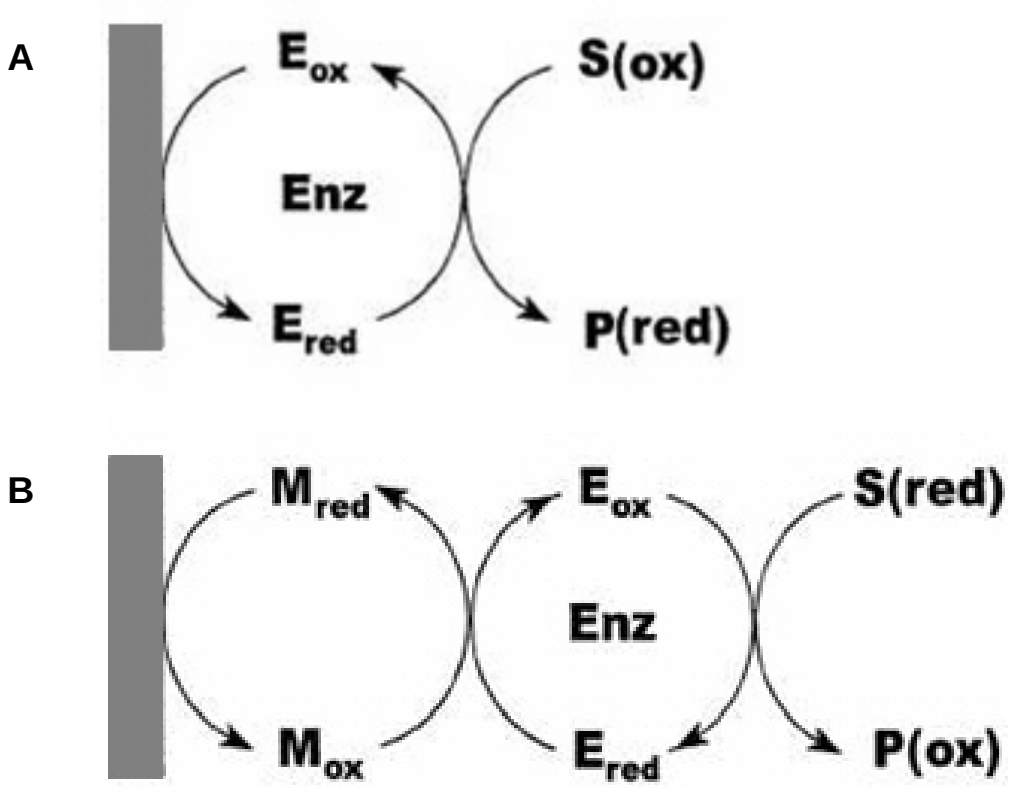

Figure I.5 Schematic representation of the A) direct electrocatalysis and B) mediated electrocatalysis; E_{ox}, E_{red}, $S_{(ox)}$ and $P_{(red)}$ stands, respectively, for the enzyme and substrate oxidised and reduced states and M_{red} and M_{oxid} represent the reduced and the oxidised mediator (adapted from Kano *et al*)[19].

The direct electron transfer in enzymatic systems, without the use of mediators, presents advantages in terms of the superior selectivity achieved, less interfering side reactions and higher transfer rates[20].

The potential imposition implies a response produced by the redox transitions of the metallic centres that, if the enzyme is active and the experimental conditions are favourable, including orientation constrains, in the presence of the substrate originates a catalytic current. The electrode substitutes the physiological partner as transfers electrons to regenerate the enzyme redox active site[16]. A schematic representation of the obtained catalytic current is displayed on figure I.6.

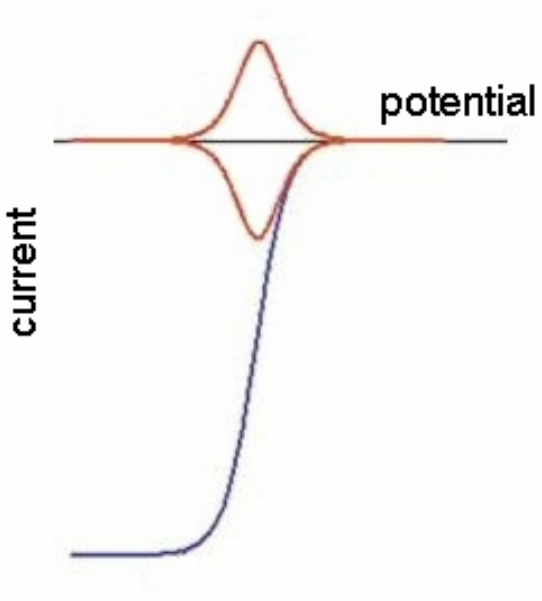

Figure I.6 Representation of the catalytic current obtained from direct electrocatalysis under a convective regime obtained with the enzyme immobilised and the use of the rotating disk electrode (adapted from Armstrong, 2005)[21].

The current response is a direct measurement of the turnover rate of the enzyme and depends on the mass transport of the enzyme, substrate and often of the reaction product, the enzyme kinetics and the electron transfer rates with the electrode surface[22]. The immobilisation of the enzymes presents the advantage of overcome the dependence of a diffusional mass transport regime. The establishment of a convective mass transport regime, by rotating electrodes, is often used to enhance the substrate and product transport overcoming the problems of the substrate depletion, in particular for enzymes with high turnover rates, and product inhibition[16].

Direct or mediated bioelectrocatalysis are both important approaches to obtain enzymatic parameters, since in general, the Michaelis-Menten model can be applied, changing the usual parameters, v and V_{max} by the electrochemical variables, I and I_{max}. So, considering the generic equation,

$$\mathbf{E + S} \underset{k_{-1}}{\overset{k_1}{\rightleftharpoons}} \mathbf{ES} \xrightarrow{k_{cat}} \mathbf{E + P}$$

Fast *Slow*

An electrochemical variation of the Michaelis-Menten equation can be defined as follows:

$$I = \frac{I_{\max}[S]}{K'_m + [S]}$$

in which, I is the current response and I_{max}, depends of the transferred number of electrons, surface area, turnover number and enzyme concentration[19].

Other factors can influence the electrocatalysis of enzymes, such as inter- and intramolecular rate constants. One interesting example of mediated bioelectrocatalysis in which the enzymatic control is essentially on the intramolecular electron transfer, can be found for the cytochrome *cd1* nitrite reductase. In fact, it has been demonstrated that the enzyme activity and, even the formation of a dead-end product, depends strongly of the experimental conditions that influence the intramolecular electronic exchange[23].

I.4 References

1. Shukla, A. K., Suresh, P., Berchmans, S., Ranjendran, A., Biological fuel cells and their applications. *Current Science* **2004**, 87, (4), 455-468.

2. Armstrong, F. A., Wilson, G. S., Recent developments in faradaic bioelectrochemistry. *Electrochim Acta* **2000**, 45, (15-16), 2623-2645.

3. Eddowes, M. J.; Hill, H. A. O., Electrochemistry of Horse Heart Cytochrome-C. *JACS* **1979**, 101, (16), 4461-4464.

4. Tilley, G. J.; Camba, R.; Burgess, B. K.; Armstrong, F. A., Influence of electrochemical properties in determining the sensitivity of [4Fe-4S] clusters in proteins to oxidative damage. *Biochem J* **2001**, 360, (Pt 3), 717-26.

5. Moreno, C.; Macedo, A. L.; Moura, I.; LeGall, J.; Moura, J. J., Redox properties of Desulfovibrio gigas [Fe3S4] and [Fe4S4] ferredoxins and heterometal cubane-type clusters formed within the [Fe3S4] core. Square wave voltammetric studies. *J Inorg Biochem* **1994**, 53, (3), 219-34.

6. Margarida M. Correia dos Santos, P. M. P. S., M. Lurdes S. Gonçalves, M. João Romão, Isabel Moura, José J. G. Moura, Direct electrochemistry of the *Desulfovibrio gigas* aldehyde oxidoreductase. *Eur J Biochem* **2004**, 271, (7), 1329-1338.

7. Anderson, L. J.; Richardson, D. J.; Butt, J. N., Using direct electrochemistry to probe rate limiting events during nitrate reductase turnover. *Faraday Discuss* **2000**, (116), 155-69; discussion 171-90.

8. Gilardi, G.; Fantuzzi, A.; Sadeghi, S. J., Engineering and design in the bioelectrochemistry of metalloproteins. *Curr Opin Struct Biol* **2001**, 11, (4), 491-9.

9. É. Lojou, P. B., Membrane electrodes can modulate the electrochemical response of redox proteins — direct electrochemistry of cytochrome c. *J Electroanal Chem* **2000**, 485, (1), 71-80.

10. Hu, N., Direct electrochemistry of redox proteins or enzymes at various film electrodes and their possible applications in monitoring some pollutants. *Pure Appl Chem* **2001**, 73, (12), 1979-1991.

11. Heering, H. A.; Wiertz, F. G.; Dekker, C.; de Vries, S., Direct immobilisation of native yeast iso-1 cytochrome C on bare gold: fast electron relay to redox enzymes and zeptomole protein-film voltammetry. *JACS* **2004**, 126, (35), 11103-12.

12. Allen, P. M.; Hill, H. A. O.; Walton, N. J., Surface Modifiers for the Promotion of Direct Electrochemistry of Cytochrome-C. *J Electroanal Chem* **1984**, 178, (1), 69-86.

13. Taniguchi, I.; Funatsu, T.; Umekita, K.; Yamaguchi, H.; Yasukouchi, K., Effect of Poly-L-Lysine Addition on the Redox Behavior of Horse Heart Cytochrome-C at Functional Electrodes. *J Electroanal Chem* **1986**, 199, (2), 455-460.

14. Murphy, L., Biosensors and bioelectrochemistry. *Curr Opin Chem Biol* **2006**, 10, (2), 177-84.

15. Zhang, W., Li, Genxi, Third-Generation Biosensors Based on the Direct Electron Transfer of Proteins. *Anal Sci* **2004**, 20, 603-609.

16. Hirst, J., Elucidating the mechanisms of coupled electron transfer and catalytic reactions by protein film voltammetry. *Biochim Biophys Acta* **2006**, 1757, (4), 225-39.

17. Banks, C. E.; Davies, T. J.; Wildgoose, G. G.; Compton, R. G., Electrocatalysis at graphite and carbon nanotube modified electrodes: edge-plane sites and tube ends are the reactive sites. *Chem Commun (Camb)* **2005**, (7), 829-41.

18. Shumyantseva, V. V.; Bulko, T. V.; Archakov, A. I., Electrochemical reduction of cytochrome P450 as an approach to the construction of biosensors and bioreactors. *J Inorg Biochem* **2005**, 99, (5), 1051-63.

19. Kano, K., Ikeda, T., Fundamentals and Practices of Mediated Bioelectrocatalysis. *Anal Sci* **2000**, 16, 1013-1021.

20. Gorton, L., Lindgren, A., Larsson, T., Munteanu, F. D., Ruzgas, T., Gazaryan, I., Direct electron transfer between heme-cointainning enzymes and electrodes as basis for third generation biosensors. *Anal Chim Acta* **1999**, 400, 91-108.

21. Armstrong, F. A., Recent developments in dynamic electrochemical studies of adsorbed enzymes and their active sites. *Curr Opin Chem Biol* **2005**, 9, (2), 110-7.

22. Heering, A. H., Hirst, J., Armstrong, F. A., Interpreting the Catalytic Voltammetry of Electroactive Enzymes Adsorbed on Electrodes. *J Phys Chem B* **1998**, 102, 6889-6902.

23. Lopes, H., Besson, S., Moura, I., Moura, J. J. G., Kinetics of inter- and intramolecular electron transfer of Pseudomonas nautica cytochrome cd1 nitrite reductase: regulation of the NO-bound end product. *J Biol Inorg Chem* **2001,** 6, 55-62.

Chapter II

Direct electrochemistry of SOR proteins

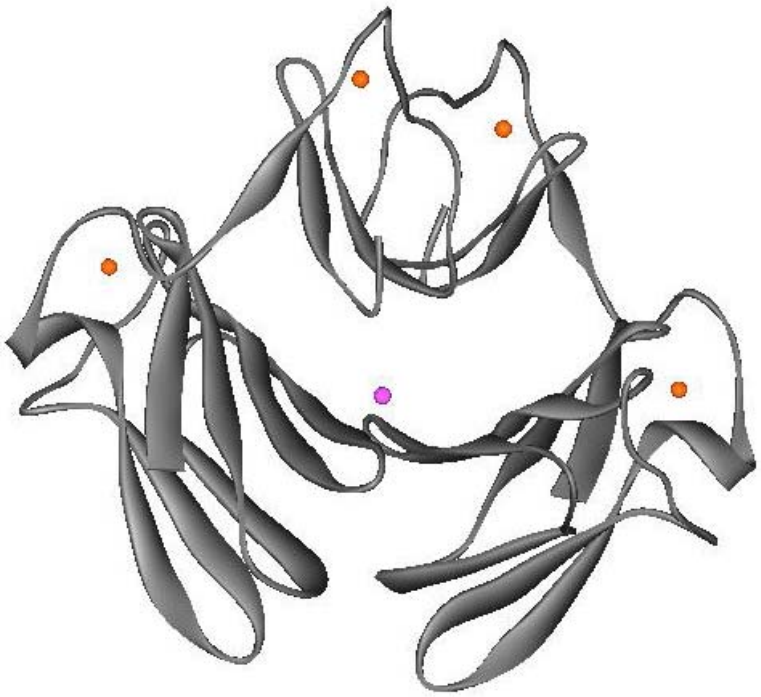

Direct electrochemistry of SOR proteins

II.1 Superoxide reductase enzymes and related proteins

Oxygen species, namely hydrogen peroxide and radicals derived from the O_2 reduction can be toxic to organisms, either aerobic or anaerobic. These molecules can be responsible for oxidative stress within an organism leading to numerous disorders, such as neurological, inflammation or cancer amongst others. One of the potential armful species is the superoxide radical O_2^-. Living organisms have developed mechanisms to avoid the toxic effects caused by these kind of molecules. One of the system uses superoxide dismutase enzyme (SOD), which is present in almost all aerobic and also in some anaerobic organisms and catalyse a dismutation reaction

$$O_2^- + O_2^- + 2H^+ \leftrightarrow H_2O_2 + O_2 \qquad (1)$$

SODs are non-hemic metalloenzymes that can differ from each other by the metal present in its redox centre. So far SOD enzymes with manganese, iron, nickel or copper-zinc present in the metallic centre have been described[1, 2]. Another defence mechanism was described more recently, occurring through the one-electron reduction of O_2^- to H_2O_2, according to the reaction

$$O_2^- + \bar{e} + 2H^+ \leftrightarrow H_2O_2 \qquad (2)$$

This later reaction is catalysed by a new class of enzymes named superoxide reductases (SORs). The first enzymes were isolated from the sulphate reducing bacteria, namely *Desulfovibrio desulfuricans* ATCC27774 and *Desulfovibrio vulgaris* Hildenborough, during the 90's[3, 4]. Without the knowledge of the enzyme function, the protein was called Desulfoferrodoxin (Dfx).

Another member of this family, isolated from *Desulfovibrio gigas*, was also reported and assigned as Neelaredoxin (Nlr)[5].

Desulfoferrodoxin (Dfx) is a homodimeric protein with two domains harbouring two mononuclear iron centres. The monomer molecular mass was determined to be 14 kDa[6]. The protein centre I is a Dx-like centre that presents the iron coordinated to four cysteines in a tetrahedral arrangement, $Fe(S\text{-}Cys)_4$ and is very similar to the iron centre of desulforedoxin (Dx)[7]. Dx is a small homodimer (about 8 kDa) with high homology with the Dfx domain I[8]. The 3D structures of Dfx and Dx proteins are displayed in figure II.1. The iron coordination, in both proteins, is assured by

cysteines 9, 12, 28 and 29[7, 8]. The Dfx and Dx metallic centres are represented in figure II.2.

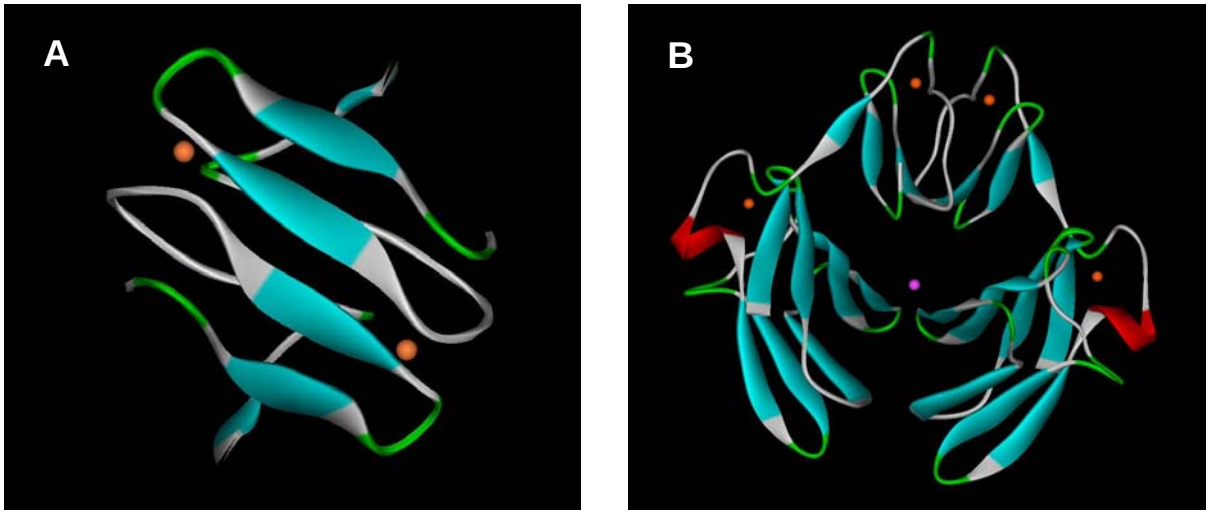

Figure II.1 Crystallographic structure of A) Dx at 1.80 Å resolution (PDB ID 1DXG)[8] isolated from *D. gigas* and B) Dfx isolated from *D. desulfuricans* ATCC 27774 at 1.90 Å resolution[7] (PDB ID 1DFX); the iron atoms are displayed at dark orange. A calcium atom in Dfx is displayed in pink.

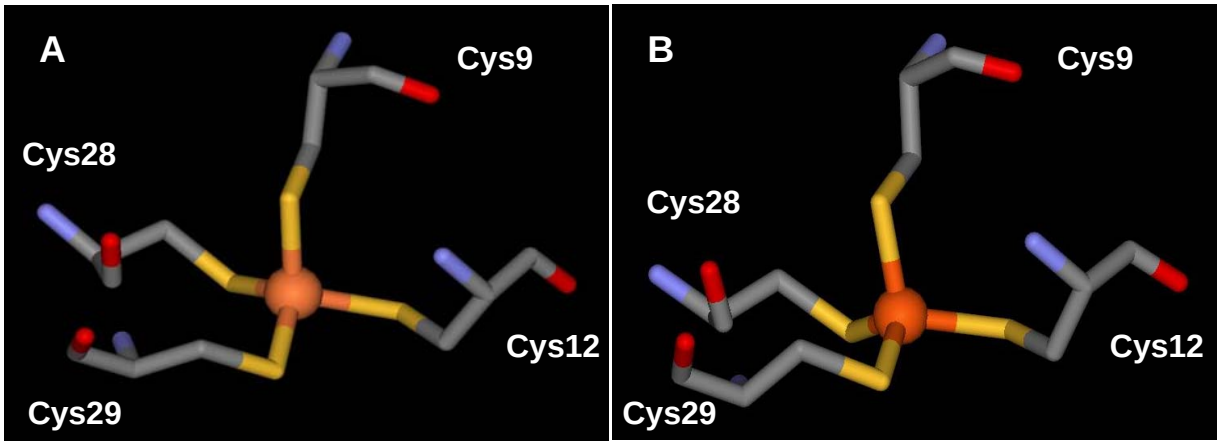

Figure II.2 Structure of A) Dx metallic centre isolated from *D. gigas* and B) centre I of Dfx isolated from *D. desulfuricans* ATCC 27774 (similar to the Dx centre), showing a distorted tetrahedral coordination of the iron atom (orange sphere) to the four sulphur from the cysteines residues.

The Dfx centre II, Fe(S-Cys)(N-His)$_4$, presents square pyramidal geometry with four equatorial histidines (His48, His68, His74 and His118) and an axial cysteine (Cys115). This centre is similar to the metallic centre of neelaredoxin (Nlr) which is a protein, with 15 kDa. Nlr is homologous to the Dfx domain II that, as mentioned before, presents SOR activity (the structure of Nlr of *T. pallidum* is presented in figure II.3).

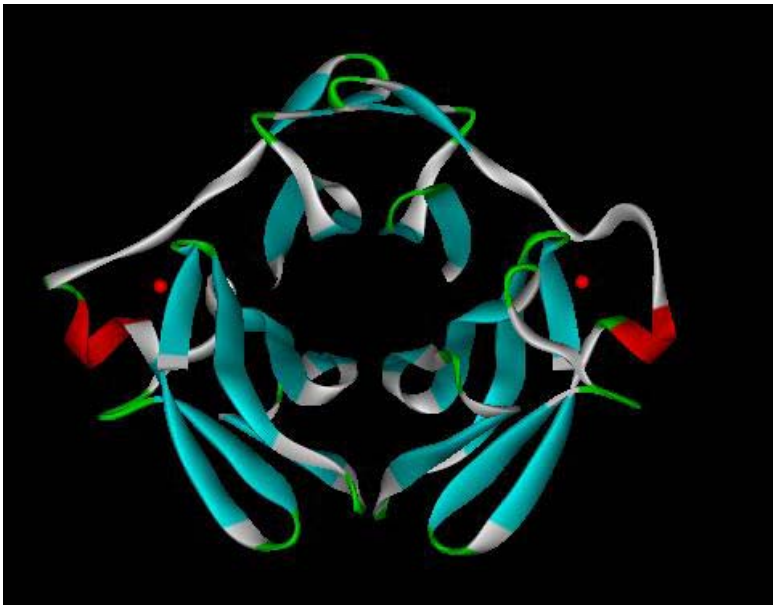

Figure II.3 Crystallographic structure of Nlr isolated from *T. pallidum* at 1.90 Å resolution (PDB ID 1Y07). The protein is a crystallographic homodimer[9].

In *Tp*Nlr the iron is also coordinated by four equatorial histidines, namely, His16, His41, His47 and His114, and an axial cysteine, Cys111, in the reduced state. However, in the oxidised state this centre can present an extra axial ligand, Glu14. The presence of this sixth ligand is variable between the subunits and also, as mentioned, dependent of the oxidation state of the protein. This suggests that the structural difference is probably related to the catalytic activity of this SOR enzyme, and may regulate the access of the superoxide anion to the centre[1, 10]. The Dfx centre II, similar to the Nlr centre, is represented in figure II.4.

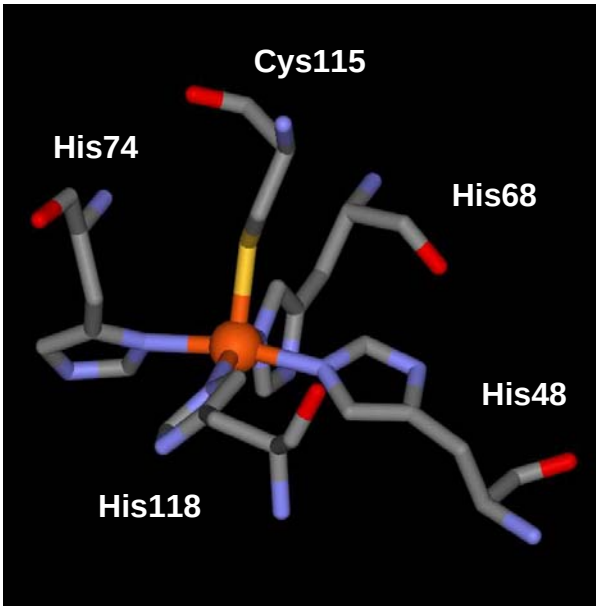

Figure II.4 Structure of centre II of Dfx isolated from *D. desulfuricans* ATCC 27774 (similar to the Nlr centre) showing a square pyramidal coordination of the iron atom (orange sphere) to the four nitrogen from the histidines residues and one sulphur from a cysteine ligand.

The SOR proteins are classified in three classes, namely I, II and III. Members of class I contain two domains with two types of iron centres, a $Fe(S\text{-}Cys)_4$ (a Dx-like type centre, corresponding to centre I in Dfx) and a $Fe(S\text{-}Cys)(N\text{-}His)_4$ (a Nlr-like type centre corresponding to centre II in Dfx). Class II proteins contain only one domain with the $Fe(S\text{-}Cys)(N\text{-}His)_4$ centre. Class III also holds only one metallic centre as class II proteins, but presents another domain, similar to the Dx, without the metal[1]. A schematic representation showing the three SOR classes is displayed in figure II.5.

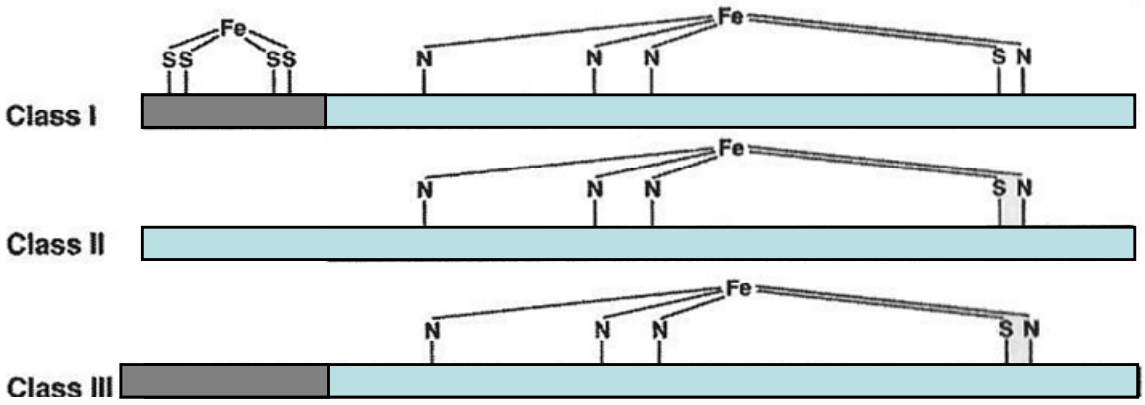

Figure II.5 Schematic representation of the three classes of SORs showing the different domain structure (adapted from Rusnak *et al*, 2002).

As mentioned before the three proteins present high homology on its amino acid sequence. The sequences alignment is presented in figure II.6.

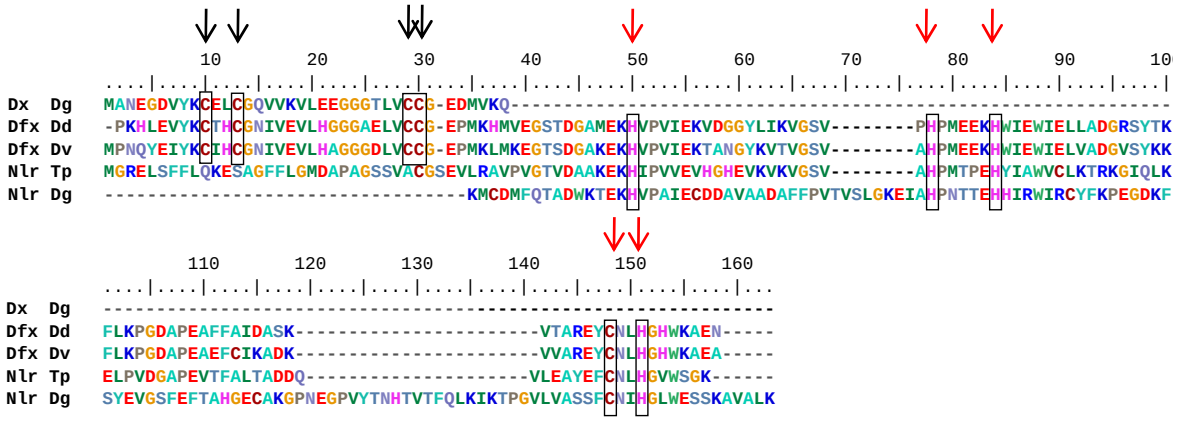

Figure II.6 Amino acid sequence allignement of the five proteins, attained with the clustal W software (available online at http://www.ebi.ac.uk/clustalw/) from the sequences on NCBI protein data base), Dx isolated from *D.gigas*, Dfx isolated from *D. desulfuricans* and *D. vulgaris* and Nlr isolated from *D. gigas* and *T. pallidum*; underline are the conserved cysteines and histidines; black arrows: Centre I, red arrows: Centre II.

Desulfoferrodoxin is isolated in two interconvertible oxidation forms, a grey, oxidised and a pink, semi-reduced form (figure II.7). The centres have significantly apart redox potential values, approximately +0 and +240 mV, respectively, for I and II, determined by potentiometric titrations[1, 4], allowing three stable oxidation states.

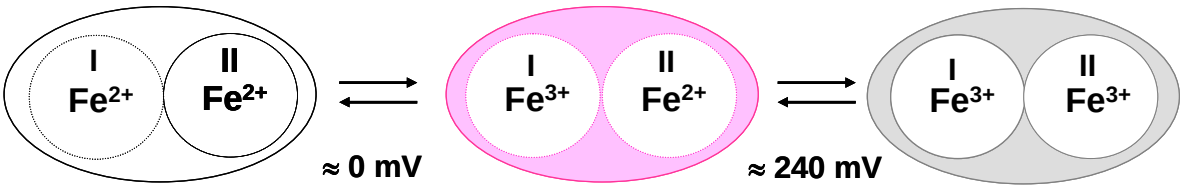

Figure II.7 Schematic representation of the redox transitions of the Dfx metallic centres. The protein displays different colours in the three different redox states[1], namely colourless, pink and grey; notation I and II represents the centre I and II.

Dfx was found in *Desulfovibrio desulfuricans* and *Desulfovibrio vulgaris* but not in *Desulfovibrio gigas* while Dx and Nlr were found in the later but not in the former two. This fact, besides its sequence and structures analogy, points to some correlation between these proteins and may correspond to two different ways to achieve the same function in each organism.

II.2 Direct electrochemistry of SOR and related proteins

Some electrochemical studies of the SOR proteins are reported in the literature. The voltammetric response of Dfx isolated from *D. vulgaris* was first accomplished by Hagen and co-workers, in 1993, with the protein in bulk and in the presence of soluble promoters (neomycin). The authors were able to observe a redox pair attributed to the centre I, but was not possible to detect centre II. The centre I midpoint potential was estimated as -4 mV vs. NHE and it was shown to be pH dependent[6]. A different approach was followed by Moura and co-workers, in 2000. In this work the electrochemical study was performed using two recombinant proteins from *D. vulgaris*, DfxC and DfxN, where the C and the N terminal domains were

expressed separately resulting in two fragments, each with one of the metal centres (DfxC presenting centre II and DfxN centre I). Square wave voltammetry yielded the redox potentials of the centres of the isolated domains, namely -2 and +247 mV vs. NHE for DfxN and DfxC respectively[11]. A more recent study, from Nivière and co-workers, 2002, have coupled FTIR spectroscopy to electrochemistry using a thin layer cell to promote the reduction/oxidation of the proteins centres[12]. By the resultant redox titration a redox potential of +290 mV vs. NHE was attributed to the Nlr from *T. pallidum*[12]. No other electrochemical studies on these proteins are reported on the literature.

A summary of the three proteins main characteristics and redox reactions is presented in table II.I.

Table II.I Published redox potential values for Dx, Dfx and Nlr.

Redox Centre	**Redox Potential / mV vs. NHE**	**Methodology[a]**	**Protein**	**Strain**	**Refs**
$[Fe(S\text{-}Cys)_4]$	-4	Cyclic voltammetry	Dfx	*D. vulgaris*	6
	-35	EPR redox titration	Dx	*D. gigas*	1, 13
	+4	UV-Visible redox titration	Dfx	*D. desulfuricans*	4
$[Fe(S\text{-}Cys)(N\text{-}His)_4]$	+240	UV-Visible redox titration	Dfx	*D. desulfuricans*	4
	+90	EPR redox titration	Dfx	*D. vulgaris*	6
	+190	Visible redox titration	Nlr	*D. gigas*	5
	+290	UV-Visible redox titration	Nlr	*T. pallidum*	12

[a] methodology for the redox potential determination

The direct electrochemistry of redox proteins is at the moment an important and attractive subject because it provides a tool to study the mechanisms of electron exchange in relevant biological systems[14, 15]. Different approaches to achieve a redox unmediated response have been tried, for instance, the use of modified electrodes

with specific films that can incorporate or interact with the target proteins, like polycations[16], surfactants[17, 18], polymers[15, 19] and several self-assembled monolayers [20, 21], among others. Also the electrode modification with protein films led to a technique called Protein Film Voltammetry with good results[22, 23]. The physical immobilisation of proteins on the electrode surface by the use of membranes is another possible procedure that has been used with success in the past years.

Physical immobilisation with a membrane electrode was the approach followed in this work because it presents significant advantages[24, 25], relatively to the modified electrodes and the “classic” solution electrochemistry. The advantages are the use of small volumes of protein, the easy preparation, the low cost of the electrodes and the approximation to the thin layer theory[26, 27]. However, some irreproducibility due to the electrodes preparation has been found during our experiments, which means that this step should be carefully performed. The details on the immobilisation procedure are presented in the experimental section (see Appendix A).

Some surface modifiers were used, namely neomycin sulphate for glassy carbon (GC) and 4,4’-dithiodipyridine for gold electrodes, aiming to the improvement of the interaction between the proteins and the electrode surfaces, as it has been currently reported by several authors[21, 25, 27, 28]. These promoters do not participate in the electron transfer but rather contribute to improve the interaction of the biological molecules and the electrode surfaces through the promotion of electrostatic interactions and hydrogen bonds.

In these assays the influence of divalent cations, namely magnesium, in the electrolyte solution was tested resulting in an improvement of the redox signal. The carbon surface (due to the carboxylic, phenolic and quinonoidal groups)[29] and the dialysis membrane (cellulose), at the experimental conditions, as well as the enzyme surfaces are negatively charged. It is documented on the literature that the inclusion of the Mg(II) should assure charge compensation and a better interaction between the electrode and the proteins[30].

The direct electrochemical responses of the Dx from *Desulfovibrio gigas*, Dfx from *Desulfovibrio vulgaris* and Nlr from *Desulfovibrio gigas* and *Treponema pallidum* were studied by cyclic and square wave voltammetry and their properties were evaluated. The comparison between the features of the three proteins should help to elucidate the role of the two iron centres in the Dfx activity.

II.2.1 Direct Electrochemistry of Desulforedoxin from *D. gigas*

The electrochemical responses of Dx, using 10 mM Tris-HCl buffer / 0.1 M KNO_3 / 2 mM neomycin sulphate, pH 7.6, as supporting electrolyte, on GC and gold electrodes, at different scan rates, are shown on Figure II.8. The cyclic voltammograms present two well defined current peaks corresponding to one electron process. These peaks are due to the redox process $[Fe(S\text{-}Cys)_4^{3+}]/[Fe(S\text{-}Cys)_4^{2+}]$ that occurs at the metallic centre of the protein. The process can be classified as quasi-reversible by the established criteria.

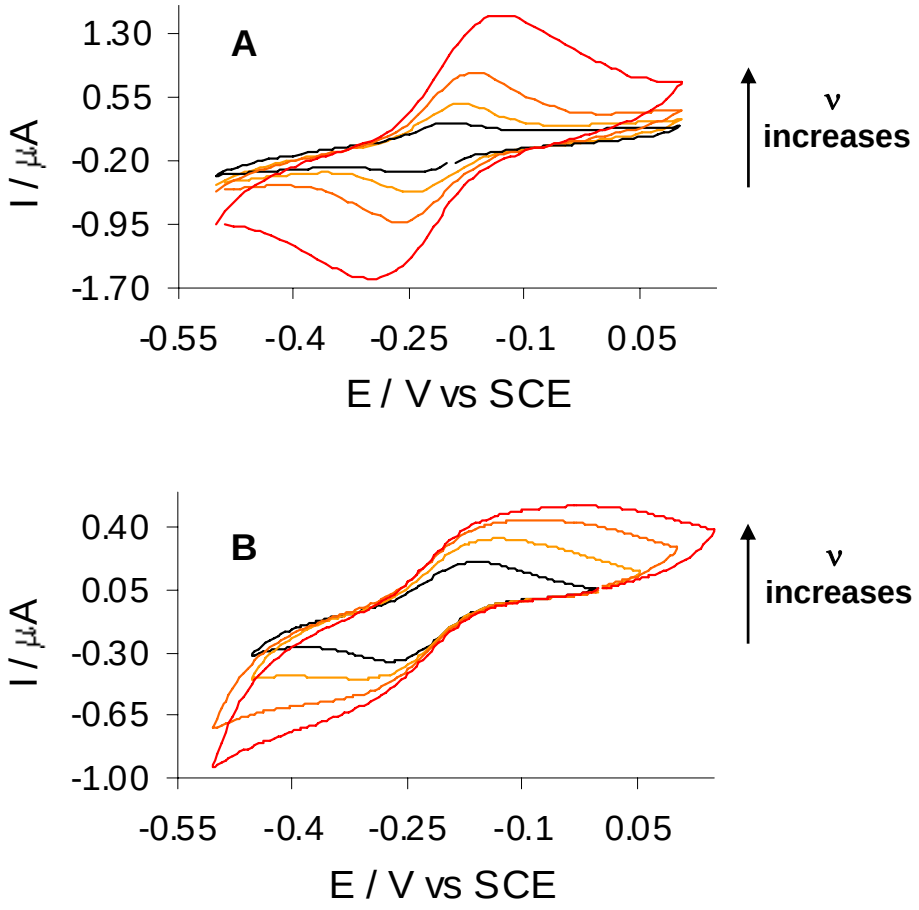

Figure II.8 A) Dx cyclic voltammograms at different scan rates (1, 2.5, 5 and 8 mV s^{-1}) on GC (A) and gold electrodes (B).

Although the position of the current peaks is similar in both electrode materials, the voltammetric features are different, showing broader peaks on gold with the scan rate increase. The broadness and the shape of the anodic peak observed on gold (Figure II.8B) may be due to a different oxidation process or, more probably in our case, to a possible interaction between the molecules at the electrode surface, which is a phenomenon well described to surface confined species[31].

The current intensity varies linearly with the scan rate up to 20 mV s^{-1} (figure II.9).

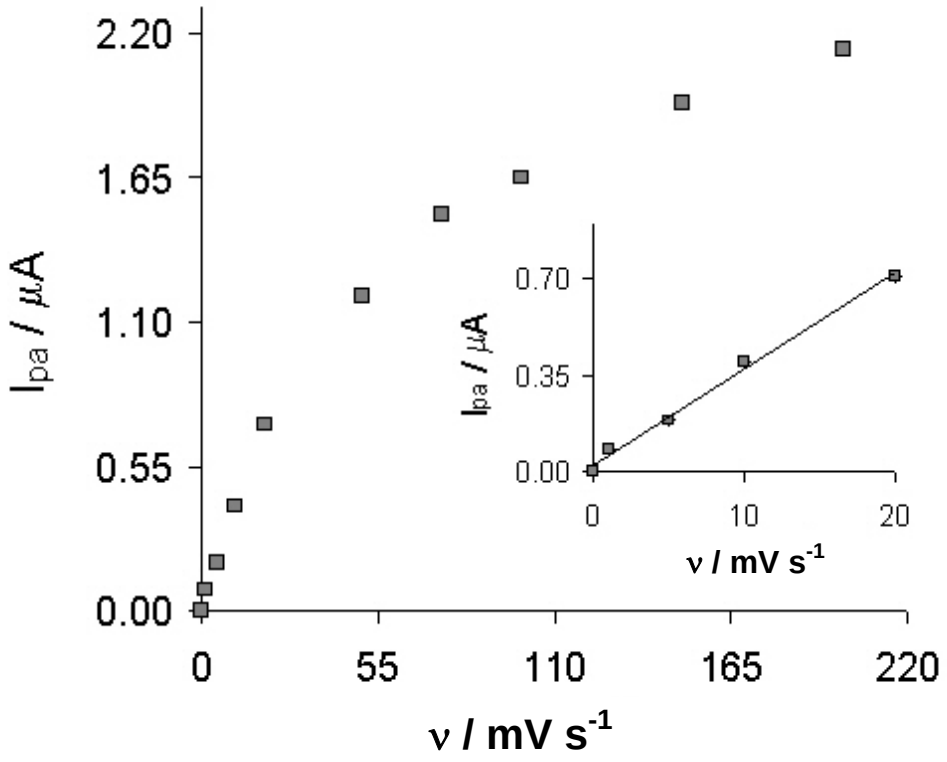

Figure II.9 Plot of the current intensity *versus* the applied scan rate.

The difference between the potential values of the anodic and the cathodic peaks, ΔE, also depends on the scan rate, exhibiting good linearity for small scan rates (figure II.10A). The slope of the plot Ep_a vs. log ν (Figure II.10B) is 53 mV, which is close to the expected theoretical value of 59 mV for the Thin Layer experimental conditions[32].

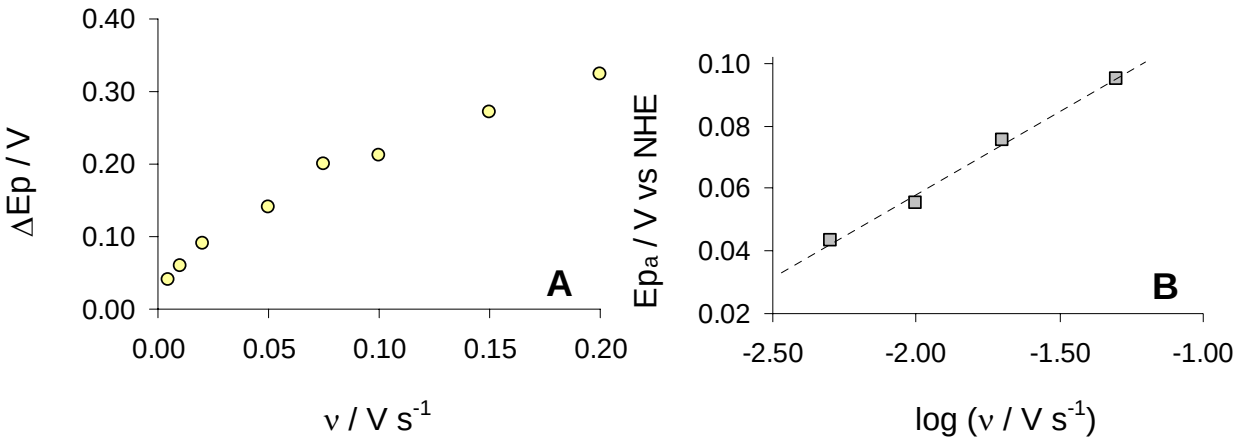

Figure II.10 Plot of ΔE *versus* the scan rate and representation of the E_p dependence on the log ν, obtained by cyclic voltammetry on the GC electrode.

The mean value of the oxidation and the reduction peak current potentials, $(E_{pa} + E_{pc})/2$, remains constant within the imposed conditions. It is then possible to consider that the immobilised Dx has electrochemical behaviour accordingly to the Thin Layer Theory[26, 32].

The formal reduction potential, Eº', was estimated by the $(E_{pa} + E_{pc})/2$ values. The Eº' found for the Dx redox process is similar on both electrode materials, namely +24 ± 5 mV for GC and +28 ± 5 mV vs. NHE for gold.

In Figure II.11 it is possible to observe a well-defined response of Dx both in GC and gold electrodes by square wave voltammetry (SWV). The obtained E_p is +23 and +20 mV vs. NHE, respectively, on GC and gold electrodes.

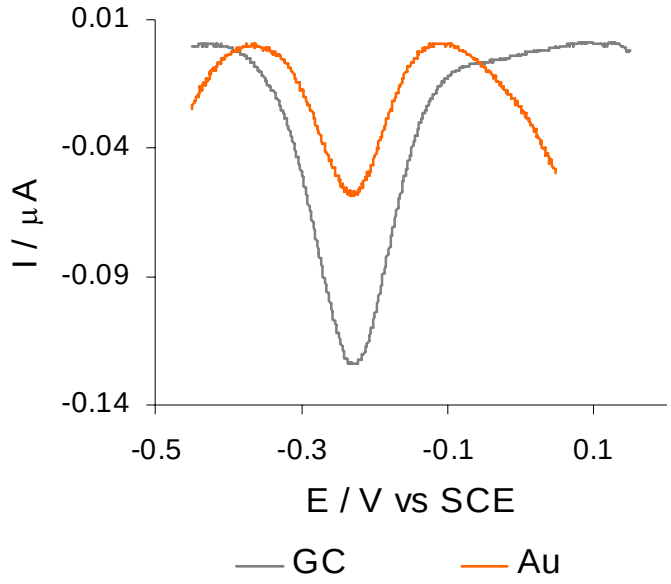

Figure II.11 Dx square wave voltammograms on GC and Au; 10 mV step potential, 50 mV pulse amplitude and 8 Hz frequency.

The protein presents reversible behaviour in both materials with $W_{1/2} \approx 127$ mV which is close to the theoretical value of 124 mV at the experimental conditions. Due to the small SWV diffusion layer thickness when compared with the membrane layer thickness (around 12 μm) it is considered that the results should be analysed considering diffusion control, as shown by some authors[25].

The heterogeneous charge rate constant, K_{sh}, of the redox process on GC was calculated based on the Laviron's mathematical formulation[32] and the value, 2.43×10^{-4} cm s^{-1} (GC) is in agreement with the published values for similar small proteins like cytochrome *c* from *P.nautica*[25].

II.2.1.1 Magnesium addition effect

The addition of a multivalent cation, Mg(II), to the electrolyte enhances the faradaic response as can be seen by the difference between the current intensities with and without magnesium ion in solution (Figure II.12). The protein surface, at pH 7, the GC surface and the used dialysis membrane to perform the immobilisation, all have negative charges. Consequently, the addition of positive species (besides neomycin) is expected to compensate the negative charge excess and minimise the electrostatic repulsion[30]. As observed in practice, the presence of positive charges improves the electrode-protein interaction in spite of this addition not being essential to obtain reasonable signals for Dx.

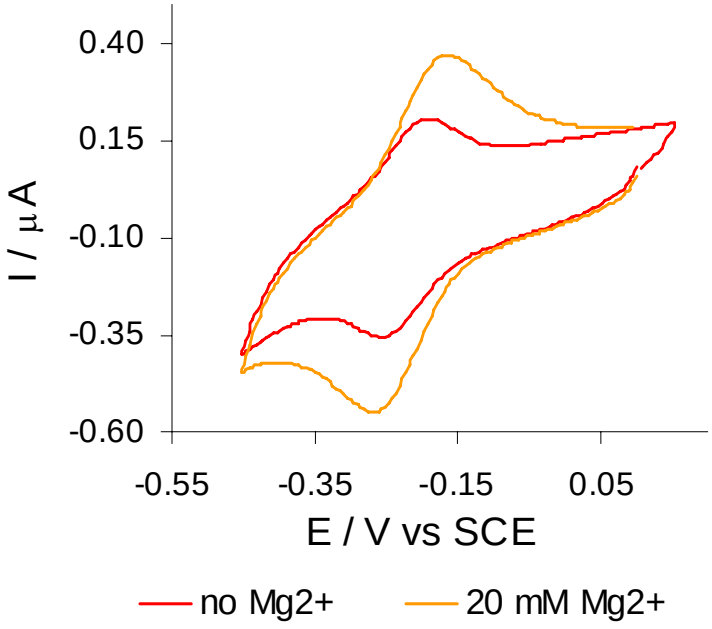

Figure II.12 Cyclic voltammograms of Dx on the GC electrode (ν = 20 mV s^{-1}): comparison of the current peak intensities with and without $MgCl_2$ addition to the electrolyte.

II.2.1.2 The pH effect

In Figure II.13 it is possible to observe the peak currents intensity dependence of the pH for the response of Dx in GC and gold (obtained by CV) which indicates that this property is due to the protein and not to the carbon surface.

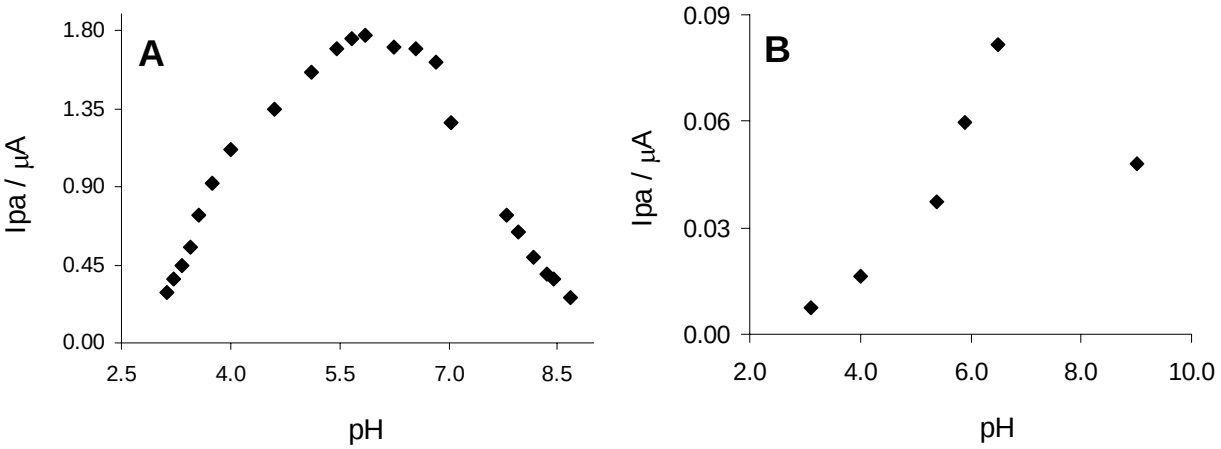

Figure II.13 Plot of the peaks current intensities dependence on the pH for the Dx protein, obtained by CV, on GC (A) and gold (B).

The Dx potential is also dependent on the pH, as shown in figure II.14, both using GC and gold. This dependence can be analysed by fitting some mathematical binding equations to the E$^{o'}$ *versus* pH curve[33]. This treatment allows to calculate the pK's values, namely pK_{red} = 4.01 ± 0.1 and pK_{oxid} = 7.06 ± 0.1 (GC) and pK_{red} = 4.64 ± 0.1 and pK_{oxid} = 7.94 ± 0.1 (gold), corresponding to the ionisation of two different residues close to the iron centre. An overview of the structure[8] reveals that Glu31 and Lys8 are residues in positions close to the iron centre that can be ionisable. In fact, Glu has a pK_a of 4.25 as a free amino acid that can explain the pK_{red} experimental values. The Lys8 (pK_a 10.5 as free amino acid), at about 13 Å of distance to the iron atom, could also interact with the very close Glu10, participating in a saline bridge. The pH dependence of this interaction could be an explanation for the observed pK_{oxid} values in the Dx.

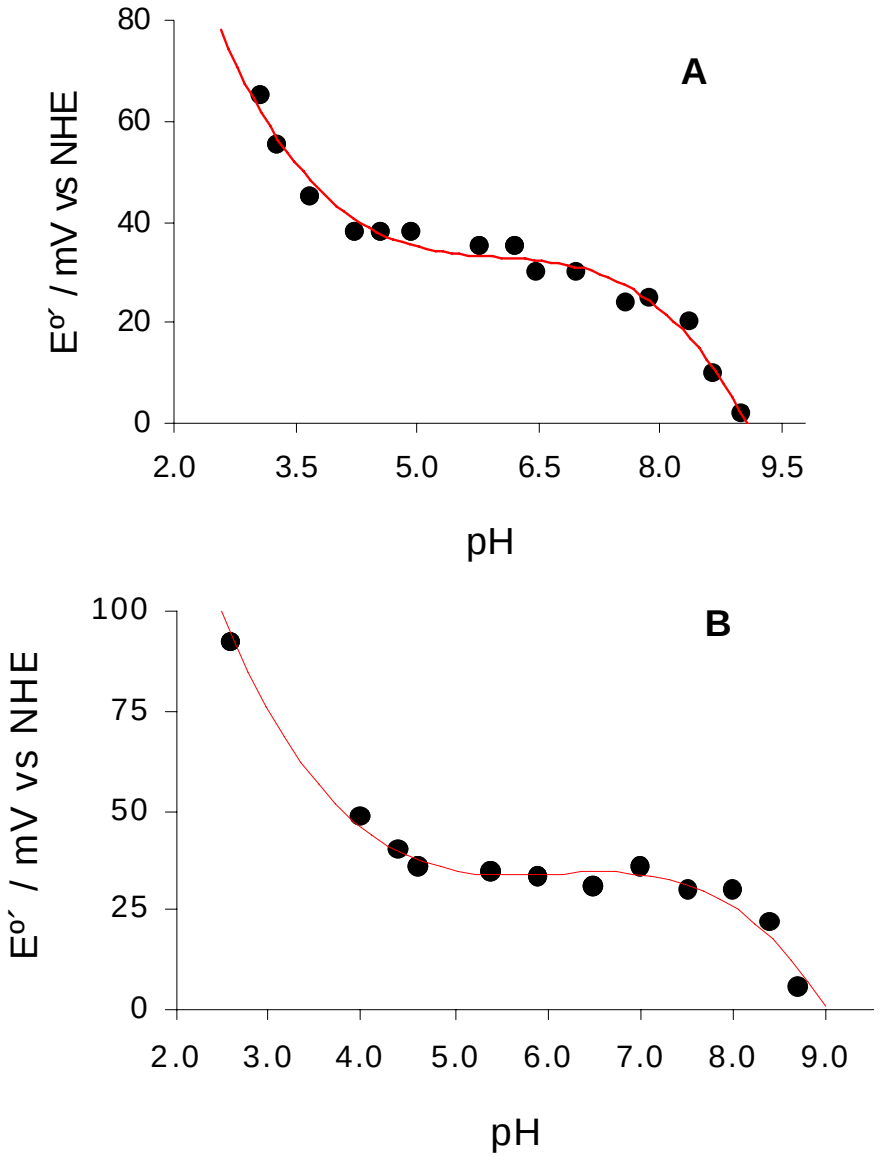

Figure II.14 Plot of the Dx potential formal dependence on the pH, on GC (A) and gold (B).

II.2.2 Direct Electrochemistry of Neelaredoxin

The direct electrochemical response of two Neelaredoxin (Nlr) proteins from *Desulfovibrio gigas* (*Dg*) and from *Treponema pallidum* (*Tp*) were attained by cyclic and square wave voltammetry.

II.2.2.1 Direct Electrochemistry of Neelaredoxin from *D. gigas*

The electrochemical behaviour of the Nlr (Dg) was tested both in GC and gold electrodes showing roughly defined cyclic voltammograms (Figure II.54). The electroactivity lowers significantly with the number of potential scans. It can be observe a reduction peak at –410 mV and an oxidation wave at –283 mV vs. SCE. On gold the oxidation process is very difficult to observe and by CV the process seems irreversible.

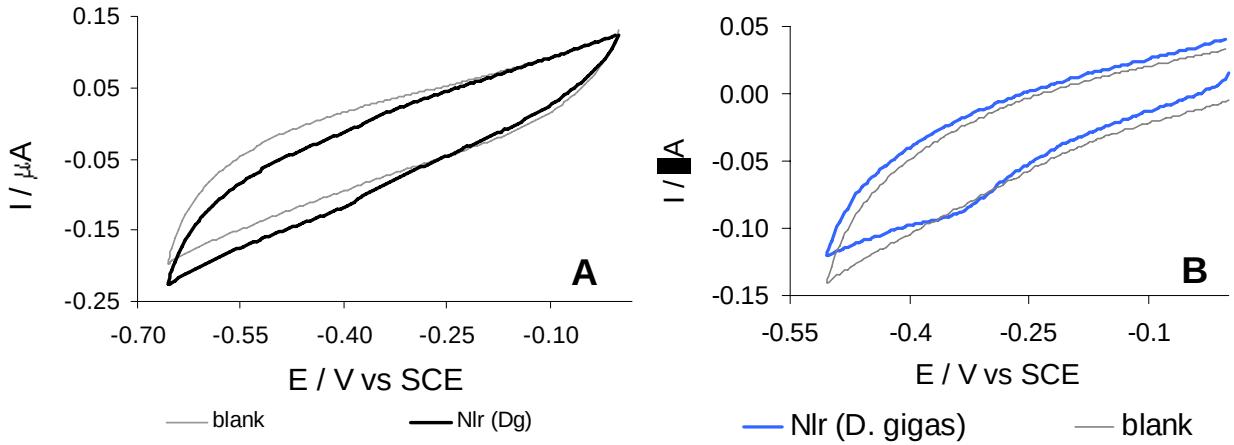

Figure II.15 Cyclic voltammograms of the Nlr (*Dg*) on GC (A) and Au (B) and comparison with the blank, ν = 1 mV s^{-1}.

Better results were attained with the square wave voltammetry technique, as observed in Figure II.16.

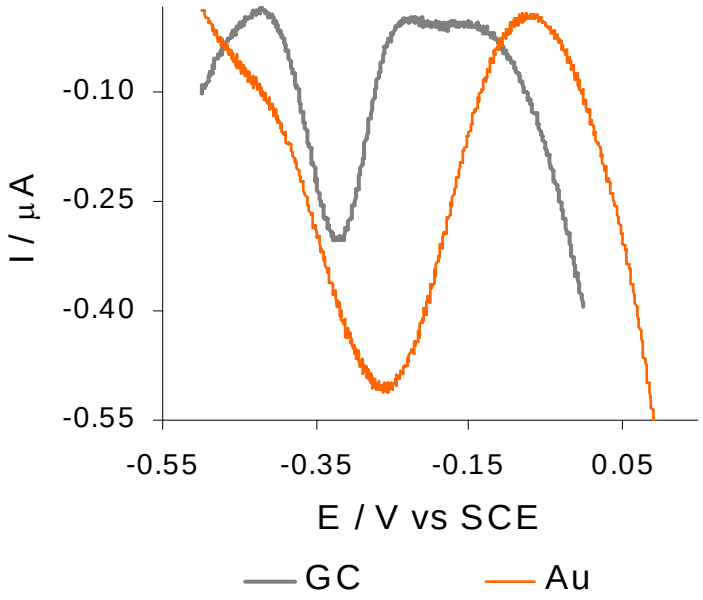

Figure II.16 Square wave voltammogram of the Nlr (*Dg*) on GC and Au; 10 mV step potential, 50 mV pulse amplitude and 8 Hz frequency.

It was possible to observe well defined shape-bell current/potential curves and the E_p and $W_{1/2}$ values remain constant with the frequency increase (Figure II.17). The calculated E°' was –197 ± 9 mV (+45 ± 9 mV vs. NHE). The obtained forward, I_f, and backward currents, I_b, (not shown) for this system are compatible with the typical profile for a reversible process. The value of $W_{1/2} \approx 86$ mV is, however, lower than expected for reversible electrochemical behaviour. This may be related to some adsorption phenomena on the electrode surface[34] and also to some changes from a regime of unrestricted to restricted diffusion[35]. The I_p presents a good linearity with the increase of the frequency (inset of figure II.17) rather than with the square root of the frequency, denoting again a shift from the expected for a reversible behaviour.

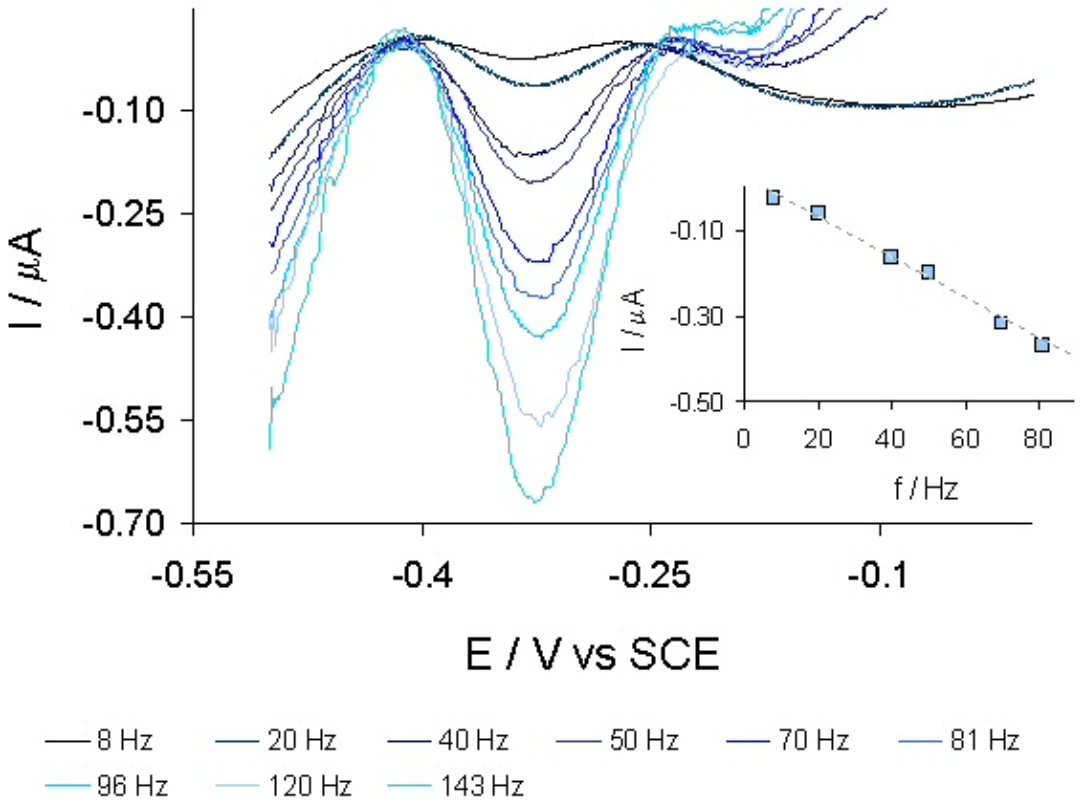

Figure II.17 Square wave voltammograms of the Nlr (*Dg*) on GC; 10 mV step potential, 50 mV pulse amplitude and different frequencies. Inset: plot of I_p vs. f.

II.2.2.2 Direct Electrochemistry of Neelaredoxin from *T. pallidum*

The Nlr *(Tp)* presents better electrochemical response, by CV, than the Nlr *(Dg)* showing a negligible decrease in the electroactivity for the first 10 cycles. In Figure II.18 the current peaks due to the redox process $[Fe(S\text{-}Cys)(N\text{-}His)_4]^{3+}/[Fe(S\text{-}Cys)(N\text{-}His)_4]^{2+}$ on gold can be seen. The peak currents increase linearly with the scan rate and the $(E_{pa} + E_{pc})/2$ values are constant. The estimated formal potential was –231 ± 6 mV (+11 ± 6 mV vs. NHE).

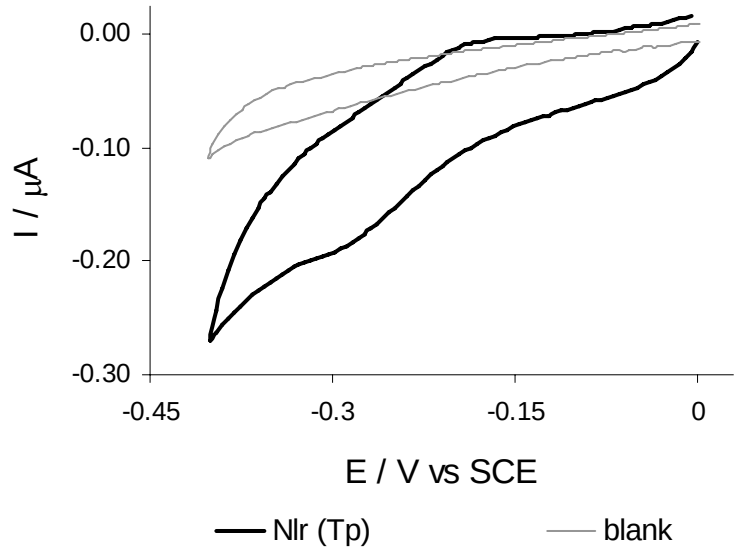

Figure II.18 Cyclic voltammograms of the Nlr (*Tp*) on Au and comparison with the blank, ν = 4 mV s^{-1}.

The SWV response for the Nlr (*Tp*) shows some characteristics that apparently seem to be attributable to some irreversibility of the process, namely the shift of the E_p towards more negative values and the enlargement of the peak width with the frequency increase[36]. The profile of the i_f and i_b currents, however, seems more compatible with a reversible process. Besides, the comparative intensity of the i_b relatively to the i_f and the enlargement of its width may also be related to the initial redox state of the protein. In fact, spectrophotometric assays of the reaction of the Nlr (*Tp*) with different oxidants allowed to find, after purification, a proportion of about 40% oxidised to 60% reduced state of the protein population[37]. This can be an explanation for the shift of the reversible behaviour observed by SWV. An example of these features on gold electrode is given in Figure II.19.

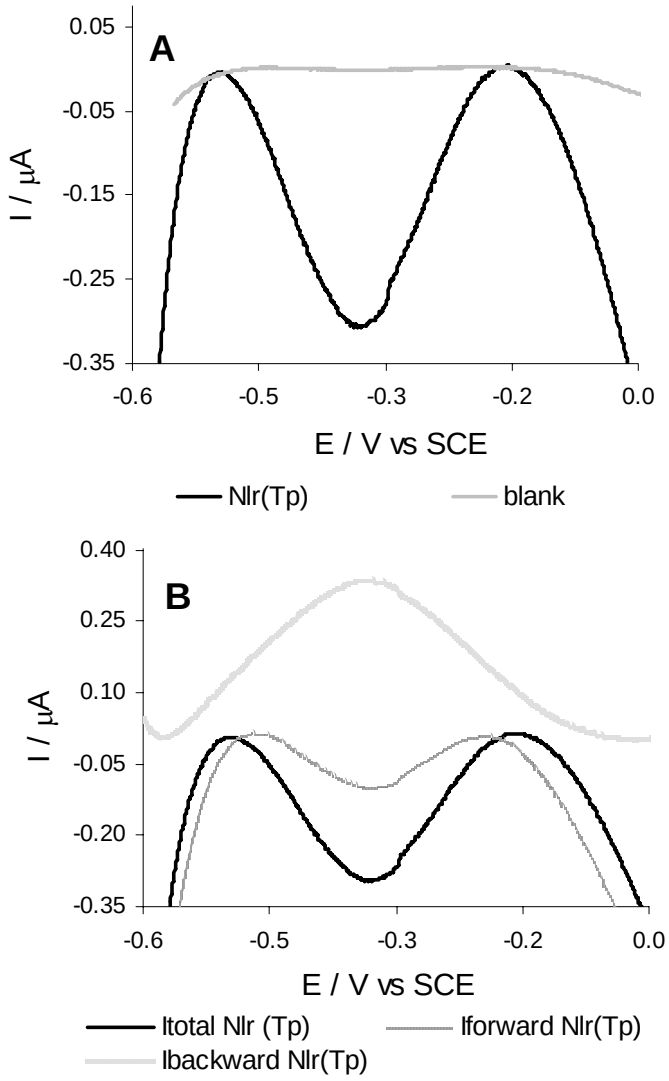

Figure II.19 Square wave voltammograms of the Nlr (*Tp*) on gold and comparison with the blank (A) and plot of the currents I_{total}, $I_{forward}$ and $I_{backward}$ for the same Nlr (*Tp*) assay (B); 10 mV step potential, 50 mV pulse amplitude and frequency 8 Hz.

The comparison between the two neelaredoxins shows that, although the protein centres are similar, the redox features observed are quite different for the same experimental conditions.

II.2.3 Direct Electrochemistry of Desulfoferrodoxin from *D. vulgaris*

In Figure II.20 the electrochemical behaviour of Dfx is displayed. It can be observed by cyclic voltammetry, on GC, a cathodic wave at approximately -300 mV and the correspondent anodic process around –200 mV vs. SCE. By comparison with the Dx results and previous results of a recombinant Dfx protein (DfxN), with only one metallic centre (Centre I)[38], these peaks were indexed to the Dfx centre I reaction, $[Fe(S\text{-}Cys)_4^{3+}]/[Fe(S\text{-}Cys)_4^{2+}]$. Although the observed shift from an ideal electrochemical behaviour, the $(E_{pa} + E_{pc})/2$ values are still constant, within the experimental error, which allowed to calculate the $E^{o'}$ = -266 ± 8 mV (-24 ± 8 mV vs. NHE).

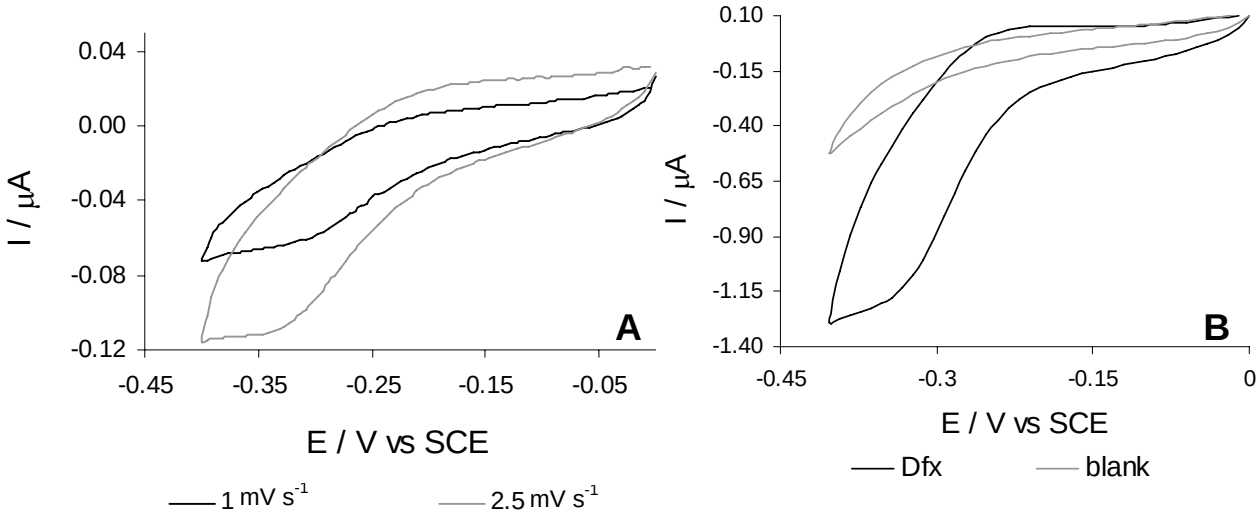

Figure II.20 Cyclic voltammograms of Dfx and comparison with the blank, obtained on GC (A), ν = 1 and 2.5 mV s^{-1}, and on gold (B), ν = 5 mV s^{-1}.

The same process at the gold electrode (Fig. II.20 B) reveals similar features but with enhanced irreproducibility and irreversible character. The potential values for the cathodic and anodic reactions are observed at –342 and –252 mV vs. SCE, respectively. A second anodic wave develops at more positive potential values around +170 mV vs. SCE and it may be related with the Dfx Centre II. The high irreproducibility and irreversibility (only an anodic process and at the first cycle) of the process did not allowed, so far, to take definite conclusions about its attribution to Centre II.

In Figure II.21 the SW response of the Dfx Centre I in GC and Au with well-defined current peaks is displayed. The I_p vs. f plot presents linearity in the applied frequency range. The E_p and $W_{1/2}$ values remain constant, and the value $W_{1/2} \approx 92$ mV is also lower than the expected for a reversible process. As discussed for the Nlr (*Dg*), this feature may be related with adsorption phenomena on the electrode surface[34, 35].

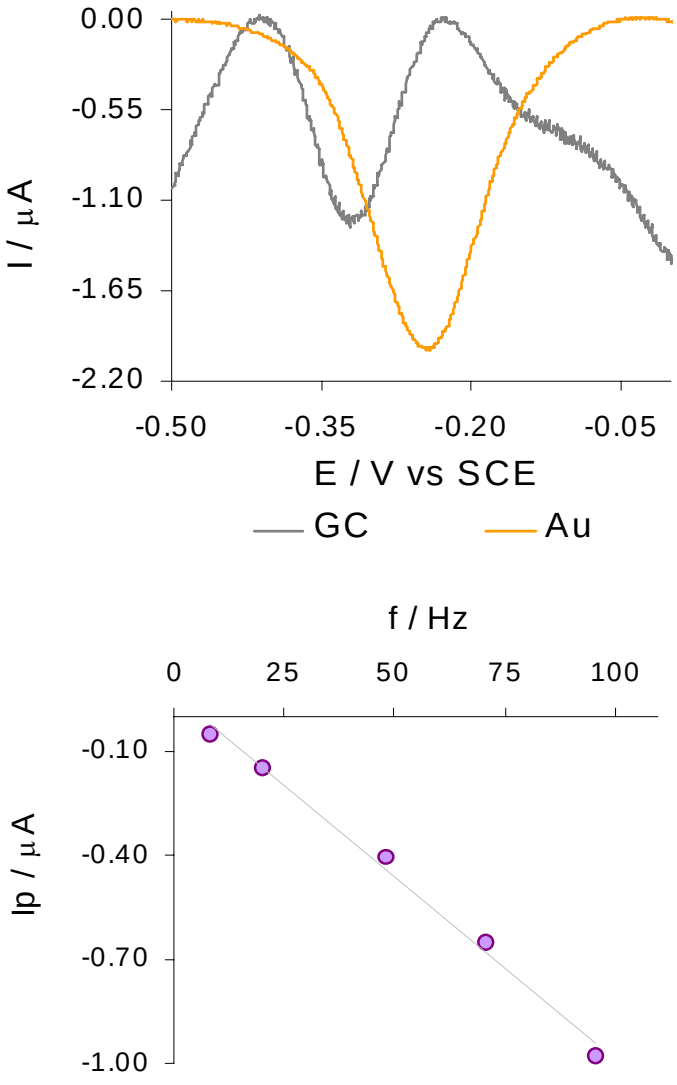

Figure II.21 (A) Square wave voltammograms of the Dfx (Centre I) on glassy carbon and gold; 10 mV step potential, 50 mV pulse amplitude and 8 Hz frequency and (B) Plot of the current peak intensity (SWV) vs. the applied frequency.

Some preliminary studies by SWV (Figure II.22), on gold, allowed to observe another process around +180 mV (+422 mV vs. NHE). This process is quite irreproducible and it is only observed at the first anodic scan of each assay. These features seem compatible with the data from CV for the second anodic peak that sometimes could be observed at +170 mV. This process may be attributed to the Dfx centre II. Previous results of a recombinant Dfx protein (DfxC), with only one metallic centre (Centre II)[38], pointed to a midpoint potential of +247 mV vs. NHE. The difference may be due to the fact that the reported experiments have been performed only with one domain of the protein which implies relevant differences, as size and global charge of the surface. Further studies are necessary to clarify this point.

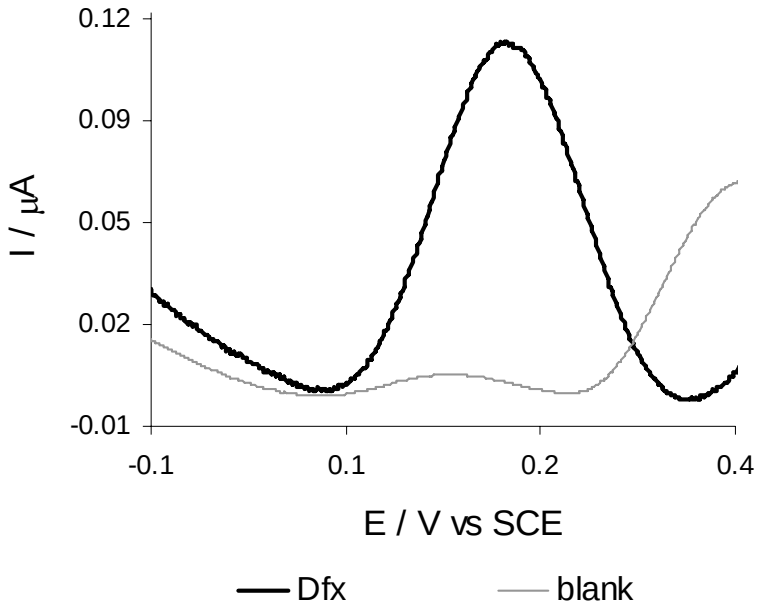

Figure II.22 Square wave voltammograms of the Dfx (Centre II) on gold and comparison with the blank assay; 10 mV step potential, 50 mV pulse amplitude and 8 Hz frequency.

II.2.3.1 Magnesium addition effect

The effect of the addition to the electrolyte solution of multivalent cations on the measured currents was also evaluated. A plot of the Dfx peak currents (Centre I) *versus* the Mg(II) concentration is shown in Figure II.23.

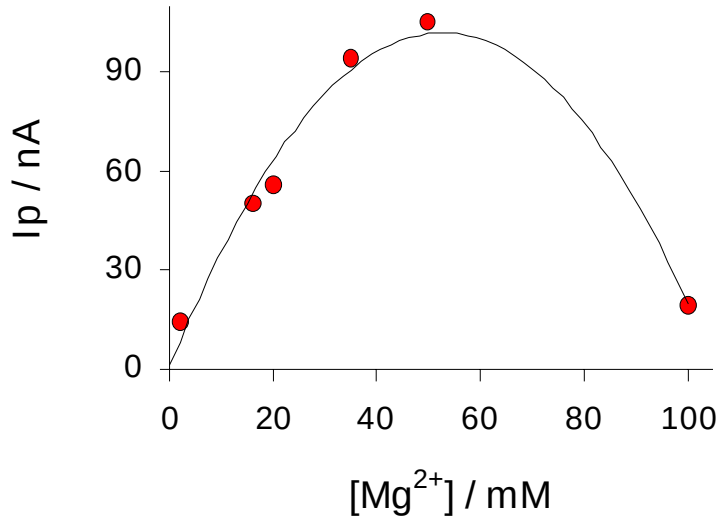

Figure II.23 Plot of the current peaks intensity of Centre I of the Dfx (obtained by CV, pH 7, on the GC electrode) *versus* the Mg^{2+} concentration (2 to 100 mM).

The faradaic response increases with increasing amount of magnesium ions, as it was observed for the Dx. A maximum value of I_p is reached at 50 mM of Mg^{2+}. The reason for this increase should be the same as discussed before for Dx, namely the need for charge compensation in order to minimise the electrostatic repulsion.

II.2.3.2 The pH effect

The current intensity dependence of the pH (Figure II.24), obtained by CV at the GC and gold electrodes, is similar to the displayed by the Dx at the same materials.

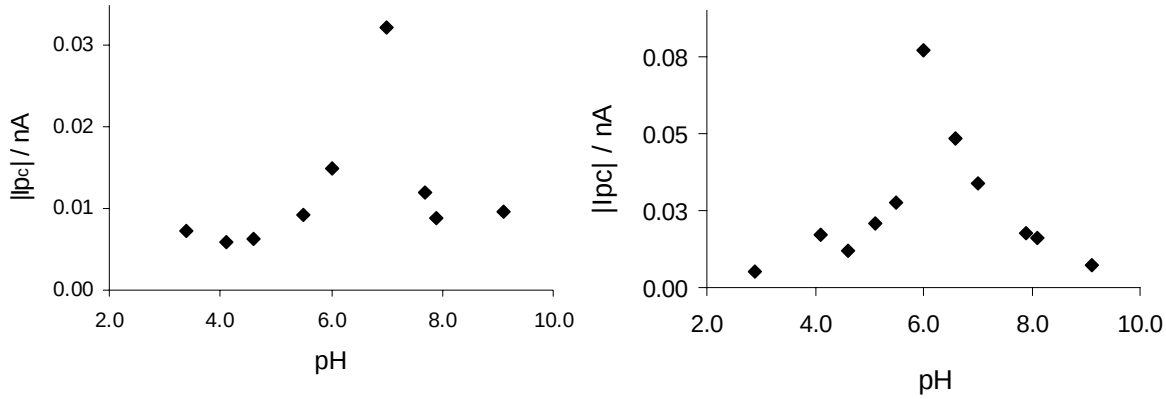

Figure II.24 Plot of the Dfx peak current intensities dependence on the pH, obtained by CV, on GC (A) and gold (B).

The Dfx potential dependence on the pH is also shown in figure II.25 both using GC and gold. The pK values determined by the analysis of the Eº' *versus* pH curve were, respectively, $pK_{red} = 4.60 \pm 0.1$ and $pK_{oxid} = 7.16 \pm 0.1$ on GC and $pK_{red} = 4.37 \pm 0.1$ and $pK_{oxid} = 7.59 \pm 0.1$ on gold. As in Dx these values should correspond to the ionisation of two different residues close to the iron centre. In this case we have examined the Dfx sequence and compared with the structure of the Dfx from *D. desulfuricans* ATCC 27774 (the crystallographic data for the Dfx from *D. vulgaris* is not available). In the Dfx sequence, as before in the Dx, we find that Glu31 is conserved and is located in the vicinity of the iron centre. Glu31 should be the responsible for the lowest pK values found in Dfx. The Lys8 is also conserved in both structures. The distance to the iron atom is, approximately, 10 Å, but the orientation of this residue seems to be contrary to the metallic centre. The highest experimental pK values, however, which are quite similar to the ones for Dx, point to the hypothesis that this may be the second residue that influences the redox behaviour of the Dfx, with the pH variation. This discussion should be reviewed when the Dfx (*D. vulgaris*) crystallographic structure is resolved.

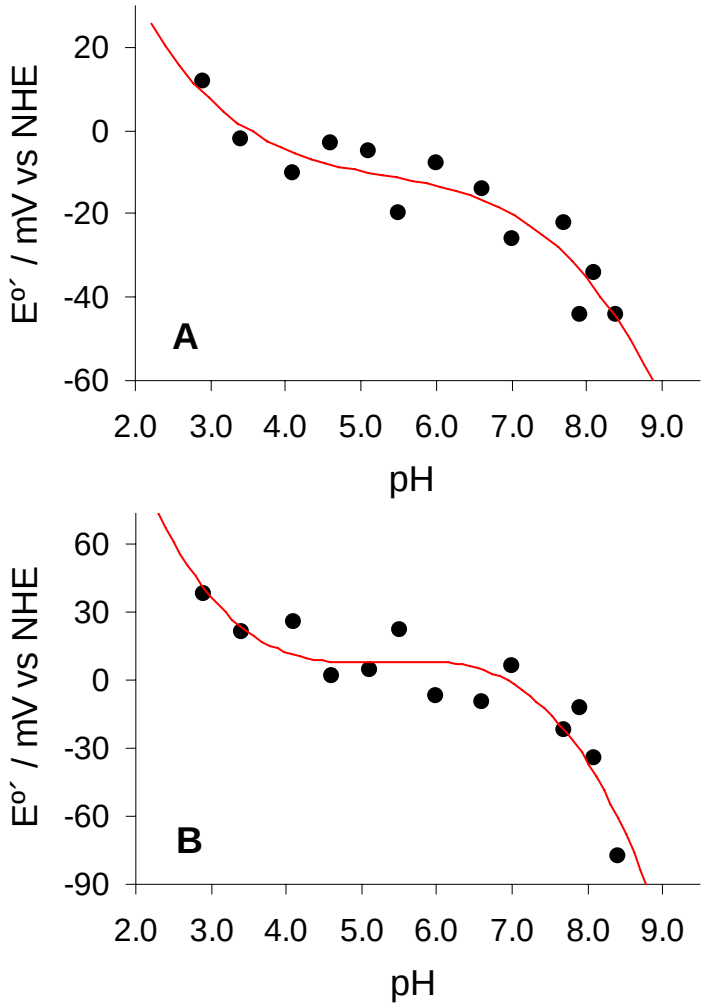

Figure II.25 Plot of the Dfx potential formal dependence on the pH, on GC (A) and gold (B).

II.2.4 Dfx comparison with Dx and Nlr

The differences of the direct electrochemical responses of the Dx and Dfx (Centre I) on GC can be clearly seen in Figure II.26. For the same experimental conditions the Dx presents redox behaviour closer to reversibility and much better reproducibility. The formal potentials are approximately 50 mV apart, with the Dfx presenting the more negative value. The Dfx features should be related to its larger structure that seems to difficult the interaction with the electrode surface.

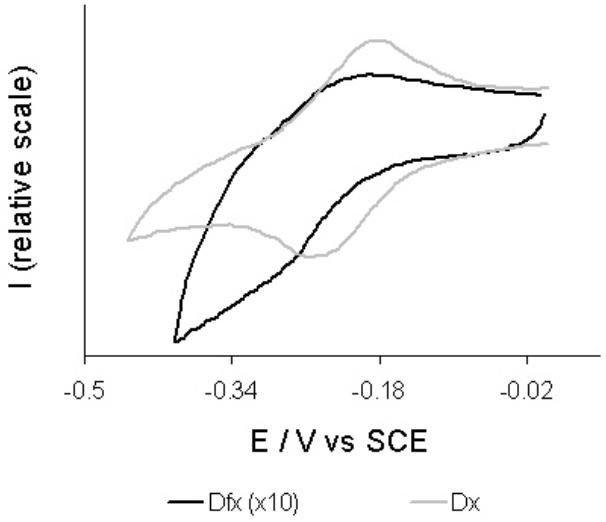

Figure II.26 Comparison of the Dfx (Centre I) and Dx cyclic voltammetry responses on GC; ν = 1 mV s^{-1}. The currents were normalised for clarity.

The SW voltammograms show, for both proteins, well-defined and reproducible bell shaped curves, as can be seen in Figure II.27. The Eº' values found on gold are very similar, -220 and –219 mV (+22 and +23 mV vs. NHE) respectively for Dfx and Dx. The difference between the E_p is more pronounced (ca. 100 mV) at the GC electrode. The Dfx apparently presents better affinity with the modified gold surface than with the carbon electrode.

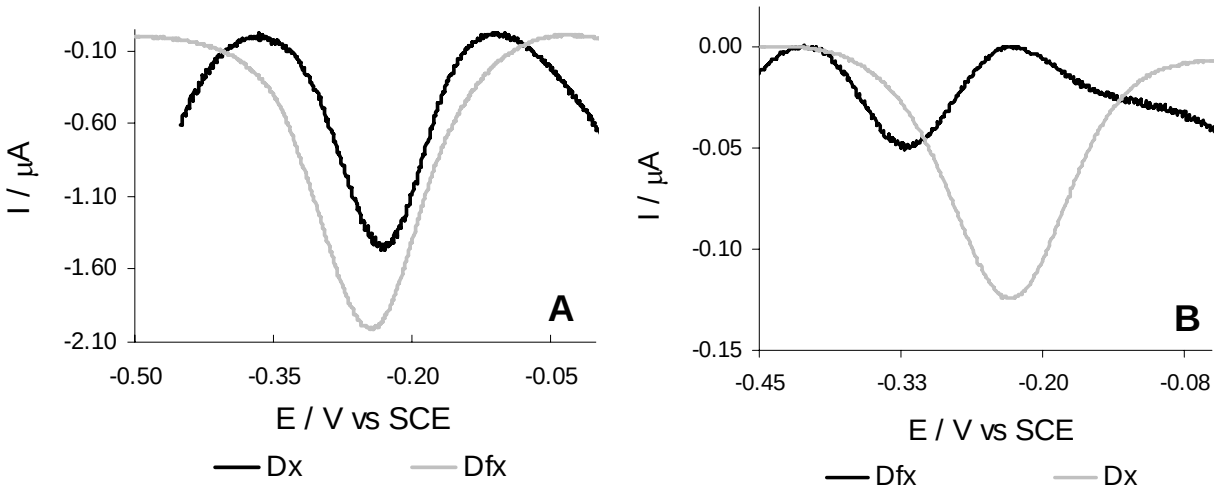

Figure II.27 Comparison between the square wave responses of the Dfx (Centre I) and Dx , on gold (A) and on GC (B); 10 mV step potential, 50 mV pulse amplitude and 8 Hz frequency.

The Nlr redox process (for *Dg* and *Tp*) appears at more negative potential values than the Centre II of Dfx. It should be notice that in Figure II.28, the Nlr current peak is obtained during the potential anodic scan (thermodynamically less favourable), that requires the previous reduction of the protein in order to be able to reoxidise it.

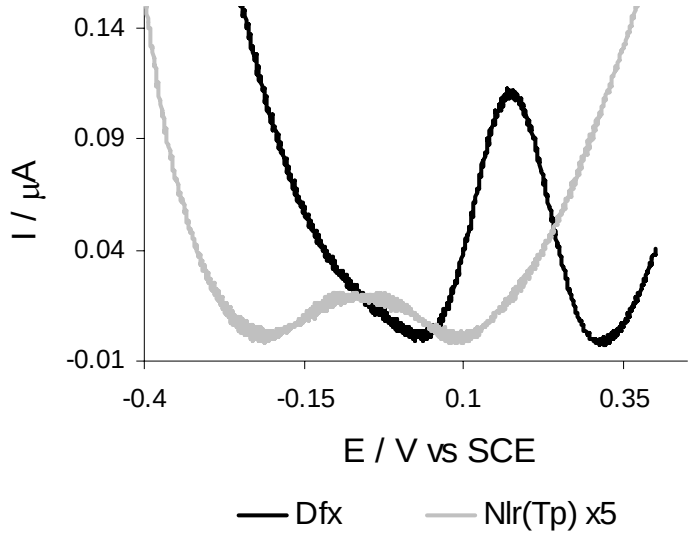

Figure II.28 Square wave responses of the Dfx (Centre II) and Nlr (*Tp*), on gold; 10 mV step potential, 50 mV pulse amplitude and 8 Hz frequency.

II.3 Final Remarks

The direct electrochemical response of the Dfx and the related proteins Dx and Nlr were observed on glassy carbon and gold electrodes by cyclic and square wave voltammetry. The Dfx centre I reveal close potential values with the Dx centre, as expected and reported before in the literature. The Dfx centre II shows, however, a considerable difference of the redox potential determined for the related proteins, Nlr. Also, it was possible to observe different electrochemical properties between the two studied Nlr‘s. The observed difference in the redox behaviour of the Dfx and the related proteins with only one of the metallic centres indicates that the Dfx global structure is a determinant influence on electron transfer properties of the superoxide reductase proteins.

II.4 References

1. Rusnak, F.; Ascenso, C.; Moura, I.; Moura, J. J., Superoxide reductase activities of neelaredoxin and desulfoferrodoxin metalloproteins. *Methods Enzymol* **2002,** 349, 243-58.

2. Niviere, V.; Fontecave, M., Discovery of superoxide reductase: an historical perspective. *J Biol Inorg Chem* **2004,** 9, (2), 119-23.

3. Moura, I.; Tavares, P.; Moura, J. J.; Ravi, N.; Huynh, B. H.; Liu, M. Y.; LeGall, J., Purification and characterization of desulfoferrodoxin. A novel protein from Desulfovibrio desulfuricans (ATCC 27774) and from Desulfovibrio vulgaris (strain Hildenborough) that contains a distorted rubredoxin center and a mononuclear ferrous center. *J Biol Chem* **1990,** 265, (35), 21596-602.

4. Tavares, P.; Ravi, N.; Moura, J. J.; LeGall, J.; Huang, Y. H.; Crouse, B. R.; Johnson, M. K.; Huynh, B. H.; Moura, I., Spectroscopic properties of desulfoferrodoxin from Desulfovibrio desulfuricans (ATCC 27774). *J Biol Chem* **1994,** 269, (14), 10504-10.

5. Chen, L.; Sharma, P.; Le Gall, J.; Mariano, A. M.; Teixeira, M.; Xavier, A. V., A blue non-heme iron protein from Desulfovibrio gigas. *Eur J Biochem* **1994,** 226, (2), 613-8.

6. Verhagen, M. F.; Voorhorst, W. G.; Kolkman, J. A.; Wolbert, R. B.; Hagen, W. R., On the two iron centers of desulfoferrodoxin. *FEBS Lett* **1993,** 336, (1), 13-8.

7. Ana V. Coelho, P. M., Vilmos Füllop, Andrew Thompson, Ana Gonzalez, Maria A. Carrondo, Desulfoferrodoxin structure determined by MAD phasing and refinement to 1.9-A resolution reveals a unique combination of a tetrahedral FeS_4 centre with a square pyramidal $FeSN_4$ centre. *Journal of Biological Inorganic Chemistry* **1997,** 2, 680-689.

8. Archer, M.; Huber, R.; Tavares, P.; Moura, I.; Moura, J. J.; Carrondo, M. A.; Sieker, L. C.; LeGall, J.; Romao, M. J., Crystal structure of desulforedoxin from Desulfovibrio gigas determined at 1.8 A resolution: a novel non-heme iron protein structure. *J Mol Biol* **1995,** 251, (5), 690-702.

9. Santos-Silva, T.; Trincao, J.; Carvalho, A. L.; Bonifacio, C.; Auchere, F.; Raleiras, P.; Moura, I.; Moura, J. J.; Romao, M. J., The first crystal structure of class III superoxide reductase from Treponema pallidum. *J Biol Inorg Chem* **2006**.

10. Yeh, A. P.; Hu, Y.; Jenney, F. E., Jr.; Adams, M. W.; Rees, D. C., Structures of the superoxide reductase from Pyrococcus furiosus in the oxidized and reduced states. *Biochemistry* **2000,** 39, (10), 2499-508.

11. Ascenso, C.; Rusnak, F.; Cabrito, I.; Lima, M. J.; Naylor, S.; Moura, I.; Moura, J. J., Desulfoferrodoxin: a modular protein. *J Biol Inorg Chem* **2000,** 5, (6), 720-9.

12. Berthomieu, C.; Dupeyrat, F.; Fontecave, M.; Vermeglio, A.; Niviere, V., Redox-dependent structural changes in the superoxide reductase from Desulfoarculus baarsii and Treponema pallidum: a FTIR study. *Biochemistry* **2002,** 41, (32), 10360-8.

13. Moura, I.; Xavier, A. V.; Cammack, R.; Bruschi, M.; Le Gall, J., A comparative spectroscopic study of two non-haem iron proteins lacking labile sulphide from Desulphovibrio gigas. *Biochim Biophys Acta* **1978,** 533, (1), 156-62.

14. Hagen, W. R., Direct electron transfer of redox proteins at the bare glassy carbon electrode. *Eur J Biochem* **1989,** 182, (3), 523-30.

15. Hu, N., Direct electrochemistry of redox proteins or enzymes at various film electrodes and their possible applications in monitoring some pollutants. *Pure and Applied Chemistry* **2001,** 73, (12), 1979-1991.

16. Lu, Z.; Lvov, Y.; Jansson, I. I.; Schenkman, J. B.; Rusling, J. F., Electroactive Films of Alternately Layered Polycations and Iron-Sulfur Protein Putidaredoxin on Gold. *J Colloid Interface Sci* **2000,** 224, (1), 162-168.

17. Chattopadhyay, K. M. S., Direct electrochemistry of heme proteins: effect of electrode surface modification by neutral surfactants. *Bioelectrochemistry* **2000,** 53, (1), 17-24.

18. Bianco, P. H., J., Electrochemistry of ferredoxin and c-type cytochromes at surfactant film-modified pyrolytic graphite electrodes. *Electrochimica Acta* **1997,** 42, (4), 587-594.

19. P. J. H. J. van Os, A. B., C. G. J. Koopal, W. P. van Bennekom, Glucose detection at bare and sputtered platinum electrodes coated with polypyrrole and glucose oxidas. *Analytica Chimica Acta* **1996,** 335, (3), 209-216.

20. Li, S. D. a. J., Self-assembled monolayers of thiols on gold electrodes for bioelectrochemistry and biosensors. *Bioelectrochemistry and Bioenergetics* **1997,** 42, (1), 7-13.

21. Pauline M. Allen, H. A., O. Hill and Nicholas J. Walton, Surface modifiers for the promotion of direct electrochemistry of cytochrome c. *Journal of Electroanalytical Chemistry* **1984,** 178, (1), 69-86.

22. J. Hirst, F. A. A., Fast-Scan Cyclic Voltammetry of Protein Films on Pyrolytic Graphite Edge Electrodes: Characteristics of Electron Exchange. *Analytical Chemistry* **1998,** 70, (23), 5062-5071.

23. Angove, H. C.; Cole, J. A.; Richardson, D. J.; Butt, J. N., Protein film voltammetry reveals distinctive fingerprints of nitrite and hydroxylamine reduction by a cytochrome C nitrite reductase. *J Biol Chem* **2002,** 277, (26), 23374-81.

24. É. Lojou, P. B., Membrane electrodes can modulate the electrochemical response of redox proteins — direct electrochemistry of cytochrome c. *Journal of Electroanalytical Chemistry* **2000,** 485, (1), 71-80.

25. M. M. Correia dos Santos, P. M. P. d. S., M. L. Simões Gonçalves, L. Krippahl, J. J. G. Moura, É. Lojou and P. Bianco, Electrochemical studies on small electron transfer proteins using membrane electrodes. *Journal of Electroanalytical Chemistry* **2003,** 541, 153-162.

26. Ana M. O. Brett, C. M. A. B., *Electroquímica-Princípios, Métodos e Aplicações*. Livraria Almedina: Coimbra, 1996.

27. Isao Taniguchi, T. F., Kazuhide Umekita, Hiroko Yamaguchi and Kazuo Yasukouchi, Effect of poly-l-lysine addition on the redox behavior of horse heart cytochrome c at functional electrodes. *Journal of Electroanalytical Chemistry* **1986,** 199, (2), 455-460.

28. M. M. Correia dos Santos, P. M. P. d. S., M. L. Simões Gonçalves, C. Ascenso, I. Moura, J. J. G. Moura, Electrochemical studies of rubredoxin from Desulfovibrio vulgaris at modified electrodes. *Journal of Electroanalytical Chemistry* **2001,** 501, (1-2), 173-179.

29. V. J. Razumas, J. J. J., J. J. Kulys, Electrocatalysis on enzyme-modified carbon materials. *Bioelectrochemistry and Bioenergetics* **1984,** 12, (3-4), 297-322.

30. Fraser A. Armstrong, P. A. C., H. Allen O. Hill, Valerie J. Lowe, B. Nigel Oliver, Metal ions and complexes as modulators of protein-interfacial electron transport at graphite electrodes. *Journal of Electroanalytical Chemistry* **1987,** 217, (2), 331-366.

31. E. Laviron, L. R., General expression of the linear potential sweep voltammogram for a surface redox reaction with interactions between the adsorbed molecules: Applications to modified electrodes. *Journal of Electroanalytical Chemistry* **1980,** 115, (1), 65-74.

32. Laviron, E., General expression of the linear potential sweep voltammogram in the case of diffusionless electrochemical systems. *Journal of Electroanalytical Chemistry* **1979,** 101, (1), 19-28.

33. Geoffrey R. Moore, G. W. P., *Cytochromes c - Evolutionary, Structural and Physicochemical Aspects*. Springer-Verlag: Berlin, 1990.

34. D. Souza, S. A. S. M., L. A. Avaca, Square wave voltammetry. Part I: theoretical aspects. *Química Nova* **2003,** 26, (1), 81-89.

35. S. P. Kounaves, J. J. O. D., P. Chandresekhar, Janet Osteryoung, Square wave anodic stripping voltammetry at the mercury film electrode: theoretical treatment. *Analytical Chemistry* **1987,** 59, (3), 386-389.

36. Janet G. Osteryoung, R. A. O., Square wave voltammetry. *Analytical Chemistry* **1885,** 57, (1), 101-110.

37. Raleiras, P. Superoxide Reductases - Structural and Functional Aspects. FCT-UNL, Lisboa, 2005.

38. Ascenço, C. Caracterização Estrutural e Funcional de Proteínas contendo Centros Mononucleares de Ferro Não-Hémico. FCT-UNL, Lisboa, 2001.

Chapter III

Direct Electrochemistry of the Periplasmic Nitrate Reductase of *Desulfovibrio desulfuricans* ATCC 27774

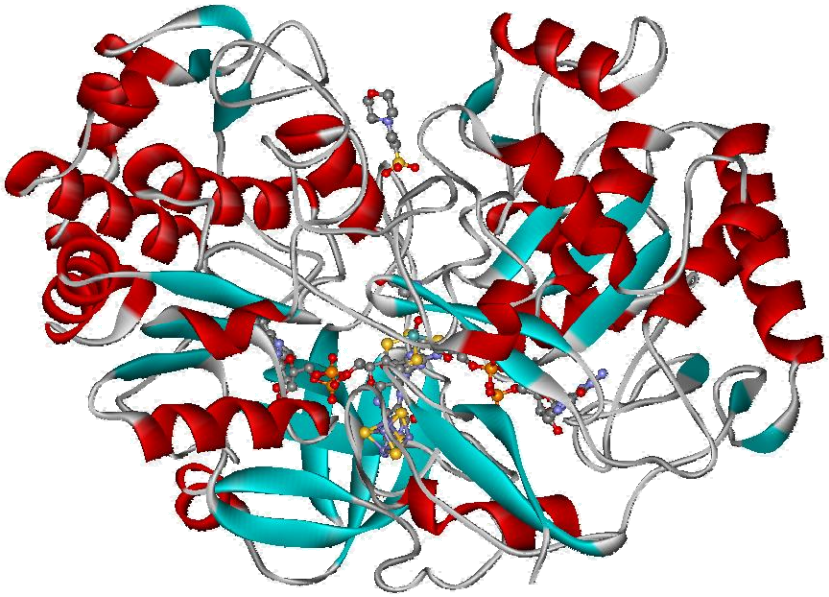

Direct Electrochemistry of the Periplasmic Nitrate Reductase of *Desulfovibrio desulfuricans* ATCC 27774

III.1 Nitrate Reductases

Nitrate reductases (NR) are enzymes involved in the nitrogen assimilation, in the dissimilatory nitrate reduction and in the maintenance of the regular cellular redox potential[1]. In the dissimilatory nitrate reduction, nitrate is converted into N_2 in respiration and into ammonia in a pathway known as ammonification[2]. NRs that take part in the nitrogen cycle catalyze the nitrate reduction reaction (figure III.1):

$$NO_3^- + 2\bar{e} + 2H^+ \rightarrow NO_2^- + H_2O$$

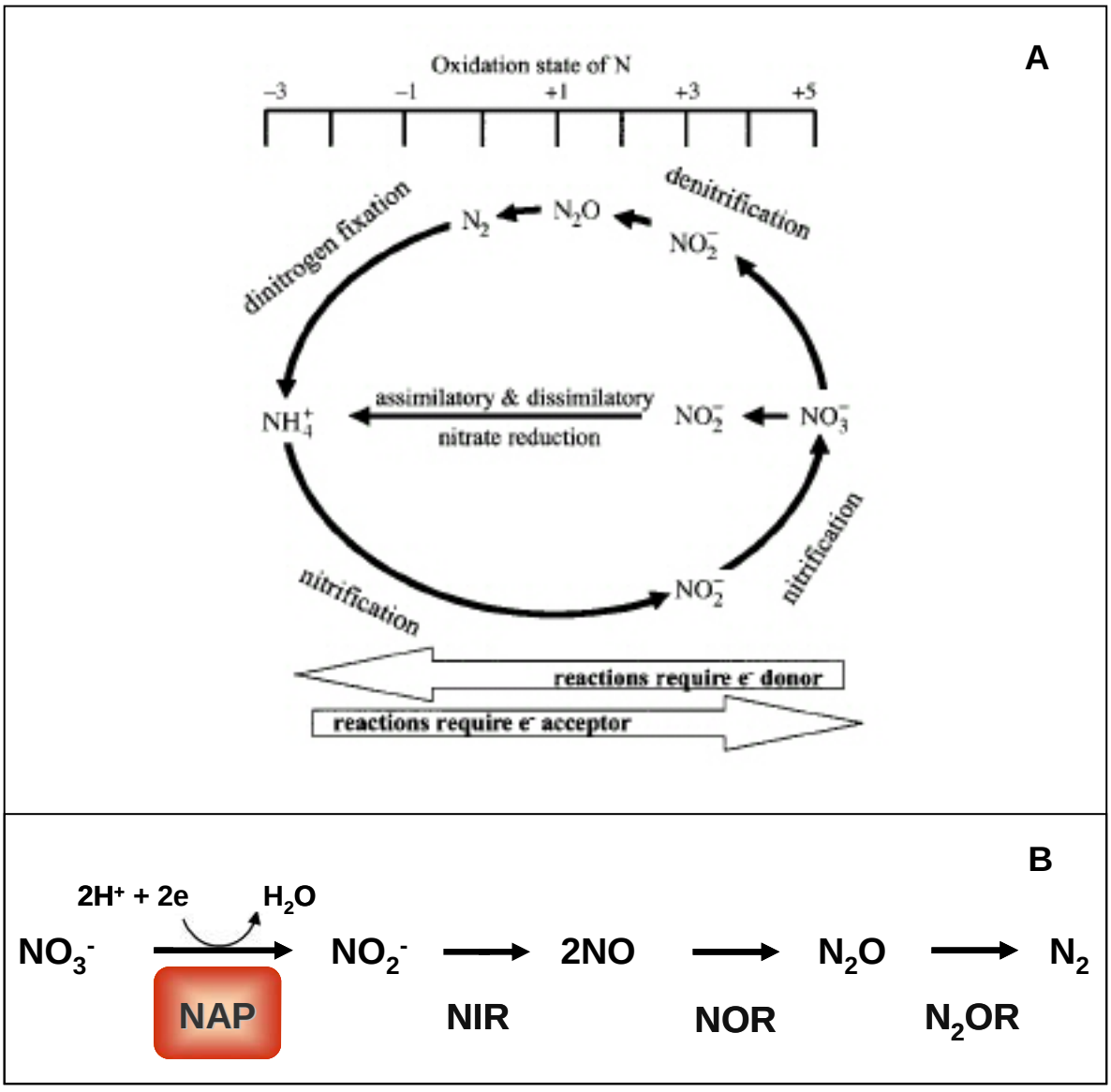

Figure III.1 A) Schematic representation of the nitrogen cycle (from Stolz, 2002)[1] and B) scheme of the denitrification pathway, showing the relative position of the periplasmic nitrate reductase enzyme.

NRs can be found in plants, algae, fungi, archaea and bacteria. The eukaryotic and the prokaryotic NRs distinguish themselves structurally. The first type belongs to the sulphite oxidase family and the second to the dimethylsulfoxide (DMSO) reductase family. All nitrate reductases found in bacteria had shown a common feature; all contain molybdenum at the catalytic centre. Also, both types of NRs contain a pyranopterin co-factor. In contrast the eukaryote's co-factor is simpler than the prokaryotic pyranopterin (figure III.2).

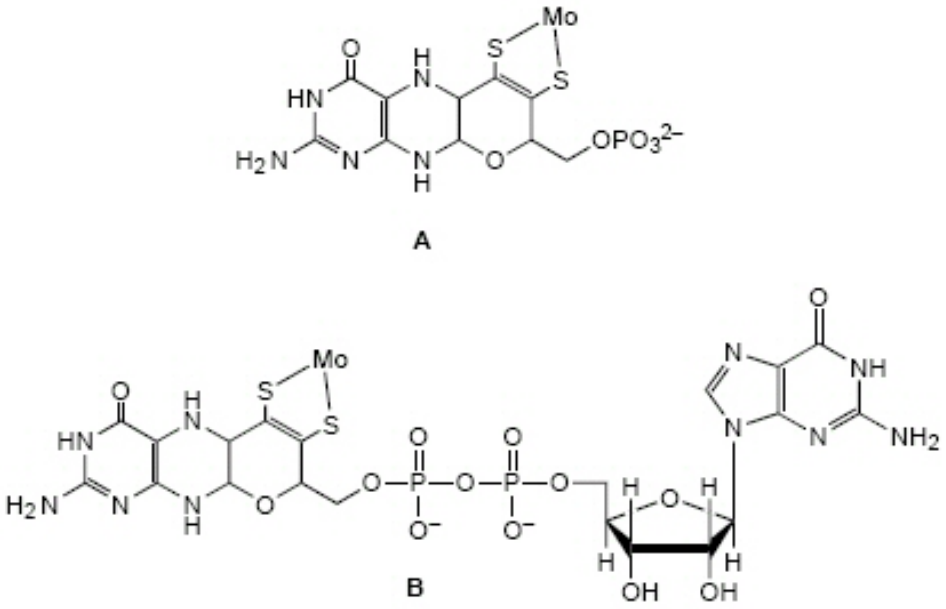

Figure III.2 Schematic representation of the pyranopterin co-factor of A) eukaryotic and B) prokaryotic NRs (from Stolz, 2002)[1].

The nitrate reductases that take part in the dinitrification or dissimilatory processes can be located in the bacteria's membrane or periplasm. The NR found at the membrane, NAR (respiratory nitrate reductase), is responsible for the generation of protons under anaerobic conditions. The periplasmic NR or NAP, is though to be involved in redox balancing, using nitrate as an electron sink, and to be responsible for the initiation of aerobic denitrification, besides the role of nitrate elimination[3, 4].

III.2 Periplasmic nitrate reductase (NAP)

The periplasmic nitrate reductase (NAP), as mentioned before, is a respiratory NR located on the prokaryotic periplasm and takes part in the dissimilatory nitrate reduction pathway[1]. NAP is usually isolated as a heterodimeric enzyme, with a large subunit, NapA (with about 90 kDa) and a small subunit, NapB (with ca. 17 kDa). NapA contains a [4Fe-4S] cluster and binds to the Mo co-factor whereas NapB holds two *c*-type hemes and has a role in the electron transfer[3]. These enzymes interact with a tetraheme cytochrome, that transfers electrons to the NapAB complex, located on the membrane, related with the quinol oxidation[5].

The NAP isolated from *Desulfovibrio desulfuricans* ATCC 27774 (DdNAP) is, however, a monomeric enzyme with only one subunit (NapA) of molecular mass ca. 80 kDa and so far, this was the only monomeric NAP described. Assays with the apo-(nit-1)-nitrate reductase, spectroscopic studies and 3D structure determinations have confirmed the presence of a molybdenum co-factor (bis-molybdopterin guanine dinucleotide, MGD) and a [4Fe-4S] centre[6, 7] (Figure III.3). The Mo atom is coordinated by four thiolate ligands from the two MGD, one sulphur from Cys140 and an oxo/hydroxo group[2].

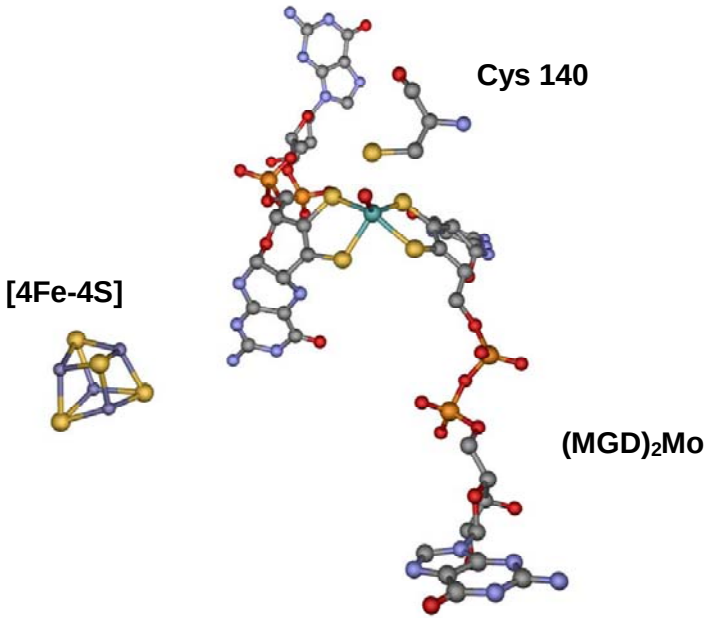

Figure III.3 Structure representation of the NAP molybdenum co-factor (bis-molybdopterin guanine dinucleotide, MGD) and the [4Fe-4S] centre (PDB ID 2NAP)[6].

The NAP approximate dimensions, determined by X-Ray diffraction at 1.9 Å resolution, are 65 Å x 65 Å x 50 Å. The structure presents a characteristic heart-shape in which can be seen a funnel-like cavity that provides access to the bis-MGD centre[3, 6]. The Mo is buried at approximately 15 Å of the surface, the iron-sulphur cluster is positioned at the molecule periphery and the MGD co-factor is extended across the molecule[6] (Figure III.4).

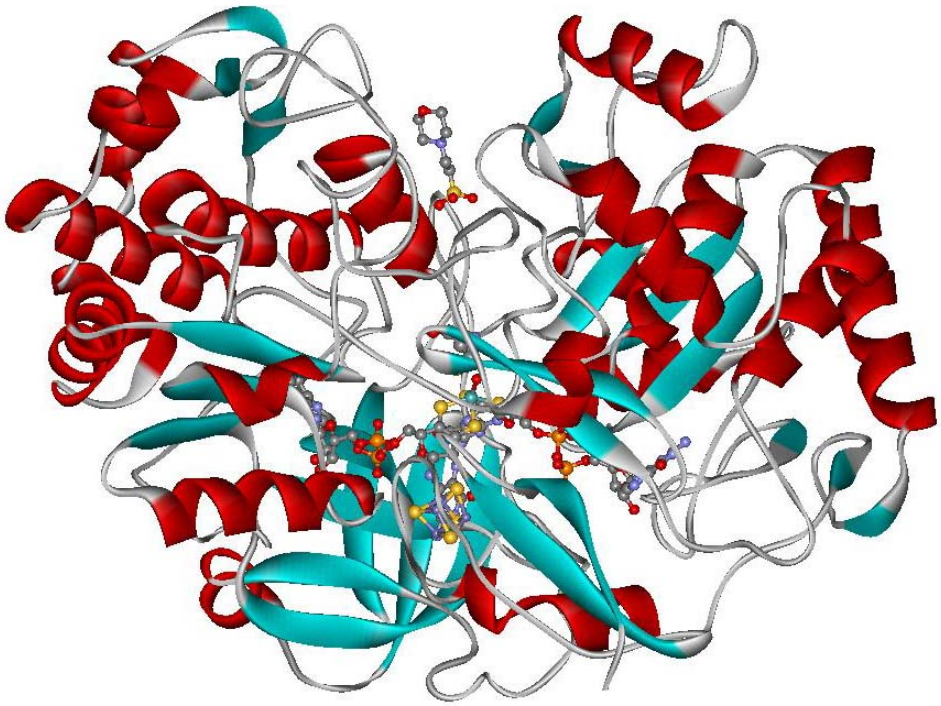

Figure III.4 NAP structure where it can be seen the characteristic heart-shape and the cavity that provides access to the MGD centre (PDB ID 2NAP)[6].

The catalytic reduction of nitrate occurs at the molybdenum co-factor when nitrate binds to the Mo at its reduced state. The NO_3^- subsequent reduction occurs with the simultaneous oxidation of Mo(IV) to Mo(VI). The Mo oxo/hydroxo ligand is directed towards the funnel channel and is linked to the oxidized Mo being lost when the metal is reduced and the current opinion is that the substrate/product entrance/exit should be done through this channel[2, 5, 6].

III.2.1 Redox behaviour

The redox potentials of the metallic centres of different nitrate reductases are reported on the literature. By EPR spectroscopy coupled with potenciometric titrations, the Mo(V)/(IV) and Mo(VI)/(V) redox potentials, from the respiratory nitrate reductase NarGHI isolated from *E. coli* were determined[8] with values, respectively, -50 $\pm$ 20 and +470 $\pm$ 20 mV.

Depending on the low-pH or high-pH form of the enzyme, differences on the Mo redox potentials were estimated. For the low-pH form the reported potentials of the Mo(VI)/(V) and Mo(V)/(IV) redox couples are, respectively, +450 and +200 mV; for the high-pH form (pH 8.1), the correspondent values are +250 and +90 mV[9]. A comparative study of the NapAB from *Rhodobacter sphaeroids* and its subunit NapA, which is very similar to the *D. desulfuricans* NAP, revealed for this one, midpoint redox potentials around –250 mV for the [4Fe-4S] cluster and +300 mV for the Mo(VI)/(V) couple[3]. Although the metal centres redox potentials have been determined potentiometrically, these couples voltammetric behaviour has only been reported in the presence of the substrate[4].

The electrocatalytic activity of NarGHI, isolated from *E. coli* and *P. pantotrophus*, was observed by cyclic voltammetry with the protein adsorbed on pyrolytic graphite. The Michaelis constants obtained in these systems are in agreement with the previous results in solution. The catalytic current develops at potential values below –100 mV[4, 8, 9].

The unmediated electron transfer response is achieved when the electrode substitutes the protein biological partner and it can be a powerful tool to provide information on the enzyme electron transfer potentials, mechanism and kinetics[10, 11].

III.2.2 Catalytic mechanism

The proposed catalytic mechanism for the nitrate reduction is based on the determined structure of the active centre (in the NAP reduced state), EXAFS and

ENDOR studies that have demonstrated the Mo centre coordination[6, 12]. In this proposal, nitrate binds to the reduced form Mo(IV) and a ligand is replaced by the nitrate molecule with this last subsequent reduction and simultaneous metal oxidation to Mo(VI). In the process, the abstraction of an oxygen atom from the binding molecule occurs and this remains as an oxo ligand of the metal (figure III.5). Finally, two protons and two electrons are transferred via the iron-sulphur cluster and the subsequent release of the oxo ligand with the Mo centre being again reduced to the initial state.

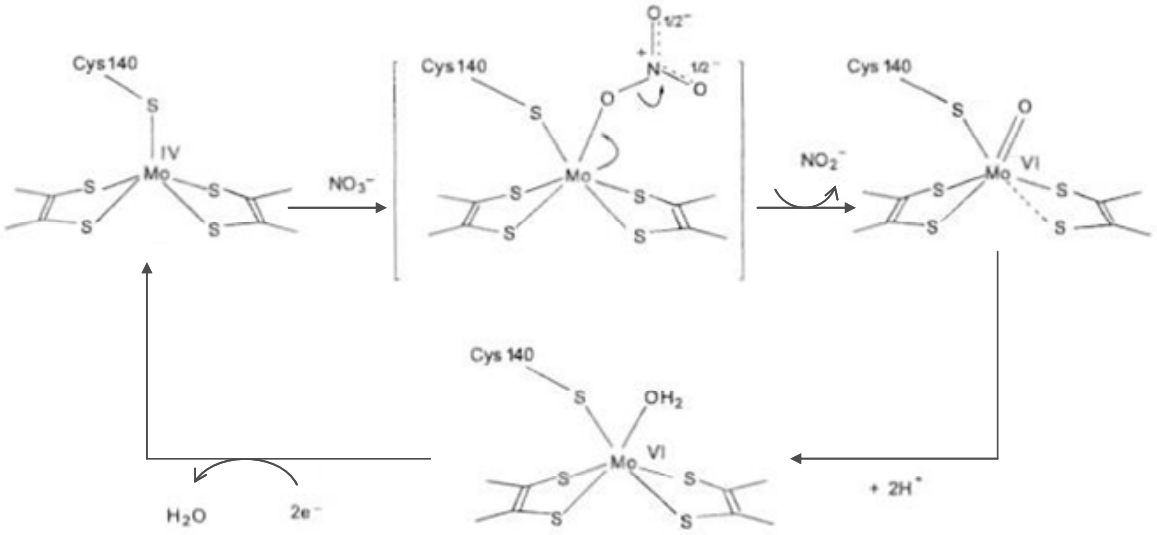

Figure III.5 Simplified catalytic mechanism for the NAP nitrate reduction (adapted from Dias *et al.*, 1999)[6].

The Mo centre has been demonstrated to have quite flexibility of coordination, with numerous active EPR species obtained at different potentials and also distinct inhibitors. The as-purified enzyme presents an EPR signal assigned to the Mo(V) species with experimental *g* values that reflect two non exchangeable species that should be due to the protons from the coordinated cysteine. The same signal under turnover conditions presents characteristics of a single non exchangeable proton, suggesting that Mo(V) may be a catalytic intermediate presenting a distorted six-coordinated site with the four sulphur from the two pterin co-factors, the Cys 140 and an oxo ligand[2, 13]. Recent discussions, based in ENDOR data, points to the inexistence of a Mo(V)-OH/OH_2 ligand, suggesting that the protonation of the oxo group occurs with the reduction of Mo(V) to Mo(IV) indicating that the reductive half

cycle may not contemplate a hydroxilated or hydrated Mo(V) intermediate[12]. This issue is still under debate and new electrochemical data may be important to its clarification.

III.3 NAP direct electrochemistry – results and discussion

We have studied the direct electrochemistry of the *Dd*NAP purified (in the laboratory)[13] from *Desulfovibrio desulfuricans* ATCC 27774 at pyrolitic graphite and gold electrodes. NAP was immobilized by adsorption on the electrode surface or using a membrane to retain the enzyme in a thin layer-like configuration electrode. The protein redox behaviour was observed and, for the first time, the metal centres voltammetric features are reported. A preliminary evaluation of the electrocatalytic activity of the *Dd*NAP obtained with the enzyme adsorbed on graphite is also reported.

III.3.1 Direct electrochemical response

The protein metallic centres, namely the [4Fe-4S] and the Mo co-factor, were investigated. NAP was studied by cyclic and square wave voltammetry using a membrane electrode (see Appendix A for the details) in 50 mM Tris-HCl medium with 0.1 M NaCl as supporting electrolyte at pH 7.

A typical response of the NAP immobilized on the membrane/gold electrode at low scan rates is displayed on figure III.5. The development of reproducible cathodic and anodic waves, attributed to the enzyme, respectively around -300 and -210 mV vs. SCE (figure III.6) were observed.

At the potential window between -600 and +400 mV, at low scan rates (1 to 50 mV s^{-1}) no further processes can be distinguished. The estimated formal potential, E°', is -244 ± 12 mV (-2 ± 12 mV vs. NHE) and it was calculated by the mean of the

anodic and cathodic peak potentials ($(Ep_c+Ep_a)/2$), which remained constant, within the experimental error, in the considered scan rate range.

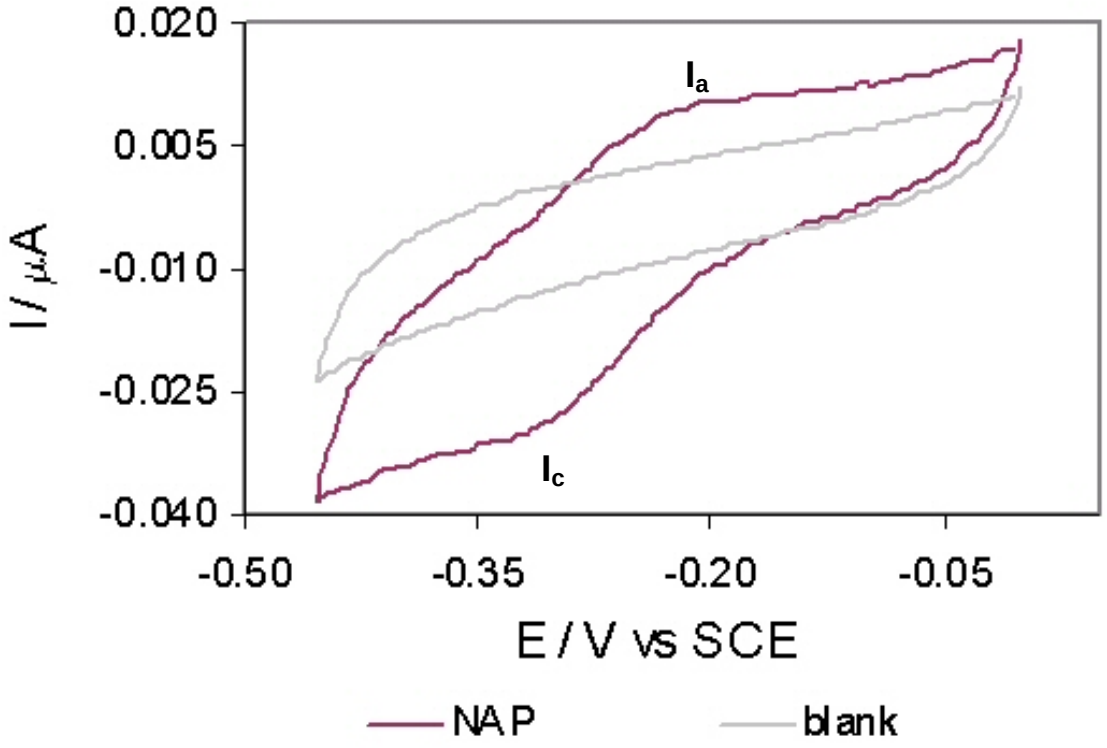

Figure III.6 Cyclic voltammogram of the NAP on Au/membrane electrode and comparison with the control assay without the presence of the enzyme; ν = 10 mV s^{-1}.

The scan rate variation shows that a good correlation, in the range 1 to 15 mV s^{-1}, is obtained between this parameter and the current intensity. At this scan rate range the separation peak values, ΔE_p, increases with the scan rate and the Ip_a/Ip_c ratio is close to unity. The cyclic voltammograms of process I obtained at different scan rates are plotted at figure III.7.

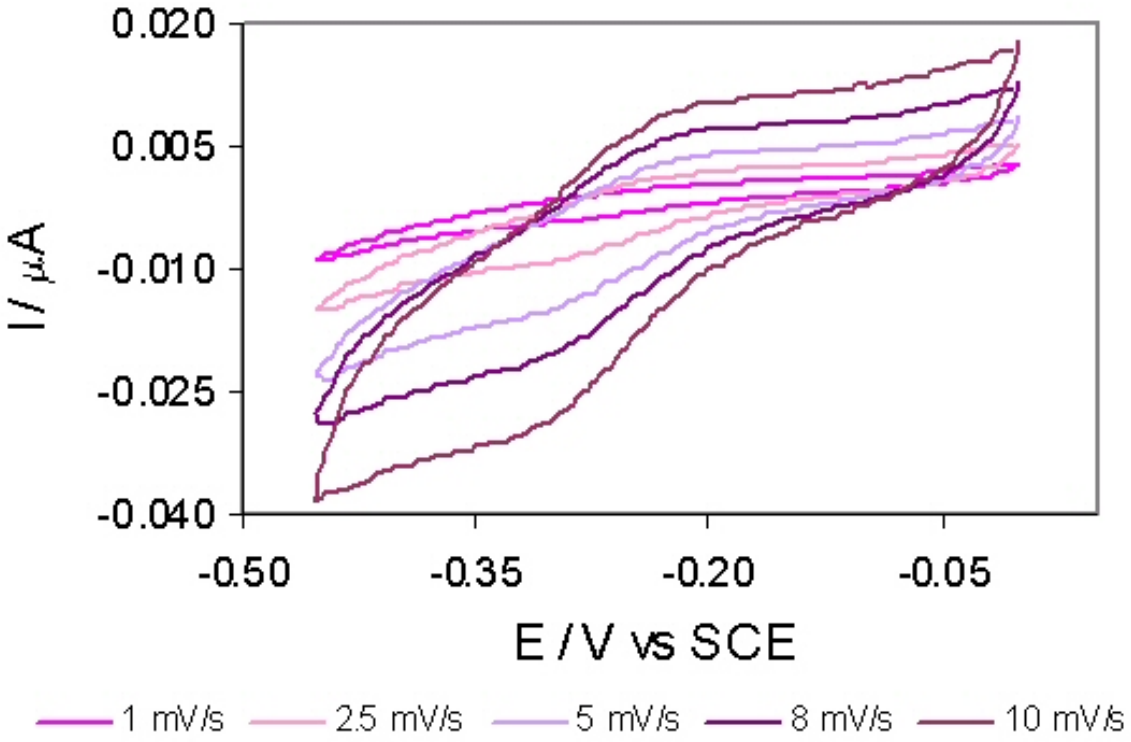

Figure III.7 NAP cyclic voltammograms at different scan rates on the Au/membrane electrode.

After the imposition of a constant potential of -600 mV for a few minutes, another redox process (denoted by II) becomes visible at more positive potential values, as displayed on figure III.8. The formal redox potential for process II, E$^{o'}$, is 19 ± 9 mV (261 ± 9 mV vs. NHE). The requirement of applying a negative potential for some time to be able to observe this redox centre, may be related to a possible rearrangement of the amino acid environment that take part in the electronic pathway.

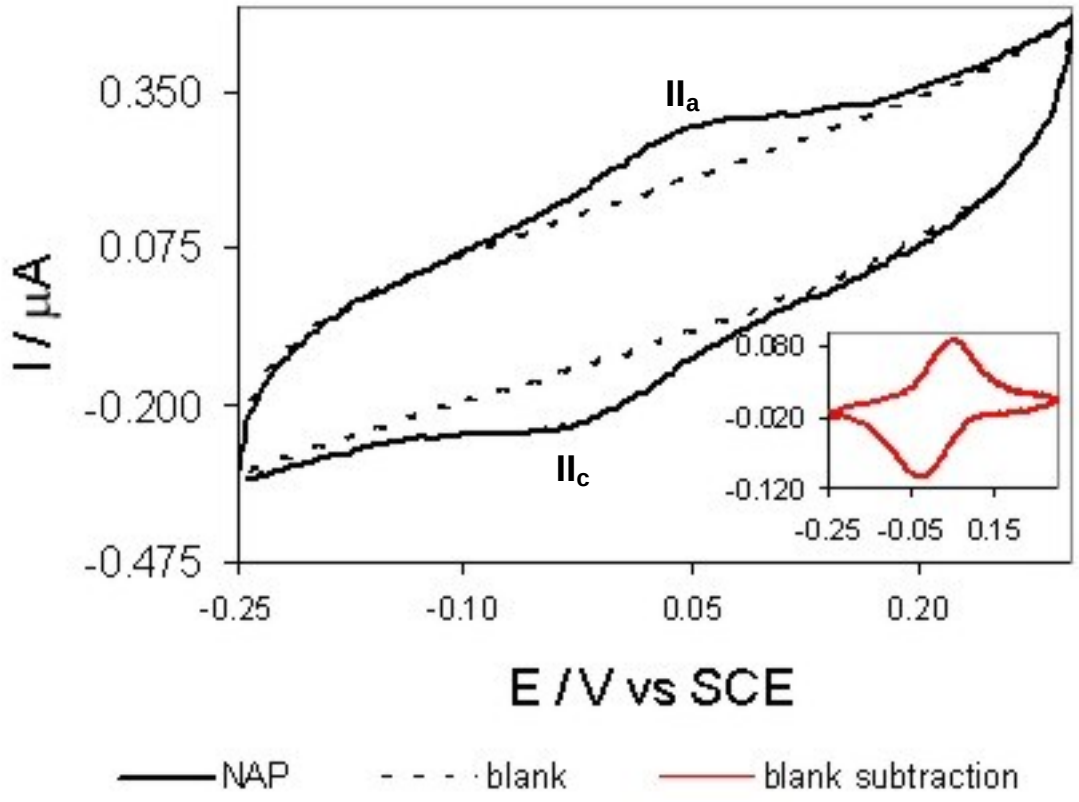

Figure III.8 Process II redox couple at the Au/membrane electrode after the imposition of –600 mV vs. SCE for 10 min and comparison with the control assay performed in the absence of the enzyme. Inset: subtraction of the control allows better observe the process.

Process II is better observed at higher scan rates. This process also presents the same features as process I, namely, direct proportionality between the current peak intensity and the potential peak separation with the scan rate, as shown in figure III.9. The Ip_a/Ip_c ratio approaches unity, especially in the highest scan rates in which process II is better discriminated.

The observed features of processes II and I are coherent with the thin layer model behaviour, as expected for a membrane electrode[14].

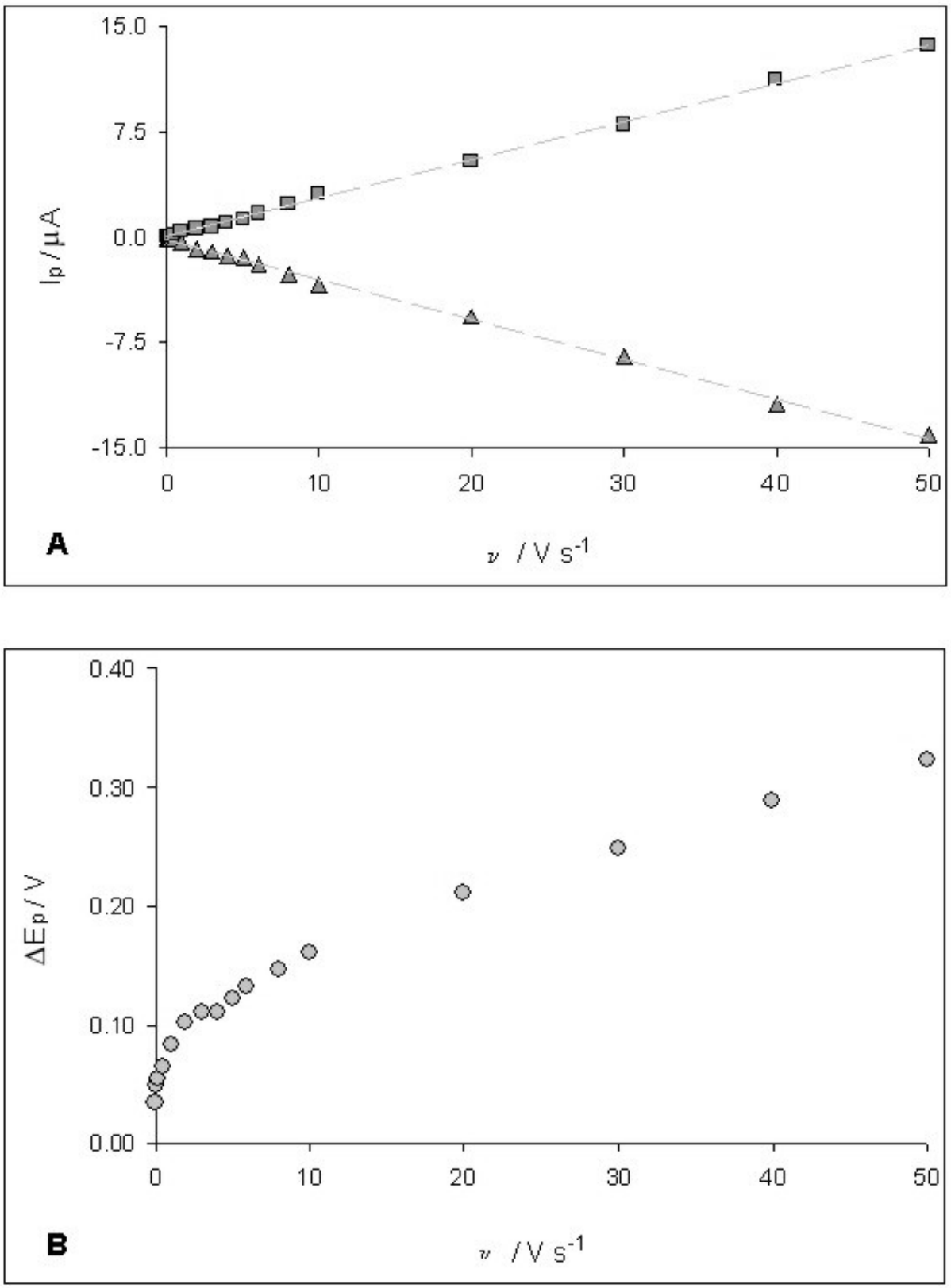

Figure III.9 Process II A) current intensity variation with the scan rate and B) the difference between the anodic and the cathodic potential peaks variation with the scan rate.

Processes II and I are also visible by SWV on the same gold/membrane electrode (figure III.10) with maxima current intensities approximately at -100 and -285 mV, respectively. The current intensity is proportional to the applied frequency, as exemplified in figure III.11 for process II. Process I, as in CV, is better seen at lower scan rates and the current vs. frequency plot is only proportional until a frequency value of 20 Hz. The value of E_p and the half-height peak width, $W_{1/2}$, remain constant within the experimental conditions. The SWV technique characteristics, in terms of its time scale, allow the discussion to be made in terms of a diffusion-controlled system[15].

The $W_{1/2}$ values found for processes I and II were 118 ± 5 and 128 ± 5 mV, respectively. These results are in agreement to the expected for a system with a behaviour close to the reversibility and with one electron transfer redox processes ($W_{1/2}$ = 124 mV theoretically)[16, 17].

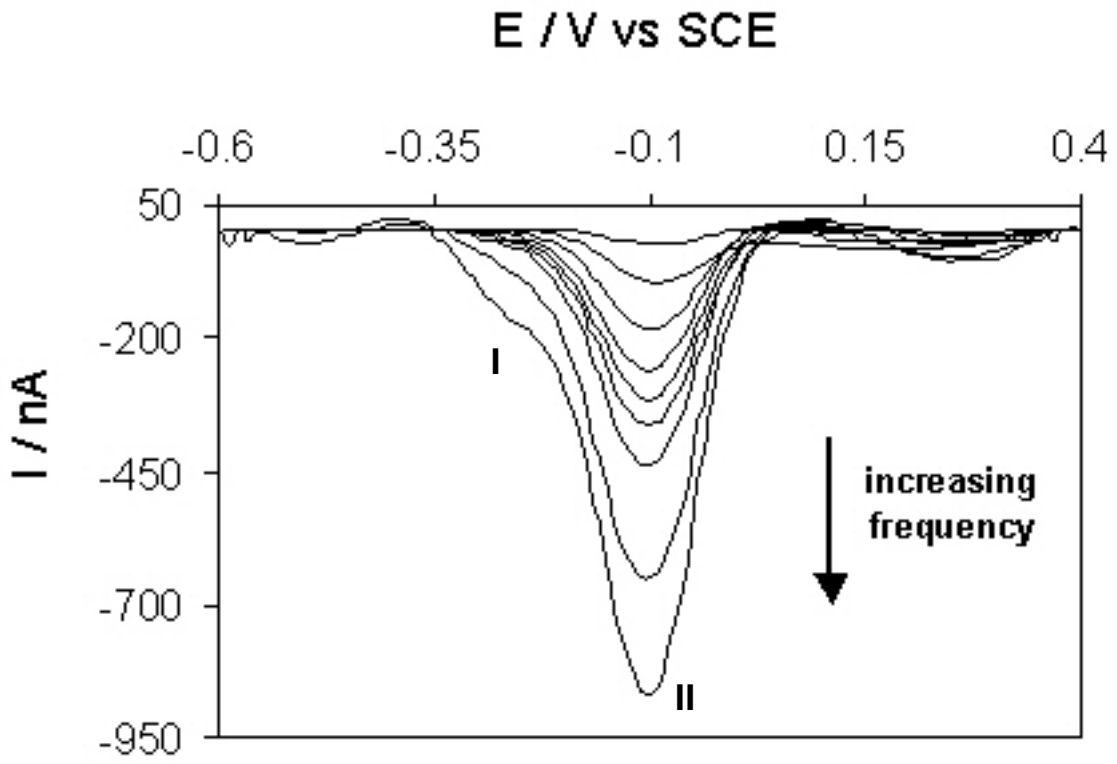

Figure III.10 SWV for the NAP at the Au/membrane electrode, showing processes I and II, observed after the imposition of a polarization potential of -600 mV for 10 min; variable frequency: 8, 20, 40, 60, 80, 100, 150 and 200 Hz; step height 10 mV and potential amplitude 50 mV.

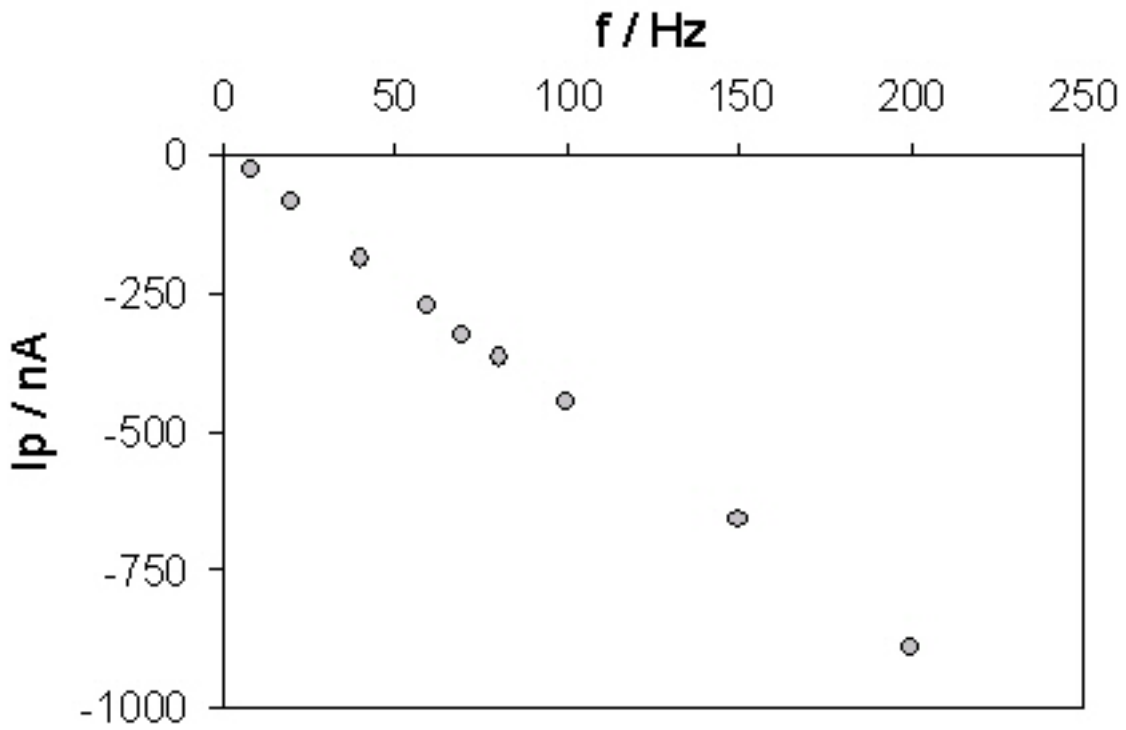

Figure III.11 Plot of the maximum current intensity of the SWV for the NAP at the Au/membrane electrode, showing processes I and II, observed after the imposition of a polarization potential of -600 mV for 10 min; SWV parameters are: variable frequency 8, 20, 40, 60, 80, 100, 150 and 200 Hz; step height 10 mV and potential amplitude 50 mV.

After multiple sequential cycles at fast scan rates it is possible to observe the development of another redox process, designated as III (figure III.12). On the cyclic voltammograms the new anodic peak, III_a, is observed around –75 mV (+167 mV vs. NHE). The cathodic counterpart, III_c, develops around -120 mV (+122 mV vs. NHE). This process can also be observed by square wave voltammetry (inset of Figure III.12) with a midpoint potential of -128 mV (114 mV vs. NHE).

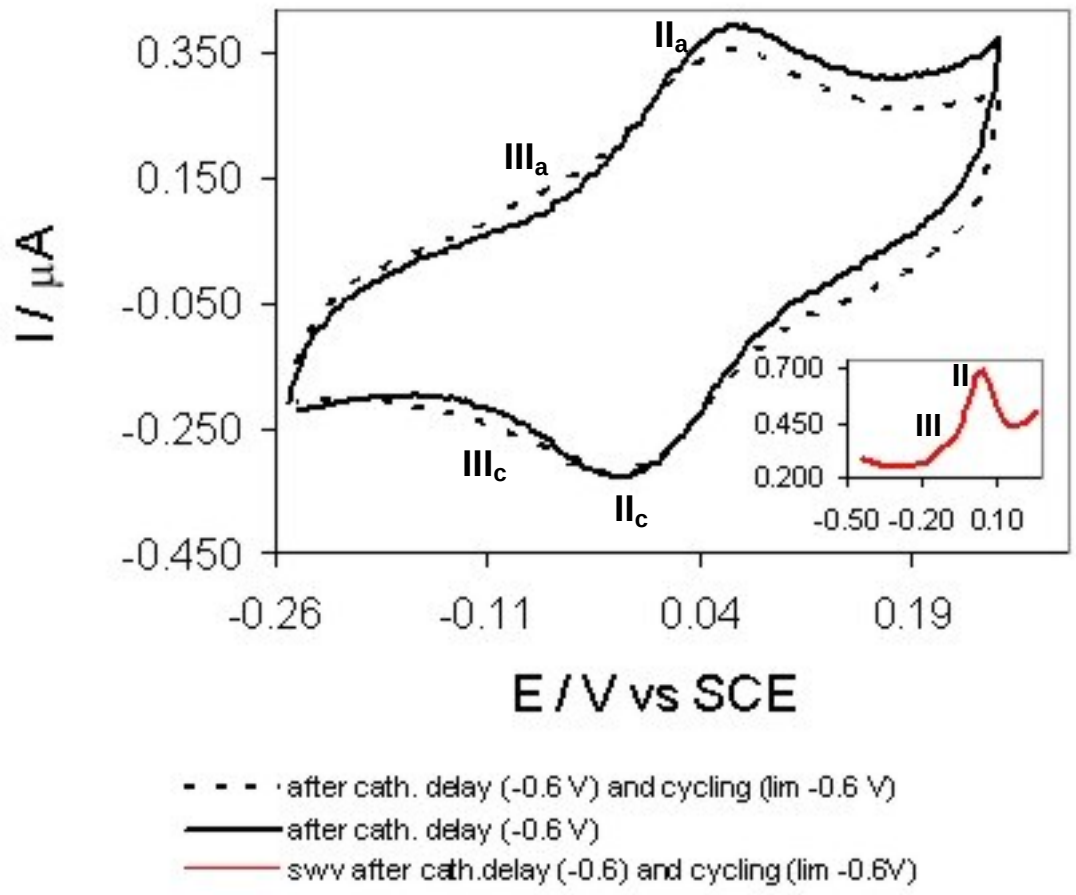

Figure III.12 After cathodic polarisation at –600 mV for 10 min and repetitive cycling over the potential range –300 to 200 mV at ν = 500 mV s^{-1}, two new, anodic and cathodic, waves are observed. The process is also observed by SWV (inset): frequency 8 Hz, step height 10 mV, potential amplitude 50 mV.

Considering a thin layer model system, the thickness of the layer can be calculated by the plot of Ip vs. ν, according to the equation

$$Ip = \frac{n^2 F^2 \nu V c}{4RT} \qquad (1)$$

where n is the number of electrons, ν, the scan rate, V the thin layer volume, c the solution concentration and R, T and F have the usual meanings. With the volume it can estimated the thickness, l, of the thin layer. In our experiments, for the Au/membrane electrode, this value is typically 3 μm. Using Laviron's mathematical formalism, for a known thickness, it is possible to estimate the heterogeneous charge transfer rate constants, k_{sh}, for processes I and II from the peak potential separation values and the scan rate[14, 18]. The heterogeneous electron rate constants calculated

for the processes I and II were, k_{sh} = $5x10^{-6}$ and $8x10^{-4}$ cm s^{-1}, respectively. The different order of magnitude of the k_{sh} is in agreement with the different behaviour of the two redox processes. In fact, process I is much better seen at low scan rates and process II, by opposition at higher scan rates. These differences are clearly observed in figure III.13, showing the evolution of the cyclic voltammograms of the two processes as the scan rate increases.

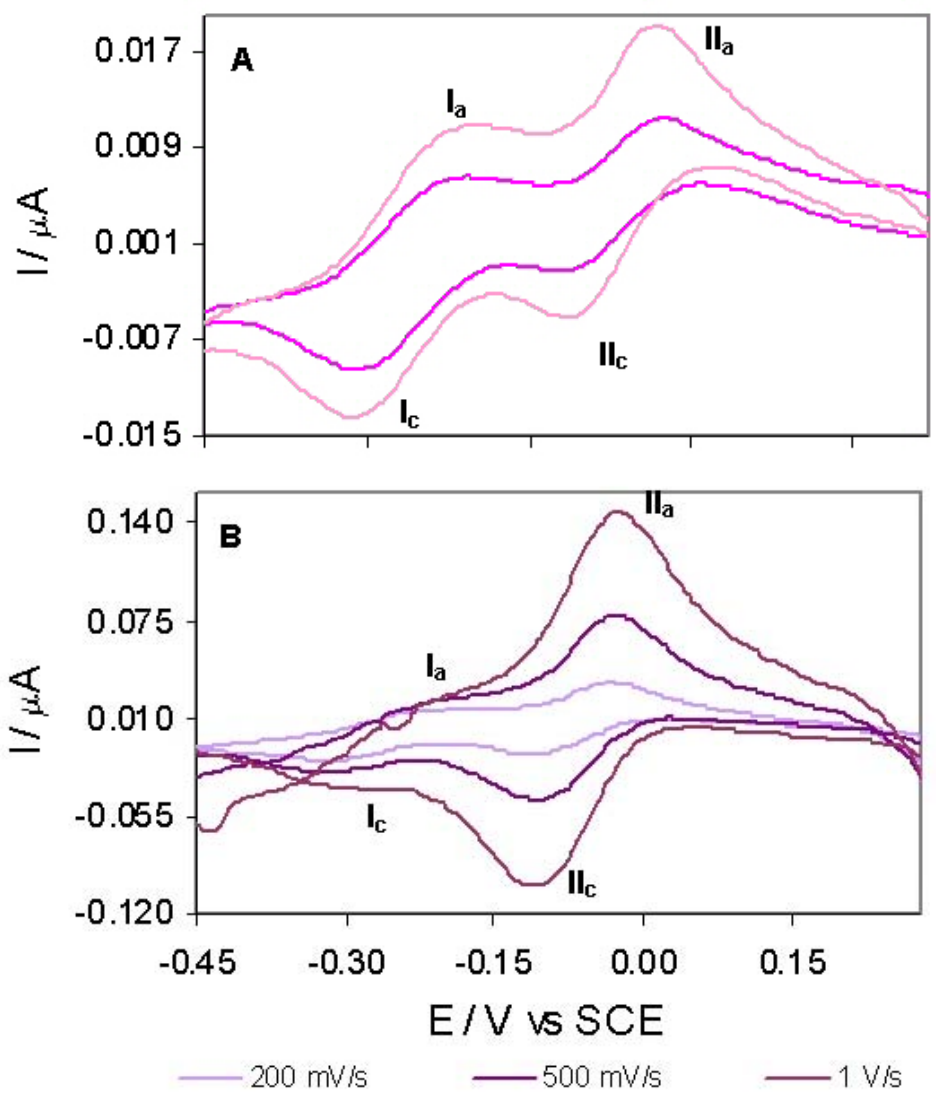

Figure III.13 Cyclic voltammograms showing the two redox processes that were attributed to [4Fe-4S] and MGD-Mo (see below in the text) different behaviour with increasing scan rates on Au/membrane electrode.

Considering that both processes are due to one electron transfer reactions and by comparison with the literature for similar systems with nitrate reductase enzymes[3, 9, 19-23] we have assign process I to the [4Fe-4S] cluster and process II to the Mo(V)/Mo(VI) redox couple. Process III that is observed at high scan rates, close to process II may be due to the Mo(IV)/Mo(V) redox couple. This couple is not frequently reported although there is a study of an *E. coli* NAR where its potential was determined by EPR redox titrations at pH 7.4, with a potential of +95 mV vs. NHE[9]. The reason why is so difficult to observe Mo(V) by potentiometric techniques may be related to its low stability.

The results show that it is possible to achieve direct electrochemistry between the protein and the gold surface. It was not possible to observe, though, the catalytic response of NAP with this electrode. The electrocatalysis was achieved with the protein immobilized by adsorption on graphite (see next section III.3.2). This raises the question of the possible NAP orientation towards the different electrode surfaces. Figure III.14 shows the protein electrostatic surface.

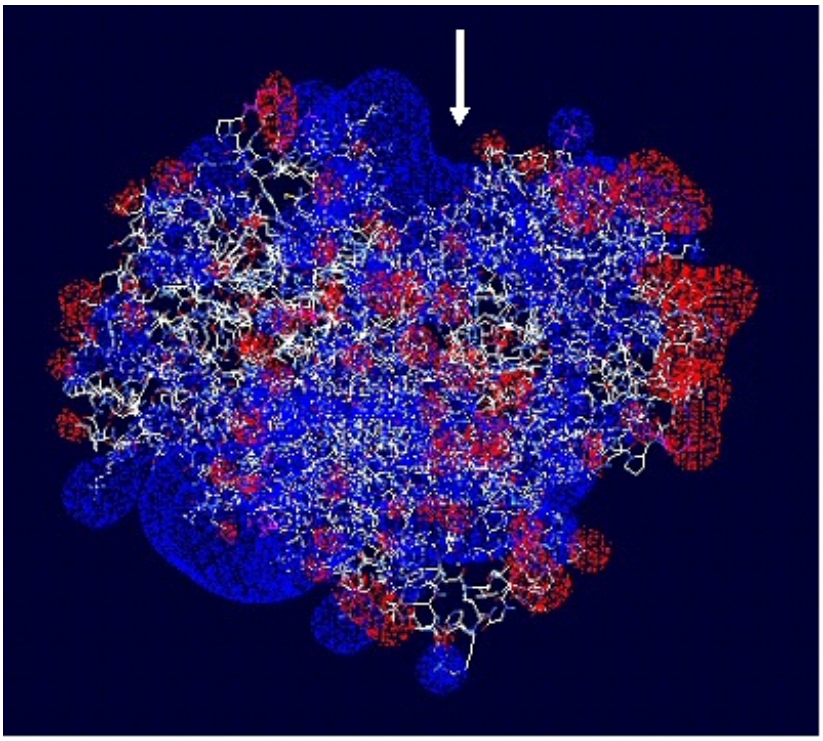

Figure III.14 NAP electrostatic surface charge, calculated with the DeepView/Swiss-Pdb Viewer software program, v.3.7 (available at http://www.expasy.org/spdbr/); showing the positive (+0.25 eV, blue) and negative (-0.25 eV, red) isopotential lines.

As can be seen the funnel-like cavity towards the Mo active site is a positive charged region. Some negative charge areas are displayed but more relevant is the extensive positively region in the opposite site of the cavity that gives nitrate access to the bis-molybodpterin centre, which should facilitate the nitrate entrance towards the MGD-MO centre.

The differences in the NAP behaviour when immobilised on gold/membrane and graphite may be due to its surface potential charge and the electrodes charge. In fact, graphite has a highly functionalized surface with different C-O groups, which confer a negative surface charge. In this case, the orientation of the protein as it adsorbs on the surface, should be influenced by strong electrostatic attraction between the extensive positively charged region of NAP and the electrode surface. The cavity that gives access to the Mo centre should, therefore, become faced to the solution and available to the nitrate entrance. It was not possible, however, to observe the centres redox features on graphite, probably due to the small protein amount effectively adsorbed.

By other hand, gold is a metallic surface with no functionality. The cellulose membrane used for the immobilisation is negatively charged. This may influence the NAP orientation towards the electrode, because the highly positive charged region is probably faced towards the membrane, opposite to the electrode surface which may result in obstruction of the nitrate into the NAP cavity, and so, no catalysis is observed. This is also in agreement with the fact that the addition of neomycin (with amino groups) to the solution enhances the currents observed at the gold electrode. In fact, neomycin is widely used to improve the interaction between negatively charged proteins and gold surfaces, namely in similar systems with Mo proteins[24].

III.3.2 Catalytic Activity

Experiments with NAP adsorbed on graphite were performed. Using this electrode material it was not possible, as mentioned before, to observe the redox features of the enzyme metallic centres. In contrast, it was possible to obtain catalytic activity towards nitrate reduction.

The influence of the nitrate concentration on the catalytic voltammetric response is shown at Figure III.15. It can be observed that the current intensity increases with the nitrate concentration. The catalytic current develops at potentials below -180 mV (+62 mV vs. NHE), which is a potential value quite apart from the redox potential assigned to the Mo(V)/Mo(VI) centre. This discrepant behaviour, showing that the catalysis develops at much lower potentials than the formal redox centre potential, has already been described by other authors for different nitrate reductase enzymes[21, 22, 25] .

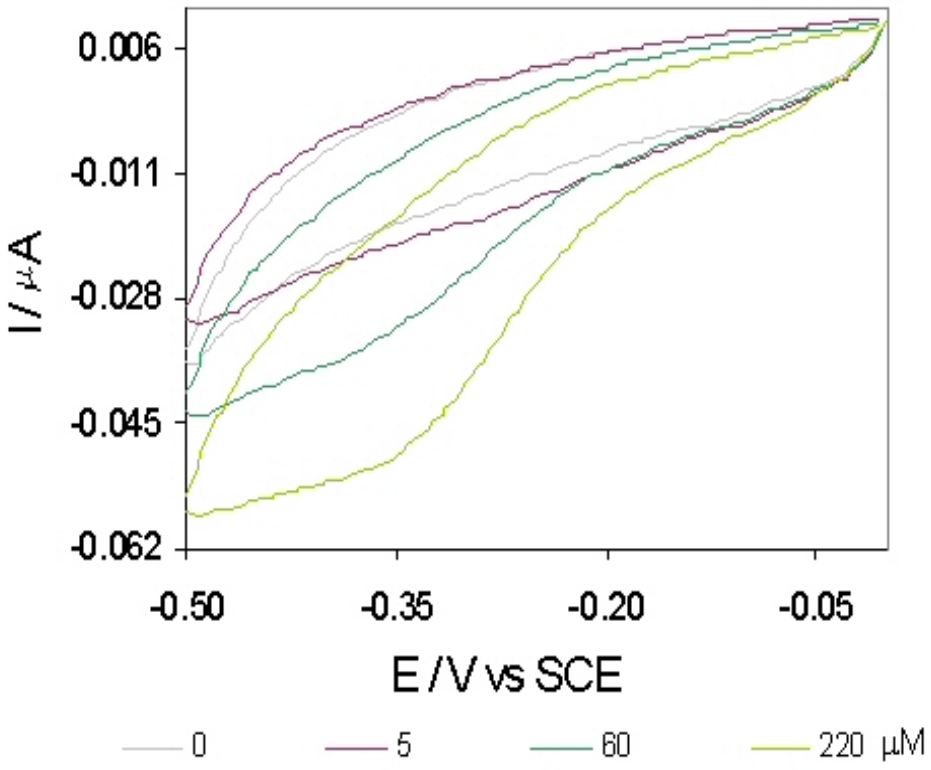

Figure III.15 Variation of the catalytic voltammetric response, on pyrolitic graphite electrode, with different nitrate concentrations; ν = 2.5 mV s^{-1}.

The broader catalytic wave, obtained at potential values much lower that the expected considering the MGD-Mo redox potentials, may be related with the catalytic mechanism features (coupling of electrochemical and chemical reactions), namely bond breaking and redox-linked reorganization[25].

The variation of the measured catalytic current density with different nitrate concentrations was fitted to a Michaelis-Menten expression (figure III.16)

$$i_{cat} = \frac{i_{\max}.C_{nitrate}}{C_{nitrate} + K_M}$$

From the fit, it is possible to calculate the values of the Michaelis constant, K_M, and the catalytic current observed at the maximum turnover rate, I_{max}. The experimental values obtained are K_M= 35 μM (nitrate) and i_{max} = 23.5 nA cm^{-2}.

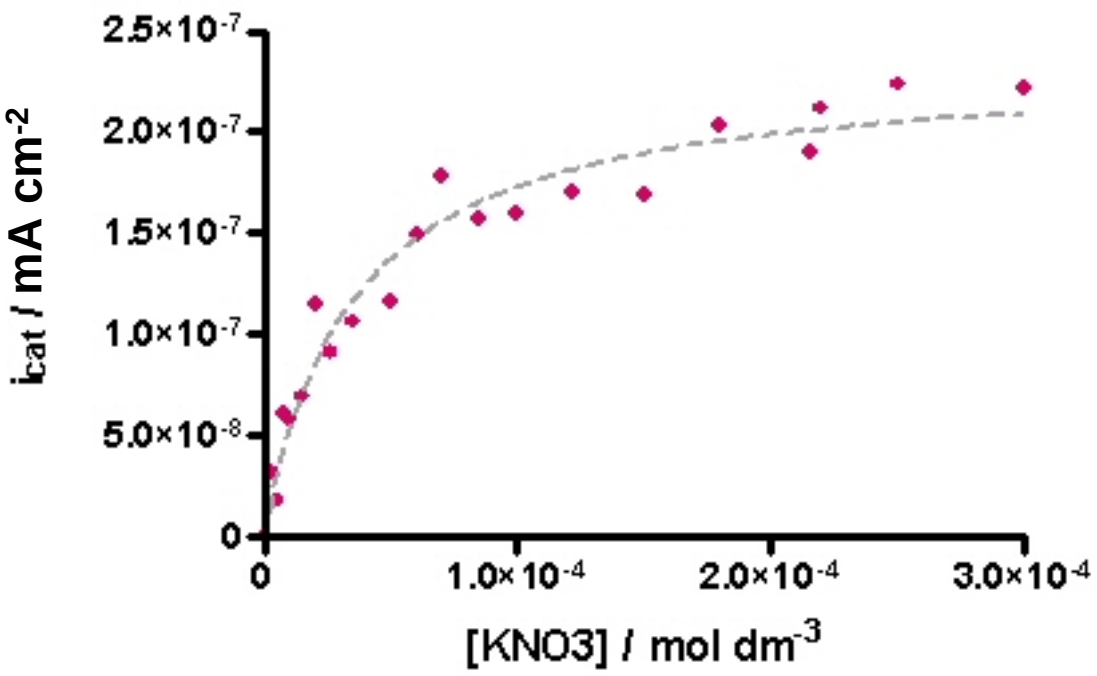

Figure III.16 Plot of the variation of the measured catalytic current density with different nitrate concentrations fitted to a Michaelis-Menten equation.

The estimated K_M is similar to the value already published obtained by spectroscopic assays with the NAP in solution[7]. This is an evidence that the adsorption of the protein does not affect its functional properties.

III.4. Final Remarks

The direct electrochemical response of the NAP was observed on gold / membrane electrodes. For the first time it was possible to observe the direct voltammetric features of the NAP metallic centres ([4Fe-4S] and the Mo co-factor) and to determine the correspondent redox potentials. Different redox features were obtained with different electrode materials.

The NAP immobilized on gold electrodes does not present catalytic activity, possibly related to its orientation towards the electrode surface. The adsorbed NAP on graphite presents electrocatalytic activity and the immobilisation does not seem to affect its properties.

III.5. References

1. Stolz, J. F.; Basu, P., Evolution of nitrate reductase: molecular and structural variations on a common function. *Chembiochem* **2002,** 3, (2-3), 198-206.

2. Gonzalez, P. J.; Correia, C.; Moura, I.; Brondino, C. D.; Moura, J. J., Bacterial nitrate reductases: Molecular and biological aspects of nitrate reduction. *J Inorg Biochem* **2006,** 100, (5-6), 1015-23.

3. Arnoux, P.; Sabaty, M.; Alric, J.; Frangioni, B.; Guigliarelli, B.; Adriano, J. M.; Pignol, D., Structural and redox plasticity in the heterodimeric periplasmic nitrate reductase. *Nat Struct Biol* **2003,** 10, (11), 928-34.

4. Martinez-Espinosa, R. M.; Richardson, D. J.; Butt, J. N.; Bonete, M. J., Respiratory nitrate and nitrite pathway in the denitrifier haloarchaeon Haloferax mediterranei. *Biochem Soc Trans* **2006,** 34, (Pt 1), 115-7.

5. Richardson, D. J.; Berks, B. C.; Russell, D. A.; Spiro, S.; Taylor, C. J., Functional, biochemical and genetic diversity of prokaryotic nitrate reductases. *Cell Mol Life Sci* **2001,** 58, (2), 165-78.

6. Dias, J. M.; Than, M. E.; Humm, A.; Huber, R.; Bourenkov, G. P.; Bartunik, H. D.; Bursakov, S.; Calvete, J.; Caldeira, J.; Carneiro, C.; Moura, J. J.; Moura, I.; Romao, M. J., Crystal structure of the first dissimilatory nitrate reductase at 1.9 A solved by MAD methods. *Structure* **1999,** 7, (1), 65-79.

7. Bursakov, S.; Liu, M. Y.; Payne, W. J.; Legall, J.; Moura, I.; Moura, J. J., Isolation and preliminary characterization of a soluble nitrate reductase from the sulfate reducing organism Desulfovibrio desulfuricans ATCC 27774. *Anaerobe* **1995,** 1, (1), 55-60.

8. Anderson, L. J.; Richardson, D. J.; Butt, J. N., Catalytic protein film voltammetry from a respiratory nitrate reductase provides evidence for complex electrochemical modulation of enzyme activity. *Biochemistry* **2001,** 40, (38), 11294-11307.

9. Elliot, S. J. H., K. R.; Heffron, K.; Palak, M.; Rothery, R. A.; Weiner, J. H.; Armstrong, F. A. , Voltammetric Studies of the Catalytic Mechanism of the Respiratory Nitrate Reductase from Escherichia coli: How Nitrate Reduction and Inhibition Depend on the Oxidation State of the Active Site. *Biochemistry* **2004,** 43, (3), 799-807.

10. Butt, J. N.; Thornton, J.; Richardson, D. J.; Dobbin, P. S., Voltammetry of a flavocytochrome c(3): the lowest potential heme modulates fumarate reduction rates. *Biophys J* **2000,** 78, (2), 1001-9.

11. Ferapontova, E. E.; Ruzgas, T.; Gorton, L., Direct electron transfer of heme- and molybdopterin cofactor-containing chicken liver sulfite oxidase on alkanethiol-modified gold electrodes. *Anal Chem* **2003,** 75, (18), 4841-50.

12. Butler, C. S.; Fairhurst, S. A.; Ferguson, S. J.; Thomson, A. J.; Berks, B. C.; Richardson, D. J.; Lowe, D. J., Mo(V) co-ordination in the periplasmic nitrate reductase from Paracoccus pantotrophus probed by electron nuclear double resonance (ENDOR) spectroscopy. *Biochem J* **2002,** 363, (Pt 3), 817-23.

13. Gonzalez, P. J.; Rivas, M. G.; Brondino, C. D.; Bursakov, S. A.; Moura, I.; Moura, J. J., EPR and redox properties of periplasmic nitrate reductase from Desulfovibrio desulfuricans ATCC 27774. *J Biol Inorg Chem* **2006**.

14. Laviron, E., General expression of the linear potential sweep voltammogram in the case of diffusionless electrochemical systems. *Journal of Electroanalytical Chemistry* **1979,** 101, (1), 19-28.

15. M. M. Correia dos Santos, P. M. P. d. S., M. L. Simões Gonçalves, L. Krippahl, J. J. G. Moura, É. Lojou and P. Bianco, Electrochemical studies on small electron transfer proteins using membrane electrodes. *J Electroanal Chem* **2003,** 541, 153-162.

16. Kounaves, S. P. O. D., J. J.; Chandreesekhar, P.; Osteryoung, J., Square Wave Voltammetry at the Mercury Film Electrode: Theoretical Treatment. *Anal Chem* **1986,** 58, (14), 3199-3202.

17. O'Dea, J. J. O. J. O. R. A., Theory of Square Wave Voltammetry for Kinetic Systems. *Anal Chem* **1981,** 53, (4), 695-701.

18. Bard, A. J. F., L. R., *Electrochemical Methods-Fundamentals and Applications*. John Wiley&Sons: New York, **1980**.

19. Magalon, A.; Rothery, R. A.; Giordano, G.; Blasco, F.; Weiner, J. H., Characterization by electron paramagnetic resonance of the role of the Escherichia coli nitrate reductase (NarGHI) iron-sulfur clusters in electron transfer to nitrate and identification of a semiquinone radical intermediate. *J Bacteriol* **1997,** 179, (16), 5037-45.

20. Blasco, F.; Guigliarelli, B.; Magalon, A.; Asso, M.; Giordano, G.; Rothery, R. A., The coordination and function of the redox centres of the membrane-bound nitrate reductases. *Cell Mol Life Sci* **2001,** 58, (2), 179-93.

21. Frangioni, B.; Arnoux, P.; Sabaty, M.; Pignol, D.; Bertrand, P.; Guigliarelli, B.; Leger, C., In Rhodobacter sphaeroides respiratory nitrate reductase, the kinetics of

substrate binding favors intramolecular electron transfer. *JACS* **2004,** 126, (5), 1328-9.

22. Jepson, B. J.; Anderson, L. J.; Rubio, L. M.; Taylor, C. J.; Butler, C. S.; Flores, E.; Herrero, A.; Butt, J. N.; Richardson, D. J., Tuning a nitrate reductase for function. The first spectropotentiometric characterization of a bacterial assimilatory nitrate reductase reveals novel redox properties. *J Biol Chem* **2004,** 279, (31), 32212-8.

23. Butler, C. S.; Charnock, J. M.; Bennett, B.; Sears, H. J.; Reilly, A. J.; Ferguson, S. J.; Garner, C. D.; Lowe, D. J.; Thomson, A. J.; Berks, B. C.; Richardson, D. J., Models for molybdenum coordination during the catalytic cycle of periplasmic nitrate reductase from Paracoccus denitrificans derived from EPR and EXAFS spectroscopy. *Biochemistry* **1999,** 38, (28), 9000-12.

24. Margarida M. Correia dos Santos, P. M. P. S., M. Lurdes S. Gonçalves, M. João Romão, Isabel Moura, José J. G. Moura, Direct electrochemistry of the *Desulfovibrio gigas* aldehyde oxidoreductase. *Eur J Biochem* **2004,** 271, (7), 1329-1338.

25. Anderson, L. J.; Richardson, D. J.; Butt, J. N., Using direct electrochemistry to probe rate limiting events during nitrate reductase turnover. *Faraday Discuss* **2000**, (116), 155-69; discussion 171-90.

Chapter IV

Electrochemistry of Nitric Oxide Reductase

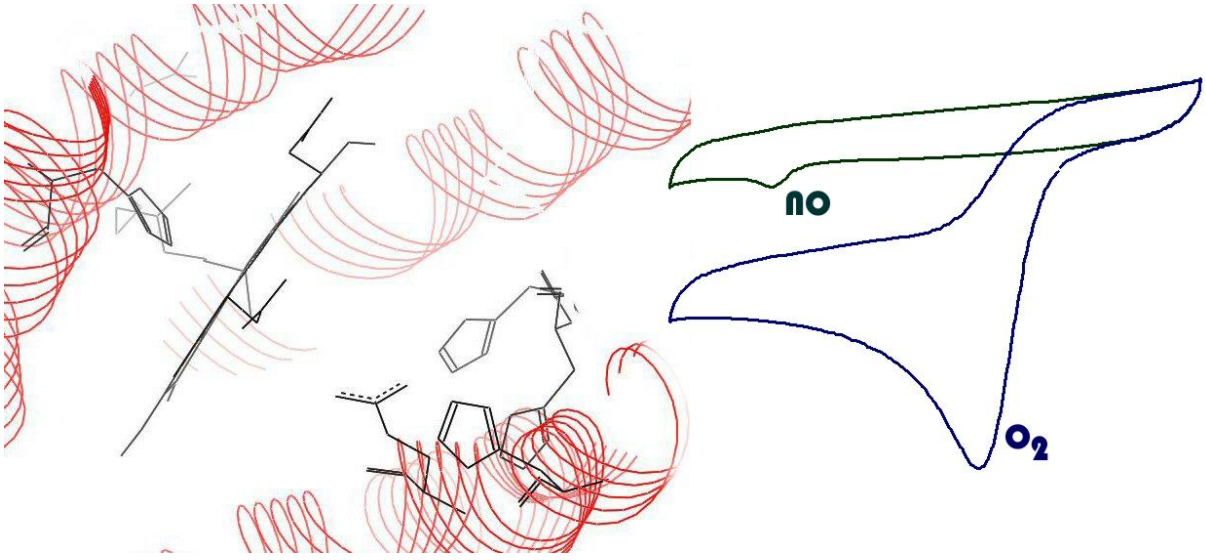

Electrochemistry of Nitric Oxide Reductase

IV.1 Nitric Oxide Reductase

Nitric oxide (NO) is a well known molecule for its toxicity. However, in the recent past it was possible to establish also important physiological roles for NO. In these are included blood pressure regulation, neurotransmission and immune response[1]. Detailed studies on NO biochemical activity are of outcome importance for scientific and even economic reasons.

Nitric-oxide reductase (NOR) is a membrane bound enzyme involved in the denitrification pathway (figure IV.1). NOR promotes the two electrons reduction of NO to N_2O, according to the following reaction,

$$2NO + 2\bar{e} + 2H^+ \rightleftharpoons N_2O + H_2O$$

with the consequent formation of a double N-N bond. This bond in nature occurs mainly during the denitrification process.

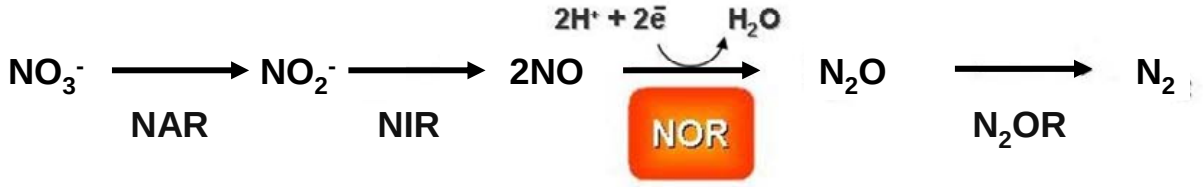

Figure IV.1 Scheme of the denitrification pathway, showing the relative position of the nitric oxide reductase enzyme.

NOR belongs, together with the cytochrome oxidases (cyt. oxidase), to the same enzyme superfamily of the heme-copper cytochrome oxidases. These oxidase type of enzymes usually catalyse the oxygen reduction in the respiratory chain. High homology was found between the NOR larger subunit and the correspondent larger subunit (the catalytic subunit) of the heme-copper cytochrome oxidases. Both reveal to be formed by 12 transmembrane helices containing six conserved histidines. This type of enzymes present two active redox centres in the catalytic subunit that are bonded by the above mentioned conserved histidines (His)[2, 3].

NOR was found and isolated from several denitrifying bacteria such as *Paracoccus denitrificans*, *Halomonas halodenitrificans*, *Pseudomonas stutzeri*, *Pseudomonas aeruginosa*, *Rastonia eutropha* or *Bacillus azotoformans*[4].

Three types of NOR were isolated, depending on the smaller subunit type. These are named cNOR, qNOR or qCu_ANOR, depending on the electron transfer subunit (figure IV.2). cNOR type is a cytochrome *bc* complex, with two subunits. The electron donors are cytochromes *c* or other small proteins such as azurin. The second type, qNOR, has only one subunit, and the electron donor is a hydroquinone or menahydroquinone molecule. The qCu_ANOR consists in two subunits but also uses menahydroquinone as the electron donor. The smaller subunit contains a Cu_A centre (binuclear $Cu_2(\mu\text{-}Cys)_2(His)_2$)[5].

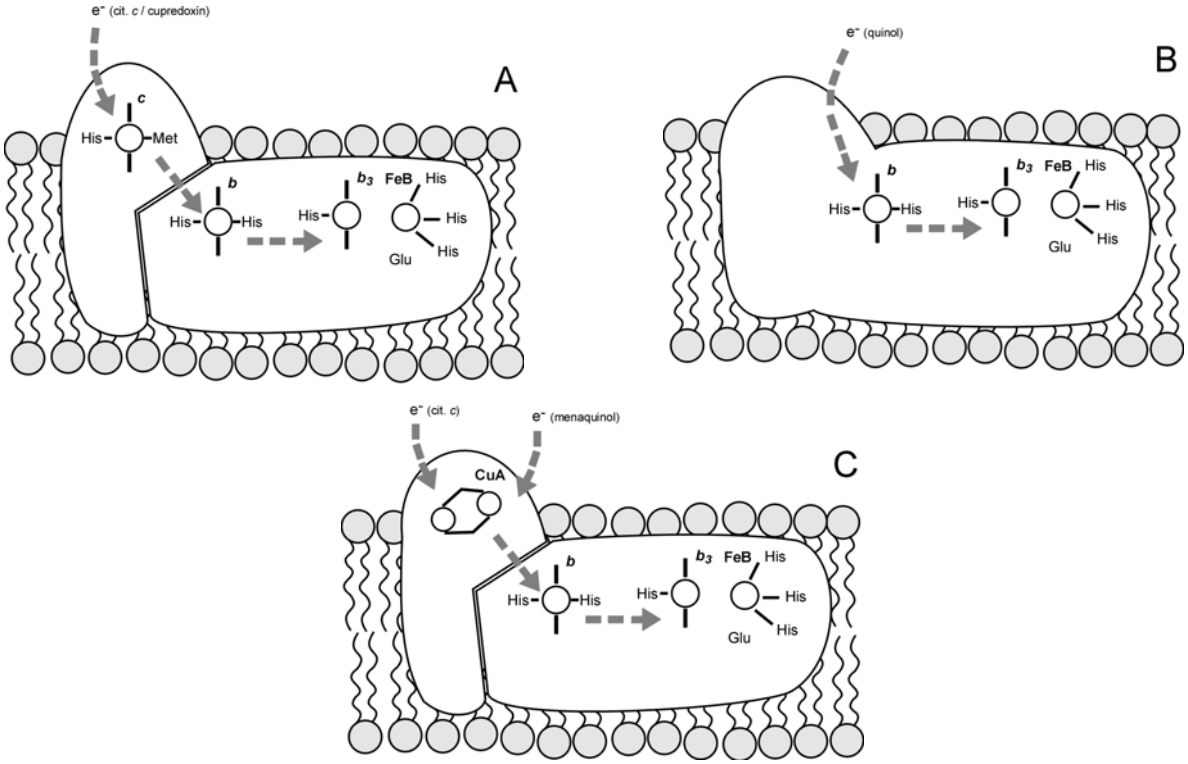

Figure IV.2 Representation of the three different nitric oxide reductase enzymes, namely A) cNOR, B) qNOR and C) qCu_ANOR (Tavares, 2006)[6].

The cNOR protein is composed by two subunits, NorC and NorB, of 17 and 56 kDa weight. The smaller subunit NorC, anchored on the cell membrane, contains a low spin heme *c*, which is the enzyme electron acceptor[7]. NorB subunit contains two *b* type hemes, a low spin heme *b* and a high spin heme b_3, and a non-heme iron (Fe_B).

Spectroscopic studies have shown that the non-heme iron should be in the ferric state and that is probably coupled to the high spin heme b_3 by an oxo/hydroxo bridge[7]. The catalytic site is described as a spin-coupled binuclear centre formed by one heme *b* (heme b_3) and the Fe_B [3, 7]. By homology with cyt *c* oxidase it is likely that four conserved histidines should be ligands of the binuclear centre (figure IV.3). The electron transfer towards the catalytic centre is accomplished via heme *c* in the NorC subunit[2].

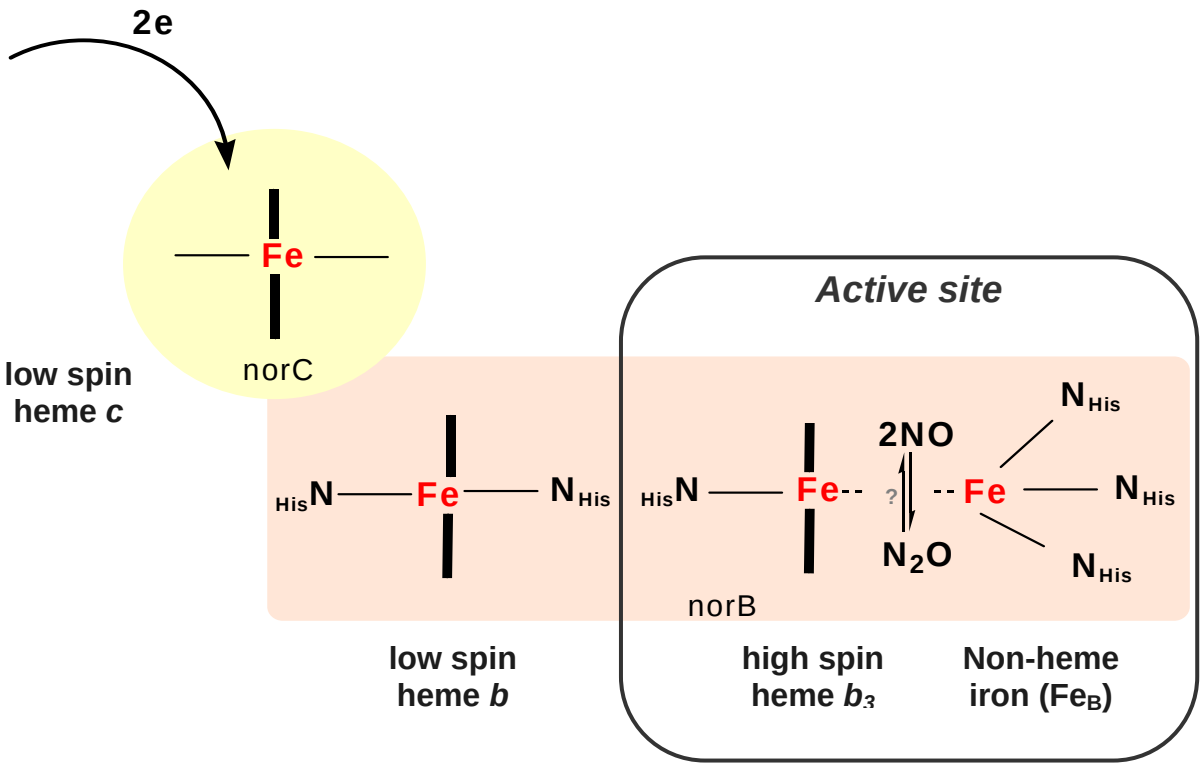

Figure IV.3 Schematic representation of the cNOR metallic centres.

The crystallographic structure of cNOR was not yet obtained. The comparison of the sequence of the NorB, the correspondent subunit of the heme-copper cytochrome *c* oxidases and the analysis of the crystal structure (cyt. *c* oxidase from *Paracoccus denitrificans*) allowed to generate a three dimensional model for the NorB from *Pseudomonas stutzeri* (figure IV.4). The model shows a highly hydrophobic molecule with small limited areas exposed to the cytoplasm and the periplasm sides of the membrane. The already mentioned 12 helices are distributed in three semi-circles forming arc-like structures[8]. The six conserved His coordinate the low spin heme *b*, the high spin heme b_3 and the non-heme iron Fe_B. In the model based on the *Pseudomonas stutzeri*, His207, His258 and His259 coordinate the Fe_B[8].

The NO reduction requires the entrance of electrons and protons. Studies with NOR incorporated inside lipossomes have proved that the turnover is electroneutral, which implies that there is no proton pumping mechanism and so, the protons needed for the catalysis are taken from the same side of the membrane as the electrons, the periplasmic side[9]. This implies that a proton pathway must exist from the periplasmic side of the membrane into the catalytic site. Based on mutagenesis studies this route seems to involve the conserved glutamate residues, namely Glu125 and Glu198, that appear to be essential to the normal NO reduction activity[10].

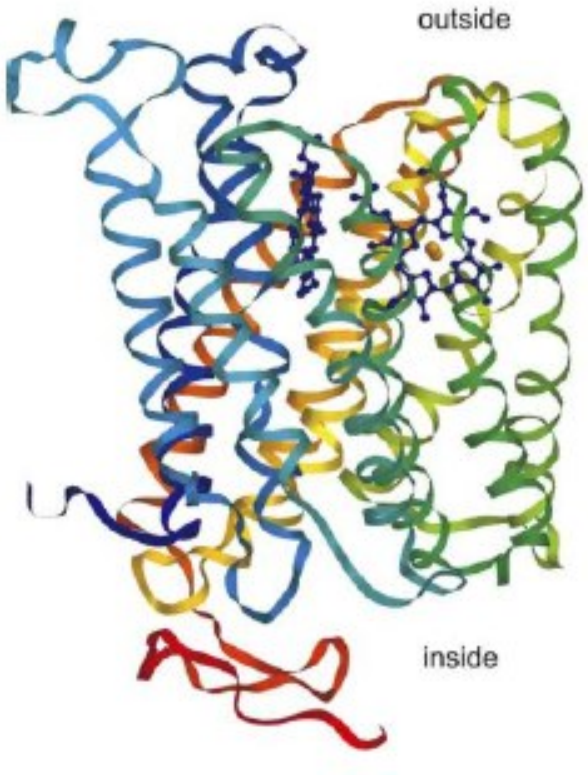

Figure IV.4 Model of the structure of the NorB subunit of the cNOR based on the crystal structure of the *Paracoccus denitrificans* cytochrome *c* oxidase (Zumft, 2005)[8]

The active form of the enzyme seems to require a three electron reduction in which hemes *b* and *c* will pass to the +2 oxidation state and Fe_B will remain in the +3 state. This implies the cleavage of an oxo/hydroxo bridge between heme b_3 and Fe_B[6]. The catalytic mechanism is still under discussion. Several models have been proposed, based in two different mechanisms (figure IV.5), namely the so-called *trans* mechanism, that requires the binding of one NO molecule to each of the iron atoms in the binuclear centre and the *cis* mechanism, in which the both substrate molecules

bond to the non-heme Fe_B[7, 11]. Some studies proved the formation of nitrosyl complexes both with the heme and the non-heme iron, but these are not sufficient to discriminate between the two mechanisms as the heme-nitrosyl complex was also interpreted as an inhibited state induced by high substrate concentrations binding to the oxidised enzyme[7].

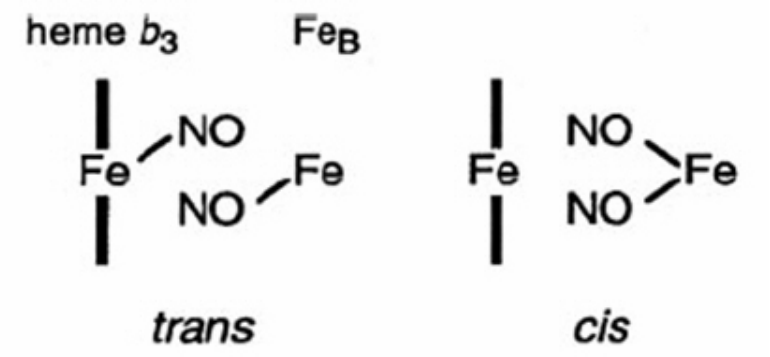

Figure IV.5 Simplified representation of the *cis* and *trans* proposed mechanisms for the NO reduction by the NOR enzyme (Shiro, 2004)[11].

Recently, some theoretical studies of the nitric oxide reduction by a heme-copper oxidase, based on DFT (density functional theory), have shown a possible mechanism in which N_2O is formed in heme *b*3, so-called *cis*:*b*3 mechanism[6, 12]. A schematic representation of the proposed mechanism is shown in figure IV.6.

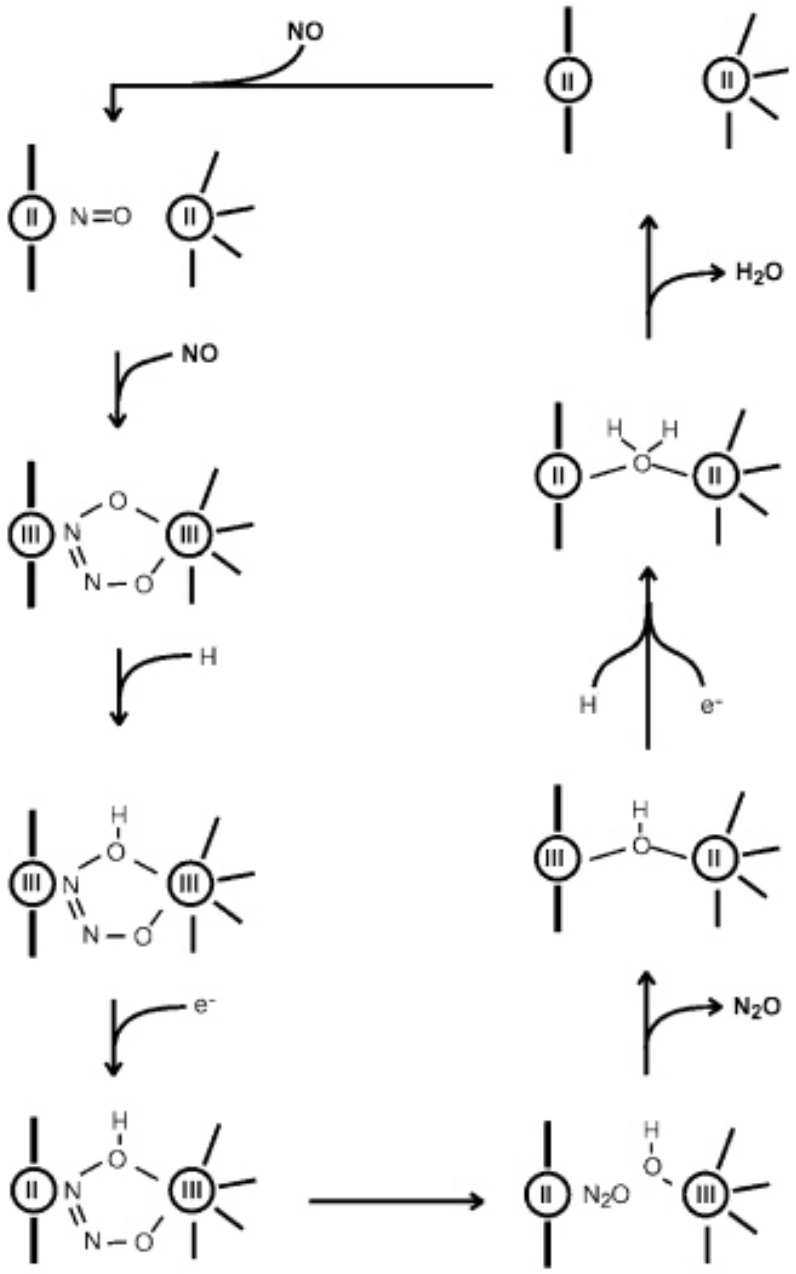

Figure IV.6 Schematic representation of the *cis*:*b*3 mechanism of the NO reduction (Tavares, 2006)[6].

Midpoint redox potentials of the different metallic centres were estimated by mediated redox titrations studies of the NOR obtained from *Paracoccus denitrificans*. The midpoint potential found for the heme *c* of the NorC subunit was +280 mV and for the heme *b* in the NorB subunit +322 to +345 mV (*versus* standard hydrogen electrode, SHE). The midpoint potential of heme *c* was also shown to shift towards more negative potential values, namely +183 mV, due to the interaction with the

subunit NorB. The potential of heme *c* is consistent with the role of the electron entrance in the protein and transference to the heme *c* of the NorB subunit, which is a currently accepted hypothesis. A much lower potential for heme b_3, circa +60 mV was found. The redox potential of the non-heme iron was estimated to be +320 mV. The low potential value of the heme b_3 produces a thermodynamic barrier for the two electron reduction of the binuclear centre. This has been interpreted as a defense mechanism against the formation of an inhibitory specie (reduced heme b_3 bonded to NO) during the catalytic reaction [8, 13].

Heering *et a*l., through mediated catalysis experiments using Iso-Cytochrome c (YCC) from bakers yeast, have accomplished to prove that the enzyme can accept electrons from YCC and it raised the question about the possibility of the existence of multiple catalytic states in NOR [14].

The direct electron transfer between the immobilised enzyme and the electrode is an important tool to understand the electron transfer mechanisms in biological systems, since the electrode replaces the physiological redox partner, allowing the gathering of thermodynamic and kinetic information[15, 16].

IV.2 Direct Electrochemistry of Nitric Oxide Reductase

In the present work, NOR purified from *Pseudomonas nautica* 617 was immobilized at graphite electrodes and its direct electrochemical response was achieved for the first time, by cyclic voltammetry. The detailed purification and characterization is described by Timóteo[17, 18].

The NOR adsorbed on graphite (see Appendix A for the experimental details) presents direct redox response that is typically observed for high scan rates (equal or above 500 mV s^{-1}), as expected for a surface process. The cyclic voltammograms present a well defined redox couple, nominated process I, (figure IV.7), corresponding to one electron transfer, with midpoint potential, $E^{o'}$= -368 $\pm$ 13 mV (-126 $\pm$ 13 mV vs. NHE).

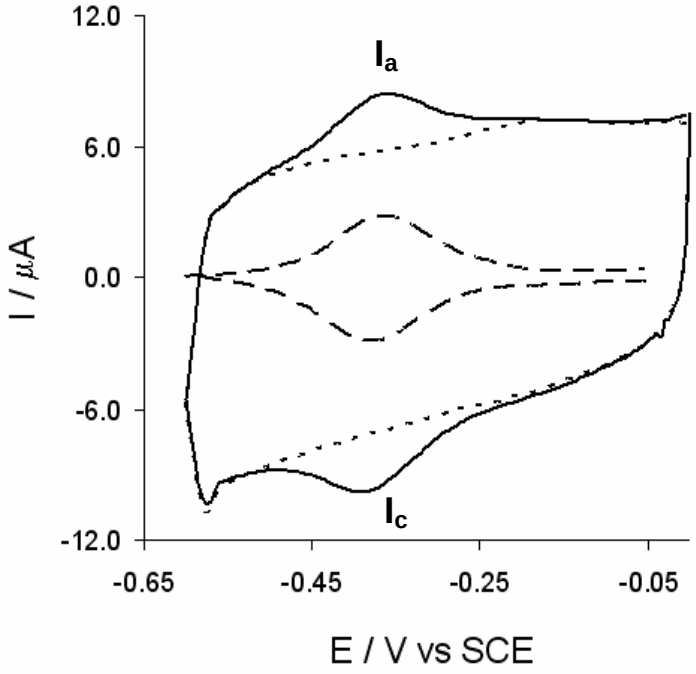

Figure IV.7 High scan rate (2 V s^{-1}) cyclic voltammograms of the immobilised NOR on graphite electrode, in a highly degassed solution (mix buffer II, see Appendix A), in 100 mM Tris-HCl, pH 7.6. Solid line corresponds to the adsorbed enzyme, thin dashed line represents the control, without enzyme, and the thick dashed line is the result of the two previous results subtraction. Subscript *a* and *c* stand for anodic and cathodic, respectively.

The calculated midpoint potential value is close to values found in other heme proteins systems[16]. In some *Pseudomonas* cells studies low midpoint potentials were also found for membrane bound cyt *c* oxidase *b*-type hemes (+64 mV at pH 7 and -8 mV at pH 9, vs. NHE)[19]. From the area of the redox peaks, and subsequently the charge, the electrode coverage with active enzyme was calculated as $(1.52 \pm 0.17)x10^{-11}$ mol cm^{-3} of immobilised NOR.

The current intensity ratio, I_a/I_c, is close to one and the peak intensity is linearly proportional to the scan rate, with a small peak separation which increases for scan rates above 5 V s^{-1} (figure IV.8) and that is a characteristic behaviour of a surface confined process with no diffusion control.

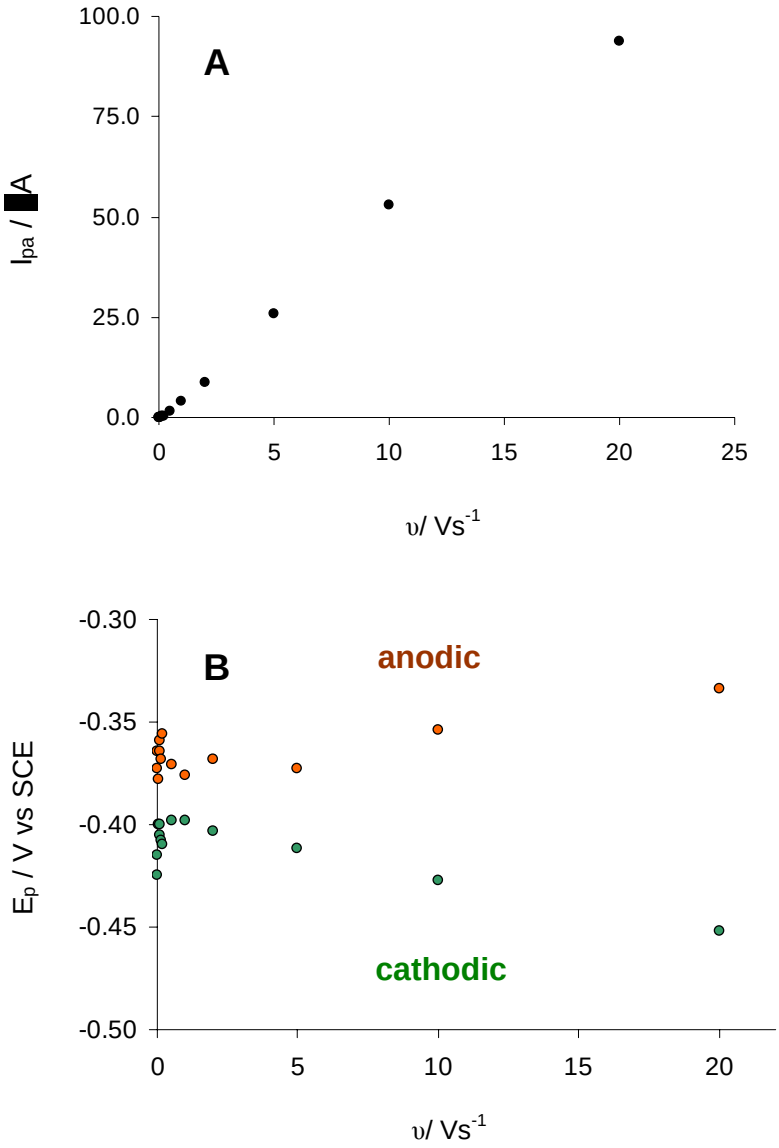

Figure IV.8 Plot of the A) maximum peak current and B) peak potential dependence on the scan rate for the immobilised NOR.

Using Laviron's formulation[20] a maximum value of the rate constant, k_s, for the redox reaction correspondent to process I was estimated (for ν = 5 V s^{-1}) as 1.73 s^{-1} (figure IV. 9). This value is within the usual estimated rate constant range for immobilised enzymes[16, 21].

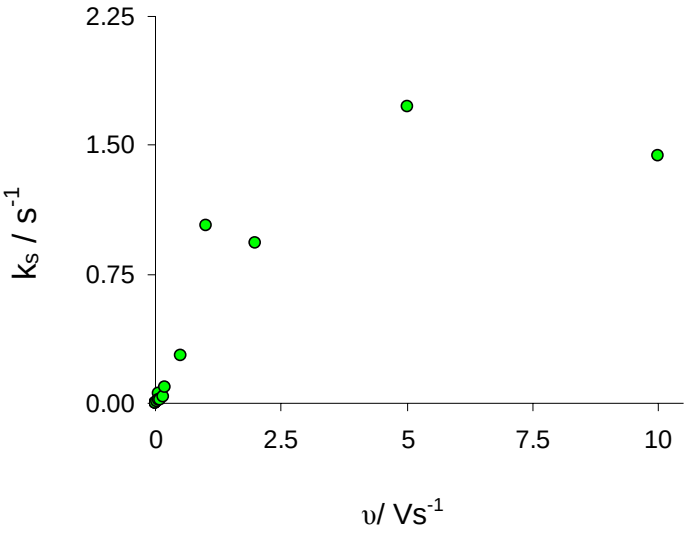

Figure IV.9 Plot of the determined rate constants, K_s, with the different scan rates, using Laviron's formulation.

The NOR modified electrode response is stable for several hours and after multiple scanning the observed electroactivity of this redox couple remains almost unaltered (see section IV.3.2).

The redox response stability of the immobilised NOR may be explained by its adsorption from a solution containing detergent (0.02% sodium dodecyl maltoside). The surfactant is known to help to stabilize the enzyme film and to retain the protein native properties[22, 23].

The observed redox couple I was ascribed to the heme b_3, reported in the literature as having a midpoint potential of +60 mV vs. NHE. This value was however estimated by potentiometric titrations performed with redox mediators in solution and using dithionite and ferricyanide as reductant and oxidant respectively[13], quite different conditions from the ones applied in the present study. These different used methodologies can also be the explanation for the difference found with the value reported in the literature. Besides, there are studies that show that the immobilisation on a surface can lower the midpoint potential value of the proteins metallic centres[24, 25]. Our results from the direct electrochemistry seem to confirm the abnormally lower potential for the binuclear centre heme b_3 taking into account the potential values found for the remaining NOR centres.

IV.3 Electrocatalytic activity

The catalytic activity of NOR was tested by cyclic voltammetry towards the oxygen and the nitric oxide reduction reactions. The experiments were performed by addition of saturated buffer with the respective dissolved gases, separately. This was the first time, for our knowledge, that the catalytic activity of this enzyme was demonstrated by cyclic voltammetry.

IV.3.1 Activity towards the oxygen reduction

In the presence of oxygen, and different experimental conditions, namely slower scan rates, the development of a reduction current at -285 ± 11 mV (-43 ± 11 mV vs. NHE) can be observed, as displayed in figure IV. 10.

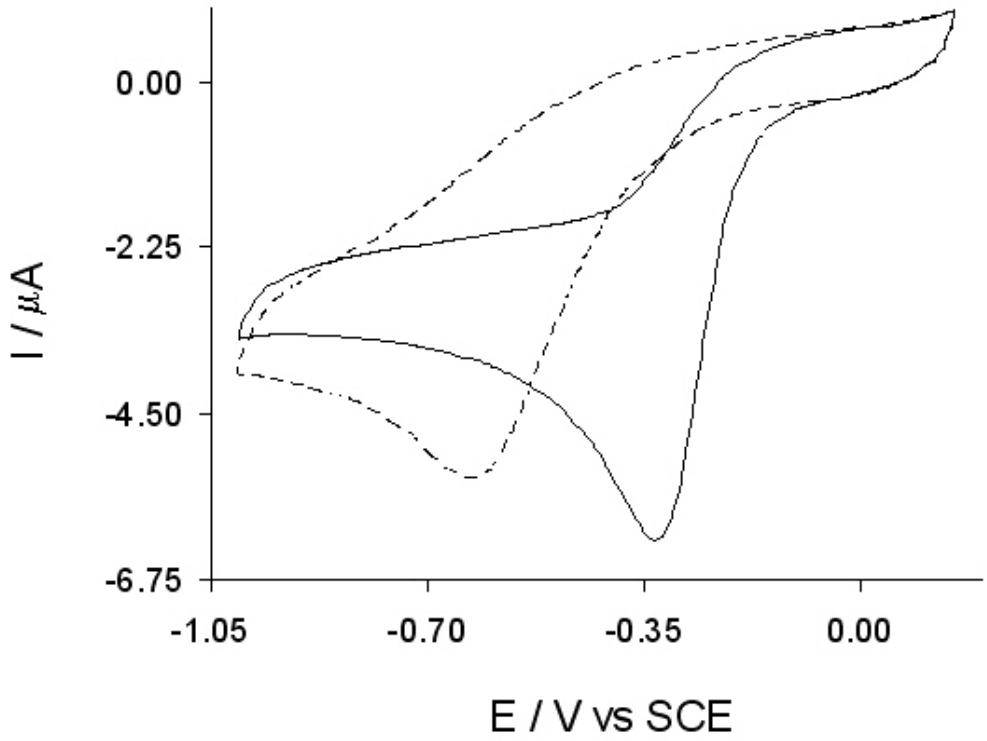

Figure IV.10 Plot of the NOR cyclic voltammograms (20 mV s^{-1}) in the presence of O_2 (solid line) and comparison with the control without the presence of the enzyme (dashed line), in a mix buffer, pH 7.5, in controlled anaerobiose conditions.

The response signal varies linearly with the oxygen concentration (figure IV.11), and so, it was attributed to the catalytic reduction of O_2 by the immobilised NOR.

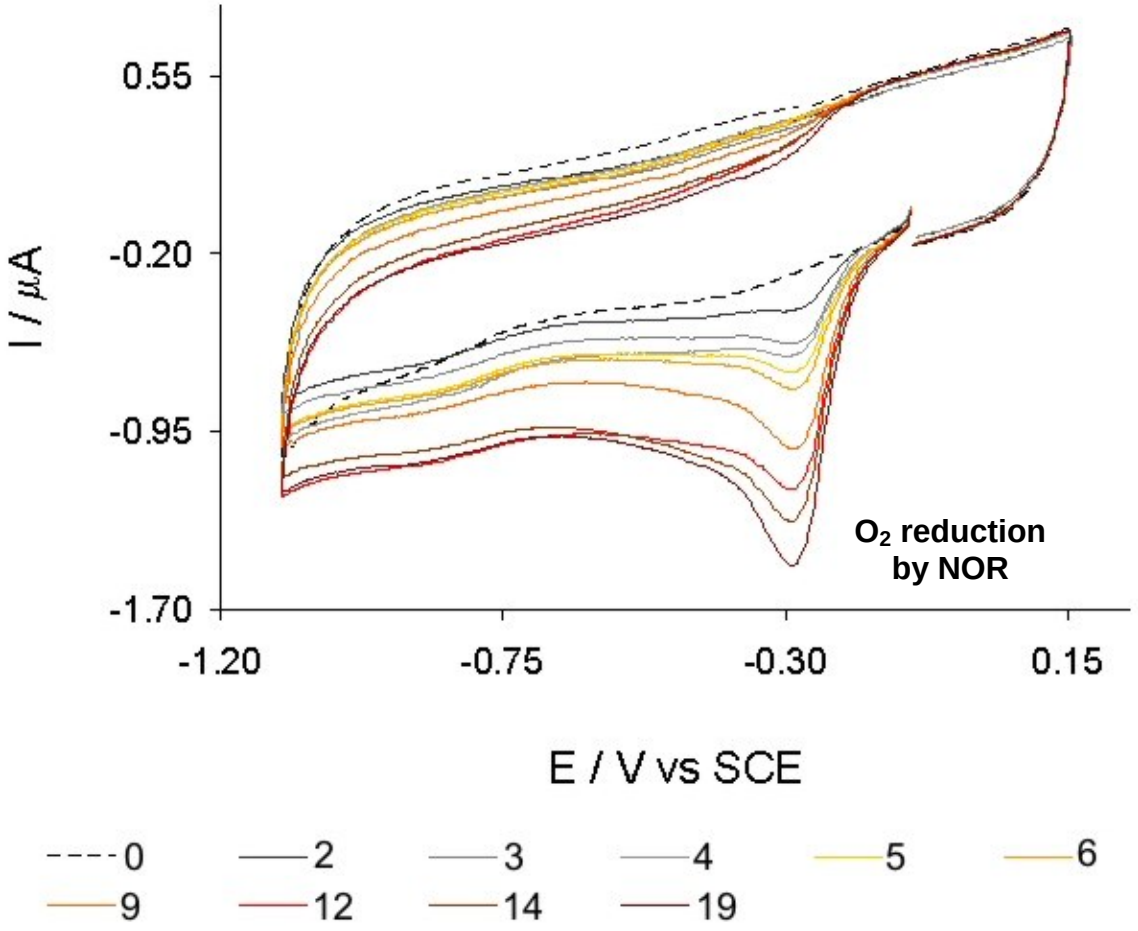

Figure IV.11 Plot of the first cycles of the voltammetric response (20 mV s^{-1}) of adsorbed NOR, with different concentrations of oxygen in solution (μM), accomplished with additions of air saturated buffer (mix buffer, pH 7.55).

The number of electrons involved in the catalytic process was not determined and so, the product of the reaction is not clear. Assays reported in the literature show that NOR can reduce oxygen, namely NOR from *Paracoccus denitrificans*. In fact for the reaction of NOR from *P. denitrificans* with O_2, using mediators in solution and measuring the oxygen consumption with the Clark electrode, have pointed four as the number of electrons involved, and so H_2O should be the final product[10]. By analogy, it seems probable for NOR from *Pseudomonas stutzeri* that the final product

should also be water. Further electrochemical studies using different conditions, namely the rotating electrode, are necessary to clearly resolve the question.

The above observation shows that the enzyme presents oxygen reduction activity like cyt *c* oxidase. In the heme-copper cytochrome *c* oxidase, heme b_3, is proposed to be involved in catalytic activity for O_2 reduction[26], catalysing the four electron reduction of oxygen to water. The reaction promotes a proton gradient across the membrane within a proton pumping mechanism. Although, as mentioned before, in NOR the reaction has been proved to be nonelectrogenic, by analogy, the assignment of this redox centre (corresponding to process I), that promotes the oxygen catalysis, to heme b_3 in NOR seems consistent. The NOR capability to reduce oxygen is reported with low turnover numbers when compared with the NO reduction. Some studies have shown that the substitution of one amino acid that affects the NO reduction also influence the oxygen reduction, implying that the mechanistic base should be similar for the both molecules[10].

The reduction of oxygen is better observed at low scan rates, as expected for an EC' mechanism, and disappears when high scan rates are employed, turning into the redox couple signal I. On figure IV.12 the conversion of the characteristic catalytic shape curve into the redox signal can be well observed.

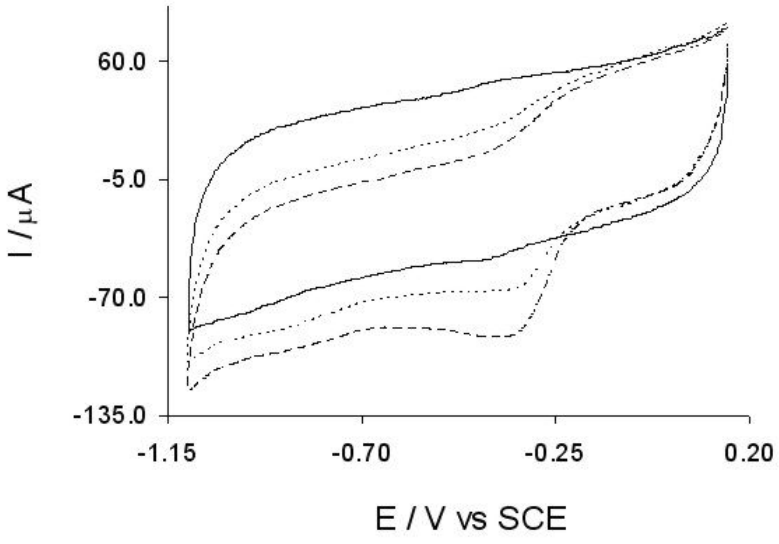

Figure IV.12 Plot of the NOR cyclic voltammograms in the presence of the same amount of oxygen (75 μM), in a mix buffer, pH 7.5, with different scan rates: 10 mV s^{-1} (dashed line), 20 mV s^{-1} (dot line) and 5 V s^{-1} (solid line). The current intensities of the 10 and 20 mV s^{-1} assays were multiplied respectively by 100 and 175 for clarity of comparison.

IV.3.2 Activity towards the nitric oxide reduction

In the presence of NO, a cathodic wave current develops (figure IV. 12), exhibiting a maximum at -730 ± 15 mV (-488 ± 15 mV vs. NHE). The NO reduction potential is quite negative when compared to the previous observed redox couple potential. This feature may be due to some conformational change that occur during the catalytic cycle and may implicate a shift in the redox potential. In fact, spectroscopic data from nitric oxide purified from *Paracoccus denitrificans* point to heme *b*3 conformational changes caused by the reduction of the binuclear centre that may have physiological relevance in the NO catalysis[27].This situation was already observed in other systems such as heme proteins, namely hemoglobin. Immobilized hemoglobin in modified electrodes also present activity towards the nitric oxide reduction and the correspondent cathodic response is also observed at more negative potential values than the redox centre midpoint potential[28].

As can be observed in the figure IV.13, the control assay, performed without the immobilised enzyme, also presents a cathodic peak corresponding to the NO reduction, but the shape and the maximum potential value is different, more negative, than when the NOR is present.

The variation of the NO concentration produces a linear variation of the current intensity, as can be observed in figure IV. 14. Because of the high turnover of the enzyme, and the limitation of solubility of the NO, it has not been possible so far to reach a current plateau with the experimental conditions used. Further work is in progress in order to overcome these limitations for NO and also to the oxygen catalysis.

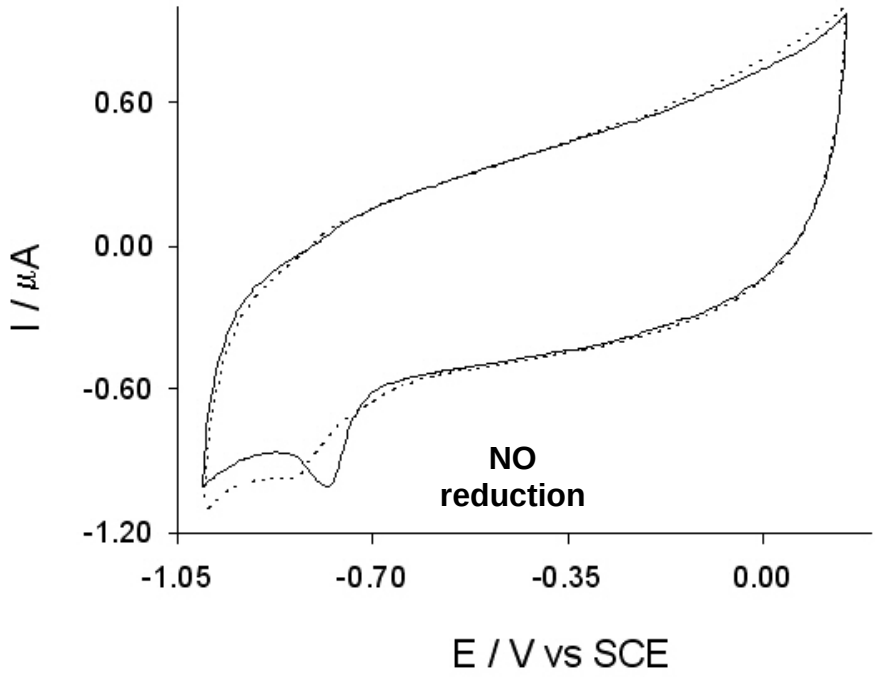

Figure IV.13 Plot of the NOR cyclic voltammograms (20 mV s^{-1}) in the presence of NO (solid line) and comparison with the control without the presence of the enzyme (dot line), in a mix buffer, pH 7.5, in controlled anaerobiose conditions.

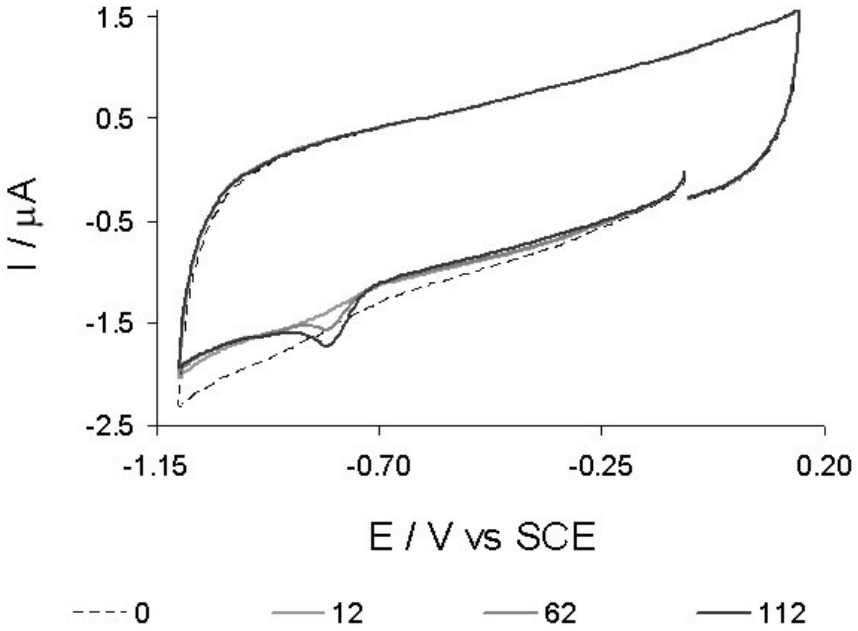

Figure IV.14 Plot of the first cycles of the voltammetric response (20 mV s^{-1}) of adsorbed NOR with different concentrations of nitric oxide in solution (in μM), accomplished with additions of NO saturated water.

In the presence of both oxygen and nitric oxide the immobilised NOR presents two distinct cathodic peaks. The potential value for the NO reduction is the same as in the experiments in which only NO is present, but the oxygen reduction is shifted to more negative potential values (figure IV.15). This shift can be due to some change in the mechanism by the presence of the nitric oxide or to some contribution from the reduction of species produced *in situ* by the reaction of oxygen and nitric oxide.

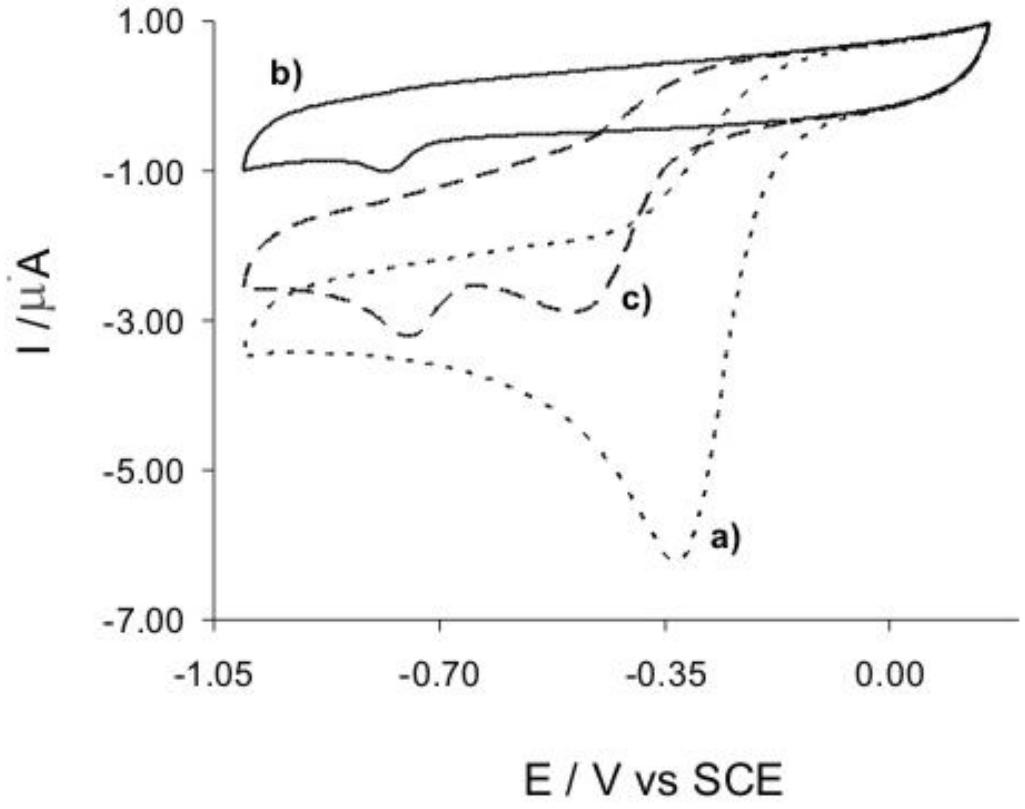

Figure IV.15 Plot of the NOR cyclic voltammograms (20 mV s^{-1}) in the presence of a) O_2 (air saturated solution), b) NO and c) both O_2 and NO in a mix buffer, pH 7.5, in controlled anaerobiose conditions. The concentrations of O_2 and NO are, respectively, ≈280 and 2 μM.

It should be pointed that the concentrations inside the protein/surfactant layer may differ from the ones in solution. In fact electrochemical studies of the cytochrome P450 entrapped in surfactant films on carbon electrodes have pointed to higher concentrations of O_2 inside these hydrophobic films than in the solution[23].

A plot with the linear variation of the electrochemical response of NOR to increasing concentrations of oxygen and nitric oxide (not simultaneously) is shown in figure IV.16.

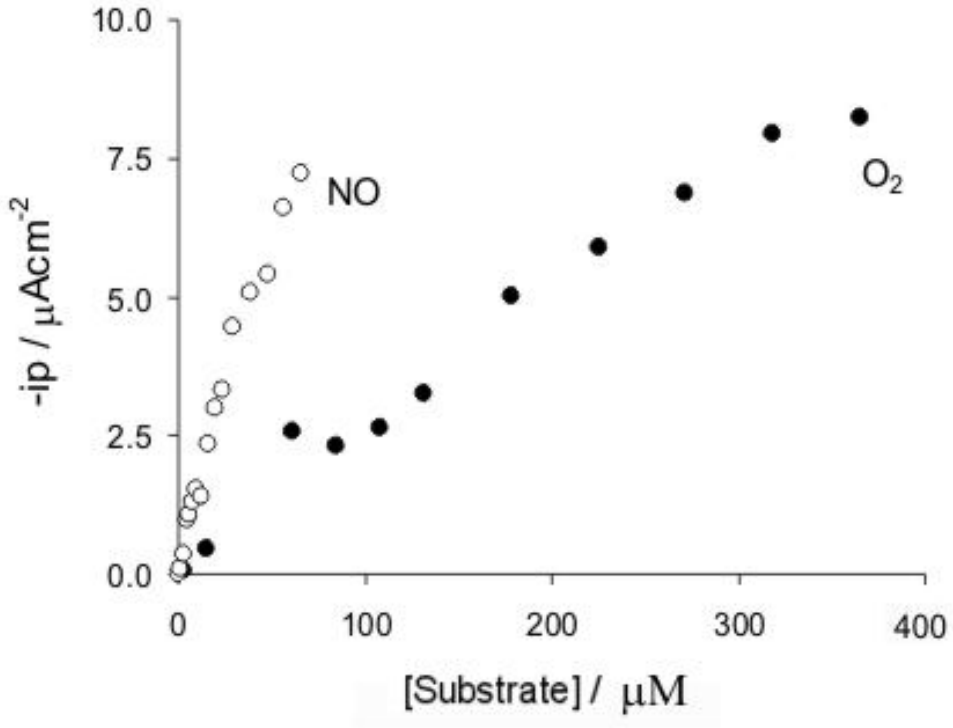

Figure IV.16 Plot of the current density *versus* the substrate concentration for assays in which O_2 and NO were present individually.

The signal of the redox couple I is stable for several hours (at least 6 hours) and the current intensity remains almost unaltered after the impositions of multiple cycles (up to around 100 cycles without catalysis). Also, after successive multicycles (at least 400 cycles for 6 hours) and the imposition of the electrocatalysis assays, the observed attenuation of the current intensity is about 50 % (figure IV.17).

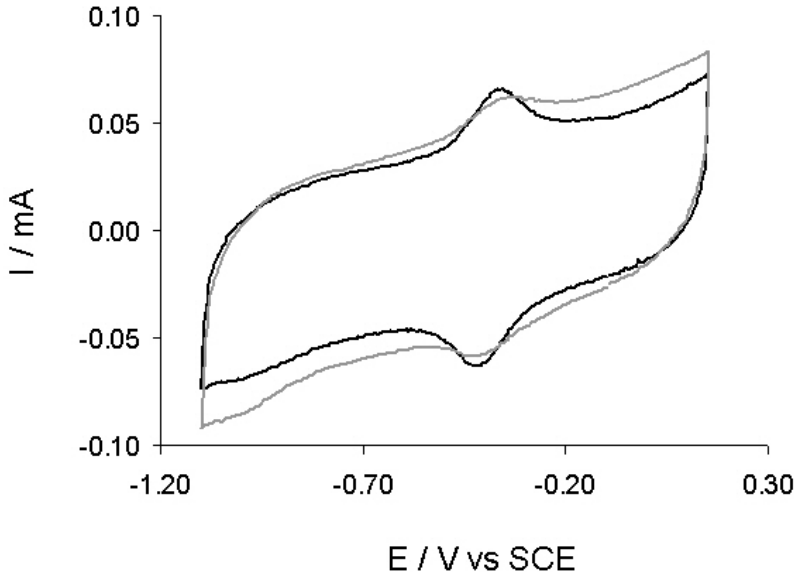

Figure IV.17 Plot of the second cycles of the NOR cyclic voltammograms (5 V s^{-1}) before (black line), corresponding to a fresh prepared modified electrode, and after (grey line) successive multicycles and electrocatalytic assays for several hours. The current intensity decreases approximately 50%.

IV.4. Effect of pH

The immobilised NOR response with the pH variation was studied. The midpoint potential of the redox couple ascribed to the heme b_3 revealed to be pH dependent. The best data fit of the obtained potential *versus* pH implies two protonation processes, resulting in four pK's values for the oxidized and reduced states, namely, pK_{ox1} = 5.0 ± 0.1, pK_{red1} = 5.9 ± 0.2, pK_{ox2} = 7.3 ± 0.1 and pK_{red2} = 8.6 ± 0.1 (figure IV.18). These values agree with enzymatic activity assays determined in solution[18], from which was possible to infer the pK_a and pK_b values, respectively, 6.9 ± 0.5 and 8.4 ± 0.5. These are consistent with the pK_{red1} and pK_{red2} considering the error range and the different experimental conditions and show that the immobilised enzyme retains its native properties.

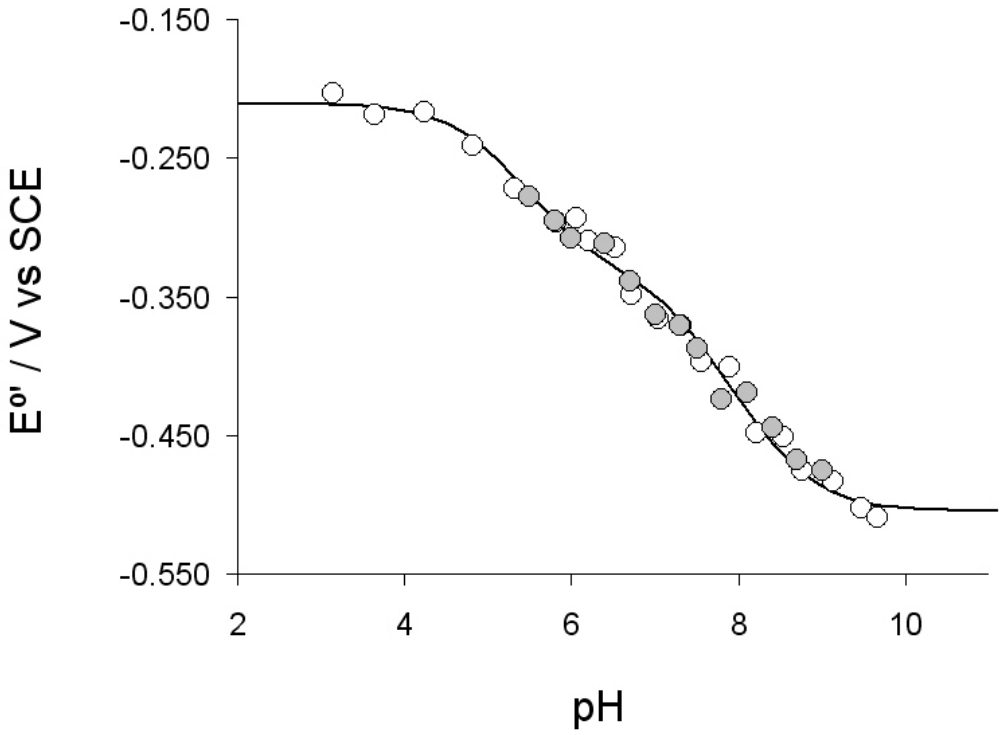

Figure IV.18 Plot of the heme *b3* midpoint potential variation with the pH, white and grey circles respect to the mix buffer with and without sodium citrate and black line is the best fit of the results.

The first protonation is proposed to be due to the Fe_B or heme b_3 coordinated histidines (His200, His251, His252, His340), which have a pK_a range 5.9-7.0. While one could still attribute the second observed pK_a value to a histidine residue, the enzyme primary sequence shows a highly conserved glutamate (Glu204) in the vicinity of Fe_B and some studies point this residue as essential for the catalytic activity in NOR from *P. denitrificans*[29]. Such a hypothesis is supported by recent studies of protein buried glutamate residues for which pK_a values of 8.5-8.8 were found[30, 31].

IV.5 Final Remarks

In this work it was possible, for the first time to obtain electrochemical data from a nitric oxide reductase resulting from direct electron transfer assays, accomplished by cyclic voltammetry. A reproducible redox couple was observed which was attributed to heme *b*3.

The demonstration of the catalytic activity towards the oxygen reduction was achieved and the reduction and catalysis of nitric oxide was also observed by direct electrochemistry.

The pH dependence of the redox processes was evaluated and the results show that the immobilised enzyme retains its native properties.

IV.6 References

1. Ford, P. C.; Lorkovic, I. M., Mechanistic aspects of the reactions of nitric oxide with transition-metal complexes. *Chem Rev* **2002,** 102, (4), 993-1018.

2. Hendriks, J.; Oubrie, A.; Castresana, J.; Urbani, A.; Gemeinhardt, S.; Saraste, M., Nitric oxide reductases in bacteria. *Biochim Biophys Acta* **2000,** 1459, (2-3), 266-73.

3. de Vries, S.; Schroder, I., Comparison between the nitric oxide reductase family and its aerobic relatives, the cytochrome oxidases. *Biochem Soc Trans* **2002,** 30, 662-667.

4. Sakurai, T.; Nakashima, S.; Kataoka, K.; Seo, D.; Sakurai, N., Diverse NO reduction by Halomonas halodenitrificans nitric oxide reductase. *Biochem Biophys Res Commun* **2005,** 333, (2), 483-7.

5. Wasser, I. M.; de Vries, S.; Moenne-Loccoz, P.; Schroder, I.; Karlin, K. D., Nitric oxide in biological denitrification: Fe/Cu metalloenzyme and metal complex NOx redox chemistry. *Chem Rev* **2002,** 102, (4), 1201-1234.

6. Tavares, P.; Pereira, A. S.; Moura, J. J.; Moura, I., Metalloenzymes of the denitrification pathway. *J Inorg Biochem* **2006,** 100, (12), 2087-100.

7. Girsch, P.; deVries, S., Purification and initial kinetic and spectroscopic characterization of NO reductase from Paracoccus denitrificans. *Biochim Biophys Acta-Bioenergetics* **1997,** 1318, (1-2), 202-216.

8. Zumft, W. G., Nitric oxide reductases of prokaryotes with emphasis on the respiratory, heme-copper oxidase type. *J Inorg Biochem* **2005,** 99, (1), 194-215.

9. Hendriks, J. H.; Jasaitis, A.; Saraste, M.; Verkhovsky, M. I., Proton and electron pathways in the bacterial nitric oxide reductase. *Biochemistry* **2002,** 41, (7), 2331-40.

10. Flock, U.; Watmough, N. J.; Adelroth, P., Electron/proton coupling in bacterial nitric oxide reductase during reduction of oxygen. *Biochemistry* **2005,** 44, (31), 10711-9.

11. Kumita, H.; Matsuura, K.; Hino, T.; Takahashi, S.; Hori, H.; Fukumori, Y.; Morishima, I.; Shiro, Y., NO reduction by nitric-oxide reductase from denitrifying bacterium Pseudomonas aeruginosa: characterization of reaction intermediates that appear in the single turnover cycle. *J Biol Chem* **2004,** 279, (53), 55247-54.

12. Blomberg, L. M.; Blomberg, M. R.; Siegbahn, P. E., Reduction of nitric oxide in bacterial nitric oxide reductase--a theoretical model study. *Biochim Biophys Acta* **2006,** 1757, (4), 240-52.

13. Gronberg, K. L.; Roldan, M. D.; Prior, L.; Butland, G.; Cheesman, M. R.; Richardson, D. J.; Spiro, S.; Thomson, A. J.; Watmough, N. J., A low-redox potential heme in the dinuclear centre of bacterial nitric oxide reductase: implications for the evolution of energy-conserving heme-copper oxidases. *Biochemistry* **1999,** 38, (42), 13780-6.

14. Heering, H. A.; Wiertz, F. G.; Dekker, C.; de Vries, S., Direct immobilization of native yeast iso-1 cytochrome C on bare gold: fast electron relay to redox enzymes and zeptomole protein-film voltammetry. *J Am Chem Soc* **2004,** 126, (35), 11103-12.

15. Armstrong, F. A.; Wilson, G. S., Recent developments in faradaic bioelectrochemistry. *Electrochim Acta* **2000,** 45, (15-16), 2623-2645.

16. Wang, S. F.; Chen, T.; Zhang, Z. L.; Shen, X. C.; Lu, Z. X.; Pang, D. W.; Wong, K. Y., Direct electrochemistry and electrocatalysis of heme proteins entrapped in agarose hydrogel films in room-temperature ionic liquids. *Langmuir* **2005,** 21, (20), 9260-6.

17. Timóteo, I. C. C. G. Estudos Estruturais e Mecanísticos em Enzimas Multihémicas Isoladas de Bactérias Desnitrificantes. FCT-UNL, Lisboa, **2004**.

18. Timóteo, C., *et al*, **in preparation**.

19. Di Tomaso, G.; Fedi, S.; Carnevali, M.; Manegatti, M.; Taddei, C.; Zannoni, D., The membrane-bound respiratory chain of Pseudomonas pseudoalcaligenes KF707 cells grown in the presence or absence of potassium tellurite. *Microbiology* **2002,** 148, (Pt 6), 1699-708.

20. Laviron, E., General Expression of the Linear Potential Sweep Voltammogram in the Case of Diffusionless Electrochemical Systems. *J Electroanal Chem* **1979,** 101, (1), 19-28.

21. Limoges, B.; Marchal, D.; Mavre, F.; Saveant, J. M., High Amplification Rates from the Association of Two Enzymes Confined within a Nanometric Layer Immobilized on an Electrode: Modeling and Illustrating Example. *JACS* **2006,** 128, (18), 6014-5.

22. Haas, A. S.; Pilloud, D. L.; Reddy, K. S.; Babcock, G. T.; Moser, C. C.; Blasie, J. K.; Dutton, P. L., Cytochrome c and cytochrome c oxidase: Monolayer assemblies and catalysis. *J Phys Chem B* **2001,** 105, (45), 11351-11362.

23. Udit, A. K.; Hindoyan, N.; Hill, M. G.; Arnold, F. H.; Gray, H. B., Protein-surfactant film voltammetry of wild-type and mutant cytochrome P450 BM3. *Inorg Chem* **2005,** 44, (12), 4109-11.

24. Hirst, J., Elucidating the mechanisms of coupled electron transfer and catalytic reactions by protein film voltammetry. *Biochimica et Biophysica Acta* **2006,** 1757, 225-239.

25. Zhang, W., Li, G., Third-Generation Biosensors Based on the Direct Electron Transfer of Proteins. *Anal Sci* **2004,** 20, 603-609.

26. Pitcher, R. S.; Watmough, N. J., The bacterial cytochrome cbb3 oxidases. *Biochim Biophys Acta* **2004,** 1655, (1-3), 388-99.

27. Pinakoulaki, E.; Gemeinhardt, S.; Saraste, M.; Varotsis, C., Nitric-oxide reductase. Structure and properties of the catalytic site from resonance Raman scattering. *J Biol Chem* **2002,** 277, (26), 23407-13.

28. Liu, X.; Shang, L.; Sun, Z.; Li, G., Direct electrochemistry of hemoglobin in dimethyldioctadecyl ammonium bromide film and its electrocatalysis to nitric oxide. *J Biochem Biophys Methods* **2005,** 62, (2), 143-51.

29. Butland, G.; Spiro, S.; Watmough, N. J.; Richardson, D. J., Two conserved glutamates in the bacterial nitric oxide reductase are essential for activity but not assembly of the enzyme. *J Bacteriol* **2001,** 183, (1), 189-99.

30. Dwyer, J. J.; Gittis, A. G.; Karp, D. A.; Lattman, E. E.; Spencer, D. S.; Stites, W. E.; Garcia-Moreno, E. B., High apparent dielectric constants in the interior of a protein reflect water penetration. *Biophys J* **2000,** 79, (3), 1610-20.

31. Fitch, C. A.; Karp, D. A.; Lee, K. K.; Stites, W. E.; Lattman, E. E.; Garcia-Moreno, E. B., Experimental pK(a) values of buried residues: analysis with continuum methods and role of water penetration. *Biophys J* **2002,** 82, (6), 3289-304.

Chapter V

Direct Electrochemistry of the Multiple Redox Centres of Hydrogenase from *Desulfovibrio gigas*

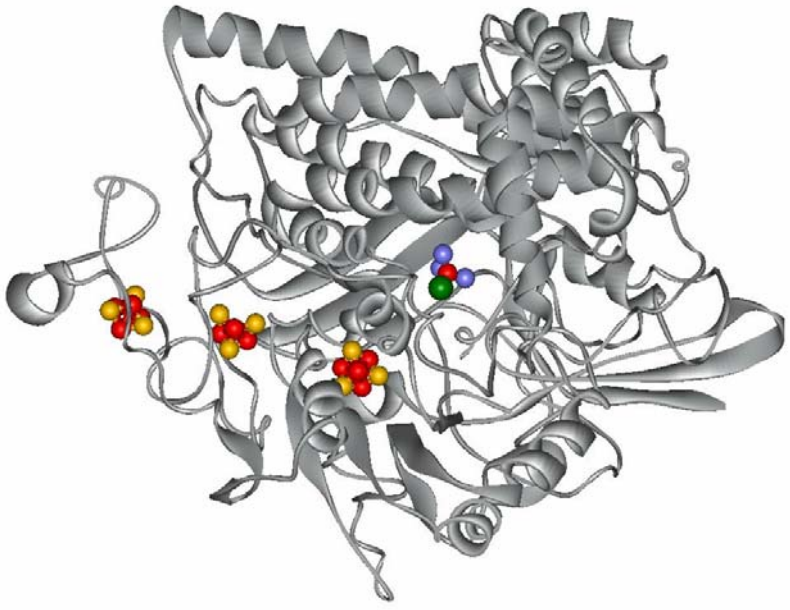

Direct Electrochemistry of the Multiple Redox Centres of Hydrogenase from *Desulfovibrio gigas*

V.1 Hydrogenase

Hydrogenases (Hases) are multicentre enzymes that catalyse the interconversion between H_2 and H^+, involved in the sulphate respiration pathway, by which anaerobic organisms obtain energy, using hydrogen not only as an electron donor (H_2 uptake) but also as an electron sink (H_2 production). These enzymes can, therefore, oxidize or reduce hydrogen[1], being responsible for the hydrogen metabolism, according to the bidirectional reaction $H_2 \leftrightarrows 2H^+ + 2e$.

Hases are also important enzymes due to its great technological interest for the H_2 production, either through the use of whole cells or the isolated enzymes. It has been shown lately that immobilised hydrogenases on electrode surfaces exhibit high electrocatalytic activity, which justifies the interest of their use in biofuel cells. Other areas of interest have been explored, such as, its use as biosensors, its role on biocorrosion mechanisms and in possible applications in environmental decontamination[2-5]. Hydrogenases high catalytic activity, with turnover numbers of 6000 s^{-1} for the *Clostridium pasteurianum* enzyme and 9000 s^{-1} for *Desulfovibrio* proteins, led to several attempts to develop biosystems to produce hydrogen. Much of these efforts have been done to achieve efficient biohydrogen production through biophotolysis, which tries to mimic the photosynthetic process with hydrogen production by water splitting[6]. In these systems, the light is capture by a photosynthetic apparatus and the generated energy is used for water splitting producing a low potential reductant that can be used to reduce the hydrogenase. These systems have, however, a limitation related with the molecular oxygen partial pressure needed to be efficient. They must operate near 1 atm of O_2 and with this pressure values, hydrogenase is very sensitive and becomes inhibited. For a practical system it is necessary that the problem of the hydrogenase oxygen sensitivity is overcome. Other possibility is to use the so-called indirect biophotolysis, where a physical separation between the oxygen and hydrogen evolution is imposed[7]. Figure V.1 shows a schematic representation of these biophotolysis processes.

Recent studies have shown that it is possible to link hydrogenase from *Ralstonia* to the cytoplasmic side of *Synechocystis* PSI, to modify photosystem I in order to photoproduce hydrogen (H_2)[8].

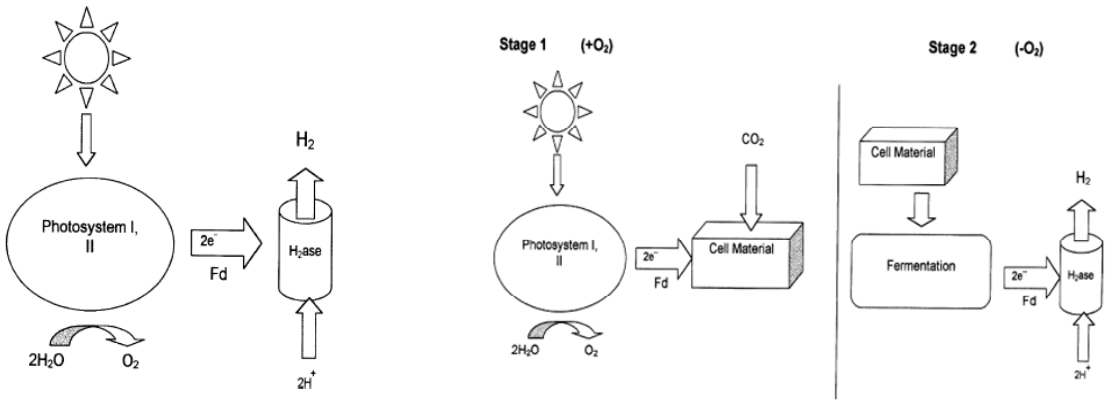

A **B**

Figure V.1 Schematic representation (adapted from Hallenbeck *et al*, *Int. J. Hyd. Energy*, 2002) of the A) direct biophotolysis (chloroplast-ferredoxin (Fd)-hydrogenase system) and B) indirect biophotolysis processes (two stage process with O_2 and H_2 production separation)[7].

In sulphate reducing bacteria the reduction of sulphate occurs on the cytoplasm and the hydrogen oxidation on the periplasm, and so, the electron transport is accomplished by redox complexes involving multiheme cytochromes, with emphasis to cytochrome c_3 (cyt c_3), that seems to be the preferential physiological partner, in spite of other small redox carriers can mediate the electron exchange between hydrogenase and the electrodes, namely ferredoxin I and II and rubredoxin[9, 10]. The electrochemical behaviour of cyt c_3 has been extensively studied and its interaction with hydrogenase has been clearly demonstrated. Studies have shown that in the presence of hydrogen, the cyt c_3 enzymatically reduced by hydrogenase from the same strain can be electrochemically reoxidated with the production of an enhanced anodic current[11]. Cyt c_3, when coupled to the hydrogen oxidation, resulted from the [NiFe]-Hase, has the capability to transfer two protons and two electrons, allowing energy transfer from the periplasm to the cytoplasm[12]. This cytochrome shows low redox potentials, typically around -300 mV vs. NHE, essential for the sulphate respiration process. The mechanism of electron transfer between cyt c_3 and Hase has been also studied by NMR and *in silico* molecular modelling of the transient complex formed between the two molecules. It has been observed that its interaction is dependent of the redox state. Site-directed mutagenesis studies also

demonstrated the importance of positive charged residues of cyt c_3, namely lysines, in this interaction and in the electronic transfer pathway[13].

There are three different classes of hydrogenases, phylogenetically distinguishable, that are classified based on the metals present in the catalytic centre, namely nickel-iron [NiFe] (a variant is the [NiFeSe] enzymes), iron-only [FeFe] and non-iron or metal-free hydrogenase, also known as Hmd (from H_2-forming methylenetetrahydromethanopterin dehydrogenase). Recently, it was proved that Hmd Hase in fact also contains Fe and CO [14, 15] incorporated in a co-factor that is essential to the enzyme activity. This co-factor is believed to be linked by a cysteine residue as can be seen schematically in figure V.2. This last enzyme does not catalyse the H^+/H_2 conversion directly but rather via the reversible reduction of the N^5,N^{10}-methenyltetrahydromethanopterin (methenyl-H_4MPT$^+$) with H_2 to N^5,N^{10}-methenyltetrahydromethanopterin (methenyl-H_4MPT) and a proton[16]. A schematic representation of the differences between the hydrogenases is displayed in figure V.2.

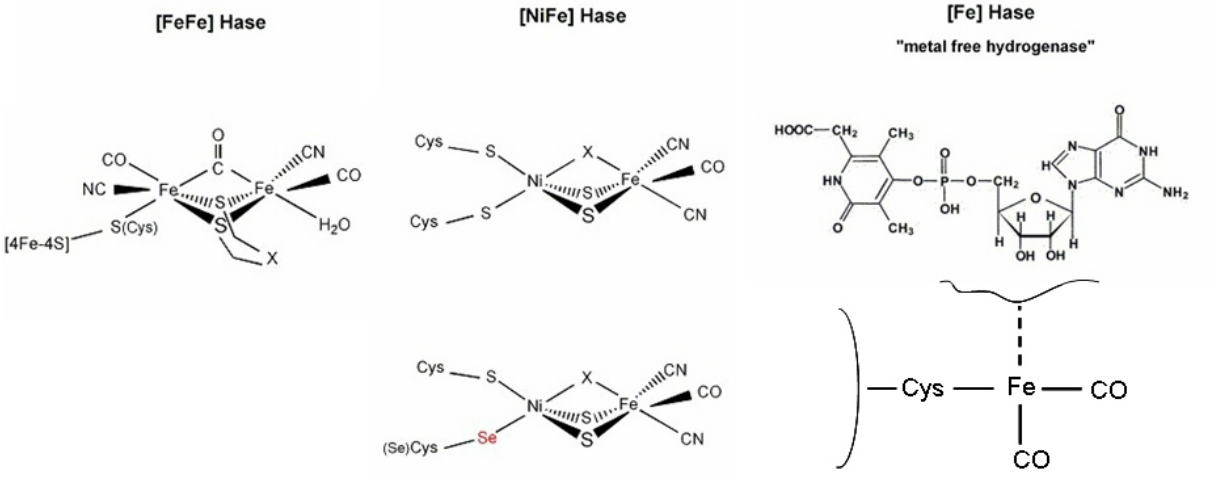

Figure V.2 Schematic representation of the metallic centres of the three different classes of Hases.

Although Ni is an abundant metal it is one uncommon element in enzymatic systems and it seems mainly related in catalytic reactions involving gases, namely, H_2 in hydrogenases, CO and CO_2 in carbon monoxide dehydrogenases and CH_4 in methyl-Coenzyme M reductase[17].

The [NiFe]-Hase from *Desulfovibrio gigas* (*Dg*) is a periplasmic enzyme with molecular weight of 89 kDa formed by two subunits (with 26 and 63 kDa), in which the larger contains the active site and the smaller one holds three iron-sulphur clusters, namely one [3Fe-4S] and two [4Fe-4S][18]. It is currently accepted that these clusters function as the electronic pathway to transfer electrons to the [NiFe] centre. The active sites of the different [NiFe]-Hases present high structural similarity. The metal centre presents one Fe atom bond to one CO and two CN ligands, which is an unusual coordination in biology [19]. CO and CN ligands, as diatomic π-acceptors, stabilize the metals in low oxidation states. The iron in this protein has only been detected so far in the +2 oxidation state. Ni is coordinated by four cysteines, two of which form a bridge to the Fe atom. The Ni oxidation states are variable[20] (reported from +1 to +3). The structure of hydrogenase from *Dg* is displayed on figure V.3.

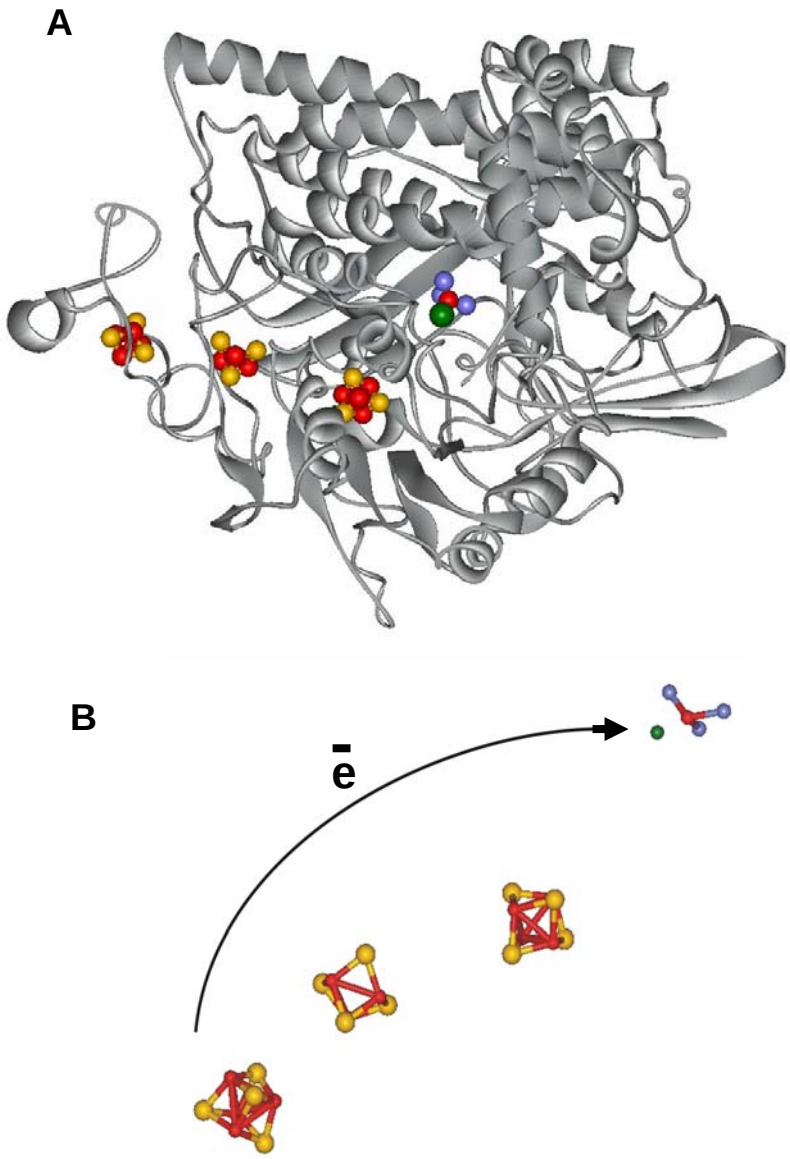

Figure V.3 A) Structure of the hydrogenase from *Dg* (PBD 1FRV) at 2.85 Å resolution[21], and B) the three iron-sulphur clusters that take part of the electronic pathway (iron in red, sulphur in yellow, nickel in green and carbon in blue).

The oxidised form of the protein presents another ligand in bridge configuration between the Ni and the Fe atoms. The nature and role of this extra ligand has been extensively discussed. It is well established that this is an oxygenated species, but the exact form depends on the catalytic site activation state and is still under discussion[22, 23]. [NiFe]-Hase presents several redox states that correspond to active and inactive forms of the enzyme. So far, at least seven different redox states,

related with the possible electron and proton transfers and ligand bonds[14, 17], have been identified. In the inactive oxidised enzyme two states are described, the so-called Ni-A "unready" and the Ni-B "ready" species, both EPR detectable, due to the Ni spin state equal to 1/2, and present in the as-isolated protein[18]. These two forms differ on the required activation time, with Ni-B being much faster (in a manner of minutes) while Ni-A requires long time (several hours) under H_2 to be active. EPR, ^{17}O ENDOR and crystallographic data suggest that the bridge ligand on Ni-A is a diatomic ligand[24] like O_2^- while on Ni-B seems to be a monoatomic oxygen species, also compatible with a hydroxide [23, 25]. Ni-A and Ni-B can be further reduced to form EPR silent states, namely Ni-SU (unready) and Ni-SI (two forms, ready and active) and the Ni-C, the so-called "active" form, and Ni-R states (fully reduced form), these last two EPR undetectable species[22, 23]. Another detected state is the so-called Ni-L which is a subproduct of the Ni-C state obtained at low temperatures by photolysis, and where the nickel is best described as +1 oxidation state[26]. A very simplified scheme showing the main states Ni-A, Ni-B, Ni-C and the silent ready and active states is shown in figure V.4.

The previous active enzyme was proved to become inactive by oxidation with O_2, in agreement with the hypothesis that the oxygenated species bond hinders the H_2 capture [27].

The discussion remains about the Ni oxidation state during the catalytic cycle, with the hypothesis of Ni(III), Ni(II) or even Ni(I) involvement[14]. Although the catalytic mechanism is still under discussion, one model for the reaction is described as the H_2 fixation to the Ni(II) at the Ni-SI form, heterolytic cleavage, that implies the presence of a base and an hydride acceptor, to form a protonated intermediate, that may be a bridge hydride between the Ni and the Fe atoms, assigned as the Ni-C form[28]. Follows the subsequent generation of the reduced state Ni-R and re-oxidation with regeneration of the Ni-SI, passing by the Ni-C form[29]. Some other pertinent studies, using X-ray diffraction (xenon diffusion) and molecular dynamics allowed the identification of a hydrophobic gas channel from the protein surface towards the Ni atom, giving support to the idea that Ni has the main role on the catalytic mechanism[30]. The observation of this gas channel proved that the H_2 does not diffuse randomly inside the protein but instead has a defined route. In [NiFe]-Hase there are two conserved hydrophobic residues (valine and leucine) at the end of this channel, but in some O_2 tolerant Hases, as the case of *Ralstonia eutropha (Re)*

[NiFe]-Hase, these residues are substituted by isoleucine and phenylalanine hindering the access of larger molecules as oxygen[31]. This can be the reason that explains the larger oxygen tolerance of some of these enzymes demonstrated in some electrochemical studies[32].

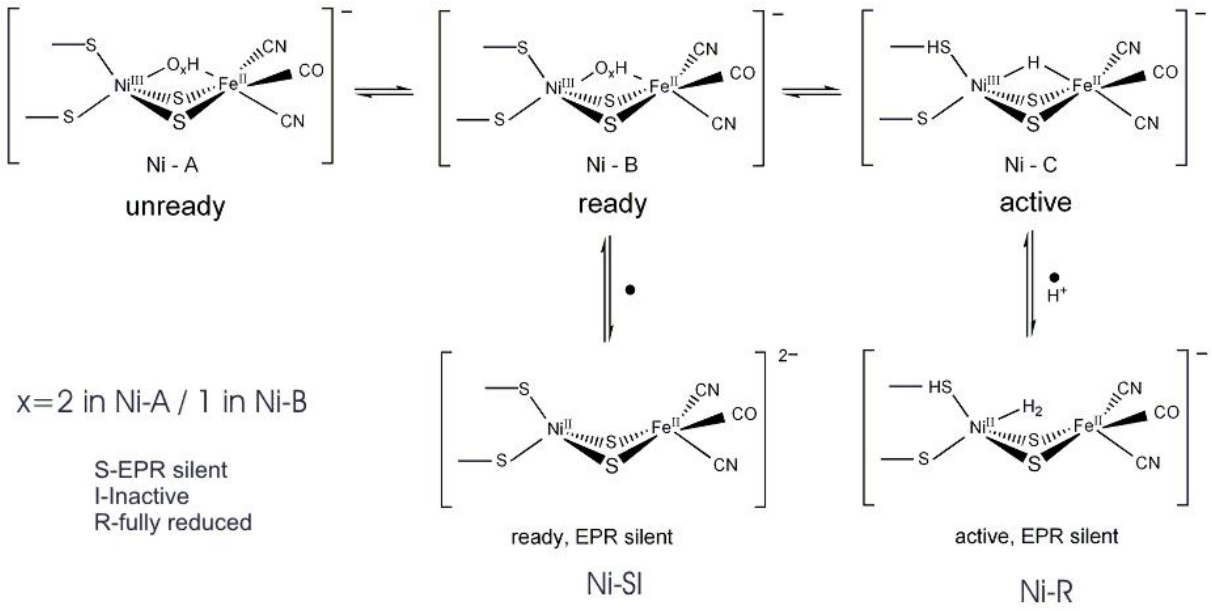

Figure V.4 Simplified scheme showing the main Hase states, namely Ni-A, Ni-B, Ni-C and the silent ready and active-fully reduced states (SI and R). The stoichiometry of the oxygenated specie that binds to the Ni-Fe centre is still under discussion.

The proposed catalytic mechanisms, based on theoretical calculations, for the above reaction are quite complex, and involve two cycles whether if it is H_2 production or consumption and if the control is electrochemical or by reduction under hydrogen[14] (later in the text).

Studies of the redox states of these enzymes have been performed for quite long time. The first studies performed were based on potentiometric assays, namely, redox titrations coupled to spectroscopic techniques as Mössbauer and EPR spectroscopies[17, 18]. The redox potentials values, for the [NiFe]-Hase isolated from *Dg*, determined by potentiometry are presented in table V.I.

Table V.I Summary of the redox potentials reported on the literature of the different *Dg* [NiFe]-Hase centres, determined by potentiometric assays[17, 18].

Centre		Redox potential (mV vs. NHE)
$[3Fe\text{-}4S]^{+/0}$	*as-isolated*	-70
$[3Fe\text{-}4S]^{0}$	*catalytic intermediate*	-290
$[3Fe\text{-}4S]^{0}$	*fully reduced*	-320
$[4Fe\text{-}4S]^{2+/+}$		-340
Ni-A	*Ni (III)*	-150
Ni-B	*Ni (III)*	*Undetermined*
Ni-C	*Ni (II)*	-310

These studies were essential for the clusters redox state determination and to enlighten the possible catalytic pathway. Other studies using a redox mediator (methylviologen) and immobilisation of the Hase on graphite have demonstrated that the modulation of the enzyme activity level is controlled by the Ni(III)/Ni(II) redox couple (-220 mV vs. NHE, pH 8.5). Based on these studies it was proposed for the first time the activation/inactivation process controlled by the imposed redox potential[33]. The pH activity dependence was also demonstrated using redox mediators (methyl and benzylviologen) with the protein in solution[34].

Dynamic electrochemical techniques are important tools to understand enzyme mechanisms and the intrinsic electrocatalytic properties. Different approaches are possible such as immobilisation by adsorption like protein film voltammetry[27, 35], or by the use of membranes[9], modified electrodes[36], or in solution[29]. Also, electrochemical studies, using cyclic voltammetry, coupled to spectroscopic methods have been performed and resulted in the demonstration of the direct response of the enzyme with the electrode surface, namely stainless steel[37].

Several studies of the electrocatalytic activity of different hydrogenases have been performed, where the rate of H_2 production and consumption is studied, either with systems where the Hase is immobilised[27] or using in bulk mediators, such as

methylviologen[29, 38]. The immobilisation of multimonolayers of biotynilated Hase at carbon surfaces was accomplished and the catalytic activity studied in the presence of methylviologen allowing the proposition of a catalytic mechanism, designated by SRC model[29]. In this model SRC, S stands for the Ni-SI EPR silent and inactive, R for the Ni-R fully reduced specie and C for the Ni-C state, and it is based on the assumption of a potential adjustable triangular mechanism that can be summarised in the following sequence:

$$\text{Ni-SI} \xrightarrow[\text{fixation}]{H_2} \text{Ni-R} \xrightarrow[\text{heterolytic } H_2 \text{ cleavage}]{} \text{Ni-C} \longrightarrow \text{Ni-SI}$$

Based on spectroscopic data (EPR and IR), density functional theory (DFT) analysis and electrochemically controlled titrations, two different catalytic mechanisms have been proposed either if the control is performed by H_2 pressure or by the imposed electrochemical redox potential, as displayed in figure V.5.

Under H_2 pressure:

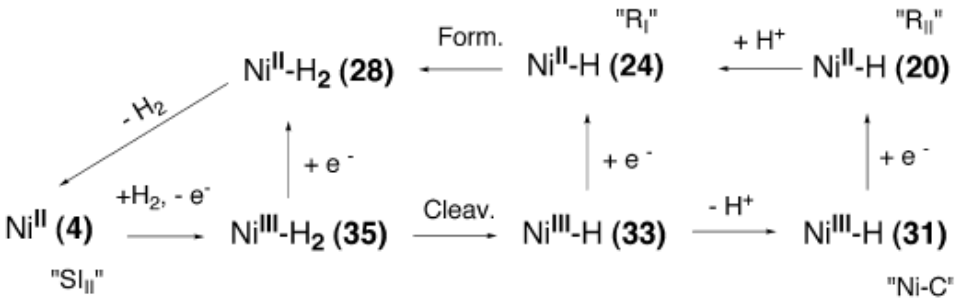

Electrochemical control:

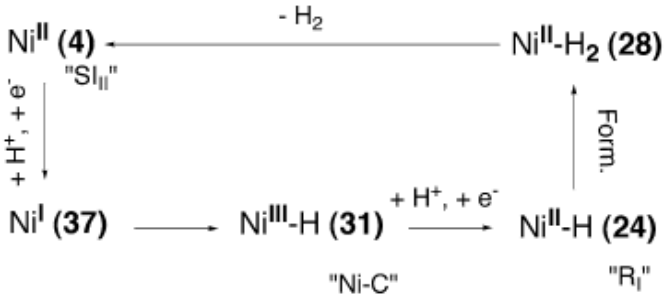

Figure V.5 Scheme of the proposed different catalytic mechanisms for the Hase activity under H_2 or electrochemical control[14].

Important progresses in the understanding of the electrocatalytic activity have been accomplished with electrochemical studies, in particular using voltammetric and amperometric techniques, with immobilised Hase, by adsorption, on the electrodes surface[32, 39]. It was observed that the catalytic activity of the immobilised enzyme is higher when its activity is determined with the protein in solution using redox mediators. The electrochemical response of the immobilised enzyme is, however, strongly dependent of the protein orientation that changes the distance of the interfacial electron transfer from the electrode surface and the protein, varying the determined electron transfer rates[40]. This direct electrochemical approach obtained by cyclic voltammetry from the adsorbed enzymes allowed the establishment of the turnover number of the enzymes, the study of the catalytic proton reduction and hydrogen oxidation of several Hase enzymes and, consequently, to infer mechanistic and kinetics implications. The results of these studies, namely the potential values of the catalytic current, its shape and pH dependence, have allowed to propose that the states and affinity of the active site in the catalytic processes are different for the oxidation and the reduction of hydrogen[41]. The electrochemical control of the catalytic activity made possible the comparison between the activity of Hase and platinum which is the most widely used catalyst for the hydrogen reduction and oxidation reactions. It was possible to observe that the [NiFe]-Hase adsorbed on pyrolytic graphite oxidises hydrogen at rates comparable to electrodeposited Pt on gold, presenting less susceptibility to CO poisoning[2]. This observation again reinforces the potential of Hase for industrial applications and the potential of the synthesis of Hase-like mimetic compounds. The problem of the oxygen inactivation however still remains and oxygen tolerance assays by cyclic voltammetry in the presence of oxygen with different Hases are reported, including the *Dg* [NiFe]. These assays have proved the different sensibility of the different Hases of [FeFe] and [NiFe] to oxidative conditions. In the case of the later enzyme, the authors observed the disappearance of the catalytic current corresponding to the total inhibition of the *Dg* [NiFe] towards hydrogen oxidation. In contrast for the *Re* [NiFe], the same conditions had almost no effect on the catalytic activity for the H_2 oxidation that persists even at atmospheric oxygen concentration[32, 35].

Although these studies were important to enlighten the catalytic mechanism, the redox signals of the individual metallic centres were not clearly observed. Armstrong and co-workers were able to observe some redox features besides the catalytic

activity for Hase isolated from *Chromatium vinosum* with the enzyme adsorbed on a rotating pyrolytic graphite disk electrode. These authors applied a CO saturated solution to the electrolyte in the presence of the Hase modified electrode and have observed that the catalytic activity towards hydrogen reduction was lost, showing that the enzyme is inhibited. In these non-turnover conditions it was possible the observation of two redox peaks attributed to one electron transitions of the iron sulphur redox centres [3Fe-4S] and [4Fe-4S][42].

The goal of the present work was to study the direct electrochemical response of the hydrogenase isolated from *Dg* and the conditions of its activation/inactivation through potential tuning.

V.2 Direct electrochemistry of Hydrogenase

In the present work we were able to observe in the absence of inhibitors, for the first time, the electrochemical response of [NiFe]-Hase redox centres, in non-turnover conditions, tuned by electrochemical control. The *Dg* Hase purification details are described on Appendix A. The enzyme direct electrochemical behaviour was studied by cyclic voltammetry. Studies were performed with the enzyme in solution or immobilised, using a membrane, at different material electrodes, such as graphite and glassy carbon. Assays with the protein adsorbed on graphite were also performed. Direct electron exchange between the electrode and the enzyme was successful. The activation of the enzyme was achieved by H_2 reduction and by electrochemical control and electrocatalytic activity was observed. Inactivation of [NiFe]-Hase was also attained through potential control, by cyclic voltammetry.

V.2.1 Activation under H_2

Electrochemical experiments with *Dg* [NiFe]-Hase were attained both in bulk and with the enzyme physically restrained with a cellulose membrane. It was possible to observe the direct electrochemical response of the *Dg* Hase using PG and GC

electrodes. The cyclic voltammograms, in anaerobic conditions (anaerobic chamber, <20 ppm O_2), with a diluted 2 μM solution, obtained after previous activation with H_2 by overnight incubation at 4 ºC, at pH 7, (ν = 50 mV s^{-1}, PG) show the development of a catalytic wave beginning at -300 mV (-58 mV vs. NHE) with a maximum reduction peak at -650 mV (ca. -400 mV vs. NHE), corresponding to the reduction of protons to H_2 (figure V.6).

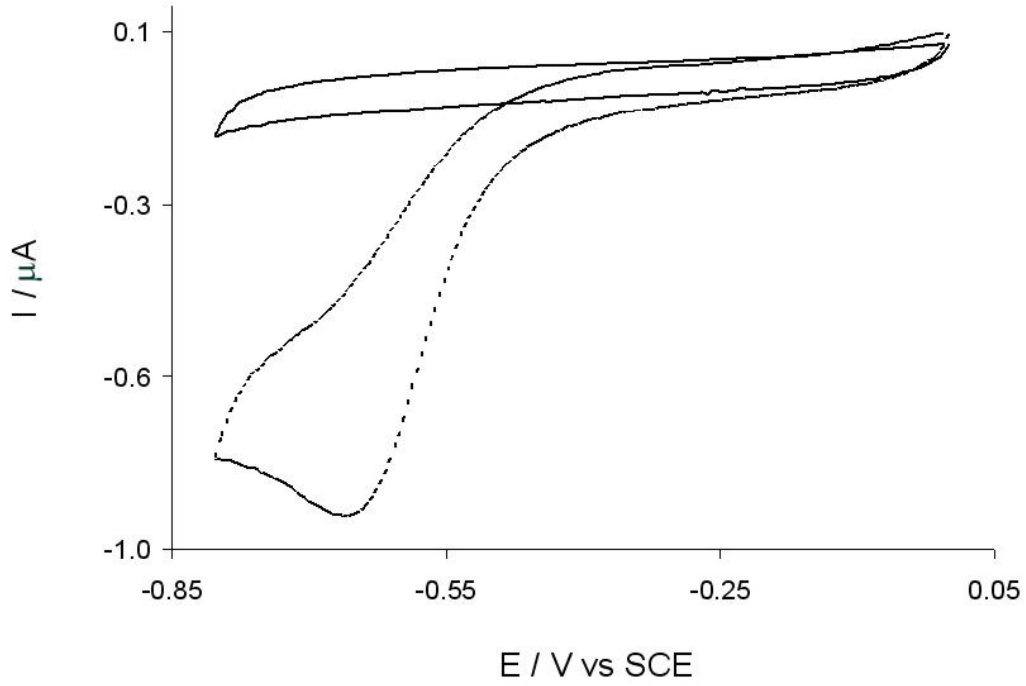

Figure V.6 Cyclic voltammograms of a diluted 2 μM Hase solution (black dashed line) in an anaerobic chamber (<20 ppm O_2), ν = 50 mV s^{-1}, after previous activation with H_2 by overnight incubation at 4 ºC, at pH 7, and control obtained in the absence of enzyme (black solid line).

After multiple cycling between 0 and -800 mV (at least 10 cycles) and a resting period (at open circuit potential, E_{oc}) long enough to obtain a stable value of the E_{oc}, in the subsequent cycles the electrochemical pattern changes and two current crossings can be observed. This phenomenon arises from the fact that the reverse scan present lower current than the forward one (in the scanning cathodic direction). The first current crossing occur at the potential value of -520 mV (-278 mV vs. NHE),

previous to the development of a cathodic current wave, with a maximum at around -350 mV (-108 mV vs. NHE), and the second crossing point at -269 mV (-27 mV vs. NHE). The cathodic peak due to the H^+ reduction reaction, is observed at a considerably higher potential value (-350 mV) than in the first assay performed with the enzyme activated by H_2 incubation and not yet subjected to the multiple cycling electrochemical assays . The initial forward scan does not present any cathodic peak. The potential at which the cathodic peak is observed on the reverse scan and the current crossings are indicative of the lower energy necessary to promote the hydrogen reduction reaction. The observed current crossings, are probably due to the formation of a hydride[43, 44] bond between the nickel and iron atoms of the active protein site. After the observation of these current crossings, the subsequent scans present the characteristic shape of the catalytic current peak (see figure V.7), in which the current starts to develop at -250 mV (-8 mV vs. NHE) in contrast with the higher potential value observed immediately after the chemical activation of Hase, as can be seen by comparing the patterns in the figures V.6 and V.7.

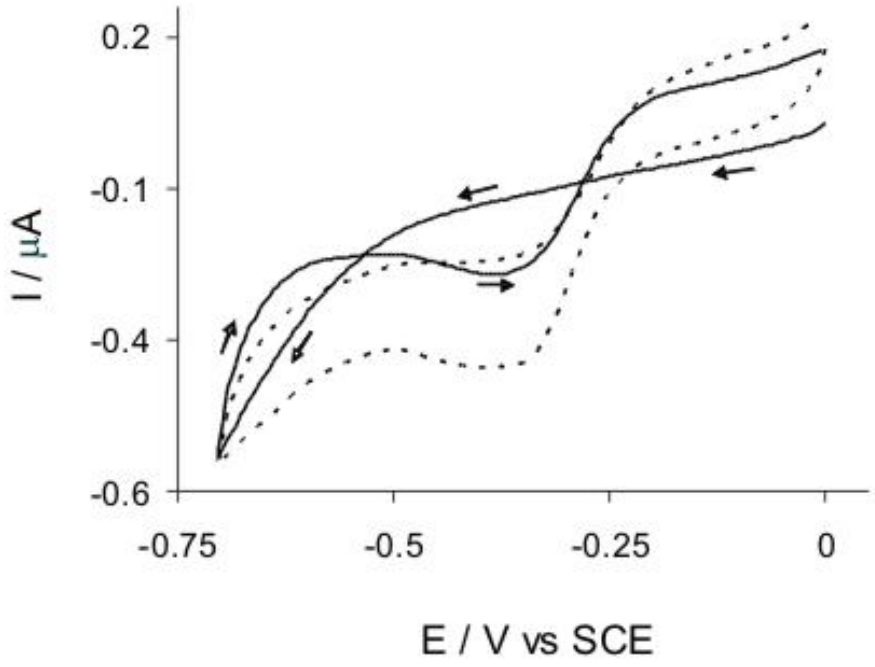

Figure V.7 Cyclic voltammograms of a diluted 2 μM Hase solution (black dashed line), ν = 50 mV s^{-1} using PG, obtained after previous activation with H_2 by overnight incubation at 4º C, at pH 7, and after multiple cycles between 0 and -800 mV vs. SCE and a resting period at the open circuit potential (1st scan black line, subsequent scans grey line).

The difference may arise from the lower energy needed to release the H_2 produced after the potential cycles imposed by cyclic voltammetry. This behaviour change and H^+/H_2 potential variation suggest that we are observing two different mechanisms by which the reaction occurs on Hase. This is in agreement with previous suggestions, based on density functional theory, that two different pathways are possible whether the potential control is made by imposing a H_2 pressure and reduction or if it is imposed electrochemically[14]. In the mentioned proposed mechanism the electrochemical controlled catalytic cycle predicts a very fast Ni(I) intermediate. This last assumption is not absolutely clear from the electrochemical data obtained at pH 7.6, although a small reduction wave observed at a more negative potential value of -650 mV (-408 mV vs. NHE) may be related with this reduced Ni form. This signal is better seen at lower pH (later on the text).

Another set of experiments was performed to study the scan rate variation effect on the catalytic current peak. The protein incubated with H_2 was subjected to multiple scans, with different scan rates (2.5 mV s^{-1} to 2 V s^{-1}), but, contrarily to the former assays without a resting period. The resulting voltammograms show a clear variation in the catalytic response pattern, that change from a typical catalytic sigmoidal curve for the smaller scan rates to a broad wave, characteristic of a diffusion controlled process (figure V.8).

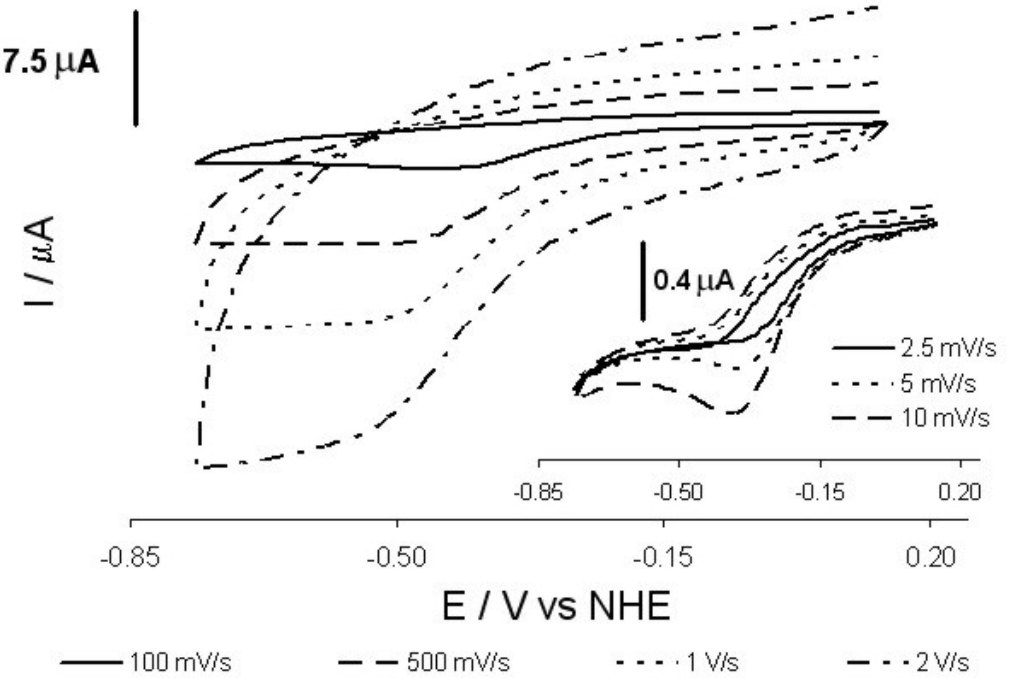

Figure V.8 Cyclic voltammograms of a diluted 2 μM Hase solution, with different scan rates, ν = 2.5 mV s^{-1} to 2 V s^{-1}, at the PG electrode, obtained after previous activation with H_2 by overnight incubation at 4 ºC, at pH 7.

It was not possible, however, to completely eliminate the catalytic reaction even with the maximum scan rate applied (2 V s^{-1}) due to the high turnover of this enzyme[35, 41].

It should be noted that the maximum of the catalytic current peak is observed at lower potential values than the obtained for the same conditions, before the imposed resting period, shown before (figure V.8). This is probably due to the fact that in this later case the protein has been already subjected to multiple potential cycles, and so, it has been electrochemically "activated".

V.2.2 Redox Centres Response

The same experimental conditions were used, with a highly degassed solution, but without a previous chemical activation step of the enzyme. The enzyme was purified

in aerobic conditions and it was kept that way previous to the electrochemical assay. In the voltammograms obtained in these conditions no catalytic wave is observed meaning that the enzyme is inhibited. There is, however, a direct electrochemical response of the protein both on PG and GC electrodes, allowing the identification of three redox processes. These correspond to the redox response of the metallic centres of the [NiFe]-Hase in non-turnover conditions.

On GC the processes are better defined and it is possible to see the redox processes clearly displayed, namely the cathodic process designated by I, around -600 mV (-358 mV vs. NHE), process II at -500 mV (-258 mV vs. NHE) with the anodic counterpart at -340 mV and the well defined redox couple, III, at -320 and -234 mV, respectively the cathodic and anodic peaks (see figure V.9). A comparison with the literature values obtained by electrochemical techniques and by EPR and Mössbauer spectroscopies together with a closer look to the structure of the enzyme was done in order to assign the observed redox processes[18, 42, 45]. Processes I and II were attributed to the $[4Fe\text{-}4S]_{dist}$ cluster and Ni (III/II), respectively. The well defined process III may be due to the [3Fe-4S] cluster, not only because of its higher potential value but also because this type of iron-sulphur clusters usually exhibit well defined and much more intense electrochemical signals than the [4Fe-4S] clusters[42, 46, 47]. Although in general, the [3Fe-4S] clusters can potentially undergo to one or two electron processes, from our data, the number of estimated electrons associated with the redox process III was 0.90 ± 0.13, indicating that this cluster undergoes a one electron transfer reaction. So, the size variations between the different centres signals must be attributed to its possible diverse accessibility and electron transfer kinetics. The estimated midpoint potential, E$^{o'}$ was -274 mV (-32 mV vs. NHE).

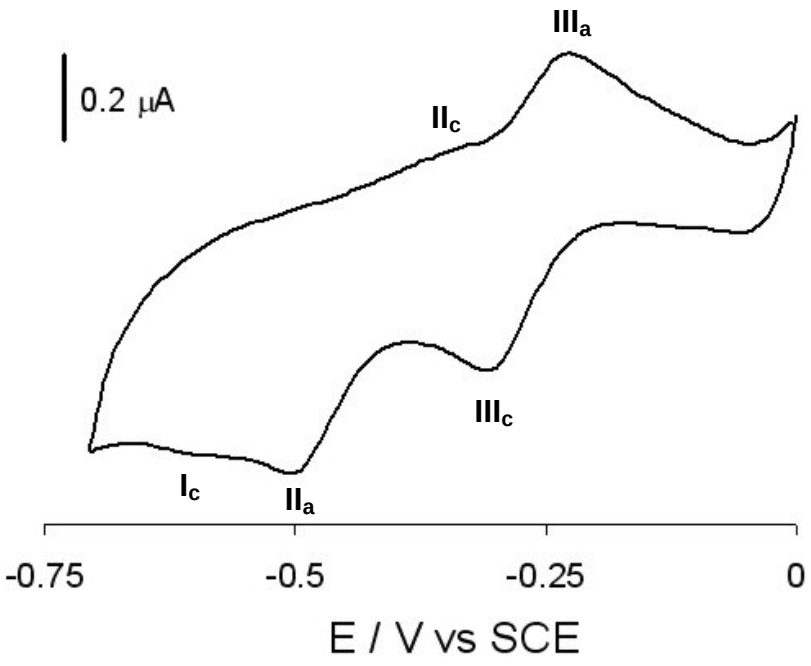

Figure V.9 Cyclic voltammogram of the *Dg* Hase in a diluted solution (2 μM), obtained in anaerobic conditions (attained with an argon flux), at pH 7, ν = 50 mV s^{-1}, using the GC electrode. The voltammogram is the result from the blank subtraction for better observation of the redox processes of the enzyme.

Figure V.10 displays the features obtained by reduction of the protein at -800 mV during different times followed by the potential scan in the anodic direction (-800 to 0 mV). In these conditions it is possible to observe two new anodic waves (I_a around -600 mV and II_a at -330 mV, approximately) related with the cathodic processes designated by I and II and that show the reversibility of the processes. A new sharp anodic peak appears at -500 mV that should be due to the oxidation of the hydrogen produced[41] at -800 mV. This phenomenon arises because the long reduction time probably implies the accumulation of an large enough amount of adsorbed molecules to the electrode surface, to allow its oxidation and consequently its detection in the time scale of the technique.

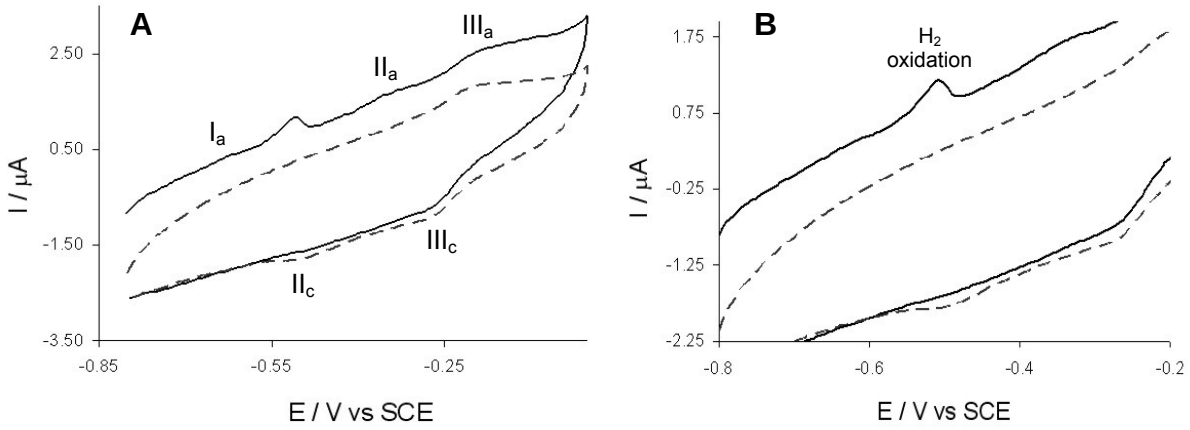

Figure V.10 A and B (ampliation of A) are the cyclic voltammograms of the *Dg* Hase in a diluted solution (2 μM), obtained in anaerobic conditions (attained with an argon flux), at pH 7, ν = 50 mV s^{-1}, using the GC electrode; dashed and solid line correspond to 0 and 600 s of potential delay at -800 mV, respectively and subscripts *a* and *c* stand for anodic and cathodic processes, respectively.

The redox behavior of Hase on PG also shows a redox pair for what it was possible to estimate the formal reduction potential, namely -635 mV (-393 mV vs. NHE). It is also possible to observe the development of a broad anodic wave around -350 mV. This seems to result from two anodic processes around -380 and -300 mV that merge in a large single broad anodic wave (figure V.11). A cathodic wave that seems related with the previous anodic broad wave also develops at -439 mV. By comparison with the results obtained on GC, these processes were attributed to processes II and III. The process with E°' = -635 mV (-393 mV vs. NHE) was attributed to process I. The same voltammograms show the development of another oxidation process at -150 mV, and its subsequent reduction on the reverse scan around -160 mV in a roughly defined cathodic wave. The processes were also observed on GC at slightly higher potential values and seem to be pH dependent. These may be due to the formation of the bridge oxo/hydroxo species on Ni-Fe corresponding to the non-active Hase forms Ni-A and Ni-B (later in the text).

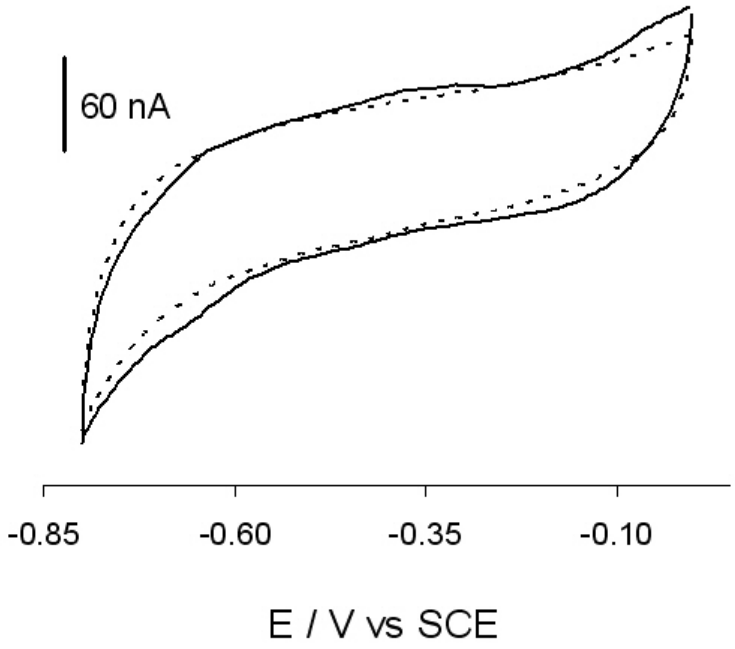

Figure V.11 Cyclic voltammogram of the *Dg* Hase in a diluted solution (1 μM), obtained with the PG electrode, at pH 7, ν = 50 mV s^{-1}, without previous activation of the enzyme.

Using a concentrated Hase solution (387 μM) the immobilisation of Hase by adsorption on graphite was also tried aiming to a better definition of the different redox processes of the enzyme metal centres. The results, however, were not satisfactory and it was not possible to improve the redox centres response. A typical result is shown on figure V.12. It is possible to detect a cathodic peak at -626 mV (-488 mV vs. NHE). By comparison with the former assays in solution this signal seems to result from an electronic transition from one of the enzyme metallic centres, probably the responsible for process I.

Pulse potential assays, by square wave voltammetry, were also performed aiming a better definition of the process observed by cyclic voltammetry (figure V.13). Two cathodic peaks were observed at -659 and -609 mV (-417 and -367 mV vs. NHE). These may be related with the processes I and II observed in the bulk experiments. The control presents a signal around -350 mV that is due to the remaining oxygen in solution that is not observable when a protein layer is on the electrode because it hinders the oxygen diffusion into the graphite surface. The enzyme adsorption, in the tried out experimental conditions, however, does not seem to be a better method than the conventional assays in solution.

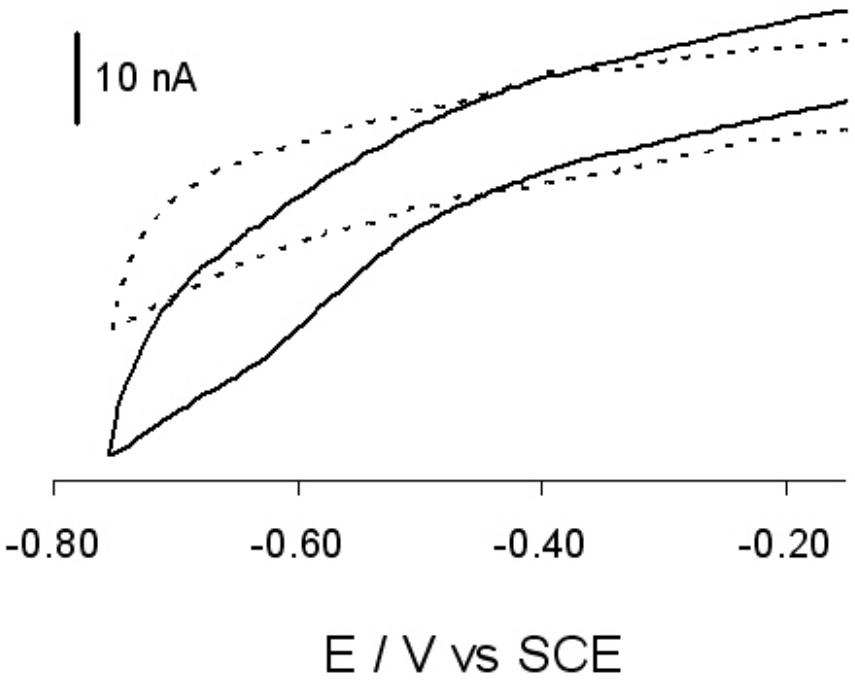

Figure V.12 Cyclic voltammogram of the *Dg* Hase adsorbed on the PG electrode, in 50 mM Tris-HCl / 0.1 M NaCl, pH = 7, ν = 10 mV s^{-1}.

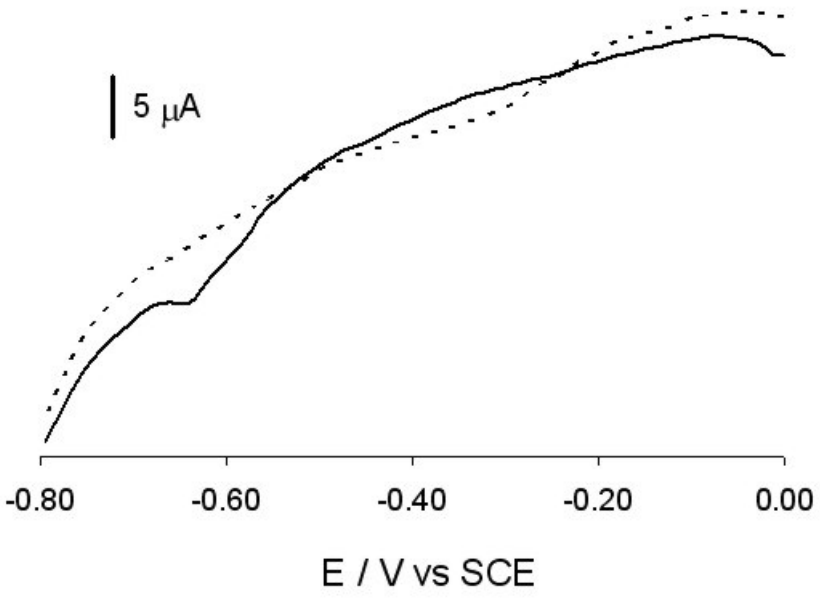

Figure V.13 Square wave voltammetry assays of the *Dg* Hase adsorbed on the PG electrode (solid line) and comparison with the control assay without enzyme (dashed line), in 50 mM Tris-HCl / 0.1 M NaCl, pH = 7, 50 mV pulse amplitude, 10 mV step potential, 8 Hz frequency.

The results from the bulk experiments, as well, as with the protein immobilised by adsorption show that it is possible to observe the metallic centres redox process starting with the non-activated Hase. This was the first time, to our knowledge, that these redox centres were observed in non-turnover conditions and without the use of any enzyme inhibitor.

V.2.3 Electrochemical Activation

The same experimental conditions as in the previous in bulk assays were again tested, with no previous activation of the enzyme. The next experiments were performed on strict anaerobic conditions (anaerobic chamber). The electrochemical activation of the Hase was achieved by multiple cycling between -50 and -1200 mV at low scan rate (5 mV s^{-1}). The cyclic voltammograms obtained show again current crossings, around -800 mV (-558 mV vs. NHE), simultaneously with some hydrogen evolution reaction (figure V.14).

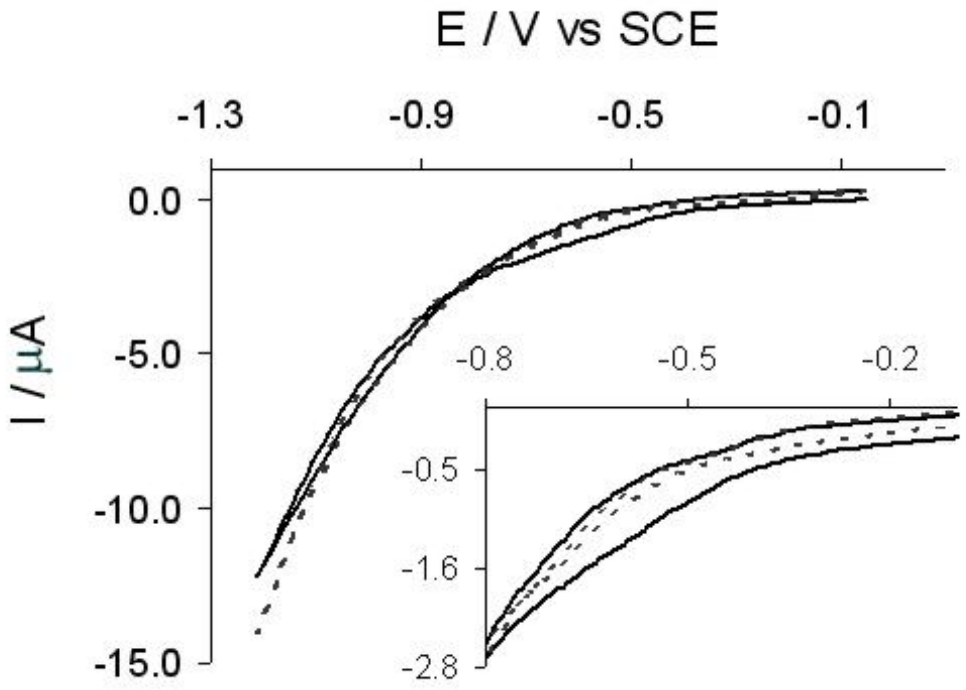

Figure V.14 Cyclic voltammogram of the *Dg* Hase in a diluted solution (3 μM), obtained in anaerobic conditions, ν = 5 mV s^{-1} at pH 4.5; A) 1st (solid line) and 3rd cycles (dashed line), inset: larger view of the potential window -200 to -800 mV.

It should be noted that a cathodic wave develops, on the first cycle, on the forward scan, around -500 mV. The reverse scan, after the current crossing, shows a smaller anodic wave at -300 mV. These can be related with the adsorption of hydrogen on the Ni-Fe centre during the process of the hydrogen fixation and/or hydride formation[44]. After cycling, a resting period at the open circuit potential was imposed, after which the same potential window was tested. The result was a typical catalytic current, showing that the electrochemical activation of the Hase was well succeeded (figure V.15). The Hase electrochemical activation was tested at different pH values. Besides the catalytic current, the subsequent voltammogram after the electrochemical activation, obtained at pH 5 or below, display another redox process at a more negative potential (inset of figure V.15). This cathodic wave after the catalytic process is probably due to a second reduction of the Ni atom, probably from Ni(II) to NI(I). This is in agreement with published data, namely potential values obtained by redox titrations[42], together with EPR experiments and theoretical calculations that point to the existence of a possible two electron reduction that would remove the hydride and generate a Ni(I) specie[48]. As mentioned before the existence of a paramagnetic Ni-L state that is obtained from the reduction of Ni-C upon illumination and at cryogenic temperatures was proven to be a reversible reaction that reverts to Ni-C with the temperature increase. DFT calculations point to the fact that this state is related with the loss of a proton from the bridging position between Ni and Fe atoms resulting in a formal oxidation state Ni(I) that seems in good agreement with the *g* values obtained experimentally[49]. In our assays, the driving force energy obtained at low potential values such as the imposed to the system at which the signal attributed to the Ni(II)/Ni(I) redox couple is observed, namely -1100 mV, is probably enough to achieve this state.

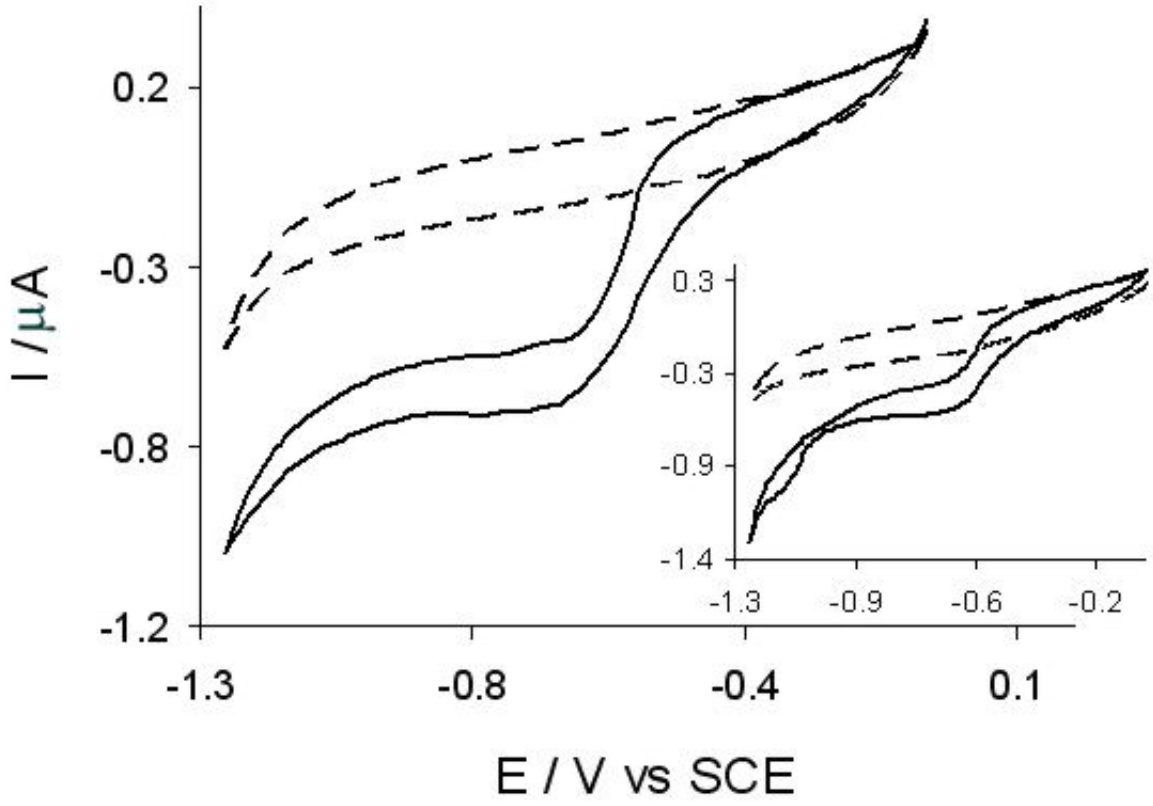

Figure V.15 Cyclic voltammogram of the *Dg* Hase in a diluted solution (3 μM), obtained in anaerobic conditions, ν = 5 mV s^{-1} after electrochemical activation with multiple scanning and a resting period (45 min) at the open potential potential (solid line) and the control assay (dashed line), inset: the same experiment at pH 5 (solid line) and the control assay (dashed line); it is possible to see the extra redox process assigned to Ni (II) / (I) (arrow).

The Hase electrochemical activation was only possible to achieve in strict anaerobic conditions. Outside the anaerobic chamber, even with highly degassed solutions with an argon flux, it was not possible to accomplish this potential modelling activation. This is probably due to the high sensibility to oxygen presented by the *Dg* [NiFe]-Hase[34] and the role of the non-active forms of the enzyme with oxo/hydroxo bridge species between the Ni and Fe atoms.

V.2.4 Electrochemical Inactivation

Another set of experiments was performed with *Dg* [NiFe]-Hase in bulk, in which a different potential window was tried, again in strict anaerobic conditions and pH 7.6. The goal was to inactivate the enzyme through potential tuning. An already electrochemically activated enzyme sample was submitted to multiple cycling in a different potential range, where the anodic limits were higher, namely from -50 to +300 mV, in a solution with pH 7.6. The first scan, beginning at the open circuit potential, in the cathodic direction, results in a typical active Hase feature, where the H^+ reduction wave is well defined. On the second cycle, however, after the protein has been subjected to the higher potential scanning, is already possible to see its inactivation (figure V.16).

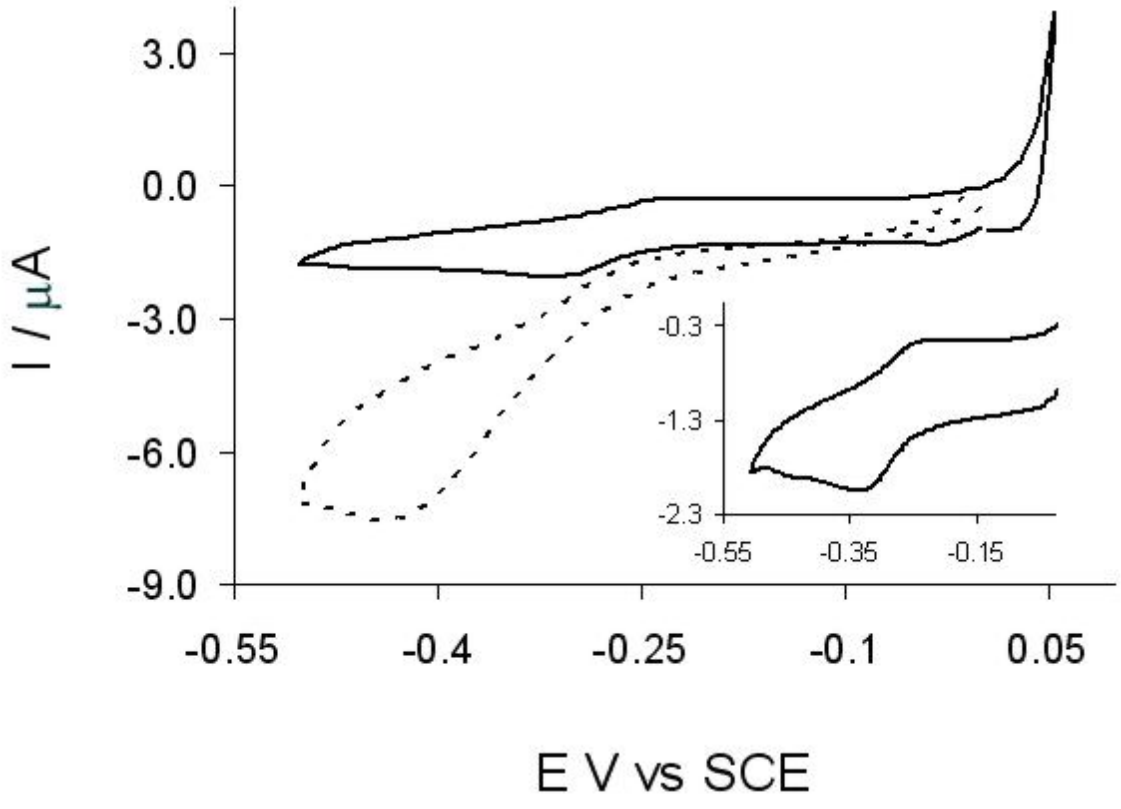

Figure V.16 Cyclic voltammogram of the *Dg* Hase in a diluted solution (2 μM), in anaerobic conditions, ν = 50 mV s^{-1}, pH 7.6, the 1st scan (dashed line) between 0 and -500 mV and 2nd (solid line) scans in a wider anodic potential limit (50 mV).

The redox centres mentioned before could again be observed, and no response due to hydrogen reduction can be observed (inset of figure V.16). In a wider potential window is possible to observe, beside these signals, the development of new signals at more anodic potential values, around -30 mV, as displayed in figure V.17.

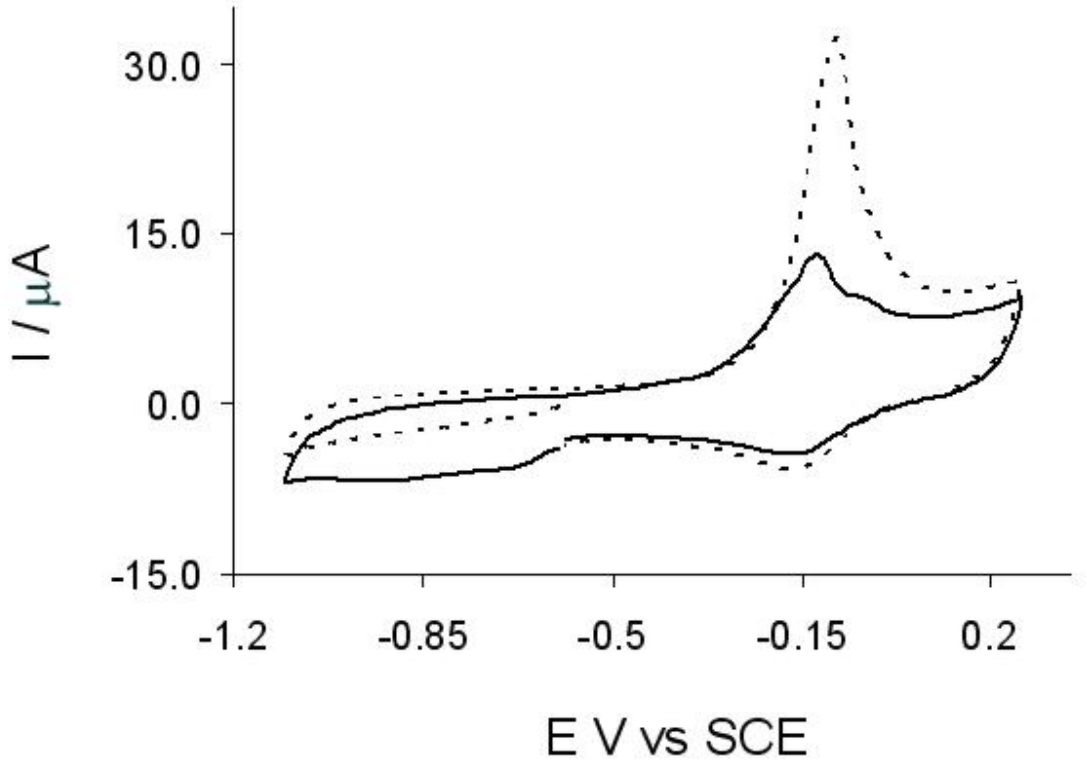

Figure V.17 Cyclic voltammogram of the *Dg* Hase in a diluted solution (2 μM), in anaerobic conditions, ν = 50 mV s^{-1}, pH 7.6 after inactivation by increasing the anodic potential limit, 1st (dashed line) and 2nd (solid line) scans.

These anodic processes at -30 mV may be associated with the formation of the Hase forms with the oxo/hydroxo bridge ligand. In fact the shape and potential domain of the above current peaks is quite similar to the ones observed by cyclic voltammetry for some nickel inorganic systems where the development of the metal hydroxides and other oxygenated species are described [50]. In the second cycle it is possible to observe new cathodic processes, in two different regions, around -150 mV, that are probably due to the reduction of the previous formed hydroxo/oxo species. Two other cathodic peaks are visible on the second scan at -700 and

-900 mV. These may be also attributed to the reduction of the oxo species formed on the first cycle and to the reduction of oxygen that is release in the first cathodic process around -150 mV. These processes seem to depend of the pH and as mentioned before may be due to the formation of the bridge oxo/hydroxo species on Ni-Fe corresponding to the non-active Hase forms Ni-A and Ni-B. In fact, no catalytic activity was observed with the Hase in these conditions. The shape and potential values at which these broad processes are observed are in agreement with the literature for the formation of α- and β-hydroxides on Ni metal, in inorganic systems[50, 51], that support the assignment of the redox peaks to the oxo/hydroxide formation.

After the described inactivation through the potential control, the electrochemical reactivation becomes very difficult. Indeed, application of the same electrochemical activation conditions as before the inactivation step did not result in the recovery of the initial current intensity for the hydrogen reduction (the maximum achieved for the reactivation was about 30% from the initial current intensity), which reflects the stability of the enzyme inactive forms and the poor reversibility of the reactions of the Hase with oxygen, as observed by other authors[35].

V.3 Electrochemical Catalytic Mechanism

Based on spectroscopic data and theoretical calculations, as mentioned before, some authors have proposed two different pathways for the [NiFe]-Hase catalytic cycle when the control is chemical, by exposure to H_2, or electrochemical[14]. Based on our experimental evidences, and taking into the consideration the literature data, we propose a scheme for the Hase activation/inactivation process electrochemically controlled (figure V.18). In this representation we assume that either starting with Ni-A or Ni-B species the enzyme can be activated electrochemically in a step that involves the hydride bridge formation and the simultaneous reduction of Ni(III) to Ni(II). This is consistent with recent studies that point to be energetically more favourable to cleave H_2 starting from a Ni(III)-H_2 precursor than a high spin Ni(II)-H_2 precursor[14]. The catalytic cycle proceeds with the H_2 release and the Ni reoxidation and restoration of the hydride bridge. After that, the Ni(II) can be further reduced to a

Ni(I) state. The role of this nickel oxidation state is, however, not well understood and may not be catalytically relevant in physiological conditions.

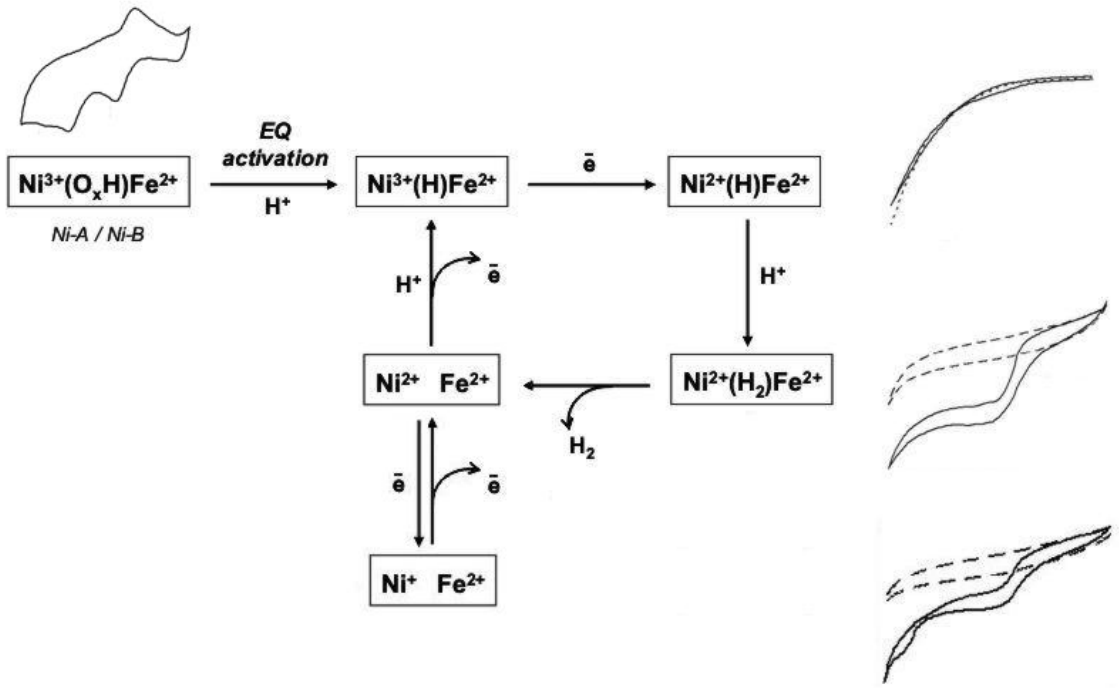

Figure V.18 Schematic representation of the proposed pathway for the Hase catalytic cycle under electrochemical control, with the correspondent voltammetric features.

V.4 Final Remarks

In this work we were able to observe the direct electrochemistry of the *Dg* Hase, in bulk solution and also immobilised by adsorption, in turnover and non-turnover conditions. For the first time the redox features of the enzyme metallic centres in non-catalytic conditions and without the addition of any of the known enzyme inhibitors were attained. Besides, we were able to tune the activation and inactivation of the Hase by dynamic potential control, where the formation of the hydride bridge was confirmed to be determinant. The potential control is also essential in the electrochemical inactivation of the enzyme through the formation of oxo/hydroxo

species within the nickel-iron centre. These results are important to better control the enzyme activity and can be of particular interest in electrochemical systems, such as biosensors or biofuel cells based on hydrogenase.

V.5 References

1. Volbeda, A., Garcin, E., Piras, C., L. de Lacey, A., Fernandez, V. M., Hatchikian, E. C., Frey, M., Fontecilla-Camps, J. C.,, Structure of the [NiFe] Hydrogenase Active Site: Evidence for Biologically Uncommon Fe Ligands. *J. Am. Chem. Soc.* **1996,** 118, 12989-12996.

2. Jones, A. K.; Sillery, E.; Albracht, S. P.; Armstrong, F. A., Direct comparison of the electrocatalytic oxidation of hydrogen by an enzyme and a platinum catalyst. *Chem Commun (Camb)* **2002**, (8), 866-7.

3. Karyakin, A. A.; Morozov, S. V.; Karyakina, E. E.; Zorin, N. A.; Perelygin, V. V.; Cosnier, S., Hydrogenase electrodes for fuel cells. *Biochem Soc Trans* **2005,** 33, (Pt 1), 73-5.

4. Beech, I. B.; Sunner, J., Biocorrosion: towards understanding interactions between biofilms and metals. *Curr Opin Biotechnol* **2004,** 15, (3), 181-6.

5. Mertens, R.; Liese, A., Biotechnological applications of hydrogenases. *Curr Opin Biotechnol* **2004,** 15, (4), 343-8.

6. Armstrong, F. A.; Albracht, S. P., [NiFe]-hydrogenases: spectroscopic and electrochemical definition of reactions and intermediates. *Philos Transact A Math Phys Eng Sci* **2005,** 363, (1829), 937-54; discussion 1035-40.

7. Hallenbeck, P. C.; Benemann, J. R., Biological hydrogen production; fundamentals and limiting processes. *International Journal of Hydrogen Energy* **2002,** 27, (11-12), 1185-1193.

8. Ihara, M.; Nakamoto, H.; Kamachi, T.; Okura, I.; Maeda, M., Photoinduced Hydrogen Production by Direct Electron Transfer from Photosystem I Cross-linked with Cytochrome c3 to [NiFe]-Hydrogenase. *Photochem Photobiol* **2006**.

9. Pieulle, L.; Morelli, X.; Gallice, P.; Lojou, E.; Barbier, P.; Czjzek, M.; Bianco, P.; Guerlesquin, F.; Hatchikian, E. C., The type I/type II cytochrome c3 complex: an electron transfer link in the hydrogen-sulfate reduction pathway. *J Mol Biol* **2005,** 354, (1), 73-90.

10. Moreno, C.; Franco, R.; Moura, I.; Le Gall, J.; Moura, J. J., Voltammetric studies of the catalytic electron-transfer process between the Desulfovibrio gigas hydrogenase and small proteins isolated from the same genus. *Eur J Biochem* **1993,** 217, (3), 981-9.

11. Haladjian, J.; Bianco, P.; Guerlesquin, F.; Bruschi, M., Kinetic studies of the electron exchange reaction between the octaheme cytochrome c3 (Mr 26000) and

the hydrogenase from Desulfovibrio desulfuricans Norway. *Biochem Biophys Res Commun* **1991,** 179, (1), 605-10.

12. Matias, P. M.; Soares, C. M.; Saraiva, L. M.; Coelho, R.; Morais, J.; Le Gall, J.; Carrondo, M. A., [NiFe] hydrogenase from Desulfovibrio desulfuricans ATCC 27774: gene sequencing, three-dimensional structure determination and refinement at 1.8 A and modelling studies of its interaction with the tetrahaem cytochrome c3. *J Biol Inorg Chem* **2001,** 6, (1), 63-81.

13. Yahata, N.; Saitoh, T.; Takayama, Y.; Ozawa, K.; Ogata, H.; Higuchi, Y.; Akutsu, H., Redox interaction of cytochrome c3 with [NiFe] hydrogenase from Desulfovibrio vulgaris Miyazaki F. *Biochemistry* **2006,** 45, (6), 1653-62.

14. Pardo, A.; De Lacey, A. L.; Fernandez, V. M.; Fan, H. J.; Fan, Y.; Hall, M. B., Density functional study of the catalytic cycle of nickel-iron [NiFe] hydrogenases and the involvement of high-spin nickel(II). *J Biol Inorg Chem* **2006,** 11, (3), 286-306.

15. Lyon, E. J.; Shima, S.; Buurman, G.; Chowdhuri, S.; Batschauer, A.; Steinbach, K.; Thauer, R. K., UV-A/blue-light inactivation of the 'metal-free' hydrogenase (Hmd) from methanogenic archaea. *Eur J Biochem* **2004,** 271, (1), 195-204.

16. Pilak, O.; Mamat, B.; Vogt, S.; Hagemeier, C. H.; Thauer, R. K.; Shima, S.; Vonrhein, C.; Warkentin, E.; Ermler, U., The crystal structure of the apoenzyme of the iron-sulphur cluster-free hydrogenase. *J Mol Biol* **2006,** 358, (3), 798-809.

17. Volbeda, A.; Fontecilla-Camps, J. C., The active site and catalytic mechanism of NiFe hydrogenases. *Dalton Transactions* **2003**, (21), 4030-4038.

18. Teixeira, M.; Moura, I.; Xavier, A. V.; Moura, J. J.; LeGall, J.; DerVartanian, D. V.; Peck, H. D., Jr.; Huynh, B. H., Redox intermediates of Desulfovibrio gigas [NiFe] hydrogenase generated under hydrogen. Mossbauer and EPR characterization of the metal centers. *J Biol Chem* **1989,** 264, (28), 16435-50.

19. Pierik, A. J.; Roseboom, W.; Happe, R. P.; Bagley, K. A.; Albracht, S. P., Carbon monoxide and cyanide as intrinsic ligands to iron in the active site of [NiFe]-hydrogenases. NiFe(CN)2CO, Biology's way to activate H2. *J Biol Chem* **1999,** 274, (6), 3331-7.

20. Armstrong, F. A., Hydrogenases: active site puzzles and progress. *Curr Opin Chem Biol* **2004,** 8, (2), 133-40.

21. Volbeda, A.; Charon, M. H.; Piras, C.; Hatchikian, E. C.; Frey, M.; Fontecilla-Camps, J. C., Crystal structure of the nickel-iron hydrogenase from Desulfovibrio gigas. *Nature* **1995,** 373, (6515), 580-7.

22. van Gastel, M.; Stein, M.; Brecht, M.; Schroder, O.; Lendzian, F.; Bittl, R.; Ogata, H.; Higuchi, Y.; Lubitz, W., A single-crystal ENDOR and density functional theory study of the oxidized states of the [NiFe] hydrogenase from Desulfovibrio vulgaris Miyazaki F. *J Biol Inorg Chem* **2006,** 11, (1), 41-51.

23. Volbeda, A.; Martin, L.; Cavazza, C.; Matho, M.; Faber, B. W.; Roseboom, W.; Albracht, S. P.; Garcin, E.; Rousset, M.; Fontecilla-Camps, J. C., Structural differences between the ready and unready oxidized states of [NiFe] hydrogenases. *J Biol Inorg Chem* **2005,** 10, (3), 239-49.

24. Carepo, M.; Tierney, D. L.; Brondino, C. D.; Yang, T. C.; Pamplona, A.; Telser, J.; Moura, I.; Moura, J. J.; Hoffman, B. M., 17O ENDOR detection of a solvent-derived Ni-(OH(x))-Fe bridge that is lost upon activation of the hydrogenase from Desulfovibrio gigas. *J Am Chem Soc* **2002,** 124, (2), 281-6.

25. Ogata, H.; Hirota, S.; Nakahara, A.; Komori, H.; Shibata, N.; Kato, T.; Kano, K.; Higuchi, Y., Activation process of [NiFe] hydrogenase elucidated by high-resolution X-Ray analyses: conversion of the ready to the unready state. *Structure (Camb)* **2005,** 13, (11), 1635-42.

26. Stein, M.; Lubitz, W., Quantum chemical calculations of [NiFe] hydrogenase. *Curr Opin Chem Biol* **2002,** 6, (2), 243-9.

27. Jones, A. K.; Lamle, S. E.; Pershad, H. R.; Vincent, K. A.; Albracht, S. P.; Armstrong, F. A., Enzyme electrokinetics: electrochemical studies of the anaerobic interconversions between active and inactive states of Allochromatium vinosum [NiFe]-hydrogenase. *J Am Chem Soc* **2003,** 125, (28), 8505-14.

28. Maroney, M. J.; Bryngelson, P. A., Spectroscopic and model studies of the Ni-Fe hydrogenase reaction mechanism. *J Biol Inorg Chem* **2001,** 6, (4), 453-9.

29. De Lacey, A. L.; Moiroux, J.; Bourdillon, C., Simple formal kinetics for the reversible uptake of molecular hydrogen by [Ni-Fe] hydrogenase from Desulfovibrio gigas. *Eur J Biochem* **2000,** 267, (22), 6560-70.

30. Montet, Y.; Amara, P.; Volbeda, A.; Vernede, X.; Hatchikian, E. C.; Field, M. J.; Frey, M.; Fontecilla-Camps, J. C., Gas access to the active site of Ni-Fe hydrogenases probed by X-ray crystallography and molecular dynamics. *Nat Struct Biol* **1997,** 4, (7), 523-6.

31. Buhrke, T.; Lenz, O.; Krauss, N.; Friedrich, B., Oxygen tolerance of the H2-sensing [NiFe] hydrogenase from Ralstonia eutropha H16 is based on limited access of oxygen to the active site. *J Biol Chem* **2005,** 280, (25), 23791-6.

32. Vincent, K. A.; Parkin, A.; Lenz, O.; Albracht, S. P.; Fontecilla-Camps, J. C.; Cammack, R.; Friedrich, B.; Armstrong, F. A., Electrochemical definitions of O2 sensitivity and oxidative inactivation in hydrogenases. *J Am Chem Soc* **2005,** 127, (51), 18179-89.

33. Mege, R. M.; Bourdillon, C., Nickel controls the reversible anaerobic activation/inactivation of the Desulfovibrio gigas hydrogenase by the redox potential. *J Biol Chem* **1985,** 260, (27), 14701-6.

34. Lissolo, T.; Pulvin, S.; Thomas, D., Reactivation of the Hydrogenase from Desulfovibrio-Gigas by Hydrogen - Influence of Redox Potential. *Journal of Biological Chemistry* **1984,** 259, (19), 1725-1729.

35. Vincent, K. A.; Cracknell, J. A.; Parkin, A.; Armstrong, F. A., Hydrogen cycling by enzymes: electrocatalysis and implications for future energy technology. *Dalton Trans* **2005**, (21), 3397-403.

36. Morozov, S. V.; Karyakina, E. E.; Zorin, N. A.; Varfolomeyev, S. D.; Cosnier, S.; Karyakin, A. A., Direct and electrically wired bioelectrocatalysis by hydrogenase from Thiocapsa roseopersicina. *Bioelectrochemistry* **2002,** 55, (1-2), 169-71.

37. Gros, P.; Zaborosch, C.; Schlegel, H. G.; Bergel, A., Direct electrochemistry of Rhodococcus opacus hydrogenase for the catalysis of NAD+ reduction. *Journal of Electroanalytical Chemistry* **1996,** 405, 189-195.

38. Tatsumi, H.; Takagi, K.; Fujita, M.; Kano, K.; Ikeda, T., Electrochemical study of reversible hydrogenase reaction of Desulfovibrio vulgaris cells with methyl viologen as an electron carrier. *Analytical Chemistry* **1999,** 71, (9), 1753-1759.

39. Rudiger, O.; Abad, J. M.; Hatchikian, E. C.; Fernandez, V. M.; De Lacey, A. L., Oriented immobilization of Desulfovibrio gigas hydrogenase onto carbon electrodes by covalent bonds for nonmediated oxidation of H2. *J Am Chem Soc* **2005,** 127, (46), 16008-9.

40. Léger, C. J., A. K.; Albracht, S. P. J.; Armstrong, F. A., Effect of a dispersion of interfacial electron transfer rates on steady state catalytic electron transport in [NiFe]-hydrogenase and other enzymes. *J. Phys. Chem. B* **2002,** 106, 13058-63.

41. Leger, C.; Jones, A. K.; Roseboom, W.; Albracht, S. P.; Armstrong, F. A., Enzyme electrokinetics: hydrogen evolution and oxidation by Allochromatium vinosum [NiFe]-hydrogenase. *Biochemistry* **2002,** 41, (52), 15736-46.

42. Pershad, H. R.; Duff, J. L.; Heering, H. A.; Duin, E. C.; Albracht, S. P.; Armstrong, F. A., Catalytic electron transport in Chromatium vinosum [NiFe]-hydrogenase: application of voltammetry in detecting redox-active centers and establishing that hydrogen oxidation is very fast even at potentials close to the reversible H+/H2 value. *Biochemistry* **1999,** 38, (28), 8992-9.

43. Soares, D. M., Hydride Effect on the Kinetics of the Hydrogen Evolution Reaction on Nickel Cathodes in Alkaline Media. *Journal of Electrochemical Society* **1992,** 139, (1), 98-105.

44. Vivier, V.; Cachet-Vivier, C.; Nedelec, J. Y.; Yu, L. T.; Joubert, J. M.; Percheron-Guegan, A., Electrochemical study of LaNi3.55Mn0.4Al0.3Co0.75 by cavity microelectrode in 7 mol 1(-1) KOH solution. *Journal of Power Sources* **2003,** 124, (2), 564-571.

45. Teixeira, M.; Moura, I.; Xavier, A. V.; Huynh, B. H.; DerVartanian, D. V.; Peck, H. D., Jr.; LeGall, J.; Moura, J. J., Electron paramagnetic resonance studies on the mechanism of activation and the catalytic cycle of the nickel-containing hydrogenase from Desulfovibrio gigas. *J Biol Chem* **1985,** 260, (15), 8942-50.

46. Chen, K.; Bonagura, C. A.; Tilley, G. J.; McEvoy, J. P.; Jung, Y. S.; Armstrong, F. A.; Stout, C. D.; Burgess, B. K., Crystal structures of ferredoxin variants exhibiting large changes in [Fe-S] reduction potential. *Nat Struct Biol* **2002,** 9, (3), 188-92.

47. Vincent, K. A.; Tilley, G. J.; Quammie, N. C.; Streeter, I.; Burgess, B. K.; Cheesman, M. R.; Armstrong, F. A., Instantaneous, stoichiometric generation of powerfully reducing states of protein active sites using Eu(II) and polyaminocarboxylate ligands. *Chem Commun (Camb)* **2003**, (20), 2590-1.

48. Foerster, S.; Stein, M.; Brecht, M.; Ogata, H.; Higuchi, Y.; Lubitz, W., Single crystal EPR studies of the reduced active site of [NiFe] hydrogenase from Desulfovibrio vulgaris Miyazaki F. *J Am Chem Soc* **2003,** 125, (1), 83-93.

49. Stein, M.; van Lenthe, E.; Baerends, E. J.; Lubitz, W., Relativistic DFT calculations of the paramagnetic intermediates of [NiFe] hydrogenase. Implications for the enzymatic mechanism. *J Am Chem Soc* **2001,** 123, (24), 5839-40.

50. Salgado, J. R. C.; Andrade, M. H. S.; Silva, J. C. P.; Tonholo, J., A voltammetric study of alpha- and beta-hydroxides over nickel alloys. *Electrochimica Acta* **2002,** 47, (12), 1997-2004.

51. Kreysa, G.; Hakansson, B., Electrocatalysis by Amorphous Metals of Hydrogen and Oxygen Evolution in Alkaline-Solution. *Journal of Electroanalytical Chemistry* **1986,** 201, (1), 61-83.

Chapter VI

Electroactive Biofilms of Sulphate Reducing Bacteria

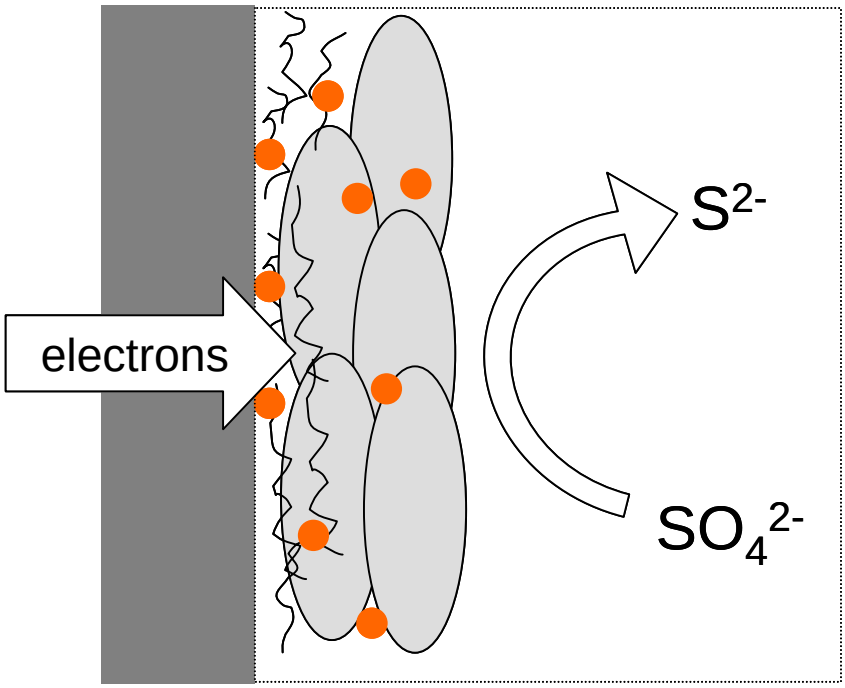

Electroactive Biofilms of Sulphte Reducing Bacteria

VI. 1 Biofilms

In natural environments, bacteria can live independently, as planktonic cells, but often form complex organism communities that survive attached to surfaces, forming biofilms. These can be formed by one single or by multiple species, with different metabolic mechanisms, which in many cases function as cooperative consortia. The positioning of bacteria and the biofilm construction is possible due to cell aggregation and attachment to surfaces. It is known that the surfaces' properties, along with other conditions as nutrient supply, the microbial biology or the hydrodynamics, can affect the biofilm structure. One common structure of biofilms presents high heterogeneity with cell aggregates dispersed in an exopolymers' matrix, mainly constituted by exopolysaccharides (EPS) that also allow the existence of water channels[1]. Besides EPS this matrix contains other components as proteins and nucleic acids. The term biofilm is referred to the all assemblage of bacteria and extracellular products at the interface.

One important aspect in the microbe-surfaces is the role of the extracellular metals, where its availability, solubility and stability are key roles. The utility of metals, either intra- or extracellular, for the microbial metabolism is dependent on the metal capacity to act as electron donor or acceptor. The most relevant redox couples in this context are Fe(II)/Fe(III) and Mn(II)/Mn(IV), not only for its abundance but also due to its formal redox potentials, compatible with the biological activity[2].

Besides the environmental influence on the biofilm formation, that includes nutritional factors, some studies have revealed that additional changes in bacteria gene expression are needed in order to adapt bacteria to a biofilm surface attached existence. One example of this is the expression of *alg*C, a gene responsible for alginate production which is an important product in the EPS matrix of biofilms, in *P. aeruginosa*. It was shown that this gene expression was activated in a manner of minutes after the contact of the cell with a surface[3]. There are three important steps in the biofilm growth. First the contact of cell with the surface, then its mobility on the surface and contact with other cell in a signalling mechanism that induces the production of molecules, typically lactones, that signals the population density and then the maturation of the biofilm with the formation of pillar-like structures in a EPS matrix[1, 3].

A schematic representation of the different stages of the biofilm formation is displayed in figure VI.1.

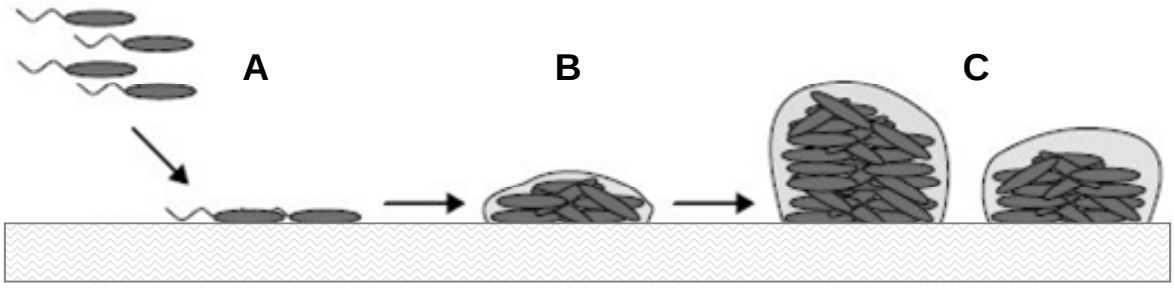

Figure VI.1 Different stages of the biofilms development, A) planktonic cells come near a surface and start cell-cell and cell-surface contact, B) formation of microcolonies and C) 3D structures of a mature biofilm (adapted from O'Toole, 2000)[3].

One of the major results of the biofilm formation is the deterioration of the surfaces due to the microbially influenced corrosion that is briefly discussed in the above section. Another area that recently has been the scope of interest is the possibility of using bacteria and biofilms in microbial fuel cells to produce electricity, reverting its occurrence to a useful application.

VI.1.1 Biocorrosion

One of the major consequences of the formation of biofilms is the possibility of an enhanced corrosion of the metallic surfaces by the result of the interactions between the metal surfaces, the inorganic corrosion and the products of the bacteria metabolism[4].

Corrosion occurs when two areas on a metallic surface have different potentials making one anodic and the other cathodic. Abiotically, without the presence of microorganisms, an electrochemical cell of this kind is formed when two different metals are in contact or, alternatively, when there are heterogeneities within one same metal or alloy. Metallic dissolution in the anode is balanced by an equivalent

reaction at the cathode where an electron acceptor, usually oxygen, is reduced. The two reactions' products combination produces metallic oxide and hydroxide which are characteristic of rust. The accumulation of the reactions' products at the metal-electrolyte interface leads to a smaller corrosion rate[5].

This process takes place in several steps, namely, an initial corrosion phase, followed by a period of low corrosion rate due to the protective character of the first layer of the formed products. After some chemical modification or rupture of the protective layer leads to a second corrosion active phase, which is frequently faster and longer than the initial phase associated with localised corrosion. This last corrosion pattern is associated to the microbial corrosion in general and to the sulphide corrosion in particular[2].

In microorganisms-promoted corrosion the initial phase can be directly influenced by its own activity, but the second phase is more likely to depend on the environmental parameters, such as the local free iron concentration, the system hydrodynamics or the presence/absence of oxygen. These factors, as mentioned before are also important for the biofilm development on a surface. The corrosion due to microorganisms can be due to many different species and mechanisms. Its effects can be specific as the Fe(II) to Fe(III) oxidation, due to *Gallionela*, the fatty acid production as in the case of *Cladosporium* or, in a more general way, as assemblages with differential aerobic/anaerobic conditions resultant of the colonies or biofilms growth[5].

The growth of aerobic microorganisms produces an oxygen gradient in which the regions below the active growth layer become rapidly anaerobic, and so, anodic towards the remaining metallic surface exposed to oxygen. This leads to the local metallic dissolution and is the more common mechanism of biocorrosion associated to the biofilms or colonies presence on metallic surfaces. The anaerobic areas on these surfaces are ideal environments for the sulphate redevelopment of anaerobic corrosion[2, 5].

SRBs are anaerobic but they can be isolated from aerobic environments. These microorganisms are frequently present in natural environments as microbial consortium members, in which the metabolic products of the aerobic species are used as nutrients for the SRBs.

The most well known model for the biocorrosion mechanism by SRBs is the so-called cathodic depolarization model[5, 6]. The model predicts that in the absence of oxygen and in acidic conditions, protons act as cathodic electron acceptors, with the formation of atomic hydrogen first and then molecular hydrogen, according with the above scheme:

$$2H^+ + 2\bar{e} \longrightarrow 2H \longrightarrow H_2$$

The reactions sequence is inhibited by the molecular hydrogen film accumulation on the metal surface that has a polarization effect on the surface. The model considers that the oxidation of this hydrogen by SRB's hydrogenase promotes the cathodic depolarization and the subsequent metal (anode) dissolution.

Another proposed mechanism considers that for pH values close to neutrality the hydrogen sulphide is the electron acceptor, with formation of molecular hydrogen, according to the reaction:

$$2H_2S + 2\bar{e} \longrightarrow 2HS^- + H_2$$

The two mechanisms propose a metallic sulphide formation, usually, iron sulphide as the corrosion product, through the two steps scheme presented below:

$$4\,H_2 + SO_4^{2-} \longrightarrow 4H_2O + S^{2-}$$

$$M^{2+} + S^{2-} \longrightarrow MS$$

Another mechanism to explain the SRB's promoted corrosion is the anodic depolarization that considers the sulphite formation as the key step. It is proposed that the protons production due to the SRB's metabolism promotes an anodic region and so, the metallic dissolution. If there is a local acidification due to the iron sulphide formation, a chain reaction can occur leading to the establishment of a stable galvanic current associated to the anode and to the beginning of the localised corrosion. The key step reaction is:

$$Fe^{2+} + HS^- \longrightarrow FeS + H^+$$

This reaction removes HS^-, reducing the buffer effect of the pair H_2S/HS^-, and so, the pH of the medium drops[2].

The kind of metallic sulphides that are formed during the corrosion are important to define the corrosion extension. It was observed that a thin, continuous and adherent

sulphide film is corrosion protector, with a similar mechanism to the oxide films that protect stainless steel in aerobic media. However, when the sulphide film is thicker and less adherent or when ruptures occur, the surface suffers extended and prolonged corrosion, independently of the microbiological activity[5]. The formation of iron sulphides protective or active towards the corrosion is dependent on the iron concentration, the temperature and the fluid dynamics of the system. A schematic representation of the current model for the microbial influenced corrosion of steel is displayed in figure VI.2.

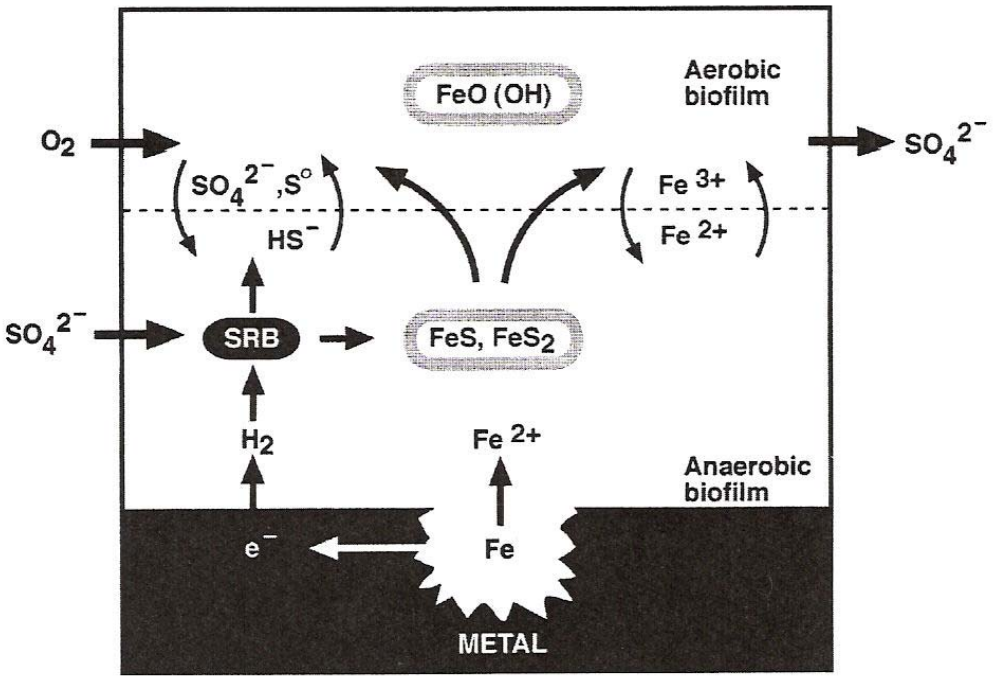

Figure VI.2 Representation of the SRB's microbial influenced corrosion of steel in a natural system with oxygen gradients (Hamilton, 2003)[2].

Some corrosion studies with iron sulphides produced abiotically, or with bacteria strains with and without hydrogenase enzyme, led to the conclusion that the microbiological activity is only related with the initial corrosion phase. Long assays (in months time scale) show that after the FeS film rupture, the corrosion rate becomes highly independent of the bacteria presence, with or without hydrogenase, and that is comparable to the normal corrosion in high corrosive media. However, as iron sulphides are not thermodynamically stable in aqueous media, for the phenomenon to occur its continuous production by SRBs is needed[5].

Recently, to explain the microbial influenced corrosion, a unifying hypothesis, based on the comparison between the SRB and manganese oxidising bacteria (MOB) influenced corrosion of steel, has been proposed. In both MIC processes, the metabolic activity of the microorganisms generates products, such as MnOOH amongst others in the case of MOB, that are thermodynamically compatible with the corrosion potentials of the metallic surfaces, and so, are able to accept electrons from these[2, 4]. This unifying theory, however, do not take into consideration that components within the biofilms matrix, namely enzymes and metal ions bonded in polymeric substances can also catalyse reactions, and may be an important component in the biocorrosion effect[4].

VI.1.2 Electroactive Biofilms

An increasing interest in biofilms, due to the capability of microorganisms to transfer electrons to electrodes, either direct or indirectly, has been shown by the scientific community.

In recent years there were several studies that indicated that microorganisms' communities have the capability to transfer electrons to electrodes. This was demonstrated in simple experiments in which an anode and a cathode electrodes were placed, respectively, into marine sediments (anaerobic) and in the aerobic over layer resulting in the production of electrical current[7].

One of the organisms family that were identified was the *Geobacteraceae*. It was observed that pure cultures of *Geobacter sulfurreducens* and *Geobacter metallireducens* can oxidise organic compounds to carbon dioxide and transfer the produced electrons to a graphite electrode. Electrical current production can also currently be obtain with other bacteria such as *E. coli* but in these systems mediators, such as potassium ferricyanide or anthraquinone, must be added in order to obtain electron transfer. In *Geobacter* the electronic transfer is direct with no mediator added[8, 9]. Other organisms as *Rhodoferax ferrireducens* or *Shewanella putrefaciens* can also oxidise glucose or lactate with an electrode as electron acceptor. The difference between these species and *Geobacter* is that the latter shows a superior

efficiency in the effective conversion of the number of available electrons into electric current[9].

The major interest in the electroactive microorganisms is its application in microbial fuel cells. In these cells the fuel can be provided by organic matter that is degraded by microorganisms, the anode accepts the electrons from a microbial culture and the cathode transfers electrons to an electron acceptor, commonly oxygen. The anode compartment is usually anaerobic and the cathode aerobic. These two compartments are usually separated by a membrane to restrict the oxygen diffusion between the two chambers. Fermentative microorganisms are the most currently used but this solution is not efficient in terms of the electric current yield.

The mechanisms by which the microorganisms can transfer electrons to electrodes are the indirect electron transfer from the reduced metabolic products with the anode, the electron transfer that is made possible by the addition of artificial mediators, the electron transfer through mediators that are produced by the microorganism themselves and finally the direct electron transfer to the electrodes[10]. As mentioned before, this last mechanism was recognised in cultures of bacteria such as *Shewanella* and *Geobacter* species. A schematic representation of a potential microbial fuel cell attained in this later case is shown in figure VI.3.

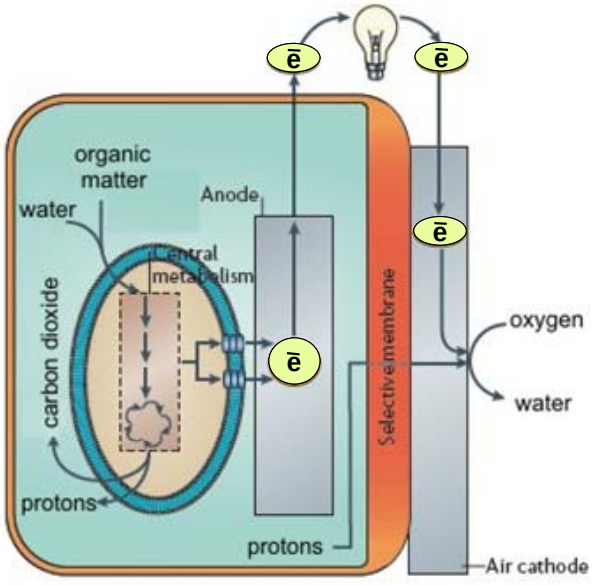

Figure VI.3 Schematic representation of a microbial fuel cell in which the electron transfer between the cells and the electrodes is direct. In the example (adapted from Lovley, 2006)[10], the authors propose that the produced electrons are transferred across the cell membranes by small electron carriers proteins, such as cytochrome *c*.

The possible use of electroactive biofilms for electricity production is a new and emergent field. The discovery of new bacteria strains with direct electron transfer capabilities, the current available tools to get genome sequences and to understand the microorganisms metabolisms and the improvements in the fuel cells technology bring an enormous potential of development in this area of knowledge. The study of pure cultures, such as the system studied in the present work, can clarify the microorganisms' mechanisms of electron transfer.

VI.1.3 The role of SRB in electroactivity

Sulphate reducing bacteria (SRB) are a group that belongs to anaerobic prokaryotes that use sulphate or sulphur as terminal electron acceptors. These organisms can be found in diverse environments in nature. A significant interest from the industry on these bacteria arise from its role in the petroleum products contamination and in the stainless steel anaerobic corrosion[11].

These organisms obtain energy through anaerobic respiration with a process of dissimilatory sulphate reduction with overall reaction:

$$4AH_2 + SO_4^{2-} + H^+ \rightarrow 4A + HS + 4H_2O$$

They can use different electron donors, generically AH_2, and they reduce sulphate or sulphur.

Some SRB's strains, such as *D. desulfuricans* ATCC 27774, are able to use not only sulphate but also nitrate as a final electron acceptor.

In respiration the electrons are generated by the oxidation of a compound and are subsequently used to reduce a second molecule that is independent of the initial oxidation pathway. The protons are transferred from the inside to the outside of the cell with the creation of a electrical potential gradient in the membrane. This driving force is used for the cell metabolic functions as for instance the ATP synthesis. The difference between aerobic and anaerobic respiration is that in the former the generated electrons are coupled to the reduction of oxygen while in the latter they are used to reduce a variety of compounds, namely SO_4^{2-}, NO_3^- or CO_2.

In the metabolism of the *Desulfovibrio* species, hydrogen plays an important and diverse role. Hydrogen can be used by these bacteria as the only energy resource in systems with acetate and CO_2 as carbon source, but it is also a metabolic product during fermentative growth if sulphate is absent. In the presence of sulphate, as mentioned before, hydrogen is produced and consumed. The proposed mechanism, by Odom and Peck in 1981, to explain the energy conservation on the *Desulfovibrio* species metabolism in lactate and sulphate media involves a hydrogen cycle where hydrogenase has a key role (figure VI.4)[12].

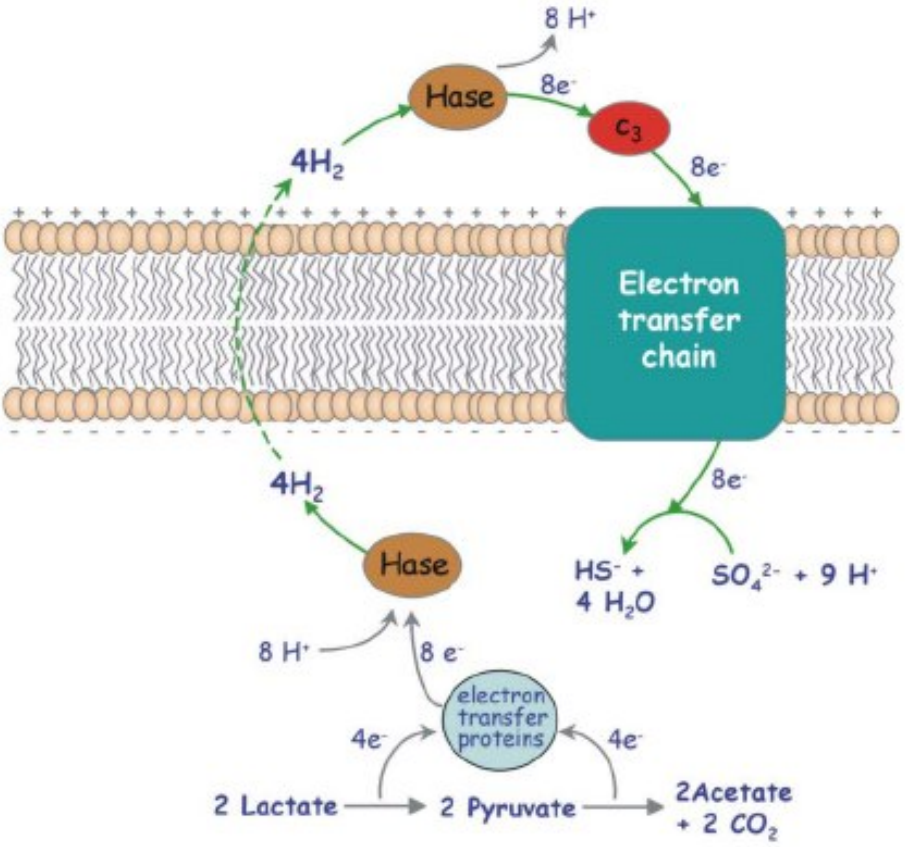

Figure VI.4 Schematic representation of the hydrogen cycling in *Desulfovibrio* species during growth in lactate/sulphate media (from Carrondo, 2005)[12].

In the above mechanism, the electrons that results from the lactate oxidation are transferred to a periplasmic hydrogenase, which reduces the available protons, producing H_2. The gas crosses the membrane and is oxidised in the cytoplasm again by a hydrogenase enzyme. The electrons that are produced are then transferred through an electron pathway chain to reduce sulphate, and consequently generating

protons that are used to the ATP synthesis. There are criticisms to the proposed mechanism, such as the need for a cytoplasmic hydrogenase that is not present in many of the *Desulfovibrio* species[12].

Besides sulphate and nitrate some of the SRB's strains, namely *Desulfovibrio vulgaris*, have the capability like other species, as for instance *Shewanella alga*, to reduce several metals, such as high valence metal ions as Cr(VI)[13], a particular important feature regarding the toxicity of this ion. Some studies with *Desulfovibrio desulfuricans* NCIMB 8307 showed that these can be used to reduce Pd(II), in a mechanism that bounds Pd(0) and that involves hydrogenase activity[13]. This element is a well known catalyst for hydrogen evolution reaction.

These bacteria ability leads to an enhanced interest because of the potential technological applications, in particular in the bioremediation field, but also for its possible application in the microbial fuel cells.

VI.2 SRB biofilms results

The aim of the present work is to study the possible electroactive behaviour of biofilms formed from pure cultures of sulphate reducing bacteria (SRB). The chosen strain was *Desulfovibrio desulfuricans* ATCC 27774. The evaluation of the response of the SRBs' biofilms formed on the electrodes was evaluated by the ratio of current obtained in the presence/absence of the biofilm and its stability in time.

VI.2.1 SRB biofilms growth characterisation on coupons

The growth of the SRB *D. desulfuricans* ATCC 27774 cells was studied previously to the polarization experiments. The cells growth with and without the presence of metal coupons was evaluated and the resulting biofilm was examined by scanning electron microscopy (SEM). The EPS yield and composition was also studied[14]. The results

correspondent to the growth conditions that were used in the polarization assays are shown below.

The growth pattern of the SRB in VMN/SO_4^{2-} without the presence of stainless steel (SS) coupons are displayed in figure VI.5.

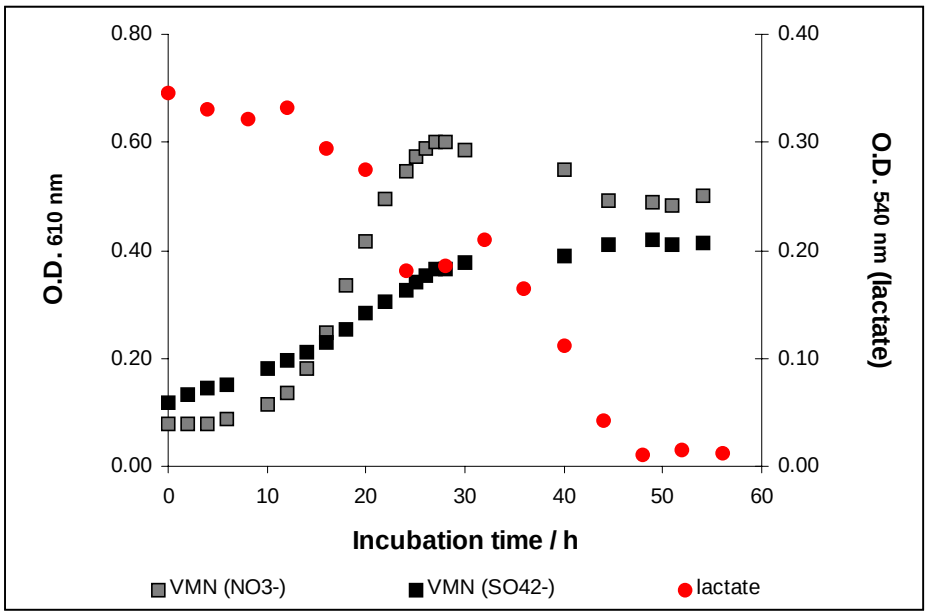

Figure VI.5 Evolution of the SRB growth in the two VMN media, with sulphate and nitrate, without the presence of coupons in bulk solution, by optical density measurements at 610 nm for the cell density and 540 nm for the control of the lactate consumption.

The pattern of growth without coupons is similar to the obtained when a stainless steel or carbon coupons are immersed in the reactor's media. Without coupons, however, the growth seems to occur faster, reaching the maximum within 1.5 days while in the presence of coupons this happens only after the third day.

A study using SEM of the biofilm growth on both VMN media was also done[14]. The coupons used were DSA (Dimensional Stable Anodes) and SS. A mature biofilm, after 15 days of growth was observed[14]. The images with different amplification are displayed in figure VI.6. The biofilm develops in both materials, although in SS the structure appears to be less compact and grown more in 3D dimensions.

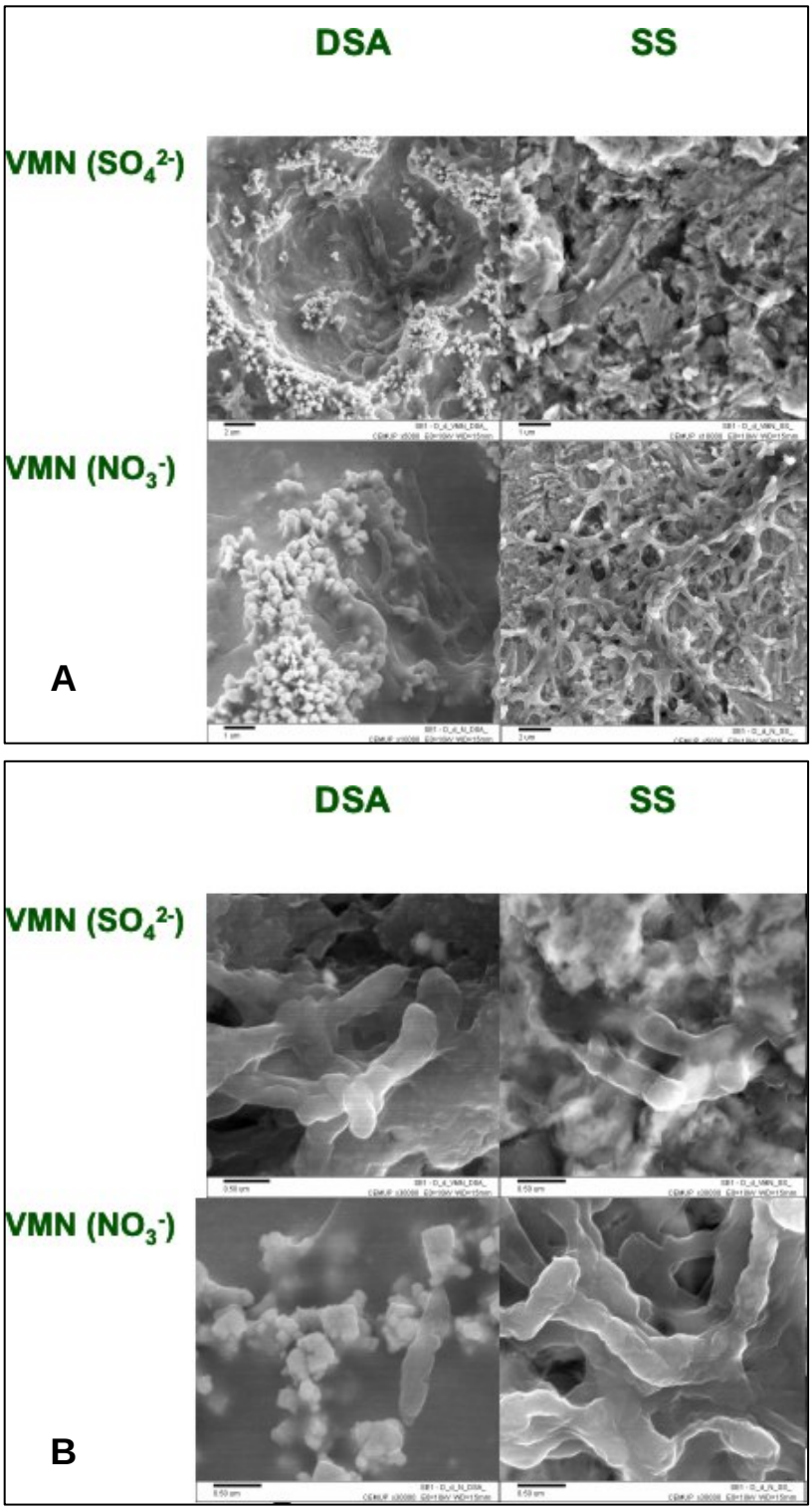

Figure VI.6 SEM images of the DSA and SS coupons after a SRB *D. desulfuricans* ATCC 27774 growth for 15 days, A and B) are the result of different amplifications; the high resolution SEM (JEOL, JSM 6301F; 10kV energy beam) was accomplished with a thin gold layer to ensure conductivity that was applied after drying the biofilm[14].

The EPS composition was also analised[14]. Table VI.I shows the EPS composition found from the planktonic and sessile cells.

Table VI.I *D. desulfuricans* ATCC 27774 biofilm composition (Martins, I., Project EA-Biofilms NEST-508866)[14].

VMN / SO_4^{2-}	**DSA**		**SS**	
	Planktonic	**Sessile**	**Planktonic**	**Sessile**
EPS yield (mg/cell)	2.5E-09	2.6E-07	2.8E-09	6.0E-08
Neutral sugars (μg/mg EPS)	12.1	57.6	13.2	44.1
Protein (μg/mg EPS)	21.4	38.5	23.3	18.2
Vc (mg/cm²day)	1.5E-03		1.2E-03	
VMN / NO_3^-	**DSA**		**SS**	
	Planktonic	**Sessile**	**Planktonic**	**Sessile**
EPS yield (mg/cell)	4.6E-09	n.d.	2.5E-09	1.2E-06
Neutral sugars (μg/mg EPS)	23.1	n.d.	18.6	26.8
Protein (μg/mg EPS)	26.2	n.d.	19.6	12.5
Vc (mg/cm²day)	2.7E-04		8.0E-04	

From the table it is possible to conclude that the production of EPS is equivalent in both materials. The values for the EPS found for the sessile cells in DSA and VMN/SO_4^{2-} are apparently higher than in SS. However, it has to be considered the much larger area of the DSA coupons' surface when compared with stainless steel. So, the discrepancy can be justified by the larger available area for the biofilm growth and EPS accumulation.

VI.2.2 SRB growth in VMN/SO_4^{2-}

The cells of *Desulfovibrio desulfuricans* ATCC 27774 were grown in VMN/SO_4^{2-} medium, pH 7, at 37 ºC temperature. The planktonic cell growth was evaluated by the optical density (O.D) at 610 nm, the lactate consumption and sulphide production (see experimental details in Appendix A). The cells were grown in the presence of polarized and non polarised surfaces of different materials, namely stainless steel, DSA and graphite. Chronoamperometry (CA) and cyclic voltammetry (CV) were used to evaluate the biofilms response. Also, EPR and CV assays were performed with the EPS of the *D. desulfuricans* strain cells in order to evaluate its role on the electrochemical response of the biofilms.

VI.2.2.1 Chronoamperometry of the SRB biofilms/VMN/SO_4^{2-}

Assays were performed using stainless steel, SS 254, as cathode and stainless steel 304 or graphite as anode in VMN/SO_4^{2-} medium, with different polarization conditions, namely, -200, -400 and -600 mV. Only the application of -400 mV on the working electrode produced a significant variation in the obtained current. The results have shown a cathodic current intensity increase starting around the 4^{th} day (Figure VI.7).

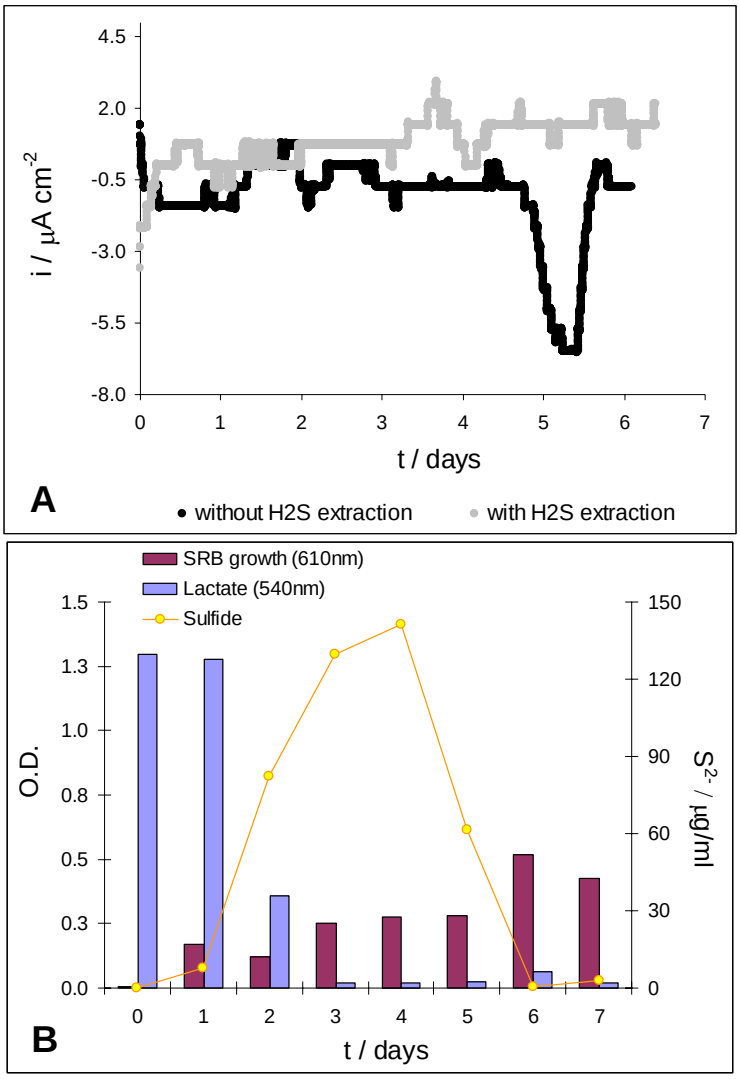

Figure VI.7 A) Current density vs. time plot from the SRB growth on VMN (SO_4^{2-}) with E_{app} = -400 mV; WE: SS 254, CE: SS 304; B) Evolution of the SRB growth, lactate consumption and sulphide production during the assay without H_2S extraction.

The maximum current intensity is 9 times larger than the residual current obtained before the current variation. After approximately 17 hours, the current starts to decrease and after one day comes back to the previous value. This result is reproducible (2 positives on each 3 essays). The blank essay (without SRB present) and the same assay with H_2S extraction did not present any current decrease. The lactate consumption is measured simultaneously with the sulphide production and the bacteria growth in bulk.

The fact that with H_2S extraction the cathodic current increase was not observed implies an interrogation regarding the role of the sulphide in this phenomenon. The

produced sulphide reacts with the Fe(II) present in the VMN medium and largely precipitates as FeS. Although this process is not electrochemical, the sulphide that remains in the form of H_2S can affect the electrode interface, for instance, changing the local pH. In order to understand the role of the H_2S vs. the biofilms activity on the current response another set of experiments with cellulose membranes protecting the working and the counter electrodes was made. The results are displayed on figure VI.8.

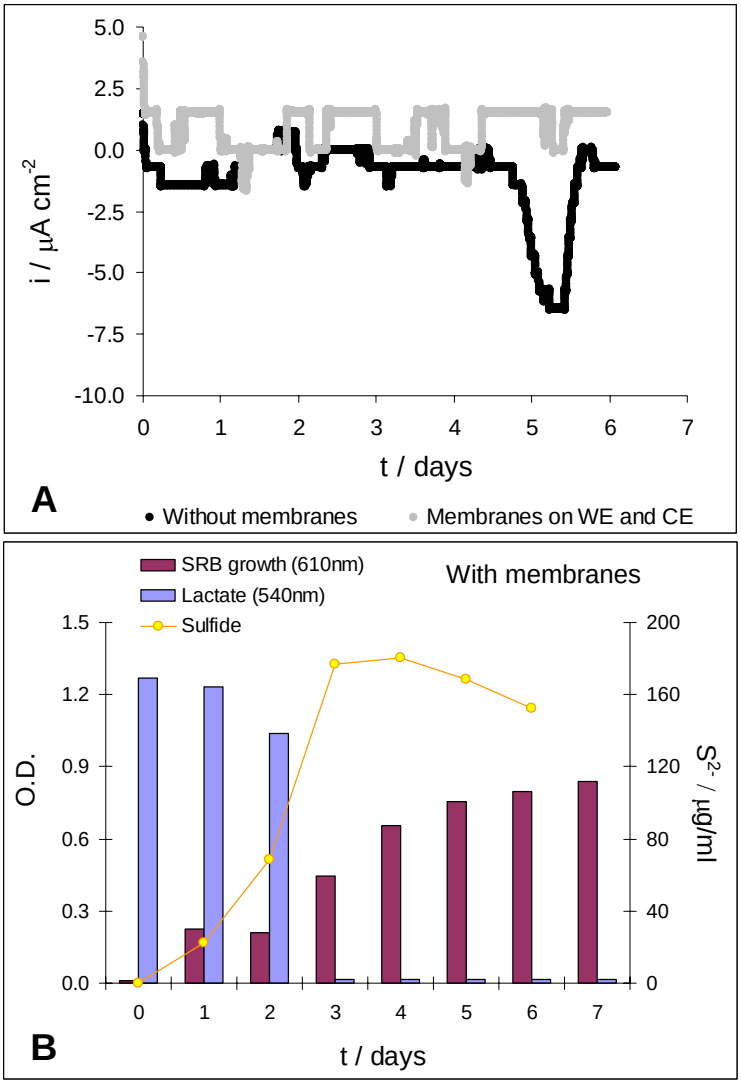

Figure VI.8 A) Current density vs. time plot from the SRB growth on VMN (SO_4^{2-}) with membranes on the electrodes, E_{app} = -400 mV; WE: SS 254, CE: SS 304; B) Evolution of the SRB growth, lactate consumption and sulphide production during the assay with membranes and without H_2S extraction.

The use of membranes hinders the biofilm formation but not the contact of the produced hydrogen sulphide with the electrodes surface. As no significant current increase was obtained using membranes, it is possible to conclude that the current is indeed due to the biofilm interaction, although a role of the H_2S in this interaction cannot be excluded.

To test the hypothesis that the observed current may be due to the result of reactions occurring on the counter electrode, due to the biofilm formation on this one, the H_2S production and subsequent change of the reactors' environment or oxidation on the CE surface (at this point SS CE was used), the CE material was changed from SS to graphite.

The same experiment, without membranes, was performed with the replacement of the CE material from SS to graphite. The obtained results are shown on figure VI.9.

It seems that the CE material influences the current response maybe because of specific reactions that may occur on the counter electrode surface. The same experiment with cellulose membranes protecting the working and the counter electrodes did not result in a cathodic current decrease.

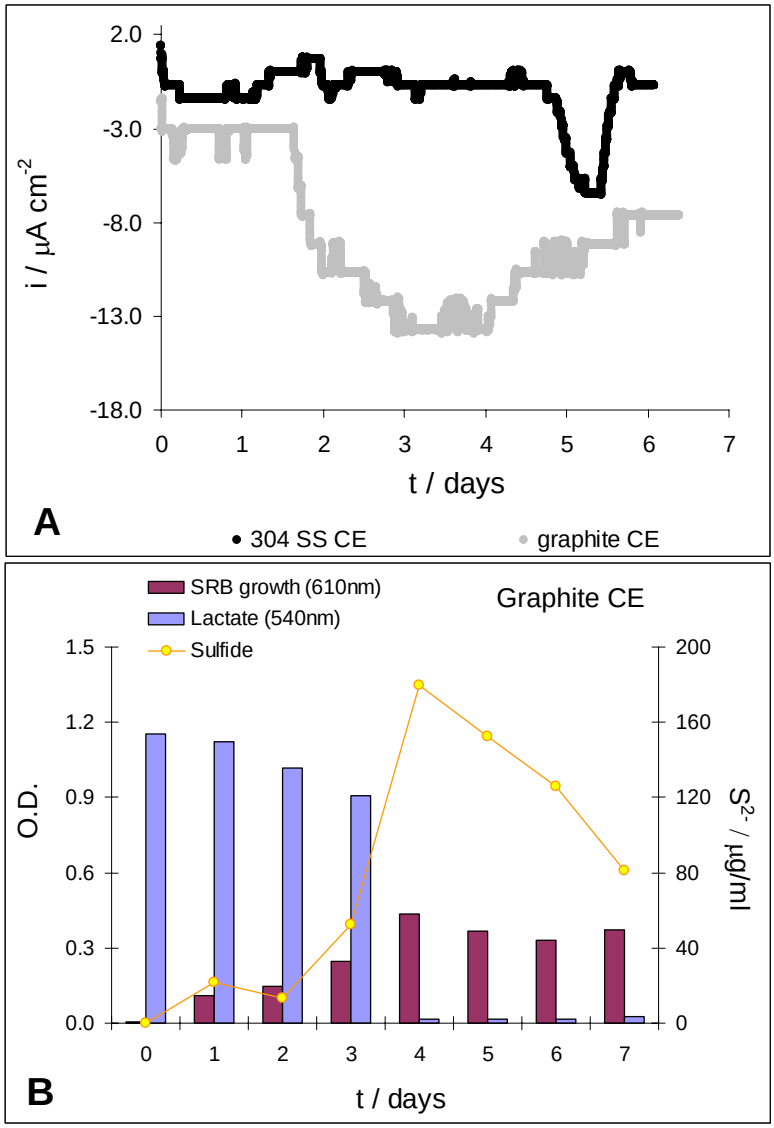

.

Figure VI.9 A) Current density vs. time plot from the SRB growth on VMN (SO_4^{2-}), without membranes, E_{app}= -400 mV; WE: SS 254, CE: Graphite; B) Evolution of the SRB growth, lactate consumption and sulphide production during the assay using graphite as CE, without membranes and without H_2S extraction

A similar experiment using fewer nutrients in the medium was performed, in this case the lactate concentration was altered to half the previous value. The working and counter electrodes used were, respectively, SS 254 and 304 SS. This assay intends to clear the hypothesis of the electrode to be working as electron donor in substitution of lactate. The results are displayed on figure VI.10.

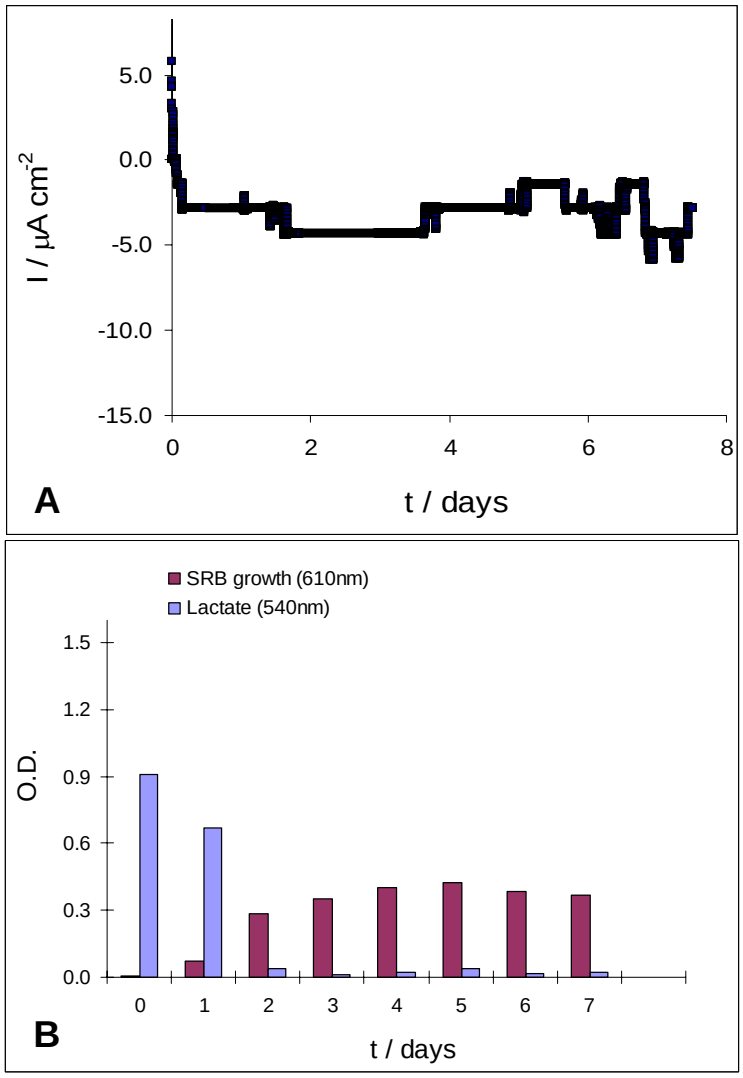

Figure VI.10 A) Current density vs. time plot from the SRB growth on VMN (SO_4^{2-}), with ½ of the initial lactate concentration, without membranes, E_{app} = -400 mV WE: SS 254, CE: SS 304 ; B) Evolution of the SRB growth and lactate consumption during the assay.

The results point to a normal growth pattern, with approximately half the number of planktonic cells obtained previously, and, as a consequence, the maximum OD reached was also half of the value. It was not possible so far to obtain a significant current variation in these conditions, probably due to the need to reach some critical mass on the electrode. Further assays are necessary to understand this situation.

Assays were performed using graphite as working electrode and also as counter electrode, using the same initial conditions of medium and temperature. The result

and the comparison with the control in which the electrodes are covered with membranes is shown in figure VI.11.

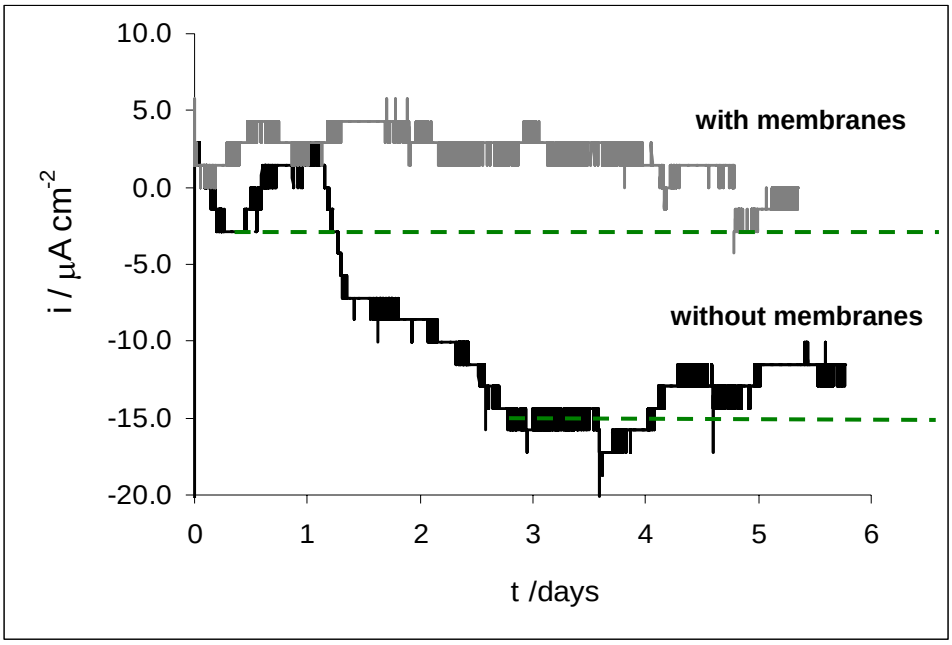

Figure VI.11 Current density vs. time plot from the SRB growth on VMN (SO_4^{2-}), with graphite electrodes as working (A_{geom} = 21 cm^2) and counter electrodes, with (grey line) and without membranes (black line) and without sulphide extraction, E_{app} = -400 mV; the maximum current variation obtained without membranes was at least 5.5 times the considered initial current (limits for the calculation are labeled in green at the above figure).

The results have shown that from the second day on is possible to observe an increase in the cathodic current. The current reaches 5.5 times the initial value, as can be seen in the above figure, and remains in this value at least for 24 h. The lactate consumption (not shown) presents the same pattern as in the previous assays.

The membranes protect the electrodes surface hindering the biofilm formation and its use implies that no significant current variation with time is obtained, showing that the biofilm interaction with the graphite surface is indeed responsible for the cathodic current increase.

Taking in consideration the above results the next assay was run, using the same experimental conditions, but with a longer time scale. The results are displayed in figure VI.12.

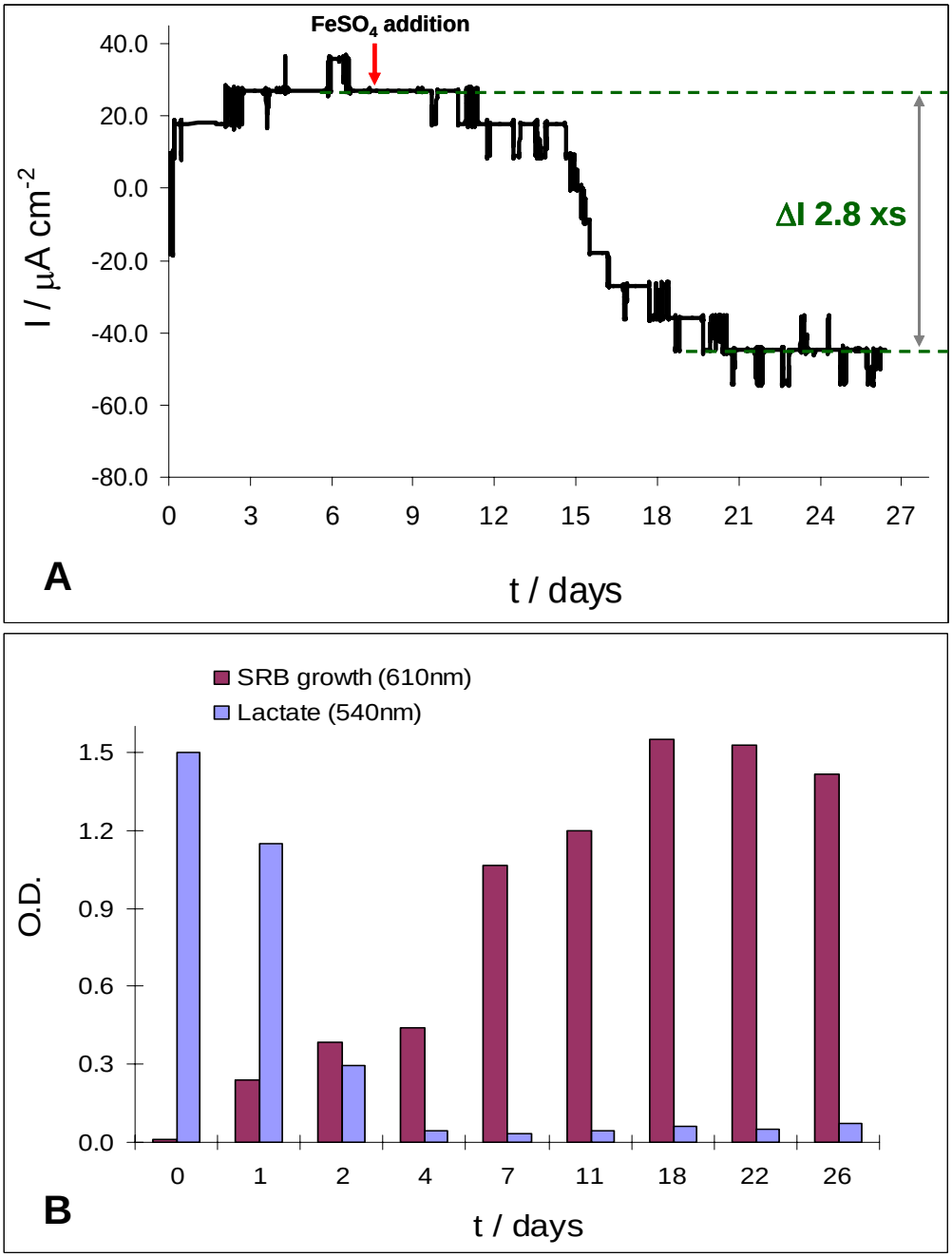

Figure VI.12 A) Current density vs. time plot from the SRB growth on VMN (SO_4^{2-}), with graphite electrodes as working (A_{geom} = 21 cm^2) and counter electrodes, without membranes and sulphide extraction, E_{app} = -400 mV; the maximum current variation was 2.8 times the considered initial current (labeled in green at the above figure) and B) evolution of the SRB growth and lactate consumption during the assay.

In this experiment iron sulphate was added at the 7th day in order to reach the initial concentration of the medium to ensure that the sulphate was not limiting the reaction.

The result was a cathodic current increase that reached 2.8 times the initial current value for at least one week long.

It was decided to run the next experiments using a different working electrode material, DSA, with the application of anodic polarization. The first set was then performed with DSA as WE and SS 304 as CE, with and without membranes on the WE. The results are displayed on figure VI.13.

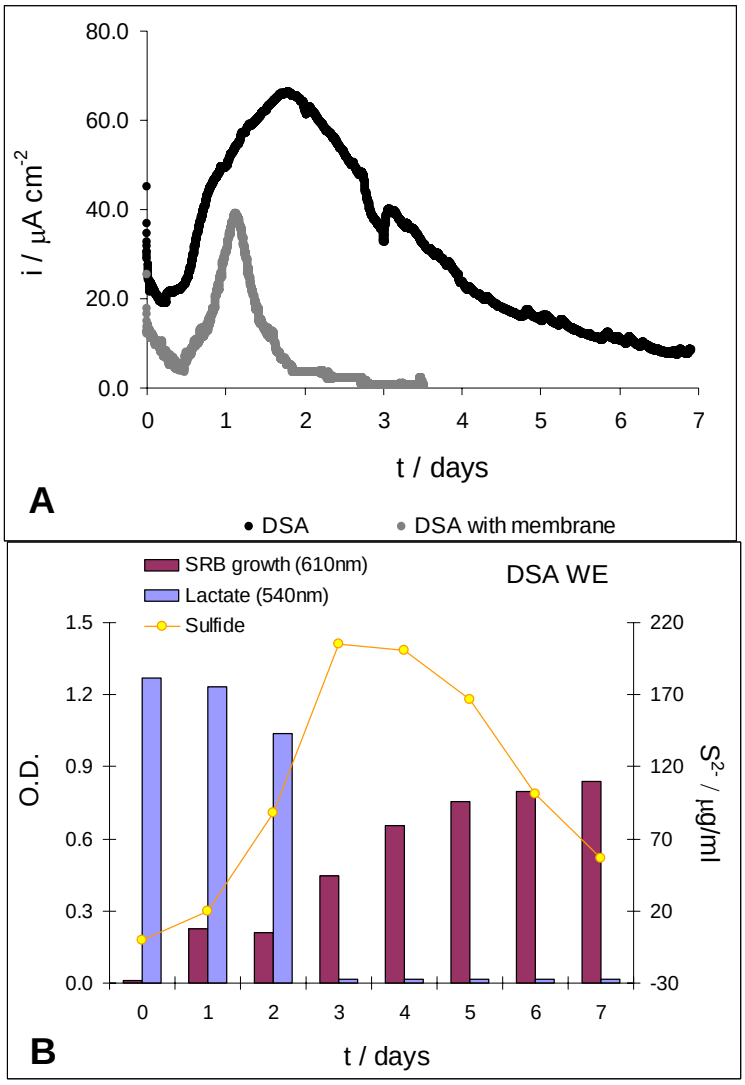

Figure VI.13 A) Current density vs. time plot from the SRB growth on VMN (SO_4^{2-}), with and without membranes, E_{app} = +200 mV; WE: DSA, CE: SS 304; B) Evolution of the SRB growth, lactate consumption and sulphide production during the assay using DSA as WE, without membranes and without H_2S extraction.

The anodic polarization with the DSA electrode has produced a large anodic current increase, with a maximum at the 2nd day, much sooner than in the previous assays. The current decreased slowly. With the membrane it was also registered an initial current increase although the current profile is quite different. The increase in the current without SRB present raises the question if the previous results are a consequence of the biofilm interaction or if it is a surface phenomenon, such as some reminiscent oxidation of the DSA typical oxides.

VI.2.2.2 SEM characterization of the SRB biofilms/VMN/SO_4^{2-}

The morphology of the biofilm on the graphite electrodes was analysed by SEM. The biofilm was developed for 32 days under a polarization of -400 mV in VMN/SO_4^{2-} medium. In this assay it was observed a variation of 17 times the initial current, with a maximum current of -150 mA m^{-2} that remained stable for approximately 10 days. In figure VI.14 the SEM images obtained with different amplifications in a region of the electrode surface are presented.

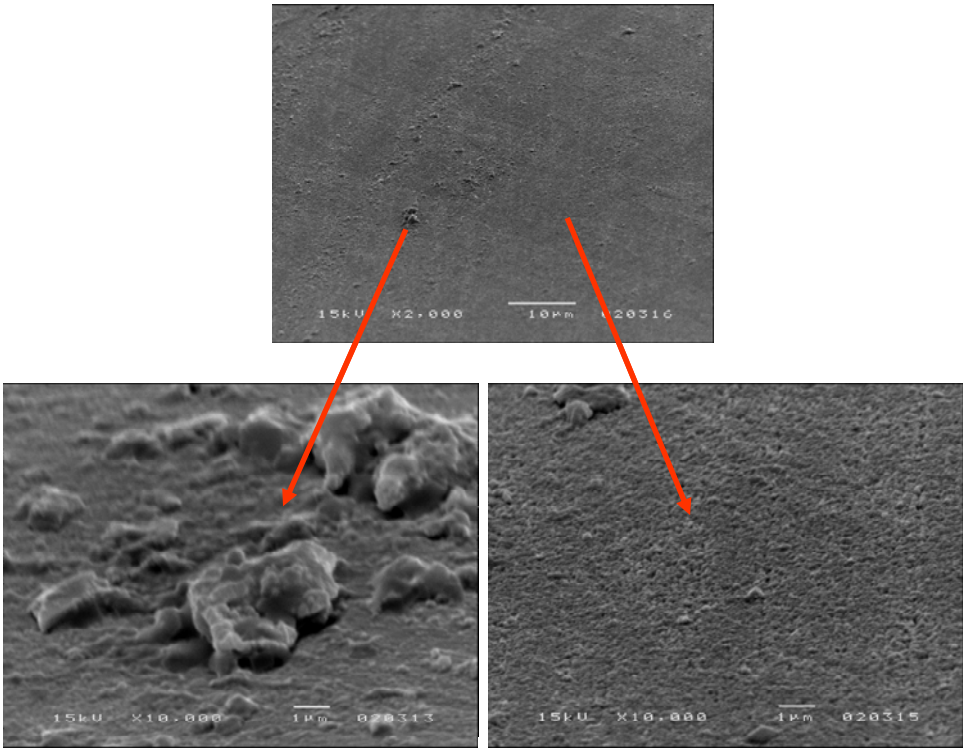

Figure VI.14 SEM images (JEOL JSM-5200 LM) of the SRB's biofilms on polarized graphite (-400 mV); a thin gold layer to ensure conductivity that was applied after drying the biofilm.

The presented images are representative of the electrode surface.

The development of the biofilm can be observed in the entire electrode surface presenting good homogeneity. It is possible to distinguish three dimensions agglomerates that emerge from the first layer, which is a typical morphology of the biofilms development.

VI.2.2.3 Cyclic voltammetry of the SRB biofilms/VMN/SO_4^{2-}

Cyclic voltammetry was used to understand the biofilms activity on the electrodes surface. The assays were done with the electrodes with and without being subjected to polarization conditions. The studied potential window was from 300 to -1100 mV and the scan rate was 20 mV s^{-1}. The results using a non polarised graphite disk are displayed in figure VI.15.

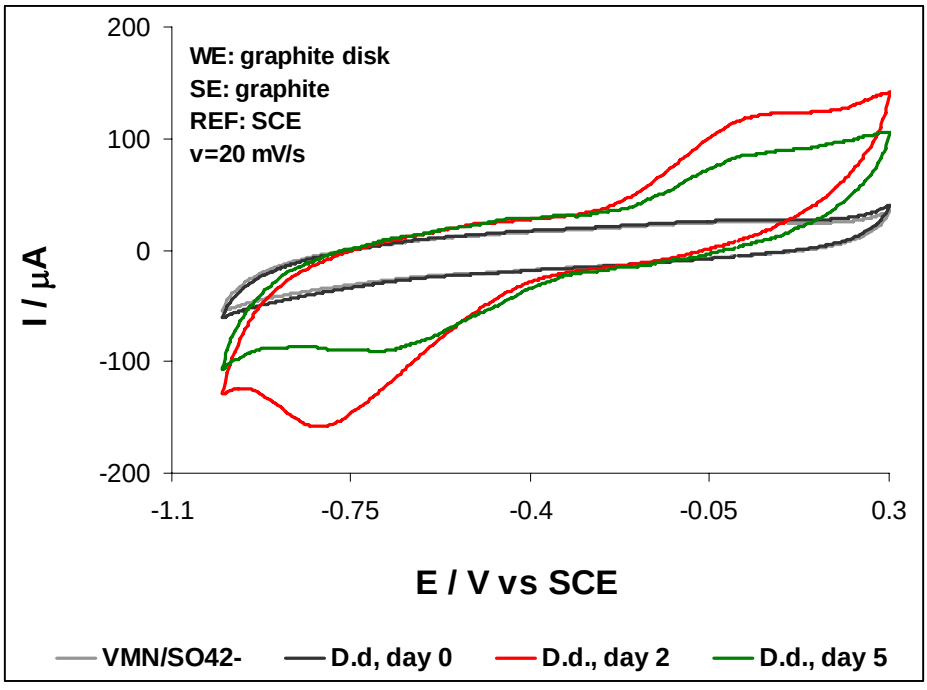

Figure VI.15 Cyclic voltammogram of a non polarized graphite disk electrode from day 0 to day 5 of the SRB growth on VMN (SO_4^{2-}) and comparison with the control assay without the presence of SRB in the medium (the control is similar throughout the time).

It was possible to observe an enhanced electroactivity when the SRBs biofilm develops on the electrode surface. The results from day 2 show the development of a cathodic wave, with maximum at -800 mV, composed by two processes in which the second is displayed at approximately –650 mV. An anodic wave develops at approximately -50 mV. The waves' current intensity is higher at day 2 and decreases from the 5th day onwards. This variation is probably related with the biofilm thickness. These processes are probably related with the reduction of the reminiscent oxygen in bulk solution. The process seems to occur in a two-step reaction and the subsequent reoxidation of the reduced species, namely H_2O_2, is also detected. The reactions should correspond to the oxygen reduction mechanism proposed, namely:

$$O_2 + 2\bar{e} + 2H^+ \rightarrow H_2O_2$$

$$H_2O_2 + 2\bar{e} + 2H^+ \rightarrow 2H_2O$$

These reactions are clearly enhanced with the presence of the bacteria at the interface. In the literature, catalysts of porphyrins and phtalocyanines derivatives have been used successfully to enhance the electrocatalytic oxygen reduction in microbial fuel cells[15]. The extracellular or even periplasmic enzymes in the biofilm can catalyse the oxygen reduction in a similar way with the consequent enhancement of the electrocatalytic activity in our system.

The same experiment with an electrode subjected to polarization is displayed in figure VI.16. In these assays it can be observed, as in the previous experiments, an enhanced electrocatalytic activity. However, in this case the activity is enhanced towards the hydrogen reduction. It is observed an increased current intensity that develops at approximately -750 mV and that is due to the hydrogen reduction reaction. Again, as in the previous results, the maximum activity is obtained at day 2 and starts to decrease at day 5. The major difference is that in this case the enhanced electrocatalytic activity is towards the hydrogen and not the oxygen reduction, clearly indicating that the polarization has a selective role in the process.

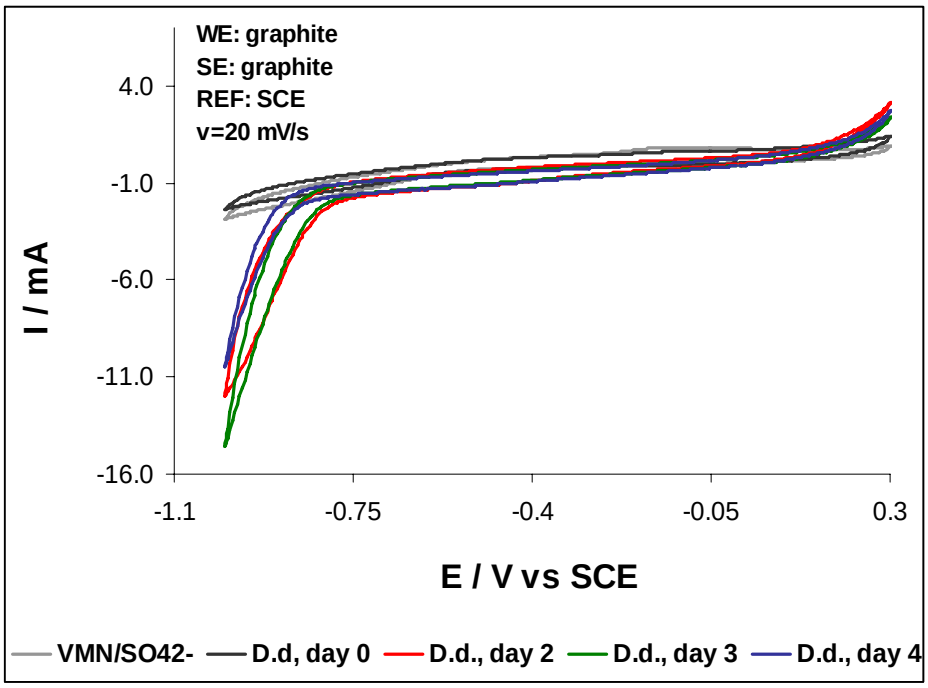

Figure VI.16 Cyclic voltammogram of a polarized graphite plate electrode (at -400 mV) from day 0 to day 4 of the SRB growth on VMN (SO_4^{2-}) and comparison with the control assay without the presence of SRB in the medium (the control is similar throughout the time).

Summarizing, biofilms from SRB present electrocatalytic activity for the oxygen and hydrogen reduction reactions according with the imposed experimental conditions. The polarization of the electrodes and the time of the biofilm development, which implies a difference in its organization and thickness, have an important role in the process.

VI.2.3 SRB growth in VMN/NO_3^-

In order to understand the bacteria interaction vs. the sulphide species' role on the current response, it was decided to grow the SRB on nitrate media. Using this medium, SS 254 as WE and graphite as CE, and imposing a constant potential of -400 and -600 mV, it was not possible to obtain a significant current intensity variation (Figure VI.17). These results on nitrate rich medium need further

confirmation, but it seems that the NO_3^- pathway is not favorable to the biofilm interaction with the electrode. Another hypothesis is that the current obtained within sulphate medium should be due to the biofilm and the consequence of the sulphide species reactions with the electrodes.

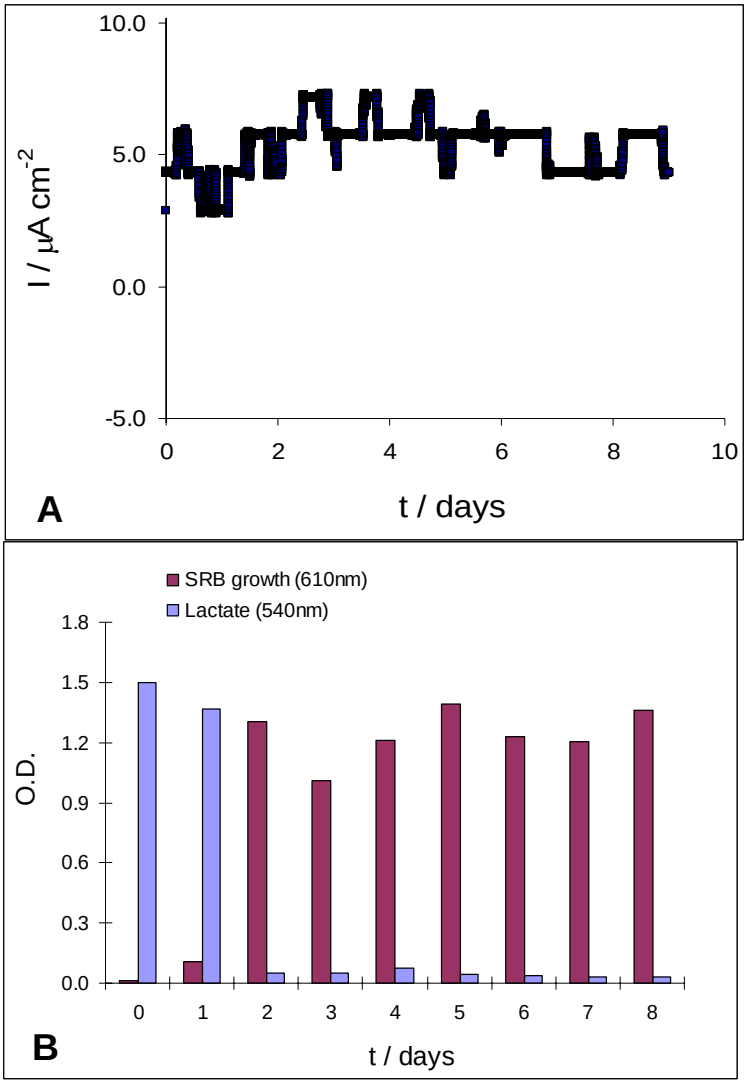

Figure VI.17 A) Example of the results of current density vs. time plot from the SRB growth on VMN (NO_3^-), without membranes, E_{app} = -600 mV; WE: SS 254, CE: graphite; B) Evolution of the SRB growth and lactate consumption during the assay.

Assays with the DSA electrode in nitrate growth medium were performed. The counter electrode used was graphite. The polarization condition tested was E_{app} = +400 mV. The results are displayed on figure VI.18. The growth pattern is the one expected for this medium. There is an initial current increase on the first day of

the assay that should be due to the DSA oxides, and it cannot be ascribed to the biofilm action. There was not any significant current increase using this electrode with anodic polarization.

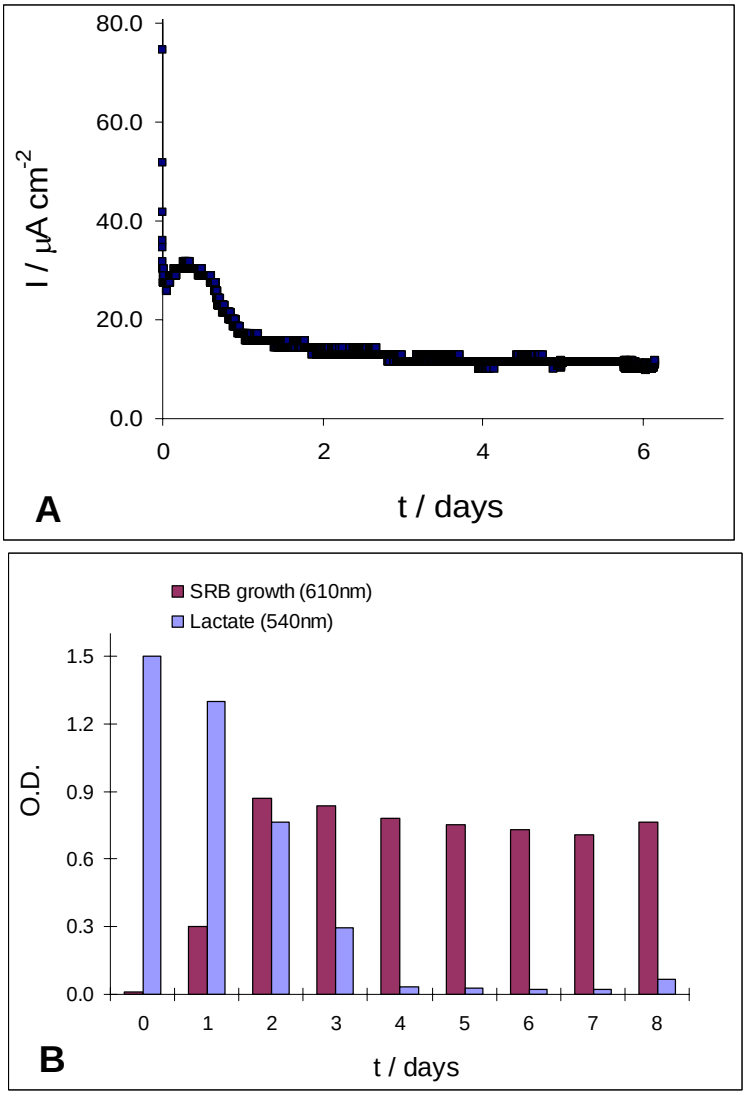

Figure VI.18 A) Current density vs. time plot from the SRB growth on VMN (NO_3^-), without membranes, E_{app} = +400 mV; WE: DSA, CE: graphite; B) Evolution of the SRB growth and lactate consumption during the assay.

VI. 3 Characterization of the *D. desulfuricans* ATCC 27774 EPS

Assays were also tried with the EPS obtained from planktonic cells of the *D.desulfuricans* ATCC 27774. EPR and cyclic voltammetry were performed in the EPS obtained with cells grown in VMN/SO_4^{2-} and VMN/NO_3^- media.

VI.3.1 EPR characterization

As mentioned earlier in this chapter, the role of extracellular enzymes can be important in the electronic transfer pathway of bacteria and the electrode surfaces. An analysis of the EPS constitution in terms of metals can help to elucidate this issue.

The EPR spectra of the EPS obtained from planktonic cells grown after 30 h were attained. The spectra of the EPS obtained VMN/NO_3^- media and the correspondent control assays, ran only with the sterilized media at low temperature (12 K), are displayed in figure VI.19. The spectra of the EPS obtained in VMN/SO_4^{2-} were not conclusive and are not presented.

The results show two signals in different *g* value regions. One at g value 4.3, also present in the control, typical of high-spin ferric iron, non specifically bonded, and the second, centered around *g* value of 2.0, corresponding to Mn(II) ion. The control spectra also present a signal around the *g* value of 2, probably also resultant from this element.

Assays with the EPS samples reduced with dithionite show no significant variation in the spectrum features, but the control presents some changes, namely the multiple signals of the manganese ion become more visible (figure VI.20).

It was not possible to obtain conclusive EPR results of the presence of enzymes, although the strong Mn(II) signals may indicate some incorporation of this metal. Further studies are needed, namely with the EPS removed from the biofilm grown in sulphate medium, to elucidate this issue.

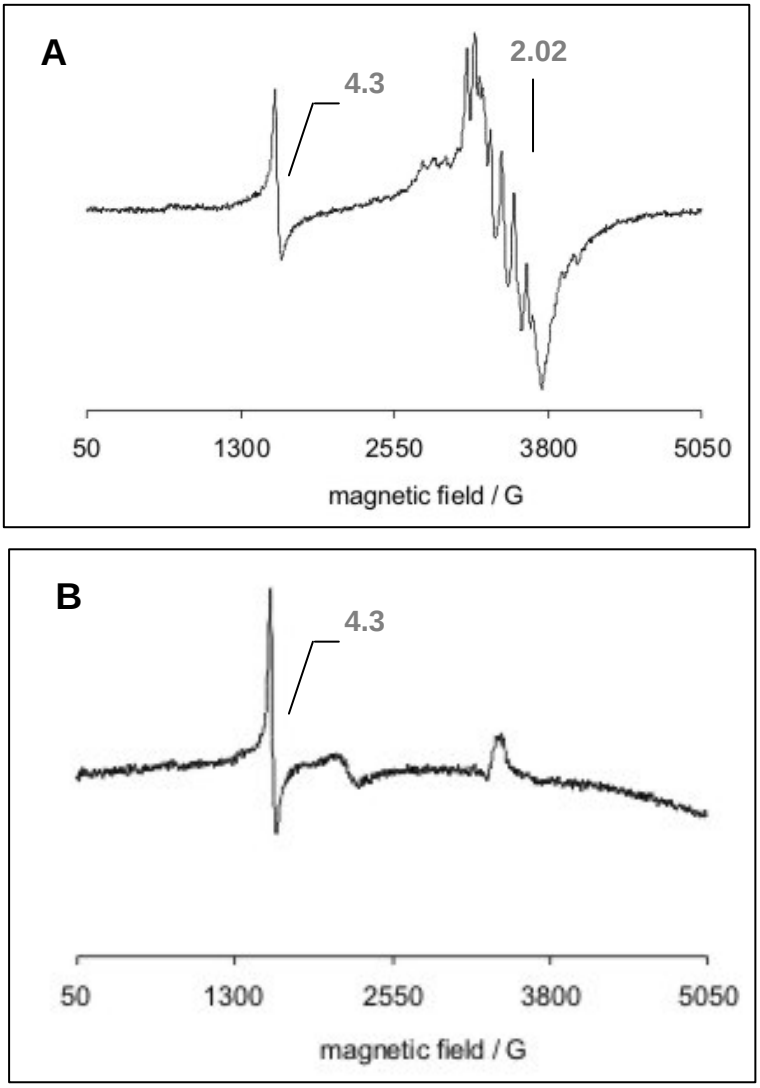

Figure VI.19 EPR spectra of the A) 30 h EPS obtained from *D. desulfuricans* ATCC 27774 cells in VMN/NO_3^- and B) the control only in VMN/NO_3^-; EPR experimental conditions are: temperature 12 K, microwave frequency 9.65 GHz, microwave power 20 mW, modulation amplitude 5 Gpp, receiver gain 10^5, 4 scans; *g* values are displayed in the figure.

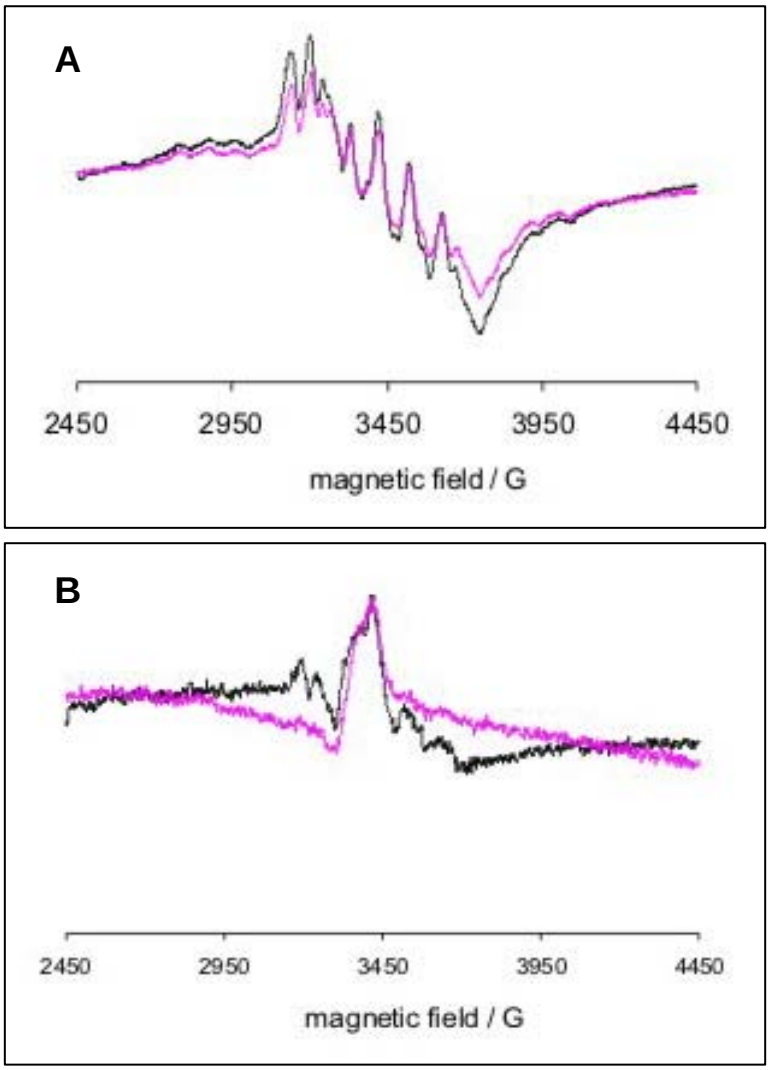

Figure VI.20 EPR spectra of the reduced samples (black line) and comparison with the native oxidized samples (pink line) of A) 30 h EPS obtained from *D. desulfuricans* ATCC 27774 cells in VMN/NO_3^- and B) the control only in VMN/NO_3^-; EPR experimental conditions are: temperature 12 K, microwave frequency 9.65 GHz, microwave power 20 mW, modulation amplitude 5 Gpp, receiver gain 10^5, 4 scans.

VI.3.2 Electrochemical characterization

Cyclic voltammograms of the EPS obtained from cells grown after 30 h were obtained at platinum electrodes (see experimental details in Appendix A). The EPS were diluted to 2.5% and NaCl to a final concentration of 0.05 M was added to assure the conductivity of the solution. The control experiments were performed in

the same conditions with the VMN media without the cells' EPS. The results obtained for the EPS of the cells grown in VMN/SO_4^{2-} and VMN/NO_3^- are displayed in figure VI.21.

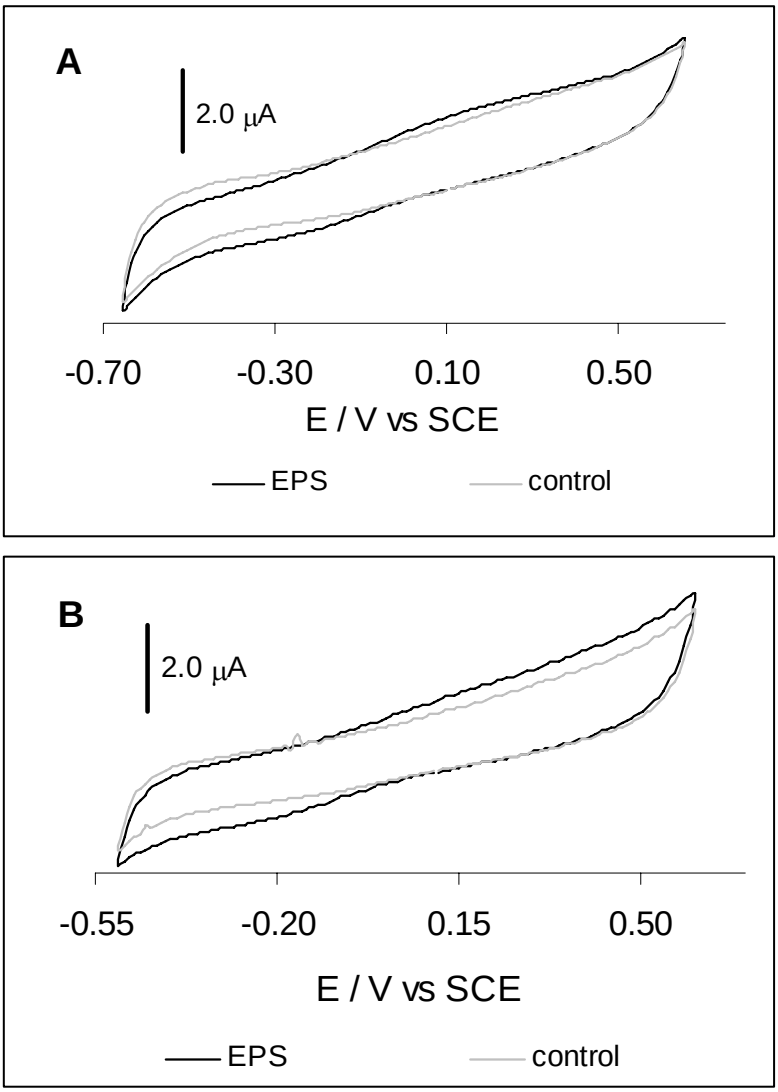

Figure VI.21 Cyclic voltammograms of the 30 h EPS obtained from *D. desulfuricans* ATCC 27774 cells in A) VMN/SO_4^{2-} and B) VMN/NO_3^-; the WE was a Pt disk, CE was a Pt wire, RE a SCE; scan rate was 50 mV s^{-1} (2^{nd} cycle displayed) and 100 mV s^{-1} (5^{th} cycle displayed) respectively for A) and B).

The results show an increase in the electroactivity when in presence of the EPS, both in VMN/SO_4^{2-} and VMN/NO_3^-, although more visible in the sulphate medium. These results confirm that EPS can have a role in the communication of the biofilm with the electrode.

VI.4 Role of the Hydrogenase on the biofilms electroactivity

The role of the bacterial enzymes on the microbial influenced corrosion and in the electron transfer between the biofilms and the metallic surfaces has been recently discussed[4]. They have been related to the ennoblement of some already passive metal layers, moreover enzymatic activities have been detected within the biofilms. The ennoblement effect (the increase of free corrosion potential) and the corrosion rate strongly depends on the local environmental conditions, namely, the oxygen and hydrogen peroxide concentrations, the presence of Mn and Fe, the local pH and also the chemistry/composition of the surfaces. Some authors have attributed some catalytic effects, namely in cathodic reactions, to the enzymes entrapped in the biofilms' EPS, and in particular enzymes related with the oxygen reduction reaction, as catalases, peroxidases and superoxide dismutases[4, 16].

Inside biofilms there are oxygen gradients that allow the occurring of SRB bacteria in natural biofilms even in oxygenated environments. The biocorrosion by the SRB has been extensively discussed. The proposed mechanisms, already mentioned in section VI.1.1, involve a hydrogen intermediate and hydrogenase enzyme activity. Hydrogenase has the capability to direct transfer electrons to metallic and other type of surfaces, such as graphite, as has been demonstrated by several authors and in the present work (see chapter V). The ability to directly transfer electrons can be of significant importance because it opens the possibility that this enzyme may be responsible not only for a SRB biocorrosion but also by the electroactivity presented by the biofilms formed from pure cultures of these bacteria. This implies an electron pathway that can carry electrons from the electrodes surface towards the hydrogenase enzyme. This pathway may be related to small proteins that are present in the bacteria membrane as well as in the EPS matrix, such as small *c*-type cytochromes[17]. Our results from the *D. desulfuricans* ATCC 27774 biofilms seem to support this hypothesis, namely the cathodic current increase with time and the enhanced hydrogen reduction reaction obtained with the biofilms formed in polarized surfaces. These results may indicate a role of the hydrogenase enzyme in the electroactivity of the biofilms and also opens new routes in the understanding of the SRB's biocorrosion mechanisms.

VI.5 Discussion and final remarks

The experiments with the *D. d* ATCC 27774 strain showed a current response with time, up to a 9 fold increase during at least one day, using SS 254 as working material with the imposition of different cathodic polarization conditions, namely, -400 and -600 mV. The best results were accomplished with the applied potential value of -400 mV. The assays with dialysis membranes allowed to correlate these results with the biofilm action and maybe also with the H_2S presence, in sulphate medium.

Experiments with half the concentration in lactate did not produce any significant current variation. This result needs further confirmation, but can be indicative that some critical mass is necessary for the bacteria to interact with the metal. The assays performed with imposed anodic potential at the DSA coupons as working electrodes, did not succeed in producing a significant current increase. The same assays were performed changing the growth medium from VMN/SO_4^{2-} to VMN/NO_3^-. These were not successful, both with cathodic and anodic polarization conditions, using respectively SS 254 and DSA as working electrodes.

Changing the electrode material to graphite, and in sulphate media, led to a significant current decrease, till 5.5 times the initial current value, and a more stable response in time. This can be an effect of the area of the electrode, that is significantly higher than the stainless steel area, but also the nature of the material can be more favorable to the bacteria or EPS components, namely small electron carriers proteins, interaction which can facilitate the electron transfer towards the electrode.

On table VI.II the obtained results with the *D.desulfuricans* ATCC 27774 strain are summarised.

Table VI.II Summary of the main results obtained with SRB's biofilms.

Organism	Media	Electrode	E_{app} / V (*vs* SCE)	ΔI	I_{max} / A m^{-2}	Time at I_{max}
D. *desulfuricans* ATCC 27774	VMN SO_4^{2-}	SS 254	-0.4	Up to 4x	-0.13	1 day
		DSA	+0.2	Not attributed to SRBs		
			+0.4			
		Graphite	-0.4	Up to 3x	-0.45	10 days*
				Up to 5x	-0.16	1 day
				Up to 17x	-0.15	10 days*
	VMN NO_3^-	SS 254	-0.6	Not significative		
		DSA	+0.4			

* with addition of $FeSO_4^{2-}$

On table VI.III the best experimental results are compared with published data, showing that SRB's biofilms can be considered very interesting from the point of view of the obtained electroactivity, namely considering the maximum high current and stability.

Table VI.III Comparison of the results obtained with SRB's biofilms and the literature data.

Organism	Media	Electrode	E / V (vs. SCE)	I_{max} / mA m^{-2}	Ref.
G. sulfurreducens *G. Metllireducens*	NO_3^-	Graphite	-0.455	-400	9
From marine environments, mainly *Geobacteracea* (MFC)	sea water	Graphite	+0.6	+130	18
D.desulfuricans (MFC)	SO_4^{2-}	Graphite	use of redox mediators	+3.74	19
From anaerobic sludge (MFC)	addition of sucrose	Reticulated vitrous carbon	use of redox mediators	+ 516	20
From compost	Addition of acetate	DSA	+0.5	+145	21
D. *desulfuricans* ATCC 27774	SO_4^{2-}	Graphite	-0.4	-150	This work

(MFC: Microbial Fuel Cell)

The cyclic voltammetry experiments have shown an enhanced electrocatalytic effect due to the biofilms' presence. The polarization of the electrodes seems to have a selective effect on the electrocatalytic enhancement, with the observation of higher currents towards the hydrogen reduction. This effect may be related with the hydrogenase activity within the biofilm and may indicate that this enzyme plays an effective role on the biofilms electroactivity.

VI. 6. References

1. Davey, M. E.; O'Toole G, A., Microbial biofilms: from ecology to molecular genetics. *Microbiol Mol Biol Rev* **2000,** 64, (4), 847-67.

2. Hamilton, W. A., Microbially influenced corrosion as a model system for the study of metal microbe interactions: a unifying electron transfer hypothesis. *Biofouling* **2003,** 19, (1), 65-76.

3. Kuchma, S. L.; O'Toole, G. A., Surface-induced and biofilm-induced changes in gene expression. *Curr Opin Biotechnol* **2000,** 11, (5), 429-433.

4. Beech, I. B.; Sunner, J., Biocorrosion: towards understanding interactions between biofilms and metals. *Curr Opin Biotechnol* **2004,** 15, (3), 181-6.

5. Hamilton, W. A., Lee, W., *Sulphate Reducing bacteria*. Plenum Press: New York, **1995**.

6. Fonseca, I. T., Lino, A. R., Chasqueira, I., Sanches, M. D., Martins, I., Corrosão do aço macio por bactérias Desulfovibrio Desulfuricans ATCC 27774 em meio de lactato-sulfato na ausência e na presença de Fe^{2+}. *Corr Prot Mat* **1998,** 17, (3), 6-13.

7. Bond, D. R.; Holmes, D. E.; Tender, L. M.; Lovley, D. R., Electrode-reducing microorganisms that harvest energy from marine sediments. *Science* **2002,** 295, (5554), 483-5.

8. Bond, D. R.; Lovley, D. R., Electricity production by Geobacter sulfurreducens attached to electrodes. *Appl Environ Microbiol* **2003,** 69, (3), 1548-55.

9. Gregory, K. B.; Bond, D. R.; Lovley, D. R., Graphite electrodes as electron donors for anaerobic respiration. *Environ Microbiol* **2004,** 6, (6), 596-604.

10. Lovley, D. R., Bug juice: harvesting electricity with microorganisms. *Nat Rev Microbiol* **2006,** 4, (7), 497-508.

11. J. M. Odom, R. S. J., *The Sulphate-Reducing Bacteria: Contemporary Perspectives*. Springer-Verlag: New York, **1992**.

12. Matias, P. M.; Pereira, I. A.; Soares, C. M.; Carrondo, M. A., Sulphate respiration from hydrogen in Desulfovibrio bacteria: a structural biology overview. *Prog Biophys Mol Biol* **2005,** 89, (3), 292-329.

13. Humphries, A. C.; Mikheenko, I. P.; Macaskie, L. E., Chromate reduction by immobilized palladized sulphate-reducing bacteria. *Biotechnol Bioeng* **2006,** 94, (1), 81-90.

14. Martins, I., In CQFB/FCT-UNL: Lisboa, **2007**; Vol. PhD.

15. Zhao, F.; Harnisch, F.; Schrorder, U.; Scholz, F.; Bogdanoff, P.; Herrmann, I., Challenges and constraints of using oxygen cathodes in microbial fuel cells. *Environ Sci Technol* **2006,** 40, (17), 5193-5199.

16. Scotto, V., Lai, E., The ennoblement of stainless steels in seawaters: a likely explanation coming from the field. *Corrosion Science* **1998,** 40, (6), 1007-1018.

17. Heidelberg, J. F.; Seshadri, R.; Haveman, S. A.; Hemme, C. L.; Paulsen, I. T.; Kolonay, J. F.; Eisen, J. A.; Ward, N.; Methe, B.; Brinkac, L. M.; Daugherty, S. C.; Deboy, R. T.; Dodson, R. J.; Durkin, A. S.; Madupu, R.; Nelson, W. C.; Sullivan, S. A.; Fouts, D.; Haft, D. H.; Selengut, J.; Peterson, J. D.; Davidsen, T. M.; Zafar, N.; Zhou, L.; Radune, D.; Dimitrov, G.; Hance, M.; Tran, K.; Khouri, H.; Gill, J.; Utterback, T. R.; Feldblyum, T. V.; Wall, J. D.; Voordouw, G.; Fraser, C. M., The genome sequence of the anaerobic, sulphate-reducing bacterium Desulfovibrio vulgaris Hildenborough. *Nat Biotechnol* **2004,** 22, (5), 554-9.

18. Tender, L. M.; Reimers, C. E.; Stecher, H. A., 3rd; Holmes, D. E.; Bond, D. R.; Lowy, D. A.; Pilobello, K.; Fertig, S. J.; Lovley, D. R., Harnessing microbially generated power on the seafloor. *Nat Biotechnol* **2002,** 20, (8), 821-5.

19. Ieropoulos, I. A., Greenman, J., Melhuish, C., Hart, J., Comparative study of three types of microbial fuel cells. *Enzyme and Microbial Technology* **2005,** 37, 238-245.

20. He, Z., Minteer, S. D., Angenent, L. T., Electricity Generation from Artificial Wastewater Using an Upflow Microbial Fuel Cell. *Environ Sci Technol* **2005,** 39, 5262-5267.

21. Dulon, S., Parot, S., Delia, M-L., Bergel, A., Electroactive biofilms: new means for electrochemistry. *J. Appl. Electrochem.* **2007,** 37, 173-179.

Appendix A

Experimental Details

Appendix A-Experimental Details

A.1 Electrochemical set-up and media

In this section the electrochemical set-up, the used electrode materials, its pre-treatment and the used media/electrolytes are described.

The potentiodynamic experiments were performed with an AUTOLAB PGSTAT 12 potentiostat / galvanostat, an AUTOLAB PGSTAT 30 (Chapter VI) or μAUTOLAB Type III potentiostat. The data acquisition was assured by a PC and the GPES software.

In all the experiments a one compartment electrochemical cell was used with a three electrodes configuration.

Except for Chapter VI assays (biofilms experiments) the used working electrodes were glassy carbon (GC), graphite and gold disks with diameters of 4 mm for GC and graphite and 2 mm for gold. The assays described in Chapter VI were performed with stainless steel coupons SMO 254 and graphite coupons, both with A_{geom}=20 cm^2, (cathodic polarization assays), and DSA (anodic polarization assays), with A_{geom}=21.2 cm^2. The EPS electrochemical characterization was accomplished using a platinum working electrode with 4 mm diameter. A platinum wire and the saturated calomel (SCE) were the counter and reference electrodes, respectively, for all experiments except Chapter VI where SS 304 and graphite coupons (same dimensions as the working electrodes) were used as counter electrodes. The working electrodes were previously treated 5.0, 1.0, 0.3 and 0.05 μm alumina and immersed in Millipore water in a ultra-sound bath for 10 min and finally thoroughly rinsed with Millipore water, except for SS and DSA electrodes, that were cleaned by:

SS: degreasing in an ethanol and acetone solution (50%v/v), immersion in an acidic solution (mixture of 65%.HNO3 and 40% HF) for one hour, and after rinsed in demineralised water for another hour; after the electrodes were left in air for 5 days for passivating;

DSA: anodic electrolysis in 0.1 M H_2SO_4 for 5 hours (galvanostatic conditions at 20 mA cm^{-2}).

A pre-conditioning in 2 mM neomycin sulfate, for GC, and 1 mM 4,4'-dithiodipyridine, for gold, was performed for 10 min when promoters have been used.

The cyclic voltammetry (CV) assays were performed at different scan rates (from 1 mV/s to 20 V/s) in a highly degassed solution through argon bubbling or in restricted anaerobic conditions accomplished inside an anaerobic chamber (MBRAUN).
Square wave voltammetry (SWV) was performed using 50 mV pulse amplitude, 10 mV step height and frequencies between 8 and 200 Hz.
Chronoamperometric experiments were performed in Chapter VI, using different polarization potentials, namely, +200, -200, -400 and -600 mV vs SCE.

The measurements were made at room temperature, except for Chapter VI, in which the assays were performed at 37ºC. All chemicals were *p.a.* grade and were purchased from Sigma.

For the different systems, different electrolytes and protein concentrations were used. Table A.1 summarizes the information concerning each system.

Table A.1 Supporting electrolytes and protein concentrations used in each Chapter.

Chapter	Supporting electrolyte	Protein concentration / mM
II	10 mM Tris-HCl (or phosphate, acetate, glycine and citrate for the pH variation essays) buffer / 0.1 M KNO_3 / 2 mM neomycin sulfate; 2 to 100 mM $MgCl_2$ was added for the effect of the magnesium ion addition study	0.3-1
III	50 mM Tris-HCl or 50 mM MOPS buffer (pH ≈ 7) / 0.1 M NaCl or KCl; KNO_3 (different concentrations) was added for the catalytic activity assays; 2 mM neomycin sulfate was added for themembrane electrode assays	0.1
IV	100 mM Tris-HCl, pH 7.6, or a mix of sodium citrate and the MES/HEPES/AMPSO buffer system with concentration of 20 mM each buffer component	0.05
V	The electrolyte composition was 25 mM Tris-HCl, Acetate, CHES or Phosphate buffer / 0.1 M NaCl / 1 mM neomicyn sulfate	1-3
VI	2.5% dilution of the initial EPS solution / 0.05 M NaCl (for EPS characterisation)	

In Chapter IV, the oxygen and nitric oxide concentration data were accomplished by the measurement of the maximum cathodic current of the oxygen or the NO reduction peak, after the addition of aliquots of water saturated with air (considering a solubility of 2.69×10^{-3} mol dm^{-3} at room temperature) or NO (maximum solubility 100 μM, at 20ºC[1]). NO saturated water was prepared from a 5% NO / 95 % He mixture (*Ar líquido*). The NO/He mixture was previously washed by bubbling in a 5 M KOH solution and through non-buffered water, at pH 3, to accomplish NO_x removal.

A.2 Protein immobilisation procedures

Protein immobilisation was accomplished either with a membrane (Medicell *visking dialysis membrane*.cellulose, 12000-14000 Da *cut-off*) adjusted to the electrodes with a viton o-ring, or by adsorption from a concentrated solution, by solvent casting, with volumes between 5-10 μL. On Chapter IV, the concentrated NOR protein was adsorbed from a concentrated solution of composition: 50 μM NOR / 100 mM phosphate buffer / 0.02% lauryl maltoside / 0.01%(v/v) phenyl ethanol.

A.3 Proteins purification

The proteins were purified following previously described methods. On table A.2 the references to the purifications are displayed for each protein.

Table A.2 References of the purification methods for the different proteins

Chapter	Protein	References
II	SORs	2-5
III	NAP	6
IV	NOR	7
V	Hase	8

The state of the as-purified *Dg*Hase was established by EPR spectroscopy. It was possible to confirm that the protein is isolated mainly in the Ni-A form as reported in

the literature[9], with a minor component with g values 2.34, 2.11 (and probably 2.01) characteristic of the Ni-B form.

A.4 Biofilms growth

The growth medium was VMN/SO_4^{2-} or VMN/NO_3^-, with the following composition:

VMN/SO_4^{2-} (for 1 dm^3):

KH_2PO_4	0.5 g
Na_2SO_4	4.5 g
NH_4Cl	1.0 g
$MgSO_4$. $7H_2O$	0.06 g
$CaCl_2$. $2H_2O$	0.04 g
sodium lactate	6.0 g
sodium citrate	0.3 g
$FeSO_4$. $7H_2O$	0.004 g
Wolfes Elixir	1 ml
Casamino Acids	2.0 g
Tryptone	2.0 g
Vitamine solution	2 ml

VMN/NO_3^- (for 1 dm^3): the same as the previous, except that 0.05 g $MgCl_2.6H_2O$ and 0.003 g $FeCl_2.4H_2O$ substitute $MgSO_4$. $7H_2O$ and $FeSO_4$. $7H_2O$.

The Wolfes Elixir and the Vitamin solution compositions are:

Wolfes Elixir (for 1 dm^3):

Nitrileacetic acid	1.5 g
$MgSO_4$. $7H_2O$	3.0 g
$MnSO_4$. H_2O	0.5 g
NaCl	1.0 g
$FeSO_4$. 7 H_2O	0.1 g
$CoSO_4$. 7 H_2O	0.1 g
$NiCl_2$.6 H_2O	0.1 g
$CuCl_2$. 2 H_2O	0.1 g
$ZnSO_4$. 7 H_2O	0.1 g
$CuSO_4$. 5 H_2O	0.01 g
$AlK(SO_4)$. 12 H_2O	0.01 g
H_3BO_3	0.01 g
Na_2MoO_4. $2H_2O$	0.01 g
Na_2SeO_3. 5 H_2O	0.001 g

Vitamin solution (for 0.2 dm^3):

B_2	0.02 g
nicotinic acid	0.05 g
B_1	0.06 g
B_5	0.06 g
B_6	0.06 g
B_{12}	0.005 g
C	0.2 g
H	0.001 g

The pH for both media was 7.45-7.55.

The SRBs growth was followed by cell counting and OD at 610 nm. The lactate consumption was monitored by the OD measured at 540 nm. The sulfide production was evaluated by a standard proceeding for the S^{2-} detection. Figure A.5 displays the experimental setup used for the biofilms growth under polarization conditions.

Figure A.1 Experimental apparatus used for the biofilm growth under polarization conditions.

A.5 References

1. Girsch, P.; deVries, S., Purification and initial kinetic and spectroscopic characterization of NO reductase from Paracoccus denitrificans. *Biochim Biophys Acta-Bioenerg* **1997,** 1318, (1-2), 202-216.

2. Czaja C., L., A. J., Naylor S., Tavares P., LeGall J., Moura J. J., Moura I., Rusnak F., Expression of the D. gigas desulforedoxin in E. Coli. *J Biol Chem* **1995,** 270, (35), 20273-20277.

3. Ascenso, C.; Rusnak, F.; Cabrito, I.; Lima, M. J.; Naylor, S.; Moura, I.; Moura, J. J., Desulfoferrodoxin: a modular protein. *J Biol Inorg Chem* **2000,** 5, (6), 720-9.

4. Coelho, A. V., Matias, P., Füllop,V., Thompson, A., Gonzalez, A., Carrondo, M. A. , Desulfoferrodoxin structure determined by MAD phasing and refinement to 1.9-A resolution reveals a unique combination of a tetrahedral FeS_4 centre with a square pyramidal $FeSN_4$ centre. *J Biol Inorg Chem* **1997,** 2, 680-689.

5. Raleiras, P. Superoxide Reductases - Structural and Functional Aspects. FCT-UNL, Lisboa, 2005.

6. Gonzalez, P. J.; Rivas, M. G.; Brondino, C. D.; Bursakov, S. A.; Moura, I.; Moura, J. J., EPR and redox properties of periplasmic nitrate reductase from Desulfovibrio desulfuricans ATCC 27774. *J Biol Inorg Chem* **2006**.

7. Timóteo, C., *et al*,, **in preparation**.

8. Teixeira, M. Estudos Espectroscópicos de Hidrogenases Bacterianas. FCT-UNL, Lisboa, 1986.

9. Teixeira, M.; Moura, I.; Xavier, A. V.; Huynh, B. H.; DerVartanian, D. V.; Peck, H. D., Jr.; LeGall, J.; Moura, J. J., Electron paramagnetic resonance studies on the mechanism of activation and the catalytic cycle of the nickel-containing hydrogenase from Desulfovibrio gigas. *J Biol Chem* **1985,** 260, (15), 8942-50.

Appendix B

Electrochemical Criteria

Appendix B-Electrochemical Criteria

B.1 Introductory note

This thesis uses extensively electrochemical tools and procedures applied to a wide range of biological systems (from isolated proteins to all cell systems). Details on experimental procedures and instrumentation used are indicated on Appendix A. Chapter I develops already an assemblage of potential applications using electrochemical methods. Here are briefly described the electrochemical techniques used and the reasons why each one was chosen (B.1). Sections B.2 to B.4 puts in evidence the main criteria used for data analysis.

B.2 Electrochemical methods

In this section a brief description of the electrochemical techniques used in the present work is given.

Cyclic Voltammetry

All the systems were studied by cyclic voltammetry. This approach has the advantage to provide fast and direct measurements of the proteins redox properties. Also it is possible to apply a wide range of potentials windows that other non-dynamic methods, such as potentiometry, cannot achieve due to the limitations of the redox mediators used. Using cyclic voltammetry it is also possible to obtain kinetic (and thermodynamic) information on the redox centres which is important to establish the catalytic mechanisms under studied[1].

In this work several approaches were followed, aiming to get the best results in each system, namely the classic bulk voltammetry and the immobilization of the biological molecules, either by physical entrapment or adsorption on the electrodes surfaces.

Square wave voltammetry

In a very simple description, the pulse techniques differ from the normal voltammetry because a potential pulse is applied and the current is sampled twice, the second time at the end of the pulse, when the charging current is already decayed. The

subtraction of the two currents gives a resulting differential pulse voltammogram. This allows an effective correction of the contribution of the charging background current and an increase of the ratio between the faradaic and non-faradaic currents with the consequent improvement of the sensibility[2].

This technique was used in chapter II and III due to its enhanced sensitivity when compared with cyclic voltammetry[3] and was demonstrated to be useful in systems with poor redox responses such as SOR and related proteins.

Chronoamperometry

In this technique a fixed potential is applied instantaneously to the working electrode, stepped from a value where no electrolysis occurs to another value where complete conversion of the species under study occurs. The current response evolution with time is observed. The current decays with time, gradually to zero (or a fixed value close to zero)[2, 3]. This method was used in chapter VI to follow the current produced by the interaction of the biofilms with the working electrodes when a fixed potential value was applied. This is a slow interaction because time is needed for the biofilms growth and cells adaptation. In this case, the current originated from the potential step is stabilised after a determined time. Additional variations of the measured current arises from new interfacial processes, namely from the interaction of the biofilms.

B.2 Electrochemical criteria for bulk electrochemical systems

The electrochemical criteria for systems with the electroactive species in bulk are summarized.

Reversible systems:

- $I_p \propto \nu^{1/2}$
- E_p independent of ν
- $|E_p - E_{p/2}| = 2.2\ RT/nF = 56.5/n$ mV (T=25ºC)

and only in the case of cyclic voltammetry

- $E_{pa} - E_{pc} = 2.2\ RT/nF = 56.5/n$ mV (T=25ºC)
- $I_{pa} / I_{pc} \cong 1$

The peak current is given by the Randles-Sevcik equation:

$$I_p = (2.69x10^5)n^{3/2}AD_0^{1/2}\ \nu^{1/2}\ C_0^* \qquad \text{B.2.1}$$

Quasi-reversible systems:

- I_p not proportional to $\nu^{1/2}$
- ΔEp increases with ν
- for $D_o = D_r = D$

the shape of the curves and parameters dependent of

Λ= ko / D1/2(nF/RT)1/2 ν1/2

The solution for the peak current is given by the equation:

$$I_p = nFAD_0^{1/2}(nF/RT)\ \Psi(E)\nu^{1/2}\ C_0^* \qquad \text{B.2.2}$$

Irreversible systems:

- $Ip \propto \nu^{1/2}$
- $(I_p / \nu^{1/2}$ independent of $\nu)$
- E_p dependent of ν
- $|E_p - E_{p/2}| = 1.86\ RT/\alpha nF = 47.7/\alpha n$ mV (T=25ºC)

for slow scan rates the systems approaches reversible behaviour

The peak current is described:

$$I_p = (2.99x10^5)n(\alpha n')^{1/2}AD_0^{1/2}\ \nu^{1/2}\ C_0^* \qquad \text{B.2.3}$$

where n' is the number of electrons in the determinant step of the reaction.

B.3 Electrochemical criteria for thin layer electrochemical systems

In this section the thin layer theory and the correspondent criteria are briefly described.

The thin layer theory is applied when all the electroactive species is confined to a thin layer at the electrode surface. If the thickness of this layer is smaller than the diffusion layer, electrolyse can be fast and complete, and the diffusion-controlled mass transfer is eliminated[4]. This type of cells typically presents thickness between 2 and 100 μm[4, 5]. Amongst the advantages are the use of small volumes, in the range of the μL, and the high sensitivity that can be achieved. In this type of cells the counter and the reference electrodes are placed outside the thin layer. Several configurations can be found, the most common being the so-called optical transparent thin layer cells and the membrane electrodes accomplished with the use of membranes (usually cellulose) that are compressed towards the electrode surface[5].

For linear scan voltammetric techniques, planar electrodes and considering that both reactant and product are soluble and with uniform concentrations in the layer, the peak current for a reversible reaction, is given by equation B.3.1:

$$I_{pc} = -\frac{n^2 F^2 \nu V[O]_i}{4RT} \qquad \text{B.3.1}$$

The equation is written for a reduction.

The reversibility criteria are[3, 5]:

- $I_p \alpha \nu$, the current peak varies with the scan rate
- $\Delta Ep \alpha \nu$, there is no separation between the anodic and the cathodic current peaks
- The curve is symmetrical around E_p
- $I_{pa} / I_{pa} \approx 1$

The thin layer cell theory is similar to other non-diffusional systems, such as the deposition and stripping of thin metallic films and the adsorbed molecules on electrode surfaces.

B.4 Laviron's mathematical approach

The use of a thin layer diffusionless regime allow to use Laviron's mathematical approach[6] to determine kinetic parameters. In this section a brief summary of this approach is presented.

For the same conditions defined in the previous sections, namely the concentrations of the reactant and product are uniform throughout the cell, it is possible to define the following equations:

$$i = nFAk_{sh}\left\{c_0 \exp\left[-\alpha nF\left(E - E^0\right)/RT\right] - c_r \exp\left[(1-\alpha)nF\left(E - E^0\right)/RT\right]\right\} \qquad \text{B.4.1}$$

$$c_0 + c_r = c_T \qquad \text{B.4.2}$$

$$i = -nFVdc_0 / dt \qquad \text{B.4.3}$$

Where I is the current, expressed in Amperes, A is the area of the electrode in cm^2, V is the volume of the thin cell in cm^3, k_{sh} is the heterogeneous rate constant in cm s^{-1},

c_0 and c_r are the concentrations of the oxidised and the reduced species in mol cm^{-3}, and the n, F, α, R and T have the usual significance.

A parameter *m* is defined by the following equation:

$$m = \frac{RTk_{sh}}{Fn\nu} \qquad \text{B.4.4}$$

When $m \rightarrow \infty$ ($\nu \rightarrow 0$), the system tends to reversibility and peak width at mid-height tends to 90.6/n mV. For $m \rightarrow 0$ (high scan rates), the system tends to irreversibility and in this total irreversible case, the width of the cathodic and anodic peaks are equal to 62.5/αn and 62.5/(1-α)n mV, respectively.

From the experimental difference between the peak potential of the anodic and the cathodic peaks, ΔE_p, and for a known α, the k_{sh} can be calculated. Two cases can be considered,

1) $\Delta E_p > 200/n$ and

2) $\Delta E_p < 200/n$ mV.

For case 1), the α can be calculated by the plot of E_p vs. log ν, with slopes equal to -2.3RT/αnF and 2.3RT/(1-α)nF for the cathodic and anodic peaks, respectively. From it is possible to calculate k_{sh} from the equation:

$$k_{sh} = \frac{\alpha nF\nu_c}{RT} = \frac{(1-\alpha nF\nu_a)}{RT} \qquad \text{B.4.5}$$

For case 2), the determination of α can not be precise, but for values close to 0.5 (between 0.3 and 0.7), the k_{sh} can still be determined with a negligible error. From a theoretical curve of $n\Delta E_p$ as a function of 1/*m*, and from interpolation of the experimental ΔE_p values, the m parameter can be found and, so, using equation B.8, the k_{sh} is estimated.

B.5 References

1. Wilson, G. S., *Bioelectrochemistry*. Wiley-VCH: Weinheim, 2002; Vol. 9.
2. Wang, J., *Analytical Electrochemistry*. Wiley-VCH: New York, 1994.

3. Bard, A. J. F., L. R., *Electrochemical Methods-Fundamentals and Applications*. John Wiley&Sons: New York, 1980.

4. Hubbard, A. T., Anson, F. C., *The Theory and Practice of Electrochemistry with Thin Layer Cells*. Marcel Dekker, Inc.: New York, 1970; Vol. 4.

5. Brett, A. M. O., Brett, Christopher M. A. , *Electroquímica-Princípios, Métodos e Aplicações*. Livraria Almedina: Coimbra, 1996.

6. Laviron, E., General expression of the linear potential sweep voltammogram in the case of diffusionless electrochemical systems. *Journal of Electroanalytical Chemistry* **1979,** 101, (1), 19-28.